Master's Thesis

FATIGUE MODEL FOR PRESTRESSED CONCRETE DECKS

Tudor Mihai Brata

Delft University of Technology

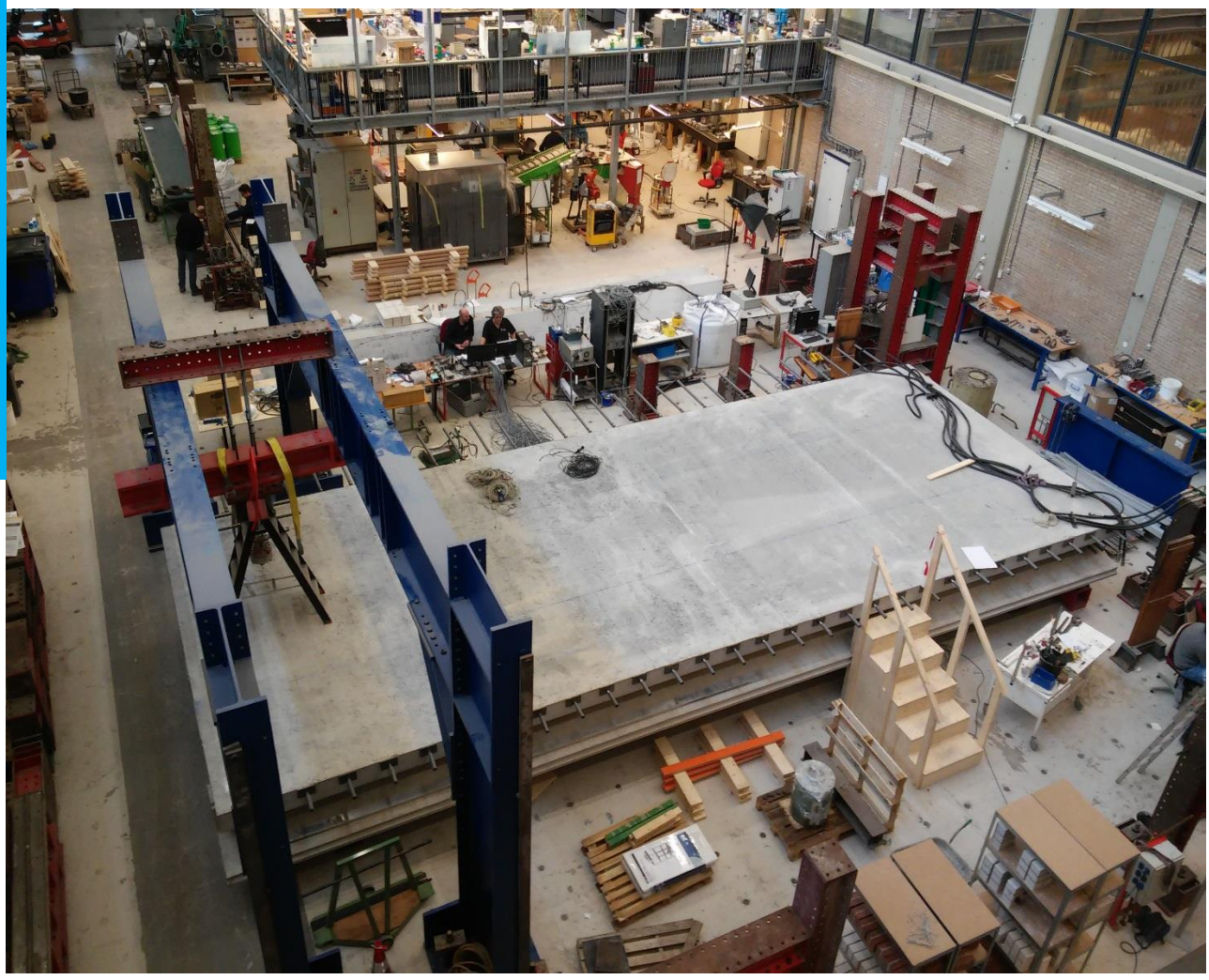

TU Delft Delft University of Technology

Challenge the future

TU Delft Delft University of Technology

Master's Thesis

Fatigue model for prestressed concrete decks

By

Tudor Mihai Brata
4418646

In partial fulfilment of the requirements for the degree of

Master of Science
in Civil Engineering

at Delft University of Technology

December 2016

Assessment Committee:

Thesis Chair:	Prof. Dr. Ir. D. A. Hordijk
Thesis Supervisor:	Dr. Ir. C. van der Veen
Thesis Committee Member:	Prof. Dr. Ir. M. A. N. Hendriks
Graduation Coordinator:	Ir. L. J. M. Houben

TU Delft Delft University of Technology

Acknowledgements

The present Master's Thesis report marks the completion of both an academic and a life cycle which would have not been possible without the help and support of a certain number of people that contributed to my personal development, both professionally and as a human being.

I would like to express my gratitude to the members of my committee: Dr. van der Veen, Prof. Hendriks and Prof. Hordijk, for their valuable advices, guidance, patience and time spent so that I could have a clear and better understanding of this topic that represents a drop in the sea that is our profession, Civil Engineering.

I want to thank my close family: my mother Dora, my father Valentin and my aunt Lia for their unconditional and always present support and love, for never stopping to believe in me and for being always by my side.

To my friends from Romania, that will never fully understand how much their presence helped me go forward, especially during the dawn of this adventure of mine that started more than two years back, thank you.

I want also to thank all the wonderful people and friends I met during my studies here. They showed me that kindness and friendship can be sought and found in all the corners of this round world.

Last but not least, I want to thank Delft University of Technology and the beautiful city of Delft for the environment that I discovered here, this gateway not only to education and Dutch culture, but also to cultures from all around the world. It has been an extraordinary experience.

Sincerely,

Tudor Mihai Brata

Summary

A high number of concrete bridges that were built in the Netherlands around half a century ago and which had a transversely prestressed thin deck, nowadays raise a series of questions regarding their structural integrity. This is because their service life has been affected over time by a substantial rise in the number of vehicles that transit them and the considerable increase in the loads applied by these vehicles upon the structure. The concern amplifies when it is highlighted that these structures were designed according to old codes that were valid during that period, codes that have been substantially modified in the course of time. Having all this that needs to be taken into account, it is of high interest to determine how safe these structures are today.

One phenomenon that in time would have left its mark on the structural integrity of these bridges is fatigue. This can be defined as the deterioration in time due to a repetitive loading. A large array of studies were dedicated to the topic of fatigue of concrete, aiming at a better understanding of its behaviour, impact and consequences upon a structure. However, throughout this extensive research that also analysed failed structures, fatigue was never found to be the primary mechanism that led to failure, but its contribution was acknowledged and, as a consequence, investigations on this topic are still of current interest. Of great importance is also the phenomenon of compressive membrane action (CMA) that is characteristic to concrete slabs and has a beneficial influence on the structure, leading to an increase in the capacity, being highly influenced by the degree of restraint

At Delft University of Technology, a couple of research programs that were performed recently tried to shed some light on both of the previously described topics. The study done on fatigue gave promising results, with its outcome being found to fit together with other researches performed worldwide. A follow-up study based solely on fatigue will start in the near future, this having as objective the impact of the loading sequence. In anticipation of this new study, in order to see to what extent the previous results can be replicated numerically and future ones forecasted, a FEA model for fatigue assessment and prediction was created and its accuracy was evaluated, this being the scope of the Master's Thesis.

For the development of the finite element model, departure points had to be set for each main phase. For the construction and calibration phase, the point of departure meant the use of a two-dimensional model for describing the behaviour of the real life structure, namely the evolution of stresses, deterioration and failure mode. For the second phase, the one related to replicating and assessing the fatigue damage, the departure point meant assuming a uniform alteration in the material properties due to the cyclic loading, modification considered at a structural level.

The FEA model was designed to be a simple 2D plane stress model, realizing that such a choice implied certain behavioural limitations. By using a two-dimensional model it was clear that this could not fully describe a three-dimensional stress state. For its development, the actual structure was used as reference, describing the full cross section for the model's geometry,

together with the reinforcing and prestressing bars. In order to obtain a realistic behaviour under loading, multiple material models were considered for the components of the FEA model, with the concrete's compressive and tensile ones being of utmost importance. Other prime constituents of the model were represented by the acting loads, support conditions and the characteristics of the performed analyses, such as the iterative or incremental procedures or the convergence criteria. For the construction of the model, the guidelines from Rijkswaterstaat on non-linear FE analysis of concrete structures were applied.

Its calibration was based on the previous performed tests and it was determined that the behaviour is influenced by a series of parameters, the most important being the considered effective width of the model. Having assumed an adequate value for it, the initial stiffness of the model was very similar to the ones obtained in the previous research programs. Other parameters that were highly influential on the capacity of the model were the considered degrees of freedom at the supports, amount of reinforcement considered - directly proportional to the width, the tensile and compressive material models for the concrete, the choice of bond for the prestressing bar or the arc-length control incremental procedure.

In the end it was decided to use two models for the fatigue assessment: one that presented the best behaviour, entitled the "best behaviour model" (BBM) and a second one, named the "realistic model" (RM). The difference between them was represented by the considered bond between the prestressing bar and the concrete element. In reality there was no bond between them, but in the case of the FEA model it was observed that if the bond is considered, the capacity is considerably increased, resulting in a behaviour more similar to the ones from the previous researches. Having decided on the models, it was studied how they behave during the analyses and the way of failure.

The next stage comprised the simulation of the fatigue tests. In order for the model to take into account the fatigue damage, the material parameters of the concrete had to be altered, with the main parameter being the compressive strength. A uniform reduction of the material properties was assumed, reduction that was considered at a structural level. For this, a formula that predicted the maximum allowed compressive stress following the cyclic loading was used, this being a function of the number of cycles and the stress or load ratio from an applied range. Subsequently, reductions for the tensile strength and both fracture energies were performed.

A series of analyses that involved a single loading range were carried out, with the results showing an offset from the confidence interval given by the prediction formula from TU Delft. The resulting force from the FEA model was larger than the one estimated by the said formula. It is thought that, apart from the model itself, this behaviour is influenced by the way the reduction in the compressive stress is performed, being too simplistic to consider only the ratio of the loads and not taking into account their values. The same simplicity in interpreting the fatigue behaviour can be assigned also to the formula that predicts the fatigue force based only on the number of cycles and the static force.

For the multiple loading ranges, two different approaches, phased and separate, were used for the analyses, but it is thought that the behaviour of the real tests was not described accurately

and it presented limitations. Regarding the impact of the loading sequence, the results showed no difference in behaviour between a low-to-high and a high-to-low analysis but a conclusive answer cannot be given in this matter. These outcomes might be due to the limitations of the model itself, since it is a simplistic one, but also due to the limited experience of the DIANA user with such type of analyses.

The current research program on fatigue that is being performed at TU Delft began in early December 2016 and has as a stated objective the clarification of the impact that the loading sequence might have on the tested specimen. The structural system for these tests was built during the summer of 2016 and it is already in the testing stage.

Table of Contents

Acknowledgements **7**
Summary **9**
Table of Contents **13**
Chapter 1: Introduction **18**
1.1 Background of the Master's Thesis topic 19
1.2 Aim of the Master's Thesis 21
1.3 Procedure for the development of the FEA model for fatigue 21
1.4 Contents of the thesis 23
Chapter 2: Literature Survey **24**
2.1 Introduction 25
2.2 Fatigue of concrete 25
2.2.1 Fatigue in plain concrete 26
2.2.1.1 Plain concrete in compression 27
2.2.1.2 Plain concrete in tension 28
2.2.1.3 Plain concrete in compression-tension 29
2.2.1.4 Additional aspects concerning plain concrete 30
2.2.2 Fatigue of reinforcing and prestressing steel 32
2.2.2.1 Reinforcing steel 32
2.2.2.2 Prestressing steel 33
2.2.3 Behaviour of reinforced concrete elements 34
2.2.3.1 Bending failure 35
2.2.3.2 Shear failure 35
2.2.3.3 Bond failure 36
2.2.4 Fatigue in bridge deck slabs – recent studies 36
2.3 Compressive membrane action in concrete slabs 43
2.3.1 General 43
2.3.2 Earlier research 44
2.3.3 Theoretical developments 45
2.3.4 Design provisions 46
2.3.5 Recent studies on CMA 47
Chapter 3: Assessment of TU Delft fatigue research program **53**
3.1 Introduction 54
3.2 Experimental program at TU Delft 54
3.2.1 Structural system and test setup 54
3.2.2 Initial static and fatigue loading tests 55
3.2.3 Fatigue and static tests from additional research program 58
3.2.4 Results 62
3.2.5 Conclusions 64

3.3 Studies outside the Netherlands 65
3.3.1 Introduction 65
3.3.2 Research programs and characteristics 65
3.4 Assessment of TU Delft testing program 73
3.4.1 General remarks 73
3.4.2 Comparison of experimental results 75
3.4.3 Conclusions 79
Chapter 4: Finite Element Analysis - Stage I 81
4.1 Introduction 82
4.2 Development of the FEA model 83
4.2.1 Plane Stress model 83
4.2.2 Geometry and support conditions of the model 83
4.2.3 Reinforcing and prestressing steel 85
4.2.4 Element types of the model 86
4.2.4.1 Plane stress elements 86
4.2.4.2 Interface elements 87
4.2.4.3 Reinforcement elements 87
4.2.5 Constitutive (material) models 88
4.2.5.1 Concrete 88
4.2.5.2 Reinforcing steel 92
4.2.5.3 Prestressing steel 93
4.2.5.4 Steel for plates 94
4.2.5.5 Interface 94
4.2.6 Loads acting on the model 95
4.2.7 Mesh properties 95
4.2.8 Features of the performed analyses 96
4.3 Calibration of the FEA model 98
4.3.1 Initial model based on the width from the experimental programs 99
4.3.1.1 Behaviour of the initial model 100
4.3.1.2 Conclusions regarding the initial model 103
4.3.2 Impact of the considered effective width 104
4.3.3 Impact of the degrees of freedom at the supports 105
4.3.4 Impact of the prestressing bar's bond 105
4.3.5 Impact of the Arc-Length Control (ALC) method 107
4.3.6 Impact of the rotation at the supports 107
4.3.7 Impact of the compressive behaviour of concrete 107
4.3.8 Impact of the tensile behaviour of concrete 108
4.3.9 Chosen FEA models 108
4.4 Final models and their behaviour 109
4.4.1 Linear analysis checks 109
4.4.2 Capacity of the models 109
4.4.3 Failure modes 110

4.4.3.1 Best behaviour model (BBM) 110
4.4.3.1.1 Stresses and strains in the reinforcing steel 111
4.4.3.1.2 Stresses and strains in the concrete 112
4.4.3.1.3 Crack width 113
4.4.3.1.4 Deflection at mid-span 114
4.4.3.1.5 Compressive membrane action (CMA) 114
4.4.3.2 Realistic model (RM) 115
4.4.3.2.1 Stresses and strains in the reinforcing steel 115
4.4.3.2.2 Stresses and strains in the concrete 116
4.4.3.2.3 Crack width 116
4.4.3.2.4 Deflection at mid-span 117
4.4.3.2.5 Compressive membrane action (CMA) 117
4.5 Conclusions of FEA – Stage I 118
Chapter 5: Finite Element Analysis - Stage II 119
5.1 Introduction 120
5.2 Changes in material properties 120
5.2.1 Compressive strength and compressive fracture energy of concrete 121
5.2.2 Modulus of elasticity of concrete 122
5.2.3 Tensile strength and tensile fracture energy of concrete 123
5.3 Single cyclic loading range analyses 124
5.3.1 Test BB23_200 125
5.3.2 Test BB24_150 127
5.3.3 Test BB26_165 130
5.3.4 Accuracy of the results 132
5.4 Multiple cyclic loading ranges analyses 133
5.4.1 Performed tests 133
5.4.1.1 Phased analysis approach 134
5.4.1.2 Separate analyses approach 135
5.4.2 Sequence effect 137
5.4.2.1 Palmgren-Miner rule 137
5.4.2.2 Phased analysis approach 138
5.4.2.3 Separate analysis approach 139
5.5 Conclusions of the FEA – Stage II 139
Chapter 6: Future research program 142
Chapter 7: General conclusions 147
Chapter 8: Recommendations 152
Annex 1 154
Annex 2 159
List of Figures 164
List of Graphs 169
List of Tables 170

List of Equations..... 170
References 171

Chapter 1: Introduction

1.1 Background of the Master's Thesis topic

In The Netherlands, 60% of the bridges were built before the mid '70s [22], with around 70 of them having a thin transversely prestressed deck which was cast in situ between the flanges of long precast girders [23]. With the passing of time and with the constant increase of the traffic loads, the question whether these structures have started to degrade or not, arises. Furthermore, considering that these bridges were designed according to the old codes, another question emerges, namely, if these structures are still safe according to the current codes that are used in today's practice.

Figure 1-1 – Dutch road network: e.g. The Ridderkerk interchange (source: Wikipedia)

When referring to bridges, from amongst the phenomena that can have a significant impact on their service life, the fatigue of concrete and the compressive membrane action (CMA) that is characteristic to thin bridge deck slabs can be distinguished. Both of these will be discussed and approached in detail in this Master's Thesis.

Fatigue, the first of these phenomena that is discussed in detail in Chapter 2, can be described as being a mechanism that in time leads to the deterioration of concrete, being caused by stress variations from repetitive loading. It is highly influenced by the stress range, the frequency of loading – which eventually will lead to the number of cycles to failure - and, to a smaller extent, the strength of the concrete. When we talk about concrete structures which are built using reinforced or prestressed concrete, steel also becomes a component that is subjected to fatigue, whether if this is reinforcing or prestressing steel. Within a structure, the stresses that can cause fatigue can be of compressive nature, tensile nature or there can be stress reversals. These can lead, for the elements within the structure, to failure through bending, shear or bond. Therefore, fatigue is a phenomenon with a negative impact, which has to be treated with caution.

The second of these phenomena described in Chapter 2, the compressive membrane action that appears in the slabs, has a positive influence on the structure since it can increase the ultimate capacity of the element and prolong its life. If it is taken into account during the design stage, CMA can lead to substantial economical savings in terms of reinforcement. In order for the arching action to develop, the element has to be restrained by at least two edges,

with the degree of lateral restraint stiffness giving the magnitude of the arching action. Other factors that influence the CMA are the percentage of reinforcement (a high percentage decreases relatively the arching action) and the concrete strength (a higher strength has a positive influence, increasing the CMA). Additionally, if a transverse prestressing of the bridge deck slab is performed, this will result in a positive effect on the CMA and also will lead to a thinner deck.

In the recent past, Delft University of Technology together with Rijkswaterstaat (Dutch Ministry of Infrastructure and Environment) conducted a research program on the compressive membrane action in prestressed concrete deck slabs, with the focus on the behaviour of this structural system under static loading [14]. A small number of fatigue tests were also performed within the said study [15], but a proper investigation on this was not done. The fatigue tests were of compressive nature only and had a constant amplitude (Figure 1-2). Subsequently, the need for studying also the effect of cyclic loading arose and a plan for a research program conducted by the same two organizations had been approved.

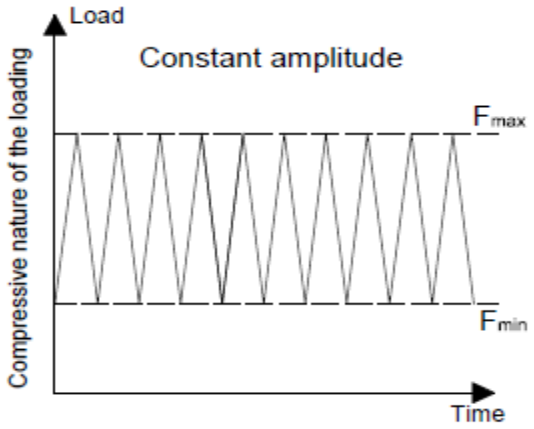

Figure 1-2 - Constant amplitude fatigue loading

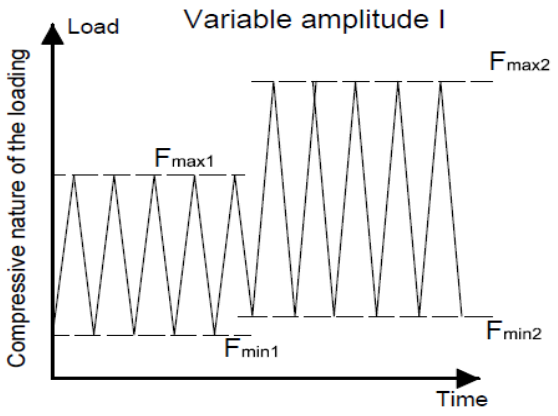

Figure 1-3 - Variable amplitude fatigue loading (I)

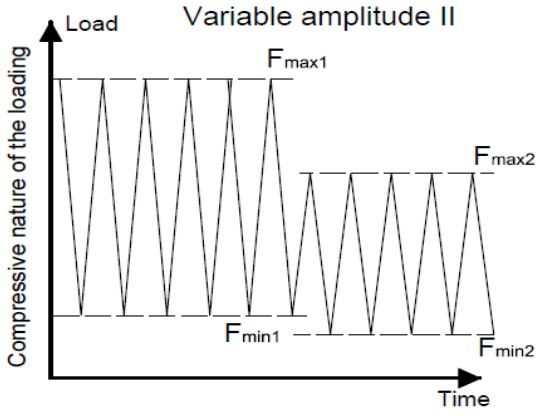

Figure 1-4 - Variable amplitude fatigue loading (II)

Besides the general fatigue problem, an additional consideration for these fatigue tests came from the following circumstances: the bridges/viaducts are designed to sustain a certain

maximum load throughout their service life; nevertheless, a few times each year this maximum load is exceeded, fact that can have serious consequences on the structural integrity of the system. Therefore it would also be of interest to study the impact of such a loading situation on the fatigue resistance, especially the loading's sequence effect and assess which case has a more detrimental impact (Figure 1-3 and Figure 1-4).

1.2 Aim of the Master's Thesis

The main goal of the Master's Thesis is to create a simplified FEA (Finite Element Analysis) model that can simulate the tests from the experimental program performed at Delft University of Technology and can be used for the prediction of the fatigue damage due to a constant amplitude loading range. It will also be tried to assess the behaviour under multiple loading ranges and also the impact of the loading sequence.

The model will be created in such a way that it will reflect as accurate as possible the experimental programs performed in the recent past at TU Delft and their outcomes, although limitations due to the model's simplified nature must be thought of. For its calibration, the results from the static tests will be used. A series of parameters within the model will be studied and varied in order to understand better their influence and the model's behaviour.

A literature survey on the topics of fatigue and compressive membrane action will be performed and presented with the scope of a better understanding of these phenomena and their interaction with the structural system.

Additionally, the author of this report will take part in the construction of the new structural system (bridge at a 1:2 scale) that is being built for the future experimental program that will be performed at TU Delft's Faculty of Civil Engineering and will focus on the fatigue loading of bridge deck slabs, more specifically, on the loading sequence effect.

1.3 Procedure for the development of the FEA model for fatigue

The point of departure for the development of the finite element model is the choice of using a two-dimensional (2D) model in order to replicate the behaviour of a real structure, behaviour that is normally described by a three-dimensional stress state (3D). This is a major assumption and simplification that has a large impact on the structural behaviour, influencing how the stresses develop within the model, how deterioration manifests itself and how the model will eventually fail.

A high number of parameters must be considered when developing the model, these being related to aspects such as the geometry, support conditions, material models, applied loads or characteristics of the performed analyses. All of them influence the FEA model's behaviour to a higher or a lower extent, this being assessed and highlighted within the thesis. Based on these

parameters, a calibration must be performed in order for the model to depict a behaviour that is very similar to the ones from the experimental program and FE analysis of S. Amir [14]. The performed analyses must be of nonlinear nature as these allow the subsequent modification of the model's parameters, specifically the ones related to the materials.

Once an acceptable calibration is reached and the static capacity of the model is determined, the next stage consists of the simulation on the FEA model of the fatigue loading cycles and their subsequent damage upon the real structure. The point of departure for this stage is represented by the assumption that the damage caused by fatigue is taken into account at a structural level, by considering a uniform decrease in the material properties of the concrete. The reduction of these properties is directly dependent on the number of cycles and on the ratio between the minimum and maximum stresses/loads within the loading range.

The assumption of having a uniform general reduction in the material properties at a structural level is a simplification of the actual behaviour of the real structure. In the case of the latter, the alteration of the material properties as a consequence of the cyclic loading does not result in the same effect on the whole structure but in a non-uniform variation of the properties, having a different reduction depending on the point or location within the structure. In fact, the real structure is loaded in bending which results in a linear stress distribution over the thickness of the concrete deck. However, it is assumed that the fatigue behaviour of the concrete deck is similar to that of a centrically loaded cylinder under compression, in which all the concrete fibres area loaded uniformly.

Therefore, it is of interest to assess to what extent the FEA model predicts correctly the structural failure load, as all of the assumptions related to the damage caused by fatigue are implemented at the level of the model's material parameters by reducing their values. The assumptions for this reduction consider a structural behaviour (Figure 1-5) that is similar to a cyclic type of loading in compression (Figure 1-6). They also consider a softening reduction correlated with the same compressive behaviour and they also take into account a reduction of the compressive and tensile fracture energies. All these parameters are connected to each other.

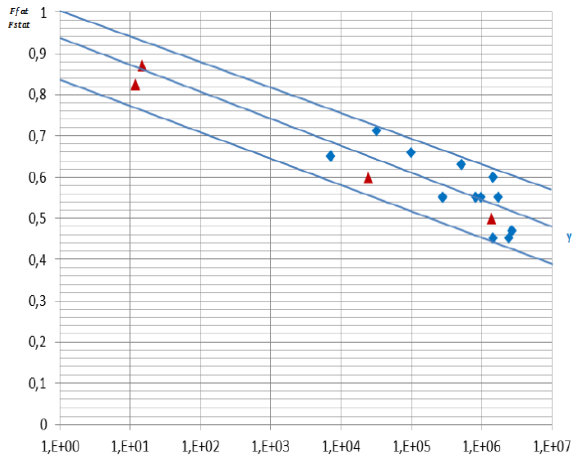

Figure 1-5 – Structural behaviour

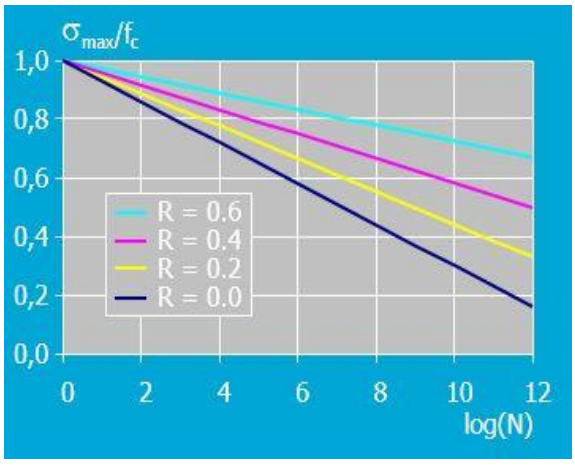

Figure 1-6 – Behaviour due to cyclic loading in compression [29]

Having made these assumptions, the behaviour of the FEA model under the cyclic loading can be assessed using nonlinear analyses, evaluating the outcome of single or multiple loading ranges, with the impact of the loading sequence also being studied.

1.4 Contents of the thesis

The current section will briefly describe the contents of the following chapters of the Master's Thesis.

Chapter 2 will present the literature survey that was performed on the topics of fatigue of concrete and compressive membrane action (CMA) in bridge deck slabs.

Chapter 3 presents the assessment of the fatigue research that was previously performed at Delft University of Technology.

In Chapters 4 and 5, the stages of the numerical analysis are presented. The finite element analysis from stage I deals with the development and calibration of the FEA model. In stage II, the analyses that try to assess the fatigue damage are presented.

The structural system for the following fatigue research experimental program and its construction stages are presented in Chapter 6.

Chapters 7 and 8 present the general conclusions and the recommendations that follow from the used procedure and the results obtained.

In the annexes, additional information will be presented concerning certain parts of the thesis that require clarification or some extra amount of data.

Chapter 2: Literature Survey

2.1 Introduction

The second chapter of the Master's Thesis work presents the literature survey on which the topic of the thesis is based. The choice for this topic was made by assessing its degree of relevance, the academic significance and possibility of accomplishment. It was decided to do a study and research on the fatigue loading of concrete focusing on bridge deck slabs and also on the effect of compressive membrane action that is characteristic to these concrete slabs. The topic of the thesis is a combination of the previously mentioned subjects.

In the following sections, both subjects will be presented, trying to describe in an accurate manner their characteristics, behaviour and influence in the civil engineering field. Reports, bulletins and articles will be used as source of documentation and information.

2.2 Fatigue of concrete

Fatigue can be defined as a deterioration mechanism that acts in time - resulting in the continuous growth of cracks - that is due to stress variations caused by repetitive/cyclic loading, which can eventually cause failure of the element or of the structure [1]. The main parameters that influence fatigue are the magnitude of the stress range, a sufficiently high number of loading cycles, the presence of a stress concentration [1, 2].

When discussing about the topic of fatigue in civil engineering, generally this is related to steel elements or structures. These are more prone to such actions and eventual failures, being mandatory to take fatigue into account since the design stage and perform adequate maintenance and checks throughout the service life, since as early as the second half of the 19th century it was known that metals fracture under frequently repeated stresses that were lower than their ultimate static strength. Wohler came to the conclusion that fatigue strength depends on the range of fluctuating stress and that reversed stresses can cause fracture [2, 3].

In case of concrete structures, fatigue has not proven to be the main reason for structural failure, but in combination with other factors and actions, such as corrosion and fretting fatigue, it can have a major impact on the service life of said structures, even to the extent to which it could lead to its end. Fatigue cracks in concrete are hard to identify since they do not have an easily recognisable surface topography like the ones in steel, therefore increased attention has to be paid during maintenance and inspection. Fatigue can occur in a concrete element when excessive cracking and deflection develops under repeated service loads. Under laboratory conditions, it was proved that concrete elements can fail under fatigue induced deterioration and, additionally, a series of real structural cases were documented by *CEB-Comité européen du beton* (now, FIB - Fédération internationale du béton) in their 1988 Bulletin No. 188 [3].

For assessing the fatigue part of this literature survey, the core of this documentation is comprised of the CEB Bulletin No. 188 ([3]) and Mallett's state of the art review on fatigue of reinforced concrete ([2]). These documents contain major data on the fatigue phenomenon that describe its behaviour and the important aspects that characterize and influence the outcome of fatigue loading on concrete structures.

In the first half of the 20th century, fatigue was not considered a problem for concrete structures. The question whether this had a detrimental effect emerged starting with the 1960's, when different types of steel started being used within the concrete and also the stresses that were acting on the structures gradually increased [2]. In the CEB Bulletin No. 188 a series of cases were presented in which a wide range of deteriorations of concrete structures was assessed, with probable or possible contribution of fatigue. Following this examination, a series of recommendations and conclusions were drawn with respect to the behaviour of the structures, with fatigue being deemed as not having a sole contribution to the deterioration, but most likely only having a contributory part [3, 2].

Two approaches can be used for assessing the fatigue life: fracture mechanics, which takes into account the energy of the loading cycles for crack propagation, or the estimation of cumulative damage, S-N/Palmgren-Miner method, which gives an acceptable probability that failure due to fatigue will not occur before a certain number of loading cycles ($\sum n/N \leq 1$). The second approach is considered to be the classical, more common approach. Fatigue characteristics can be presented using S-N curves and Goodman diagrams [2].

There are two types of fatigue loading cycles that can be distinguished: low-cycle fatigue and high-cycle fatigue. During low-cycle (amplitude) fatigue, the stress levels of the applied load are high and the number of cycles is low (e.g. earthquake). For high-cycle fatigue the stresses are lower and the number of cycles is higher, this situation being more common in practice [3, 4].

In terms of nature of the loading that can cause fatigue, this can be one or a combination of the following: wind and wave loads, loads for highway and railway bridges, loads for crane runways, freezing temperatures, thermal gradients. It must be mentioned that in a high number of cases the load that causes fatigue is considerably influenced by the dynamic response of the system [3].

2.2.1 Fatigue in plain concrete

Concrete is a non-homogeneous material. When talking about fatigue in concrete, this is a process within which the structure of the material continuously changes, with the possibility of appearance of micro-cracks which will propagate and eventually form macro-cracks. These cracks have a direct impact on the remaining fatigue life since they are synonyms with cross-sectional reduction and concentration of stresses. The important features of the fatigue process are the stress/strain changes under cyclic loading and the mechanics of crack growth [2, 3].

There are different methods to compare the development of fatigue damage under cyclic loading as it can be seen in the below graph made by Holmen ('79). The distinguishable methods are: ultrasonic pulse velocity, acoustic emissions, strain development [2, 3].

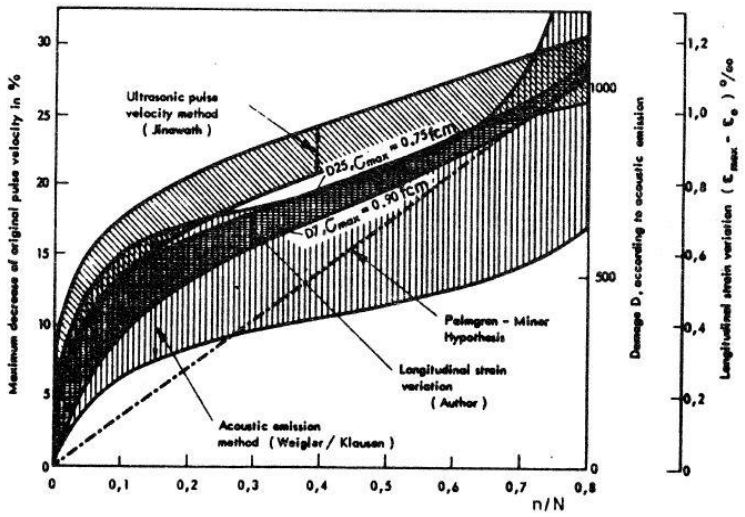

Figure 2-1 - Development of fatigue damage [2, 3]

2.2.1.1 Plain concrete in compression

The fatigue strength of concrete is defined as a fraction of the static strength that can be sustained repeatedly for a certain number of loading cycles. It can be represented by S-N/Wohler curves (stress-fatigue life curves). In common practice, these curves are plotted for a given constant minimum stress or for a constant ratio between the minimum and maximum stresses [2, 3].

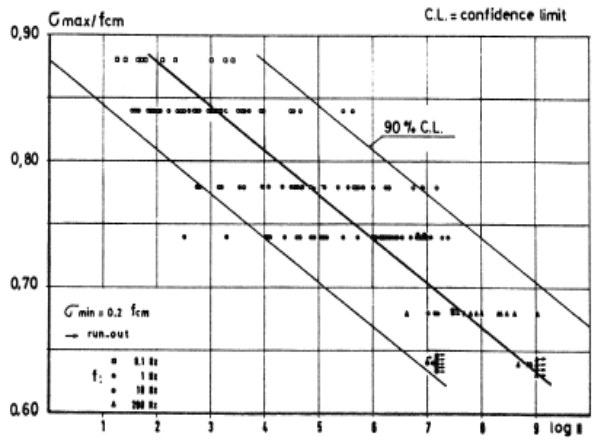

Figure 2-2 - Example of a Wohler diagram (S-N curves) [2, 3]

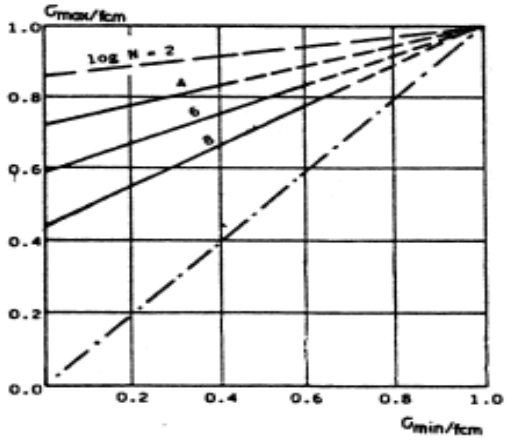

Figure 2-3 - Example of a Goodman diagram [3]

With the use of Goodman diagrams (Figure 2-3) the effect of the fatigue strength depending both on the maximum and minimum stresses in the loading cycle can be assessed. It was observed that the fatigue strength for a given number of cycles increases with the increase of the minimum stress. Unlike steel, there is no fatigue limit for concrete, meaning that there is no known stress below which the fatigue life is infinite and no damage will occur [3].

Studies on the longitudinal strain (the sum of elastic and inelastic strain) of compression fatigue revealed that this has two components, one related to the endurance of the specimen and

one that is time independent and analogous to a creep deformation. The strain has a three stage development: a rapid increase up to 10% of total life, a uniform increase from 10 to 80% and a final rapid increase until failure. The way the strain develops can help assess the remaining fatigue life and the ultimate strain could be a criterion for fatigue failure [2, 3]. Figure 2-4 presents the development of cyclic strain.

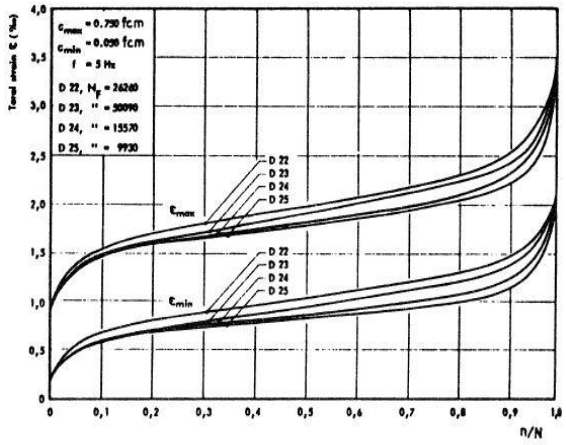

Figure 2-4 - Development of cyclic strain [2, 3]

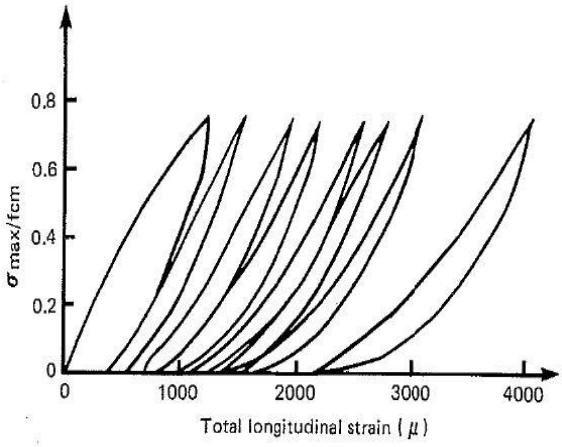

Figure 2-5 - Cyclic stress-strain curve for concrete in compression [2, 3]

Figure 2-5 presents a cyclic stress-strain curve for concrete in compression that varies with the number of cycles. The shape of the line changes from concave, to straight, to convex, with the degree of convexity being an indicator for how close is the concrete to failure. At lower stress levels fatigue failure is not reached and the stress-strain curve appears to remain constant, with no reduction of the secant modulus. The elastic strain increases with the number of repetitions [3].

2.2.1.2 Plain concrete in tension

Assessing the fatigue behaviour of concrete under tensile stresses has an importance for determining the susceptibility of a structure to cracking under repeated loading. Following series of tests, it was observed that if the fatigue stress is expressed in terms of static strength, the obtained results are similar to those obtained from flexural tests. Furthermore, it is claimed that parameters such as moisture conditions, age, mix design etc. have a similar effect on the fatigue strength, irrespective if the load is compressive, tensile or flexural. The stress-strain diagrams have almost linear curves throughout the life time, with the strain increasing after each loading cycle. Overall, the total and residual strain increase, but the elastic one remains almost constant [2, 3].

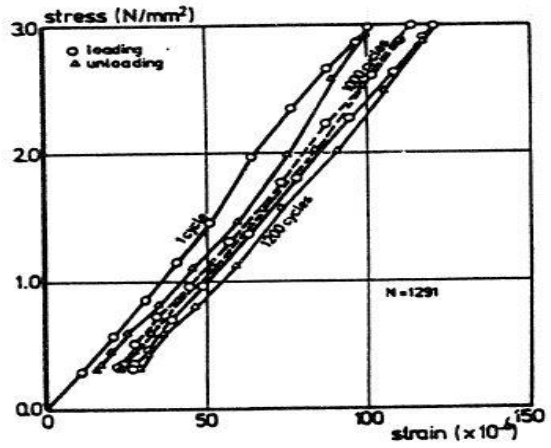

Figure 2-6 – Cyclic stress-strain curve for concrete in tension [3]

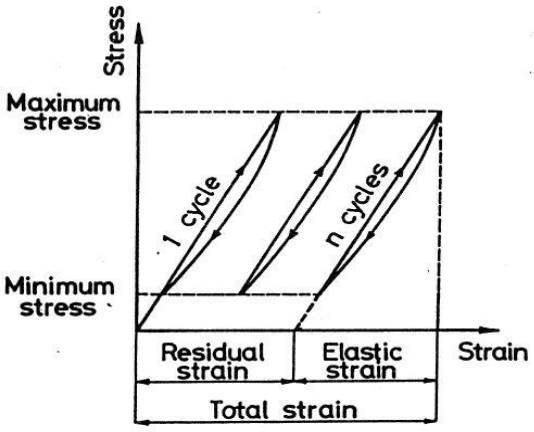

Figure 2-7 – Development of the tensile strain components [3]

2.2.1.3 Plain concrete in compression-tension

The tensile fatigue strength of concrete seems to be affected by stress reversals, with the minimum compressive stress levels reducing the number of cycles to failure considerably. The outcome of a stress reversals with a low minimum stress level – high compressive stress – is that compressive failure is generated. When alternating compressive and tensile stresses, the compressive one has a higher negative effect on the fatigue life than the tensile one [2, 3].

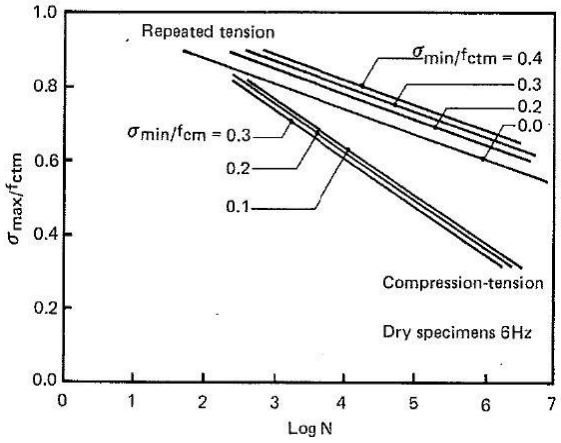

Figure 2-8 - Cyclic stress-strain for reversals [2, 3]

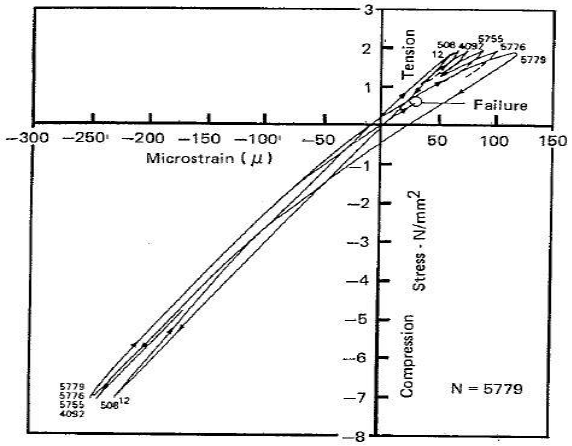

Figure 2-9 – Detrimental effect of stress reversals [2, 3]

During stress reversals, in the early cycles a compressive strain is produced, this remaining almost constant, whilst the tensile strain increases leading to hysteresis and failure (Figure 2-9) [2, 3].

2.2.1.4 Additional aspects concerning plain concrete

- The scatter in tests results and the variability in S-N lines is due to the scatter of the static strength [2, 3]
- The fatigue strength of concrete, if expressed as a fraction of the static strength, is almost the same for compression and tension [2, 3]
- If the fatigue strength is expressed in terms of static strength, parameters such as cement content, water-cement ratio, curing conditions, age of loading, entrained air do not have an influence on the fatigue strength [2, 3]
- Lightweight concrete has a similar fatigue behaviour as regular concrete, with the strength of the aggregates playing an important role. High strength concrete presents a reduced fatigue strength [2, 3]
- The fatigue strength does not seem to be affected by a load frequency between 1 and 15 Hz as long as the maximum stress level is not higher than 75% of the static strength. If the stress levels are higher, the fatigue strength will decrease with decreasing frequency. Fatigue life, in time units, will decrease at increasing cycle rates. Accelerated fatigue tests overestimate the fatigue life under use conditions, especially for high cycle stresses [2, 3]
- Rest periods seem to have a beneficial effect on the fatigue strength, resulting in a higher fatigue life, but it depends on the time between the cycles [2, 3]
- The moisture effect on the fatigue strength is complex and depends on the moisture content. Dry concrete has a better fatigue behaviour than wet concrete, this having a lower number of cycles to failure. An explanation for this behaviour is that dry concrete exhibits lower creep, which influences crack propagation in concrete that undergoes fatigue loading [2, 3]

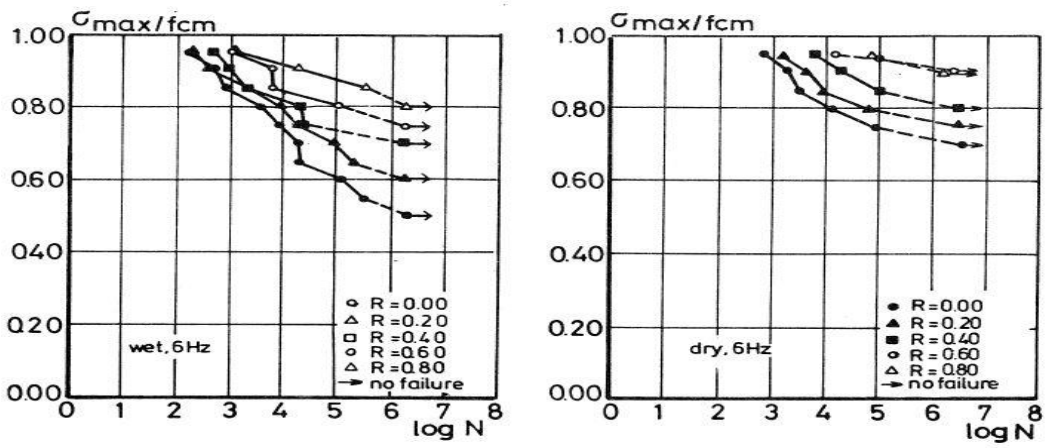

Figure 2-10 - S-N diagrams for wet (left) and dry (right) concrete [2, 3]

- Curing has an influence on the fatigue strength, this being larger for proper cured and aged concrete [2]
- Strength and stiffness are affected by loading and deformation history. Static compressive preloading improves stiffness but cyclic preloading has a negative effect on stiffness and reloading effect, with the worst situation being cyclic tensile preloading [2, 3]
- The prediction of fatigue life based on Miner's rule, including variable amplitude loading, is not sufficiently accurate [2, 3]

- Reliable material models are needed for an accurate computation with the aid of computer software, with respect to fatigue and deformations. In order to describe the relation between stress and strain, the models use the development of cyclic strain and Young's modulus as an input. These give the behaviour for uncracked concrete. In order to describe the behaviour of cracked concrete, the post-peak properties of the material are needed. Following tests, stress-strain diagrams can be obtained for concrete undergoing compression or tension. These models take into account the softening properties of the material which is caused by the formation of micro-cracks [3].

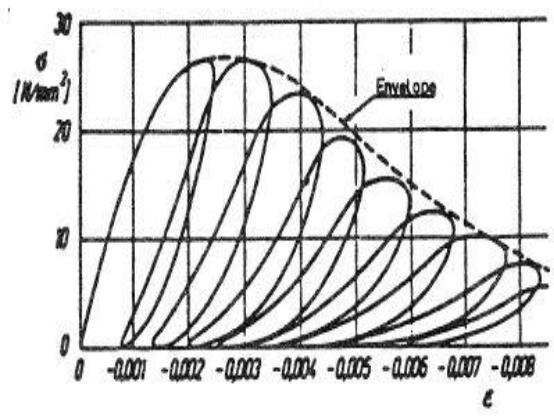

Figure 2-11 - Stress-strain relation with post-peak cycles for concrete in compression [3]

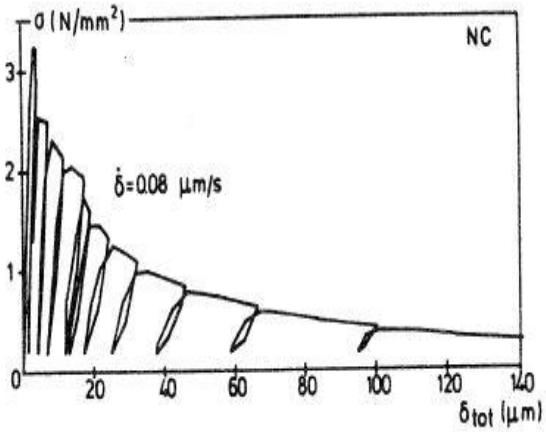

Figure 2-12 - Stress-strain relation with post-peak cycles for concrete in tension [3] (from Reinhardt, Cornelissesn and Hordijk, 1986)

- In his thesis, Hordijk [13] aimed for a better understanding of the causes and mechanisms of the fatigue of concrete and the development of a model based on fracture mechanics. For reaching his goal, he also did an extended research on the tensile behaviour of concrete, since this property of the material was essential for a proper development of the model. Following the tests, he proposed a model for the tension softening curve, this being used in both analytical and finite element model calculations [13].

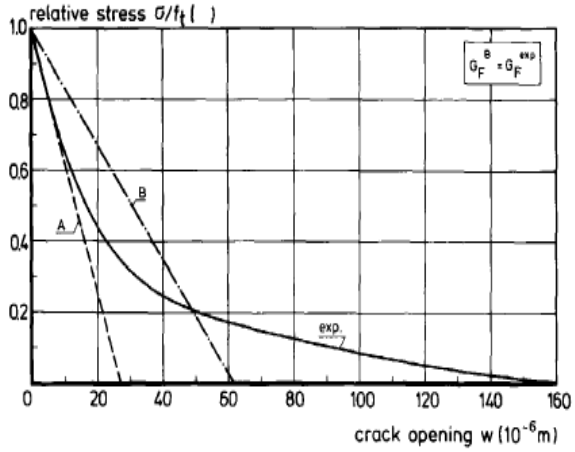

Figure 2-13 - Linear softening relations and an experimentally determined relation [13]

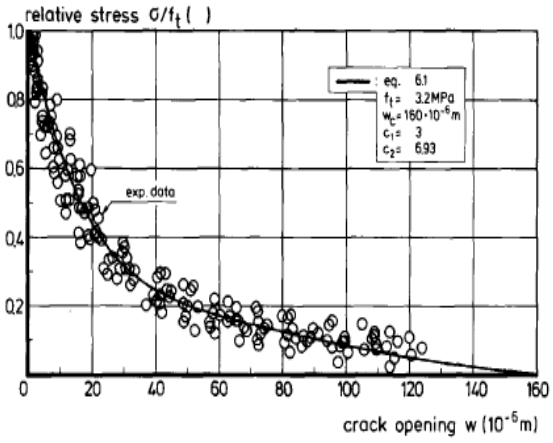

Figure 2-14 - σ-w relations, and data points [13]

2.2.2 Fatigue of reinforcing and prestressing steel

2.2.2.1 Reinforcing steel

There are different types of steel and steel reinforcing bars, each having their own properties. The studied cases mentioned in Bulletin No. 188 that reported fatigue damages undergone by concrete structures, exhibited cracking or spalling of the concrete, with no fatigue damage of the reinforcing bars. Nevertheless, there are situation that require a proper assessment of the fatigue performance of the bars, such as in the case of increased cyclic loading or corrosion of steel due to deterioration of concrete. It can be difficult to assess if the reinforcing bars have failed since there can be no obvious sign except for local cracking of concrete. The fatigue strength of bars is expressed in terms of the stress range and S-N curves [2, 3].

For testing continuous bars there are two methods at use, axial testing in air and bending tests on concrete beams (considered more relevant for service conditions). The disadvantage of the axial test lays in the gripping of the test specimen which can cause local stresses and early failure, whilst the disadvantage for the bending tests consist of usage of low cyclic frequencies in order to avoid heating problems. During axial tests, fatigue cracking is initiated at minor surface defects, whilst for bending tests the fatigue is initiated in the vicinity of the ribs. On average, axial tests exhibit a lower fatigue performance, around 20% lower than bending tests [3].

The ribs on the reinforcement bars were designed to improve the bond with the concrete and for a higher pull-out strength, but they can also cause stress concentrations. There are several factors that can cause premature failure, including intersecting ribs, small radii of the ribs, poorly designed identification markers, fabrication effects [2, 3].

It was found that the fatigue strength decreases with the increase in bar diameter, mainly due to the higher probability of existing manufacturing flaws on the surface of the bars. A similar effect was noticed on the static strength [2, 3].

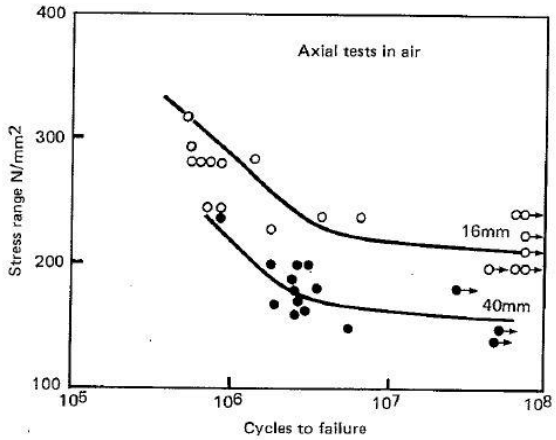

Figure 2-15 - Size effect on bars [2]

In the case of bent bars, it was shown that these have a lower fatigue strength than straight bars. The reduction of strength increases as the bend diameter decreases with respect to the bar diameter. The cause of this reduction is due to cold working and residual and bending stresses [2, 3].

Three types of connections are used for reinforcing bars in concrete: overlapping, mechanical and welded. The straight overlapped bars have a very similar fatigue strength to continuous bars. Mechanical and welded connections reduce fatigue life [2, 3].

Corrosion also has a negative effect on the fatigue strength of reinforcing bars and subsequently reduce the fatigue life of a structure. Local corrosion is more dangerous than general corrosion since it results in deep pits and is harder to detect. This can lead to significant reductions of the cross-section (even up to 50%) and stress concentrations [2, 3].

2.2.2.2 Prestressing steel

Fatigue behaviour of prestressing steel, from the bare steel point of view, is similar to that of reinforcing steel. Concerning prestressing steel, initially it was thought that fatigue is not an issue, since all the concrete members were fully prestressed and no cracking occurred. Since subsequently partial prestressing became used more often and the stress ranges increased, it was required for a better understanding of the fatigue behaviour of prestressing steel. With respect to their type, they can be classified according to their strength, shape and manufacturing process [2, 3].

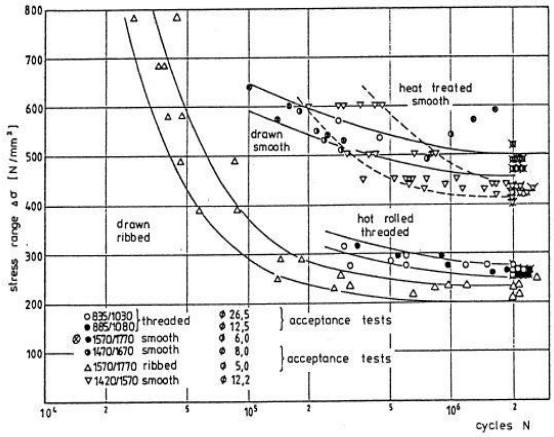

Figure 2-16 - S-N curves for wires and bars [2, 3]

The fatigue performance of steel is considered at a stress range - referred to also as the endurance limit - of constant amplitude for two million cycles, given a maximum stress. The parameters that influence the fatigue behaviour are the stress range, the mean stress (drop in fatigue strength with increasing mean stress), length of the specimen (drop in fatigue strength with increase of the specimen's length) and frequency (lower frequencies lead to lower fatigue strength) [2, 3].

Fretting corrosion has a negative effect on the fatigue strength since it can damage the tendons. Fretting can occur between the wires of a strand, between tendon and the empty duct or between wires and anchorages. Slip and mechanical transverse pressure are the main parameters that influence fretting corrosion. The worst form of corrosion is pitting corrosion and generally, prestressing steel is much more sensitive to corrosion than regular bars [2, 3].

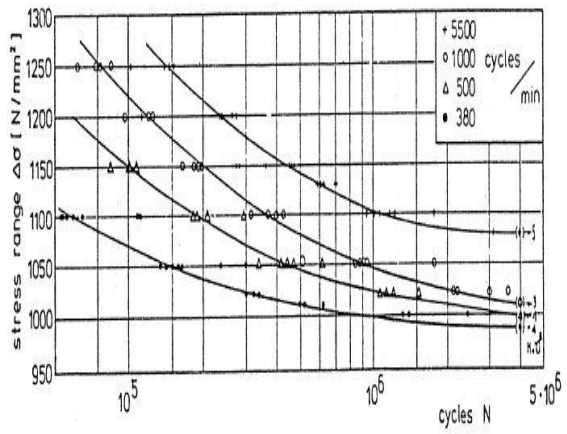

Figure 2-17 - Influence of frequency [2, 3]

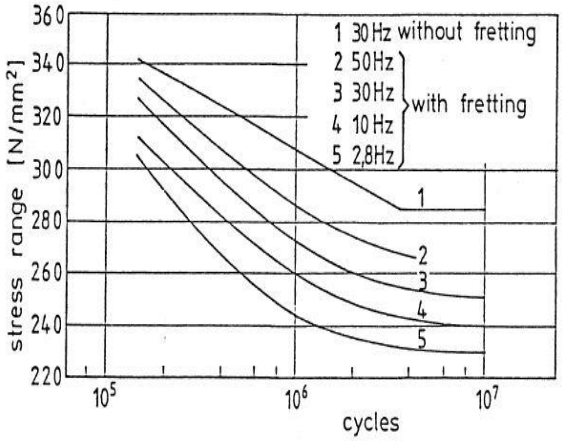

Figure 2-18 – Fretting at different frequencies [2, 3]

Redistribution of stresses can occur in a cracked section that contains both active and passive reinforcement. This is caused by different bond behaviour of both types of reinforcement and it leads to a decrease of stress in the prestressing steel if the regular reinforcing bars have a better bond. On the other hand, the increase of stress in the reinforcing bars can be up to 25% [3].

Additional characteristics that were revealed after considerable testing include:
- Smooth steel has a better behaviour than ribbed steel
- Curved cables in concrete beams have lower fatigue strength than bare cables.
- Steel ducts are worse when compared to plastic ducts
- Tendons in the beam have a considerably lower fatigue strength than tendons in the air, between 40 and 70% lower
- Coupled beams have considerable lower fatigue life than uncoupled beams, due to earlier cracking, fretting and local bending [2, 3].

2.2.3 Behaviour of reinforced concrete elements

A reinforced concrete structure is a composite structure and its fatigue properties are given by the interaction and properties of the composing materials, concrete and steel. The steel's purpose is to carry tensile forces when the concrete cracks, with this happening when the tensile strength is reached in the concrete. The concrete, whilst designed to undergo compression stresses, in the tensile zones it will be subjected to different levels of tensile stresses up to the moment of cracking, when, due to redistribution, the stresses will be taken by the steel. Since fatigue depends on the stress level, the susceptibility of fatigue in the structure will be varied. With the progressing of fatigue and propagation of cracks, there will be

deformations and stress redistribution changes so that fatigue failure could be given by a different mechanism than for static failure. When determining the stresses in the reinforced concrete, simplified models are used. Additionally, taking into account the diversity of materials and loads, it can be observed why there is such a large scatter in fatigue test results [2, 3].

The fatigue properties of an under-reinforced member failing in bending are related to the reinforcement. Heavy reinforced members undergoing bending failures or members where shear or bond are governing have more complicated conditions [2, 3].

2.2.3.1 Bending failure

For this type of failure there can be two situations: failure of the concrete in compression or failure of the tensile reinforcement. In the first situation, compression zone at bending, there is a stress gradient which allows for stress redistribution as the zone with the highest stress starts to deteriorate due to the cyclic loading. It was proved that it is safe to assess the compression zone of beams using uniaxial compression fatigue data. With respect to the fatigue of tensile reinforcement in bending, it was discovered that the relative fatigue strength has a low value. High yield steel reinforcement has only a slightly better fatigue performance compared to mild steel [2, 3].

2.2.3.2 Shear failure

In practice, shear failure is avoided being considered a brittle type of failure. The ductile failure, which is desirable in the ultimate limit state, is about yielding of the reinforcement. However, it was acknowledged that there were situations when similar specimens (beams) failed in shear, when they were exposed to cyclic loading, and bending, when they were exposed to static loading [2, 3].

Beams without shear reinforcement present some specific characteristic that were outlined following series of tests. Their crack pattern is developed after the first few loading cycles, with the critical shear crack appearing after limited crack elongations. The formation of the critical crack, which intersected the bending cracks, lead to the failure of the element. In some cases, the longitudinal moment reinforcement separated from the web concrete, without having a direct impact on the failure of the specimen. At the beginning of the loading cycles, the deflections and the strains increased substantially, but this behaviour got reduced with cycling. After the formation of the critical shear crack, the number of cycles to failure is difficult to predict. Concrete has a similar fatigue behaviour for shear and bending [2, 3].

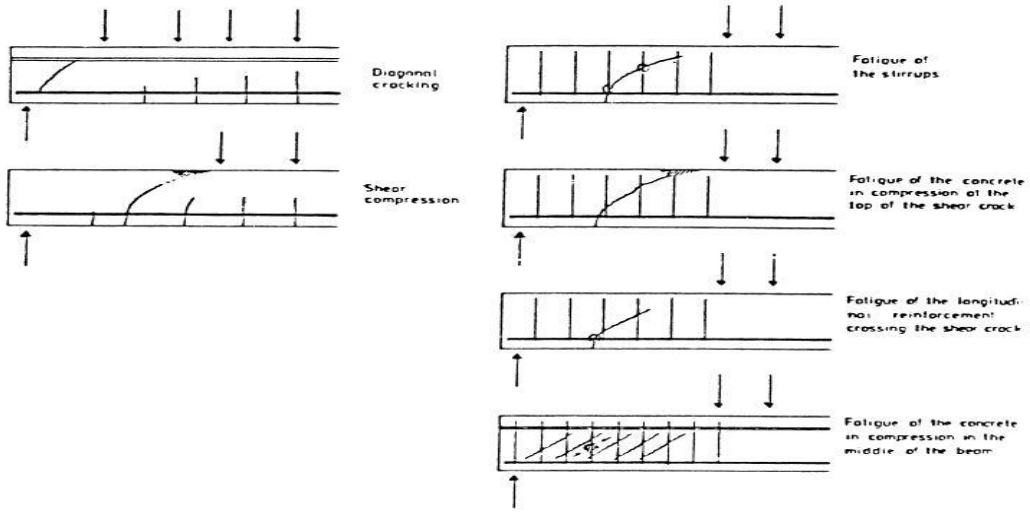

Figure 2-19 - Failure modes for beams without stirrups (left) and with stirrups (right) [2, 3]

The fatigue properties of beams with shear reinforcement are dependent on the properties of the reinforcement. Their behaviour is affected by the stress history of the stirrups, the occurrence of failure at the lower bends of the stirrups and the fact that shear cracks cross the stirrups at skew angles. Size and scale effects influence the fatigue resistance [2, 3]

2.2.3.3 Bond failure

There are several factors that influence the bond, such as the type of reinforcing bar, the geometry of the surrounding concrete, the existence of confinement, load time history, transverse pressure or tension, maximum load level (compared with the ultimate static load). There can be distinguished three types of bond failure:

- failure due to excess of shear strength between the bar and the concrete
- if there is sufficient shear strength between the reinforcing bar and the concrete, the tensile stress will lead to the cracking of the concrete, with the bond force being directed outwards, such that the surrounding concrete may be split away by the pressure of the bar
- if the splitting resistance of the surrounding concrete is high enough, in the situation of a deformed bar, the bond failure will also occur as a shear failure in the concrete along the perimeter of the bar

The reduction of bond strength due to fatigue depends on how the previously mentioned strengths are affected by the cyclic loading. Usually the bond stress is not uniformly distributed along the bond length [2, 3].

2.2.4 Fatigue in bridge deck slabs – recent studies

After CEB's Bulletin No. 188 publication in 1988, which had the purpose of presenting the research previously done and setting guidelines with respect to the fatigue behaviour of concrete and reinforced concrete structures, in the following decades more studies were conducted on this topic since it still represents an important aspect in the field of civil

engineering, where fatigue of concrete can be a mechanism that has a significant impact in the life of a structure.

In this section, a few articles that were based on researches done on fatigue in the past years will be presented, including the description of the tests, parameters and their conclusions. The outcome of these investigations should be rooted in the general knowledge of CEB's no. 188 bulletin, providing a deeper insight of the topic, but also extending the knowledge with better understanding of the phenomenon that is fatigue and the parameters that influence its behaviour.

The first study presented was performed by Carvelli, Pisani & Poggi, 2010 [5] and focused on the fatigue behaviour of concrete bridge deck slabs reinforced with GFRP (Glass Fibre Reinforced Polymer) bars. This type of bars are an alternative to the traditional steel reinforcing bars, mainly due to their extremely good behaviour in terms of corrosion resistance. For the experimental part, four full scale bridge deck specimens were subjected to cyclic loading and their fatigue behaviour was assessed [5].

The reasoning behind the use of GFRP bars, although they have lower mechanical properties, was that the normal steel bars in bridge decks are affected by corrosion due to the use of de-icing salts and temperature variation. Corrosion of the rebars will cause cracking and spalling of the concrete deck, which in the end will affect the durability of the structure and will raise additional costs [5].

The design of the specimens and the loads that were taken into account followed the European codes. The dimensions of the slabs were choses so that they would reflect as accurately as possible structural solutions used on a global scale and the boundary distances were chosen in such a way that the system would mimic a continuous slab [5]. The dimensions of the specimens, amount of reinforcement and the loading setup can be seen in the figure below.

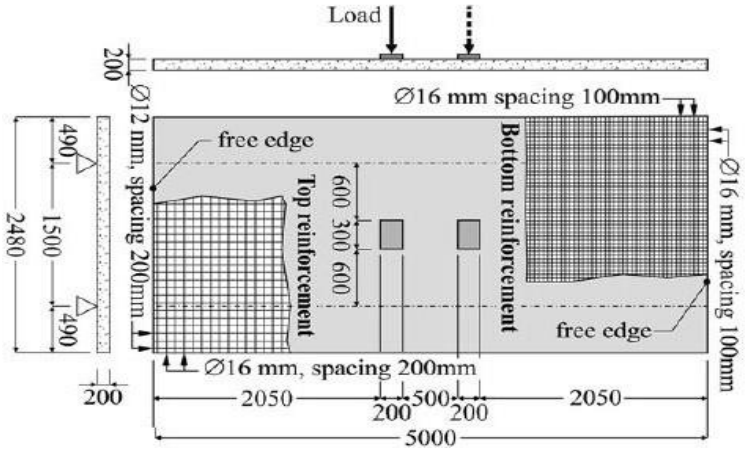

Figure 2-20 - Specimen dimension, reinforcement and loading setup [5]

The stress spectrum produced by the traffic and which is the cause of fatigue depends on multiple parameters such as axle load, vehicle geometry, vehicle spacing etc. Although the European codes specify different load models, the authors of the study decided to increase by

50% the maximum load from the codes and also reduce the wheel contact area. All this was done in order to reduce the number of cycles to failure during the experimental tests [5].

The GFRP bars had a tensile strength 1.5 times higher than regular steel bars, but a modulus of elasticity that was 5 times smaller, the latter being similar to the one from concrete, making the GFRP bars useless in aiding the concrete under compression forces. Combined with a weak resistance to shear stresses, they are not capable in taking punching also. Other aspects concerning this type of rebar is the possible low fatigue endurance and bond under cyclic loading [5].

According to the European codes, the strength verification for concrete under cyclic loading is performed using the Palmgren-Miner rule. Following this procedure, a hypothetical number for cycles to failure was determined. The design punching shear strength of the specimen was also determined following the codes [5].

The setup tried to reproduce closely the actual working situation of a bridge. In order to simulate a simple support boundary condition, the slabs were constrained by two longitudinal beams on two of the sides. The loading was performed by using two hydraulic jacks, with a frequency range varying between 0.2 and 1.25 Hz. The loading was applied in such a way that it mimicked the real wheel load, always having one jack delivering the maximum load, whilst the other one was at its minimum. Two of the slabs were subjected to cyclic plus static loading, one slab only to cyclic loading and the last one only to static loading [5].

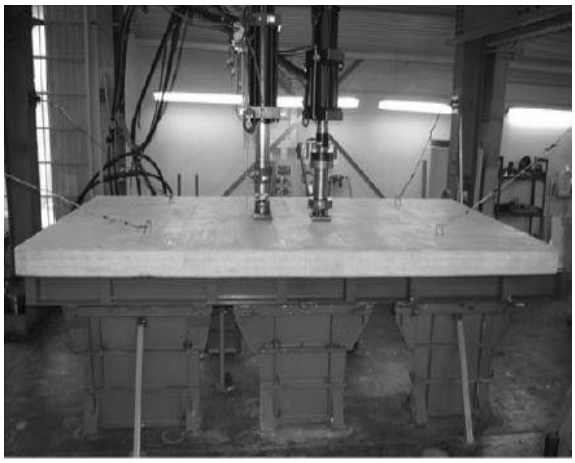

Figure 2-21 - Experimental setup [5]

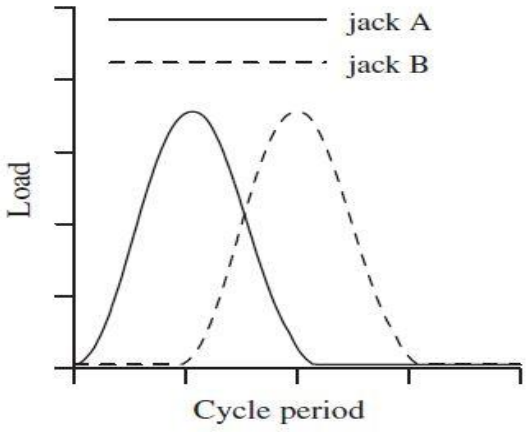

Figure 2-22 - Shape of load variation [5]

The slabs that did not collapse following the cyclic loading (S1 and S2), were subsequently loaded statically up to failure, with a single concentrated load. Tensile tests were performed on the rebars and compressive tests were performed on concrete specimens, all these to determine the properties of the materials. The slabs that underwent cyclic loading, each had a different maximum load within the cycles. The variation of the frequency did not show any influence on the behaviour of slab S1, which had the lowest maximum load. The cracks showed a radial distribution from the contact zone of the load. After 1.5 million cycles the test was stopped since the slab reached a stable response. Slab S3, which was the last specimen subjected

to cyclic loading and had the highest load, failed after a very low number of cycles (≈400). S2 was somewhere in between and S4 was loaded only statically to failure [5].

Slab S1 proved to be stiff enough to resist the loading cycles without major damage and had a very low displacement at the mid-span of the free edges. According to the codes, slab S1 should have failed long before the test was stopped, case similar for slab S2 also. The GFRP rebars showed no signs of debonding even after collapse. The displacement of these slabs increased during the first period of cycle loading, matching the predictions from literature: the strain in the concrete increases until the stability curve is reached. The collapse mechanism in all the static tests was punching, which is characteristic for reinforced concrete bridge decks. The experimental punching shear strength for these specimens was only slightly higher than the one given by the codes [5].

The study concludes that the experimental behaviour of the specimens, under both low and high cyclic loading, is better than the one predicted by the codes. It is believed that GFRP bars are a viable solution for severe environments [5].

In another study performed in Switzerland by M. Schlafli and E. Bruhwiler in 1998, the fatigue of existing reinforced concrete bridge deck slabs was investigated [6]. In the second half of the 20^{th} century, most of the bridges that have been constructed in Switzerland were made out of reinforced concrete. Since this is a material that degrades over time and the traffic loads increase constantly, the necessity of evaluating the performance of these bridges emerged [6].

The bridge decks are the most loaded elements of a bridge, being prone to fatigue. This subsequently may lead to the damage of concrete and the steel rebars. Fatigue damage has been observed mainly during tests since it is hard to distinguish in a real structure, but there are cases where it was determined that fatigue damage occurred. The assessment of fatigue is based initially on codes and assumes a worst case scenario, this leading to a conservative approach, which might be acceptable for new structures but costly for the already existing ones [6].

Examining a certain number of existing bridges, some conclusions were drawn. Amongst these, it was found that normal stress reversals in the longitudinal direction leads to cracking of the slab in the transverse direction; due to positioning of the load, fatigue safety could be insufficient in section that met structural safety requirements and vice-versa; the thickness of the pavement/deck has a big influence on load distribution and stresses [6].

The behaviour of concrete under fatigue loading is described, considering the main relevant situations. Plain concrete under compressive or tensile fatigue loading exhibits a high strain increase during the first cycles. This is followed by a steady, but slow increase of the strain. During the last cycles before failure, again the strain increases rapidly. Throughout the loading cycles, the modulus of elasticity decreases due to the formation of micro-cracks. In both situations, uniaxial compression and tension, the fatigue loading is dominated by the propagation of cracks, with the cement matrix or the interface suffering from micro-cracking. In the case of stress reversals, the concrete is deteriorated rapidly since the micro-cracks have different orientations, following from alternating compressive and tensile stresses [6].

For assessing fatigue there are several models in use: S-N approach, fracture mechanics and damage accumulation [6].

The S-N approach is based on stress S versus number on load cycles N curves. Tests are performed to assess the resistance to fatigue and checks are made to see if the fatigue resistance is larger than the fatigue loading. For steel reinforcement, the important parameter are the stress range, number of load cycles and discontinuities. For concrete, fatigue is defined by a maximum and a minimum stress and their effect over a number of cycles is represented by a Goodman diagram. When stress reversals occur (e.g. due to a moving load), the resistance to fatigue is significantly reduced. Other parameters relevant for fatigue behaviour are the concrete strength and the size factor [6].

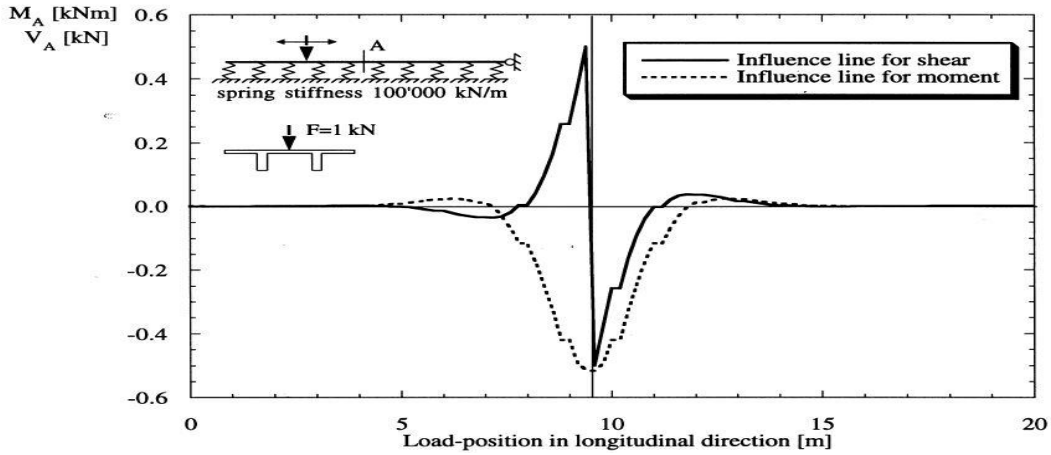

Figure 2-23 - Influence line for a moving load – stress reversal occurrence [6]

Fracture mechanics for steel rebars describe the crack growth as a function of material parameters, crack size geometry and specimen geometry. A linear elastic approach is used in case of steel structures. The development of fatigue is considered to have 3 stages: crack initiation, propagation and unstable crack growth until failure. In the case of concrete, a softening crack is introduce by the means of fracture mechanics, resulting in a decrease in the stress transfer with the increase in crack opening [6].

The third model for evaluating fatigue, damage accumulation, allows the prediction of damage by assessing the varying stresses. The Palmgren-Miner hypothesis is the most common. This is a linear damage accumulation model and describes the sum of the damage from each individual cycle, being based on S-N curves [6].

The research conducted by the authors focused on the remaining fatigue life of existing bridges. Their testing program included beam specimens that resembled slabs, they had no shear reinforcement. The loading on the beams was either static or cyclic (4.5 Hz, sinusoidal load). Only after the maximum fatigue load was increased to more than 60% of the final static load, fatigue damage was observed. The deflection and the strains increased significantly during the first thousand cycles, followed by a period on slow but constant increase. Following the results from the tests, based on which observations were made by the authors, a procedure was proposed to examine existing bridges [6].

A third article published by Hwang et al. [7] dealt with the punching and fatigue behaviour of long-span prestressed concrete deck slabs. Such slabs are used in order to minimize the weight of the deck and to make the structural system more economical. Additionally, prestressing increases the flexural, punching and fatigue strengths but there are questions whether the same formulas from reinforced concrete deck slabs can be applied to the prestressing situation. Static and fatigue tests on long-span prestressed concrete decks were carried out by the authors in order to obtain reliable design formulas for punching and fatigue strength [7].

In order to have a wider and more reliable base for the design formulas of punching shear and fatigue, the authors selected four formulas for punching and one for fatigue. The ones for punching were chosen due to their use in official codes or mechanical considerations, whilst the one for fatigue was chosen because it was the only one that took into account a moving wheel load [7].

For the experimental program 10 one-way slab specimens were produced on a 1:3 scale of a real bridge components, but with identical sectional detail. The level of prestressing was classified into 5 sub-stages (from fully prestressed to none), with the tendons being disposed eccentrically in order to maximize the efficiency of the section. The slabs are connected to the supporting girders by shear connectors, in order to reproduce the real life situation [7].

Since the strength of the specimens decreases with the increasing number of cycles, the accumulated fatigue damage had to be estimated by comparison with the static strength, this being obtained following a static load test. For the fatigue tests, an equipment that simulated the passing of a wheel was used, this being also able to perform static tests. A track made of steel blocks that was placed on the specimens was used as a runway. Due to their setup, the specimens were considered to have fixed and fully supported boundary conditions. During the tests, the strains and the deflections were measured [7].

Figure 2-24 – Static test [7]

Figure 2-25 – Wheel load fatigue test [7]

For the static tests, the specimens that were subjected to punching exhibited different behaviour depending on the concrete strength and level of prestressing. The failure mode was punching shear or a combination with flexure. Prestressing increases the arching action and

seems to influence the failure mode. For the specimen without prestressing, the cracks started at the bottom of the slab, having a mixed failure mode. For the specimens that were prestressed, the cracks had a radial pattern, a trademark for punching shear. In this situation, failure occurred before yielding of the tendon and reinforcing bars in the longitudinal direction. In terms of ultimate strength, all the prediction formulas used gave a lower strength than the one obtained from the test, with an accuracy between 60 and 85%. The formula from the Eurocode is considered to be reasonable for the estimation of punching strength. It appears that the punching strength is proportional to the level of prestressing [7].

The cyclic wheel loading gives more conservative results than the fixed-point cyclic loading. To shorten the testing period, large loads and load increments were chosen. Specimens failed by sudden subsidence at the centre of the slab. The cracks at the bottom resembled the punching cone from the static tests [7].

Figure 2-26 - Failure shape of fatigue test specimen, top [7]

Figure 2-27 - Failure shape of fatigue test specimen, bottom [7]

The specimens that were subjected to high wheel loading values (up to 50% of the predicted static strength) failed after ≈35000 cycles. The short fatigue life is given by the accelerated cyclic loading damage combined with the occurrence of cracks in both longitudinal and transverse directions. The specimens that were fatigue loaded in two stages, underwent a considerably higher number of cycles, especially in the first stage of loading. Cycles of $5x10^5$ and $8x10^5$ were performed without any significant damage to the specimens, having the deflection of the slab and the strains of the bars monitored. The number of cycles which led to failure during the second stage was very low, since the load was increased substantially. At the bottom of the slabs, the transverse cracks progressed to form a grid shape, with a distribution similar to that of the punching cone from the static tests [7].

It is generally accepted that minimum fatigue strength is thought of being achieved if after two million loading cycles there is no observable damage to the specimen. This is done since there are no clear specifications or guidelines for fatigue evaluation. If the prediction of Miner's rule is applied, this will give a much too conservative result. This was observed by comparing the actual deflections of the slabs and strains of the transverse tensile bars, with the theoretical prediction from Miner's method. According to the latter, the specimens should have

failed at a much lower number of cycles, but in reality the damage corresponding to that number (or equivalent no. of cycles at a different load) was very small. A prediction formula is derived by the author by combining Miner's rule with the test result, but provides also conservative results. According to it, the test specimens studied in this paper have sufficient fatigue strength and durability [7].

2.3 Compressive membrane action in concrete slabs

2.3.1 General

The second subject that will be treated in the literature survey of the Master's Thesis refers to the compressive membrane action (CMA) in concrete slabs. A phenomenon that initially was neglected and therefore not considered, CMA was subsequently researched to a higher extent when it was understood the highly beneficial outcome from it.

The design of bridge deck slabs has been based throughout time on the concept of a wheel load distributed over a certain effective width, with the methods that were behind this approach being developed in the first half of the 20th century by Westergaard. This type of design meant that only the bending effects were taken into account, assuming that the shear capacity that would result is adequate. By doing so, the in-plane forces were neglected, although it was known to a certain extent that they might have a significant effect on the behaviour of the slab. The strength of the slab is enhanced if the in-plane forces are of compressive nature [8].

The effect, in the concrete slabs, of in-plane compressive struts (forces), which provide an arch or dome effect, is called "compressive membrane action" (referred to also as "arching action"). This phenomenon is due to the restrained movements of the slab at the supports, with the slab panels having the tendency to act as arches between the supports. This type of behaviour can increase significantly the load capacity of the slab, so that bridge slabs that are designed for bending, will normally fail in punching shear. The actual failure load can be several times higher than the predicted flexural strength [1, 8, 9].

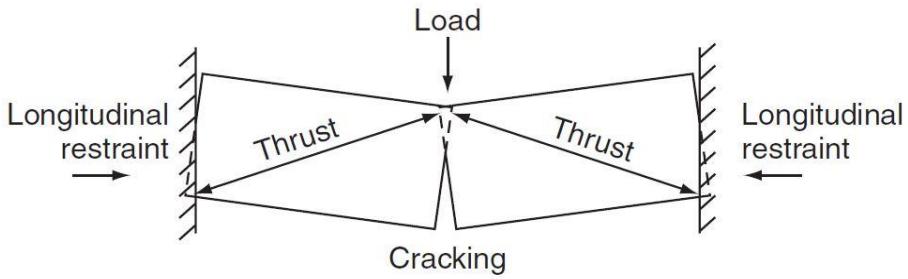

Figure 2-28 - Arching in concrete element [1]

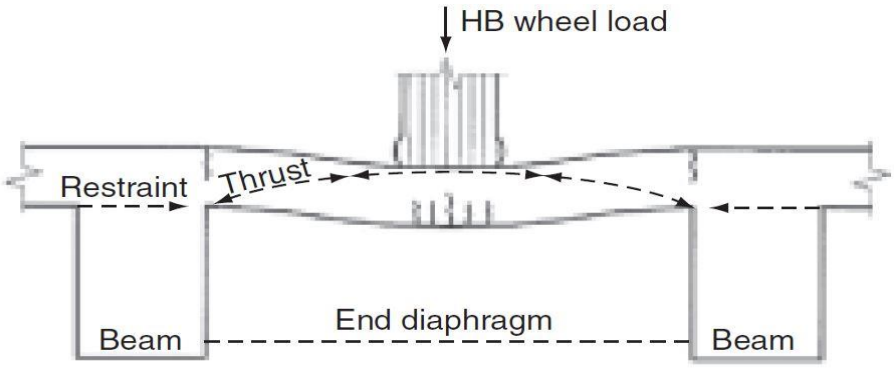

Figure 2-29 - Compressive membrane action in bridge deck [1]

In order for the CMA to be certain that it is initiated, the slabs require restraints along all four boundaries. Depending on the type of slab, these restraints differ. For floor slabs or cellular structures, the adjacent slabs can be considered as restraints or the stiff frame around the slab. In the case of bridge deck slabs, the restraint in the longitudinal direction can be provided by bending stiffness of the abutment walls, whilst for the transverse direction, adjacent areas of the deck can be considered as restraints. Another possibility of development of CMA is between deck beams [1, 9].

Based on studies on CMA started in the late '60s at Queen's University in Canada, where it was discovered that the arching action in bridge deck slabs can be estimated accurately for certain systems, an empirical design method was developed and put in use for assessing most of the bridge slab systems. This method admits the occurrence of CMA and, as a consequence, it results in lower reinforcement percentages [8].

2.3.2 Earlier research

Studies related to the previous mentioned method started in the first half of the 20th century, with shear being one of the main interests. It is a general opinion that bridge deck slabs fail due to punching shear rather than bending (flexural) failure. Although initially it was regarded as a feature of beam behaviour, the arching action was later acknowledged to develop also in relatively thin slabs, with subsequent investigations confirming the existence of the CMA and the effect of edge restraint. A common observation for the studies performed was that slabs fail in punching when are subjected to concentrated loads. The first rational model for punching failure was developed and refined at the beginning of the 1960s [8].

The first reports on CMA emerged in the '50s. It was shown that CMA develops in unreinforced cracked slabs, in a reinforced cracked slab where additionally there is flexural action that resists the load, but CMA is not developed if the material of the slab has the same stress-strain relationship in compression and tension. Maximum CMA occurs at low deflections of the slab, being superimposed on the flexural action. The effect of horizontal restraints on punching strength was also investigated, the obtained results showing a substantial increase (up to 60%) depending on the edge restraints [8].

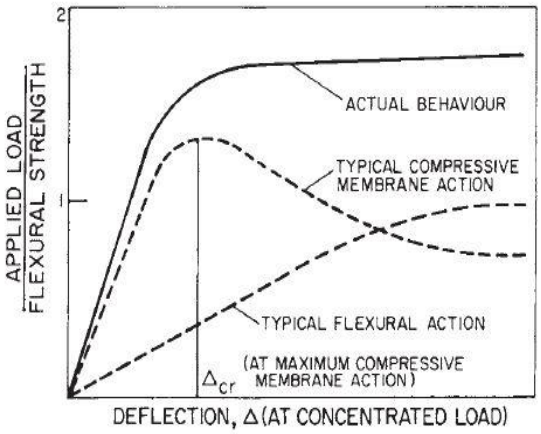

Figure 2-30 - Components of load deflection curve for a partially restrained slab [8]

The investigations on bridge deck slabs acknowledged that compressive membrane action was a direct effect of the restraining against horizontal movements of the edges of the slab panel and this leads to an increase in strength. Punching failure becomes predominant in deck slabs subjected to concentrated loads. Due to the many variables that such a complex problem poses, a universal design approach could not be reached, instead empirical methods were used [8].

2.3.3 Theoretical developments

Investigations at Queen's University in Ontario led to the conclusion that the traditional methods for bridge deck slab design were highly non-economical. Subsequently, a modified version of a previously proposed model was considered accurate enough to predict punching shear strength for typical bridges deck slabs. The said model had incorporated edge restraints due to bending and membrane forces [8].

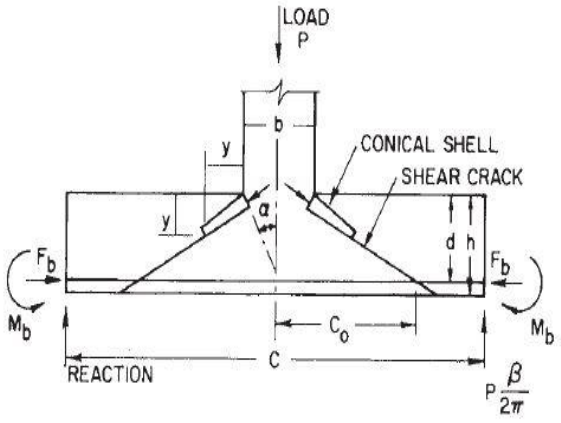

Figure 2-31 - Punching failure model, boundary forces [8]

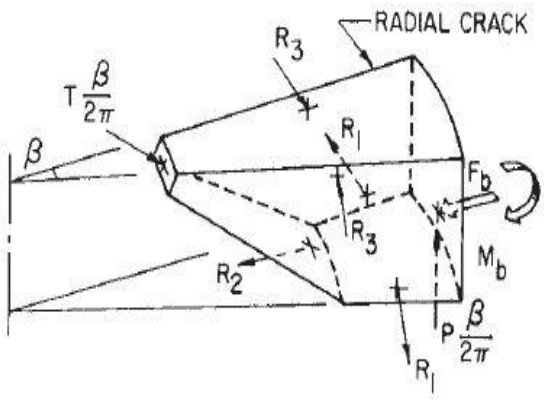

Figure 2-32 - Punching failure model, forces on sector element [8]

The effect on the punching load of the variation of boundary restraints was also studied, having varied the values of the force and moment at the boundary. The model predicts an increase in the punching strength with the increase in the boundary forces. With respect to the model, it was concluded that the predicted results are very good [8].

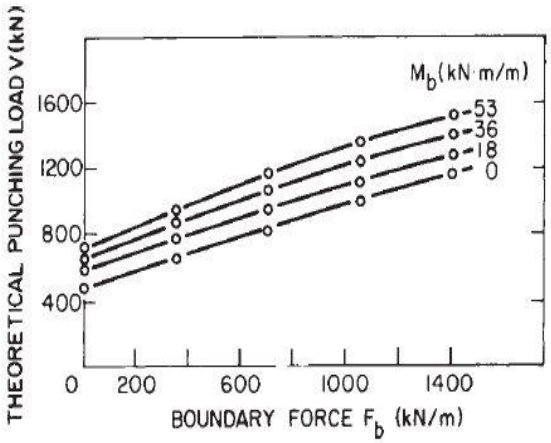

Figure 2-33 - Variation of punching load with boundary forces [8]

Determining the values of the boundary restraining forces for all the situations was impossible, therefore a restraining factor was introduced (η). The extremes would be 0 when considering a simply supported slab and 1 for a fully restrained slab. With the aid of a computer software and using data from previous tests, curves for punching load versus restraint factor were developed [8].

This empirical method was applied and tested on a larger scale with good results, but with additional requirements needed in order to be deemed efficient and safe. Its proper use will lead to a more economical design, having considerable savings in terms of reinforcement, without having the safety compromised [8].

2.3.4 Design provisions

The *Design manual for roads and bridges* [9] provides guidelines that must be considered when designing bridge deck slabs and taking into account the compressive membrane action. The manual defines general principles, the design approach with considerations for serviceability and ultimate limit states, assessments of these analyses and a simplified method for determining the local capacity of the bridge deck slabs.

For the simplified method it is assumed that the slab reinforcement makes no contribution to the local load carrying capacity. This method was first formulated by Kirkpatrick et al. in 1984 when, after series of tests, it was discovered that the CMA provides significant additional strength to such extent that the failure load is almost independent of the amount of transverse reinforcement. The increase in the punching strength due to the CMA is considered by an equivalent percentage reinforcement factor, with the actual reinforcement being neglected. This method is also presented in the *ICE Manual for bridge engineering* [1], but there are some small

differences between the two. The design manual [9] presents also the limitation of this approach [1, 9].

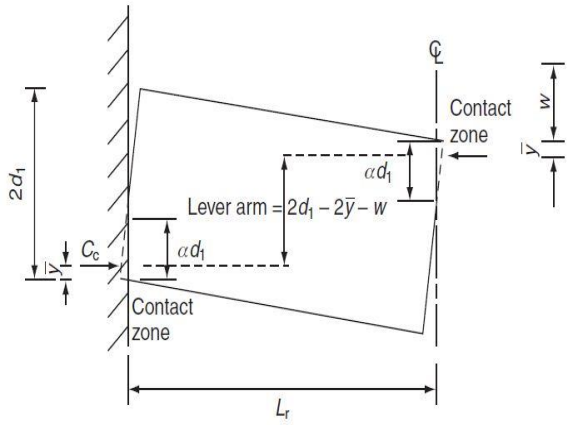

Figure 2-34 - Idealized mode of arching action [1]

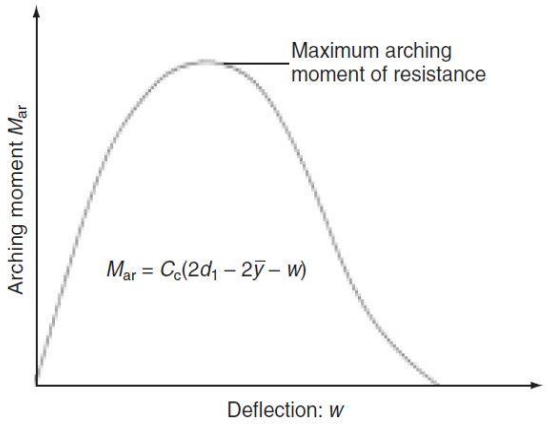

Figure 2-35 - Arching moment of resistance [1]

2.3.5 Recent studies on CMA

A recent study publish in 2015 by Zheng et al. [10] dealt with the influence of CMA on shear behaviour of laterally restrained concrete bridge deck slabs, having the slabs reinforced with GFRP bars. For the experimental program, 17 full-size one way slabs were casted and tested, with the variables consisting of lateral restraint stiffness, reinforcement configuration and concrete strength. Based on these parameters, the effect of the compressive membrane action was analysed. The choice for GFRP rebars was based on durability issues. Reinforcing steel is subjected to corrosion, phenomenon which affects the service life of a bridge. To avoid such an occurrence, glass fibre reinforced polymer is considered an optimum solution since it is more economical than other FRP, more suitable for infrastructure works and already has a service history. GFRP bars have a higher rupture strength but a much lower elastic modulus [10].

It is known that bridge deck slabs can fail in shear (punching or one-way) due to the in-plane restraints and the concentrated or distributed loads of larger magnitude. A compressive membrane action (or arching action) occurs as the slab is deflected due to the restraints provided by the boundary conditions (e.g. beams, diaphragms). The shear capacity of elements reinforced with FRP is smaller compared to a similar member reinforced with steel [10].

During tests, to observe the arching capacity, the lateral restraint stiffness was varied three times and also for one phase of the tests it was removed completely. With respect to concrete, also three types were used during the experimental program. Reinforcement percentages and configurations were also varied and assessed, additionally having besides de GFRP slabs, a slab reinforced with steel [10].

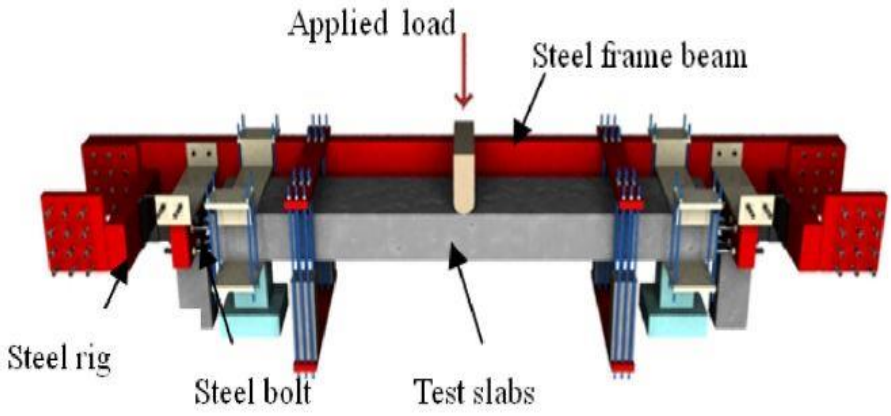

Figure 2-36 - Test slab and lateral restraint configuration [10]

To simulate the horizontal in-plane restraints from actual service life, a steel frame was used. The lateral restraint stiffness is a combination of the axial stiffness of the steel bolt and the bending stiffness of the steel frame. The specimens were tested under three point bending, with a line load applied at mid-span. The specimens were equipped with strain gauges and deflection transducers for data acquisition. Each specimen was incrementally loaded to failure, during which time the deflection, the crack width development, the strains in concrete and bars were measured [10].

Increasing the restraint stiffness resulted in smaller crack widths, effect which was similar with increasing the percentage of reinforcement. The failure mode for the restrained slabs was shear-compression failure, with the concrete being crushed due to the arching action. The slabs that had no lateral restraints failed in bending. The amount of reinforcement and the degree of restraint had a similar effect on controlling the main diagonal crack, which was formed at around 50-60% of the ultimate load. Once the applied load exceeded the flexural crack load, the horizontal deflections were enhanced, this being a sign for the development of the arching action. Increasing the FRP rebar percentage reduces the contribution of the arching action, but also reduces the strain of the bars. The shear strength is increased with the increase of external restraint, meaning that the CMA is enhanced with the increase in restraint stiffness. The load carrying capacity increases also with the increase of the concrete compressive strength [10]

There is a difference between the behaviour of elements reinforced with steel and FRP and this makes it hard to predict their shear behaviour. As a consequence, a number of shear strength prediction models were developed by different researchers, without including the arching action. The authors of the article, [10], compared their test results with results given by some of the prediction models but in most cases these turned out to be too conservative. Their recommendation is that the effect of the arching action should be included in the shear strength prediction methods. This can be done by assuming an increase in the reinforcement percentage, as it was concluded from the experimental part. This approach has already been considered and presented in papers such as [1, 9] and their references. By using this method, the authors obtain accurate results, with a small conservative tendency [10].

Another recent study, part of a doctoral research program at TU Delft, was performed by Amir, van der Veen and Walraven [11] and dealt with the bearing capacity of prestressed concrete deck slabs, the influence of the compressive membrane action being a point of high interest. The tests carried out examined parameters such as the transverse prestressing level, type of loading, geometry of deck and their influence on the punching shear strength [11].

In the Netherlands, old bridges with prestressed decks no longer achieve safety requirements if the shear capacity is determined using current design codes. Since these bridges were designed using flexural theories, their safety poses a big concern, as in the past decades it has been proved that bridge deck slabs are most likely to fail in punching shear. Compressive membrane action is a phenomenon that comes to aid the structural behaviour of such elements by enhancing their overall strength [11].

For the experimental program a scaled model (1:2) of a bridge was built, being designed in such a way that failure would occur in the deck slab. A pallet of lower bound parameters were considered in order to account for the least favourable effects, such as higher centre-to-centre distance between transverse reinforcement or two transverse prestressing levels. The whole system consisted of four precast concrete beams placed in the longitudinal direction, two cast in-situ concrete beams placed in the transverse direction and a cast in situ deck slab, which subsequently was transversely post-tensioned. The loading was of static type, with multiple positions across the area of the deck slab, having either one point load or two point loads [11].

Figure 2-37 - Test setup, laboratory [11]

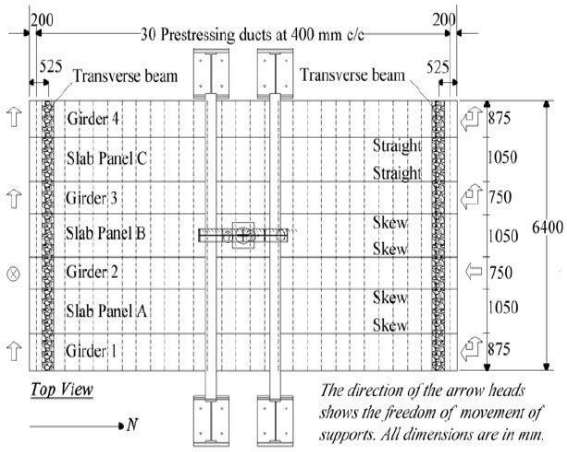

Figure 2-38 - Test setup, scheme [11]

Until the publication of the article, 16 tests have been carried out, most of them between the prestressing ducts, therefore the results can be categorized as low boundary. Except the case when the load was applied at mid-span (failure by flexural punching), for all the other tests the failure mode was brittle punching shear. When the tests were performed above the ducts, an increase in the transverse prestressing level is certain to give a higher bearing capacity, therefore have a positive effect. The cracking pattern at the bottom of the slab, for the brittle punching mode, is in the form of a punching cone, which is the already known pattern for punching shear failure. For the flexural failure mode, although there was a significant increase in the prestressing bars due to rotations at mid-span, failure occurred by punching of one of the loaded

plates. Analysing the data, it was confirmed that a higher level of prestressing in the transverse direction delayed the moment of cracking. Single loads or loads at mid-span presented lower cracking when compared to loads applied close to the support/interface or double loads [11].

The punching capacity of the slabs was predicted using both the European EC2 code and ACI 318 from the US. Both codes underestimate the punching shear capacity as they do not take into account the compressive membrane action. Nevertheless, there are other methods or codes that do take into account the CMA (e.g. UK BD81/02 or the method of Park et al. - 1980). By using Park's et al. method for determining the flexural capacity which considers CMA in reinforced concrete structures, a higher estimate than the actual failure load is obtained, proving that the punching shear is critical. Calculating the punching failure capacity following the UK standard, a lower value is obtained than the ones from the test, most likely since the prestressing effect is not accounted for, the method being developed for reinforced concrete only. In case of the two point loads at mid-span, the flexural capacity is considered to be the sum of the arching moment capacity and the bending moment capacity. A method developed by Taylor et al. (2002) appears to give a good estimation [11].

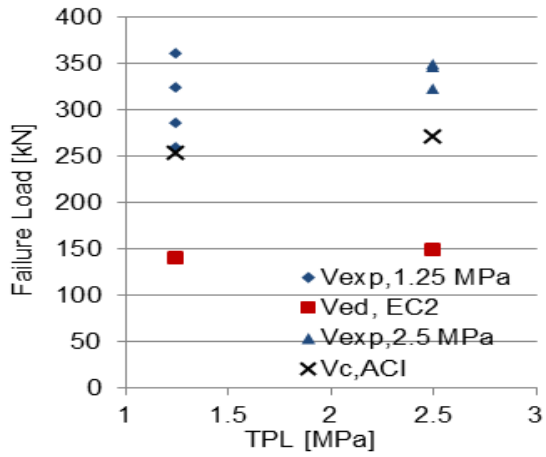

Figure 2-39 - Punching failure load predictions: EC2, ACI [11]

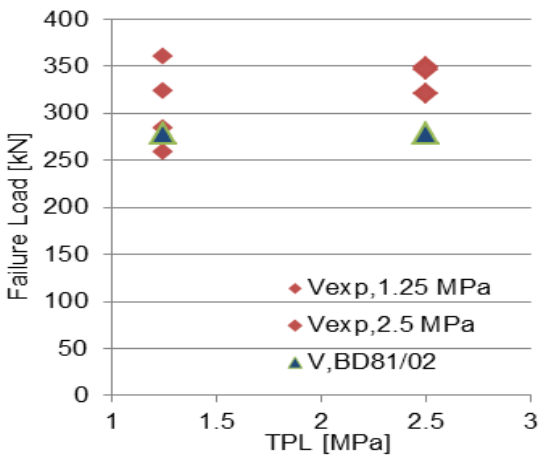

Figure 2-40 - Punching failure load calculated from UK BD81/02 with CMA [11]

At the beginning of the years 2000s, Graddy et al. [12] conducted a research on the punching shear behaviour of bridge decks under fatigue loading, taking also into account the compressive membrane action. The study comprised an experimental and an analytical part. For the experimental part, static and cyclic fatigue tests were performed on the specimens and their behaviour was analysed [12].

It has been studied and confirmed that the arching action improves the overall capacity of the slab, both bending and punching shear. This increase in flexural capacity will make the punching shear to be governing and dictate the design of the bridge. Up to the moment of cracking, the bridge deck will resist traffic loads through transverse flexure. Following the occurrence of cracks, a compressive membrane action develops in the slab, its magnitude depending on the degree of edge restraint. According to the AASHTO standard, the large distance between the axles of a vehicle allows for the CMA to form. A problem emerges in the

situation where there are multiple loads applied simultaneously at a close distance, this leading to a decrease of the arching effect and posing the question whether the slab can sustain such loading scenario. Having this combined with fatigue deterioration will lead to a great concern in bridge design [12].

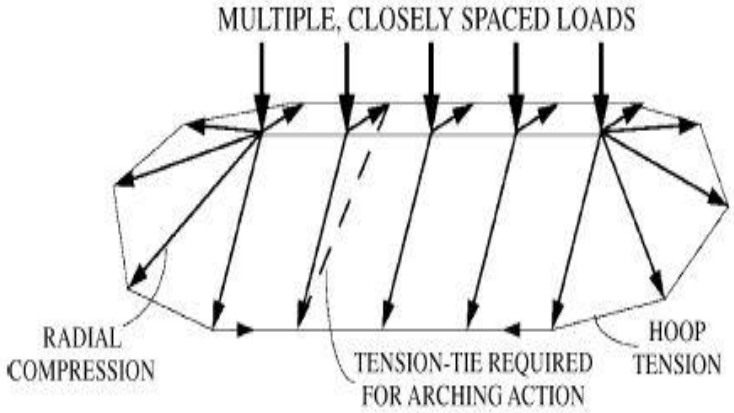

Figure 2-41 - Scheme of reduced effectiveness of arching action due to multiple close loads [12]

The specimens used during the testing procedure simulated the behaviour of parts from a real bridge deck, being designed to fail in punching shear. Some of them were cast on place, whilst others where made of precast and prestressed panels with a cast in-situ topping. The load applied on the specimens was considered to be given by a two wheels tandem. Finite element and analytical models were used for the development and verification of the capacities of the specimens [12].

The punching shear capacities of the slabs were analytically determined using a similar procedure from both AASHTO and ACI codes. For determining the flexural capacity of the specimens in both directions, moment-curvature analyses were used. Based on these capacities an overall flexural capacity was determined using yield-line analysis, but the CMA was not accounted for. The arching effects were subsequently included following finite element analysis but their contribution was small [12].

A steel frame was used for testing the specimens. The value of the minimum cyclic load was around 10% of the cycle's maximum load value. A high percentage of flexural reinforcement was used to avoid flexural failure of the cast-in-place specimens. For the precast specimens it was also made sure that they would not fail in bending. The deflections of the slabs at various locations and the strains of the reinforcing bars were measured. For the pulsating fatigue tests in case of the precast slabs, the dimensions of the footprint were reduced in order to increase the punching shear stress without increasing the load, therefore avoiding bending failure. The fatigue load was sinusoidal, having a frequency between 1 and 4.5 Hz [12].

For the cast-in-place specimens two static tests were performed which ended in punching shear failure. The bending cracks started forming at low values of the force and propagated in both directions. During the pulsating fatigue tests, the majority of flexural cracks formed during

the first loading cycle, propagating into the specimen and towards the supports. Fatigue deterioration was observed as the numbers of cycles increased, presenting wide cracks and considerable loss of material after more than 500000 cycles [12].

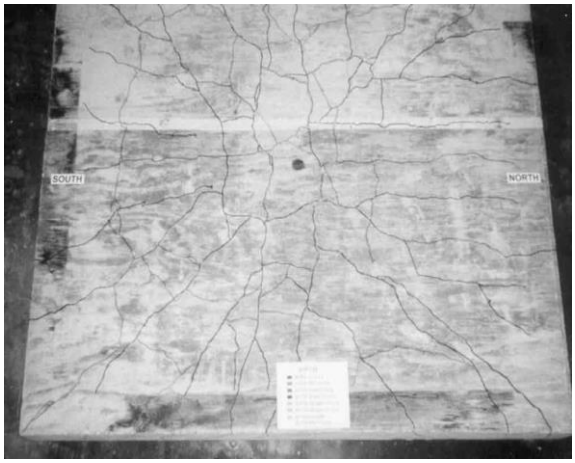

Figure 2-42 - Pattern of cracking on bottom surface of cast-in-place specimens after punching shear fatigue failure [12]

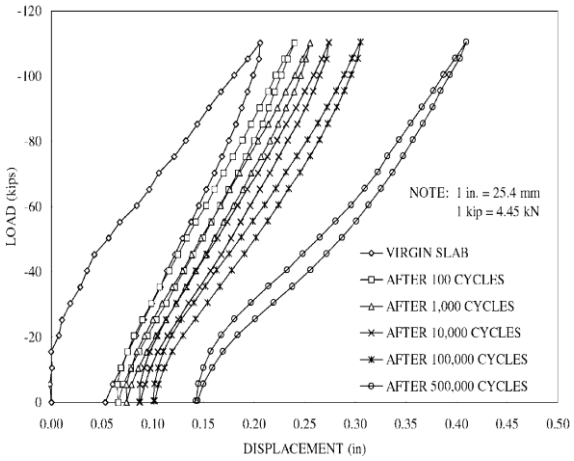

Figure 2-43 - Load-deflection behavior of cast-in-place specimens under fatigue [12]

The precast slabs underwent two static tests, both failing in punching shear but at lower load values than for the other type of slabs. There were also two fatigue tests. Bending cracks formed during the first cycle, but new ones formed as the cycles progressed [12].

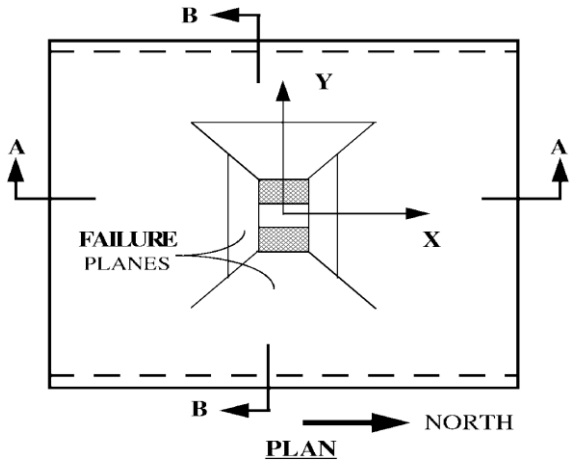

Figure 2-44 - Schematic plan view of combined failure mode for precast specimens [12]

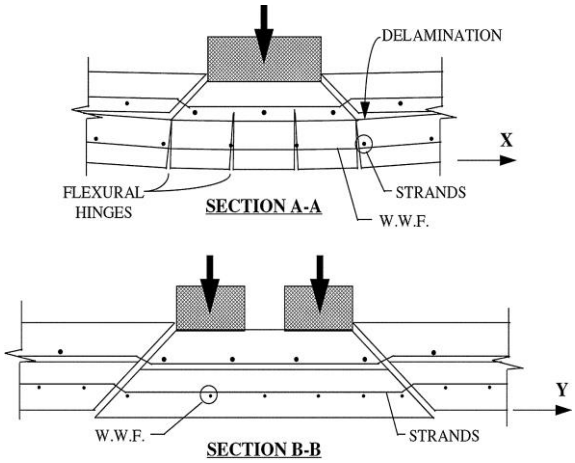

Figure 2-45 - Schematic section view of combined failure mode for precast specimens [12]

Later is was discovered that the specimens that were tested under fatigue failed due to the delamination at the neutral axis caused by high shear stresses. Since the precast specimens failed at values much lower than expected, it was assumed that this is due to a combined failure mode. The influence of the supports was analysed and it was found to be highly responsible for the unusual combined failure mode. The obtained results were also compared to analytical predictions, turning out to be significantly higher than the predictions from AASHTO and ACI codes [12].

Chapter 3: Assessment of TU Delft fatigue research program

3.1 Introduction

As stated previously, the majority of bridges in The Netherlands were built before the mid-1970s. Since then, the traffic has increased significantly and the loads also became larger as time went by, leading to a possible degradation of these structures. Taking all of this into account, it is of concern whether the safety requirements of these bridges are still fulfilled when referred to the present day design codes. To arrive at an answer, a series of studies were or will be performed, with their conclusions hoping to shed some light on this important aspect.

In the recent years, at Delft University of Technology a research study was conducted on the compressive membrane action (CMA) in prestressed concrete deck slabs under static loading, study that was organized together with Rijkwaterstaat, which is part of the Dutch Ministry of Infrastructure and Environment (reference 14). Although the main point of interest in terms of the nature of loading was the static type, a series of fatigue tests were also performed. The outcome of these cyclic tests was presented in the report "*Vermoeiingssterkte voorgespannen tussenstort"* - report number 25.5-14-06 from December 2014 (ref. 15). This report will be a primary source of information for the third chapter of the Master's Thesis and will depict the way fatigue loading was treated during this study at TU Delft. In the following, an overview of the tests will be presented together with the structural system, characteristics of the loading cycles and results. For the second part of this chapter, other testing procedures from different studies will be presented as a comparison and discussed. Based on all of these, an assessment of the procedure utilized at TU Delft will be performed and comments related to its suitability and reliability will be made.

3.2 Experimental program at TU Delft

3.2.1 Structural system and test setup

The structural system used (12 meters x 6.40 meters) for the experimental testing program was a 1:2 scale model of a real life concrete bridge. This was composed of precast, prestressed longitudinal T girders (12 meters in length, with 0.75 meters being the width of the top flange), with a concrete deck cast in-situ between the flanges of the girders. The deck was transversely post-tensioned using bars. Additionally, two transverse cross-beams were casted in-situ at both ends of the structure in order to increase the stiffness of the structural system and deploy the compressive membrane action, resulting in a higher bearing capacity. The cross-beams were also post-tensioned after casting. All the elements of the structural system were properly cured before prestressing. The bars used for prestressing of the deck slab and the cross-beams were not bonded in order to allow for change in the transverse prestressing level. In order to avoid non-uniform stresses, the prestressing followed a certain sequence in terms of prestressing force and order of the bars. The cross-beams were initially prestressed to 1 MPa before the casting and prestressing of the deck, subsequently having their level increased to that of the deck [14, 15].

Figure 3-1 – T girders before casting of the deck and the cross-beams [14]

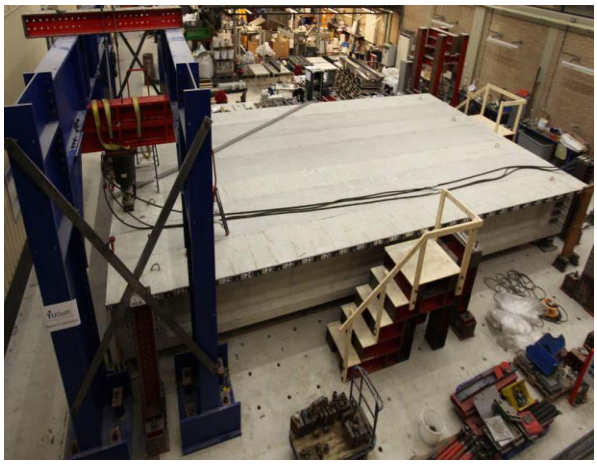

Figure 3-2 – Structural system after casting of the deck and the cross-beams [14]

The tests were performed using an electro-hydraulic actuator system, which, by introducing a concentrated load, simulated an actual wheel load applied to the concrete bridge deck. The actuator was attached to a frame that was bolted to the floor, the whole setup having the ability to be moved from one testing position to another once the test was complete. The loads applied to the concrete bridge deck were either single loads or double loads, these being transmitted from the actuator to the loading plates (steel and rubber, depending on the situation) via an H-profile steel beam. In terms of measurements, a high range of parameters were monitored such as: applied load, mid span and interface deflections, horizontal and vertical displacements, support reactions and prestressing forces, crack pattern [14].

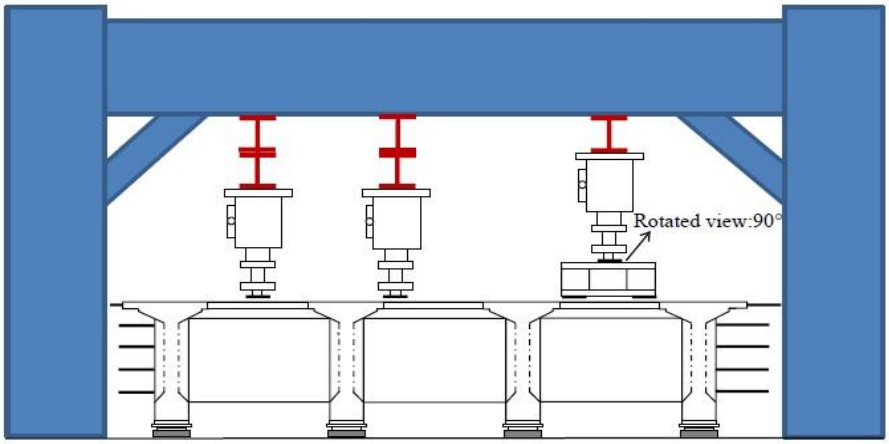

Figure 3-3 – Loading setup scheme: single load and double load [14]

3.2.2 Initial static and fatigue loading tests

On the original structural system from S. Amir's PhD research program (ref. 14), besides the static tests, a couple of fatigue tests were also performed, these being linked to an acoustic emission study, since in the case of the latter, the load was applied in an alternating manner. Additional static loading tests were performed in order to have an order of magnitude for the ultimate capacity of the slab for this extra study [15].

In the case of the static tests, these were conducted by applying a single point load with a load area of 200 mm x 200 mm and an increment of 50 kN. Failure occurred within 45 minutes after the start of the tests, with a mean value for the failure load of 335 kN. This value was higher than the one that resulted from conventional bearing capacity theories since those do not consider the effect of the compressive membrane action [15].

For the two tests involving acoustic emissions, the same load step of 50 kN was applied, similar to the static tests. When the desired load was reached, this was maintained for 10 minutes, with each loading step being repeated three times. Failure occurred after 5 (for test no. 1) and 8 (for test no. 2) hours and at an average load of 283 kN, which was reasonably lower than the value from the static tests. Due to the alternating nature of the load which is similar to a fatigue type of behavior, the strength was reduced by 16%, a value that cannot be neglected [15].

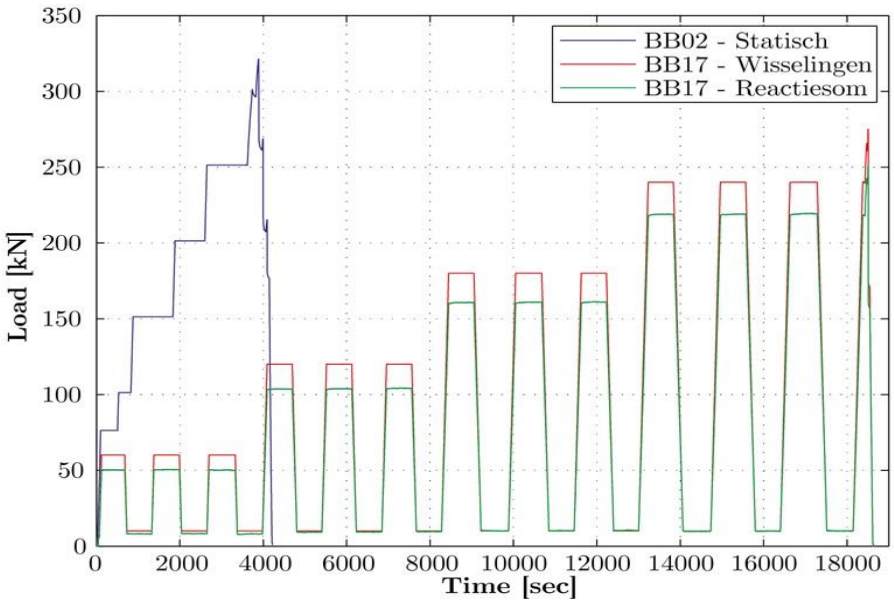

Figure 3-4 – Loading scheme for static (blue line) and alternating loading [15]

As mentioned previously, two fatigue tests were also performed on the original prestressed concrete deck, at a frequency of 1 Hz (1 cycle/sec). These tests were performed on the middle section (strip) of the structural system. The thickness of the slab was 100 mm, having 30 transverse prestressing bars passing through Φ40 mm sheath tubes at a spacing distance of 400 mm, with a transverse prestressing level of 2.5 MPa (compressive stress in the concrete between the girders). The load was transferred to the slab through a steel plate with a thickness of 20 mm and a rubber plate of 10 mm, both having the same in-plane dimensions of 200 x 200 mm^2. The tests simulated a single wheel loading situation, applying only compressive stresses, with the lower limit of the load having a value of 10% of the maximum applied load. For each fatigue test the maximum applied load was different: 200 kN in case of the first tests and 150 kN in case of the second test. The load was applied between the prestressing bars and not directly above one, in order to consider a least favorable situation [15].

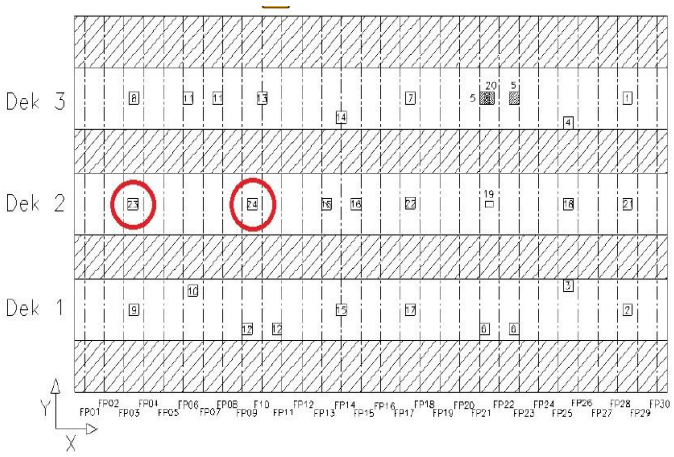

Figure 3-5 – Position of the fatigue tests [15]

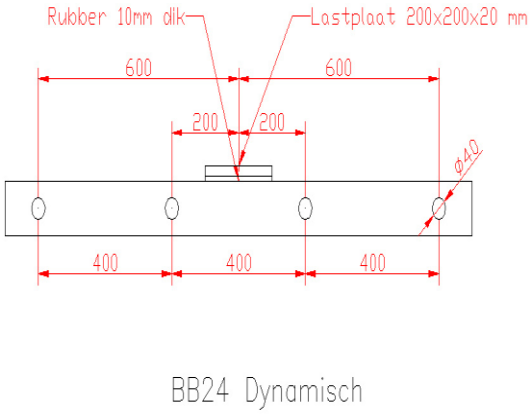

Figure 3-6 – Position of the applied load [15]

The 200 kN maximum load from the first test represented 60% of the average failure load from the static tests. The number of cycles to failure had the low value of approximately 24800 cycles, with a maximum crack width of 0.4 mm after 1000 cycles. The radial cracking pattern increased with the increasing number of cycles. The cracks due to shrinkage that were observed before the tests were not considered to have a negative effect but, on the contrary, it was assumed that this would represent even more the actual service life of such a structure. Following the failure of the slab, large transverse cracks were observed along the tubes that served as sheathing for the prestressing bars. A huge bending crack was also present in the middle area, parallel to the girders [15].

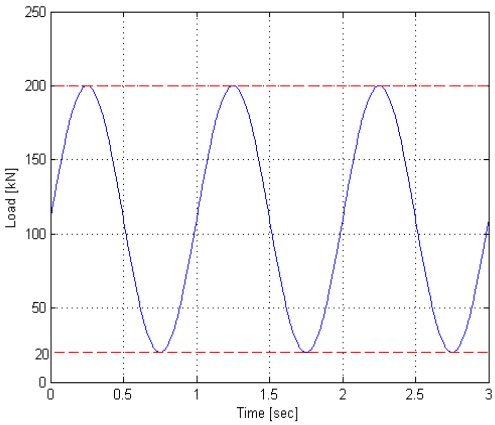

Figure 3-7 – Loading during the first fatigue test [15]

Figure 3-8 – Failure of specimen during the first fatigue test [15]

For the second dynamic test, only the values for the maximum and minimum load had been changed. It was chosen a maximum loading value of 150 kN which represented 45% of the average static strength. The corresponding minimum value was 15 kN, representing 10% of the maximum one. Since the specimen did not fail after 1.5 million cycles, it was decided to continue the test by applying a static load, this eventually leading to failure at a value of 330 kN, a load that was extremely close to the average static strength of 335 kN. Following this result, it seemed that the cyclic loading had almost no impact. In terms of cracking, at 150 kN there was observed an opening of 0.25 mm, this increasing to 0.3 mm after 1000 cycles.

Between 1 and 1.5 million cycles the crack width increased to 0.6 mm. In the end, the crack pattern at failure was similar to the ones from the tests that were of static nature only [15].

Figure 3-9 – Crack pattern at failure, fatigue test no. 2 [15]

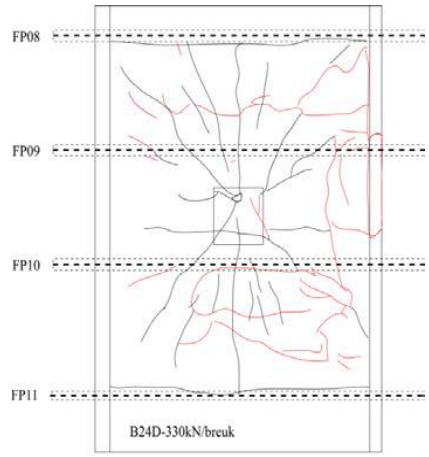

Figure 3-10 – Crack pattern at 330 kN [15]

3.2.3 Fatigue and static tests from additional research program

Following the results from the initial fatigue tests, it was decided to continue the study on this phenomenon with an additional research. In order to do this, the central strip of the original bridge deck that got damaged during the previous tests was replaced, resulting in a brand new structural system in the central area, with a length of 12 m and a width of 1,05 m. The diameter of the casing pipes was changed to 30 mm from 40 mm in the previous tests. At two locations along the slab (A, B, C and D, E, F) dummy tubes are installed with a center to center distance of 300 mm. In these areas there are no prestressing bars but the average level of compression in the concrete between the girders (2.5 MPa) is maintained by prestressing at a higher level the other bars. For the casing tubes that have prestressing bars passing through, their center to center distance remained 400 mm. In total, a number of 3 static tests and 5 dynamic tests (frequency of 1 Hz) were performed, with one test from each category being performed at the locations that lacked prestressing bars [15].

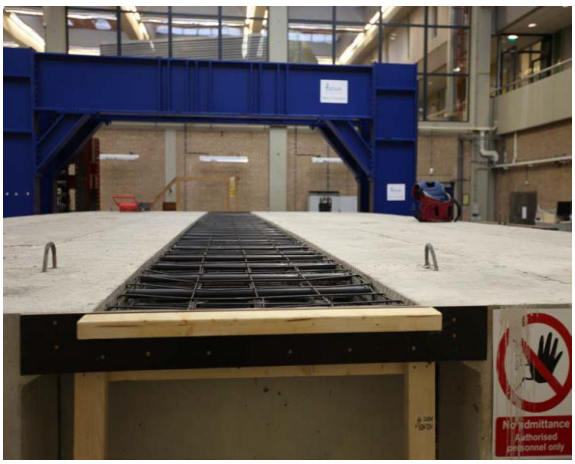

Figure 3-11 - New deck slab before casting [15]

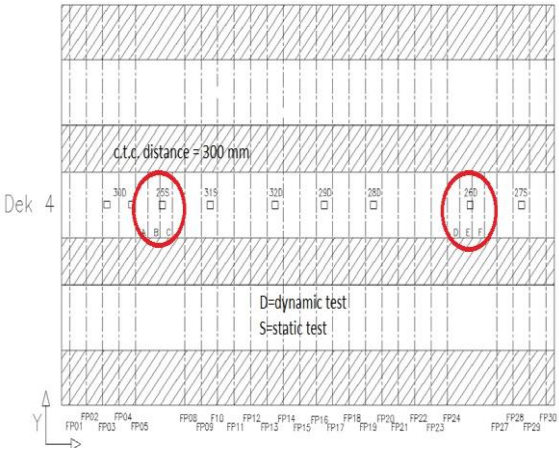

Figure 3-12 – Position of static and dynamic tests [15]

For all of the tests, the size of the steel plates that simulated a scaled wheel print was 115 x 150 mm^2, with a thickness of 20 mm. In 6 out of the 8 tests, a rubber plate of 10 mm thickness was used between the steel loading plate and the concrete slab. Each of the tests performed had at least one parameter that was characteristic to that test alone, resulting in a series of tests that were unique and which covered a wider range of variables [15].

The first static test was performed at one of the locations with dummy tubes (spaced at 300 mm) and had the single point load transferred to the slab by means of the steel plate only, missing the rubber one. The load was applied in increments of 50 kN up to the failure load of 330 kN. The cracks started forming below the loading plate and increased rapidly as the failure load was being reached, forming the characteristic cracking pattern that is known for punching shear. Outside the area of the loading plate, the cracks were considerably smaller in width: 0.25 mm compared to 0.9 mm below the plate [15].

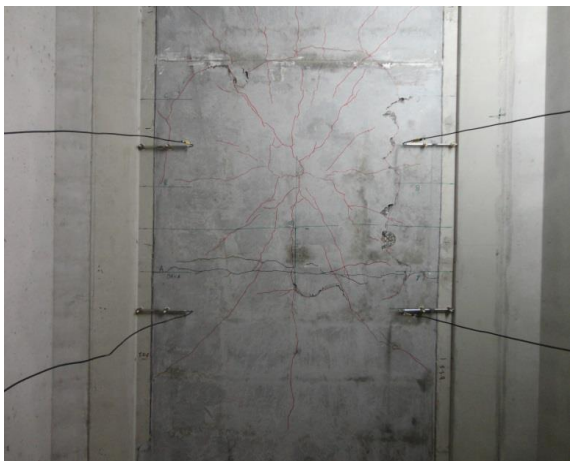

Figure 3-13 - Crack pattern at failure, static test no. 1 [15]

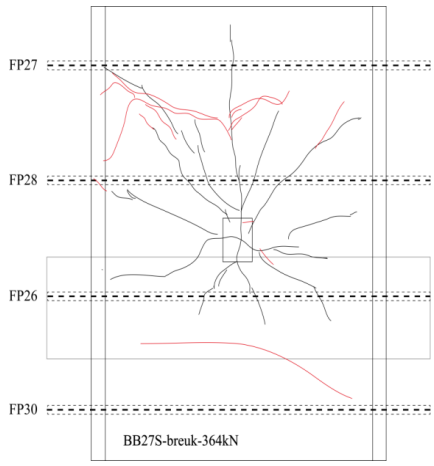

Figure 3-14 - Crack pattern at failure, static test no. 2 [15]

For the second static test, the steel plate and the rubber plate were positioned at mid distance between two prestressing bars (c.t.c. = 400 mm). The load was applied in increments of 50 kN up to the failure of the slab, this having a value of 364 kN. Regarding crack development, same observations can be made as for the first test. A different aspect from the previous test was that failure came gradually under controlled deformation [15].

In case of the third static test, again the plates were positioned at mid distance between two casing pipes that had a center to center distance of 400 mm. Similar to both previous tests, the load was applied in increments of 50 kN until failure, this load having a value of 331 kN. The steel plate had in-plane dimensions of 115 x 150 mm^2. Same observations can be made with respect to the development of the cracks. These could be already measured at 100 kN and had an opening of 0.2 mm. They increased gradually up to 200 kN, subsequently reaching in a short period of time a width of 0.9 mm at failure. The cracking pattern again depicted a punching shear type of failure [15].

The first fatigue test was performed at the other location where dummy tubes were installed with a 300 mm spacing between them. There was no rubber between the loading plate and the concrete. The applied load was of compressive nature only, with a maximum value of 165 kN and a minimum value of 16.5 kN (10% of the maximum). As stated previously, the

frequency was 1 Hz. The specimen failed after more than 1.4 million cycles. The cracks started forming under the loading plate and had an initial width of 0,3 mm, this growing up to 0.45 mm at the moment of failure, with the cracks that formed outside the loading plate area having a much lower width. This observation was made also for the static tests. The failure was considered as being the result of a "push through" action of the jack [15].

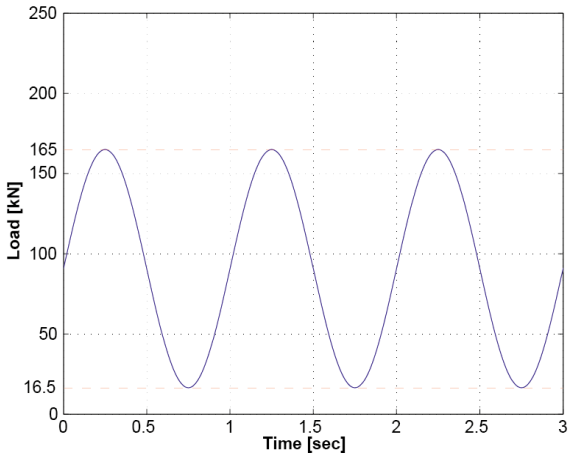

Figure 3-15 – Load values for fatigue test no. 1 [15]

Figure 3-16 – Failure pattern for fatigue test no. 1 [15]

The second fatigue test was located at mid distance between two casing tubes with prestressing bars passing through them (c.t.c. = 400 mm). The loading cycles had three different maximum values: 165 kN, 200 kN and 240 kN. For each of these set of cycles, the minimum value of the load was 10% of the maximum one, at a loading frequency of 1 Hz. For the first set of loading cycles (max. load of 165 kN) there was no failure after 1.5 million cycles, with the range of the crack width below the loading plate spanning from 0.25 mm to 0.4 mm at 1.5 mil. cycles. Outside the loading plate area the cracks were substantially smaller. Since the concrete slab did not fail, it was decided to increase the value of the load within the cycles to 200 kN. Even so, there was no failure up to 1 million cycles. The width of the main cracks increased from 0.4 mm to 0.6 mm. Finally, it was decided to increase the upper loading force even more, to 240 kN. This led to failure after a little over 7000 cycles, with a maximum crack width of 0.8 mm [15].

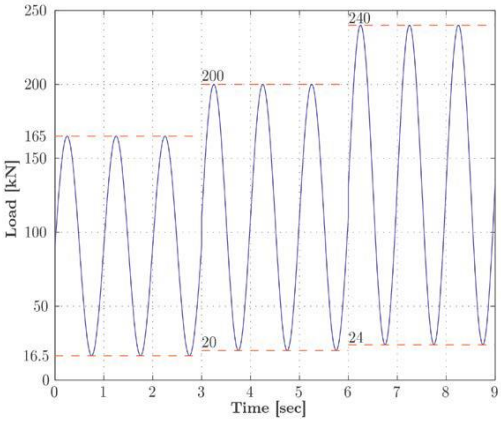

Figure 3-17 – Loading sequence for fatigue test no. 2 [15]

Figure 3-18 – Failure pattern of fatigue test no. 2 [15]

The next dynamic test was located at a similar position as the previous one, at mid distance between two prestressing bars. The loading cycles had two different maximum loads, 200 kN and 220 kN, with the minimum load being 10% of the max. With the maximum load of 200 kN, the specimen did not fail after 1.5 million cycles (1 Hz). The crack width ranged between 0.35 and 0.5 mm. Subsequently, the loads were increased to 220 kN (max) and 22 kN (min), this leading to failure after approx. 265000 cycles. The crack width below the loading plate remained at a constant value of 0.6 mm until failure [15].

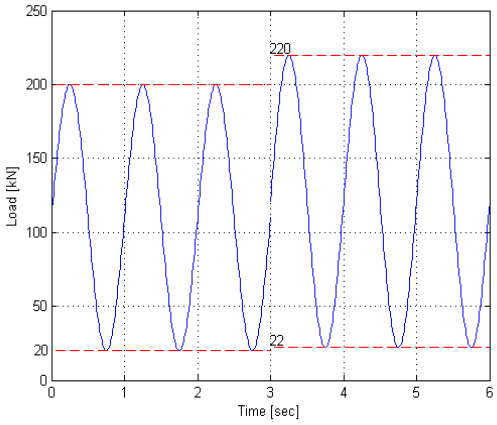

Figure 3-19 - – Loading sequence for fatigue test no. 3 [15]

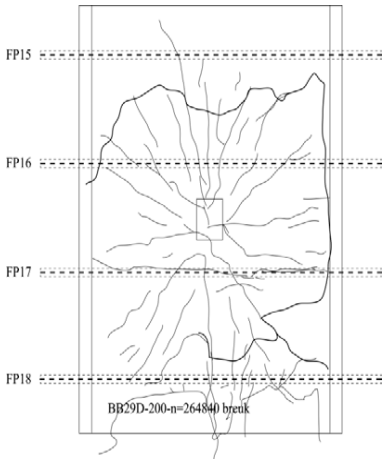

Figure 3-20 – Crack pattern at failure, fatigue test no. 3 [15]

The fourth fatigue test was the only test where a double point load was applied. The two steel plates were positioned at 600 mm center to center distance from one another, having in-plane dimension of 115 x 150 mm^2 and a thickness of 20 mm. between the steel plates and the concrete a rubber plate of 10 mm thickness was applied. The loading sequence was more complex than in the previous tests, having five different maximum loading values: 280 kN, 240 kN, 280 kN, 320 kN and 360 kN. The minimum load was always 10% of the maximum one. For the first loading sequence at a maximum load value of 280 kN, the crack width grew rapidly from 0.35 to 0.7 mm in the first 100000 cycles (1 Hz). Fearing that the specimen would fail, the maximum load was decreased to 240 kN, using this value to reach 1.5 million cycles and a maximum crack width of 0.7 mm. Since no failure occurred, the load was increased again to 280 kN until 2.25 million cycles were reached and a maximum crack width of 1.5 mm. The load was increased for the second time to 320 kN for 500000 cycles and for a final time to 360 kN. Failure eventually occurred after approx. 33000 cycles performed at the last loading value. The maximum crack width had a value of 2 mm [15].

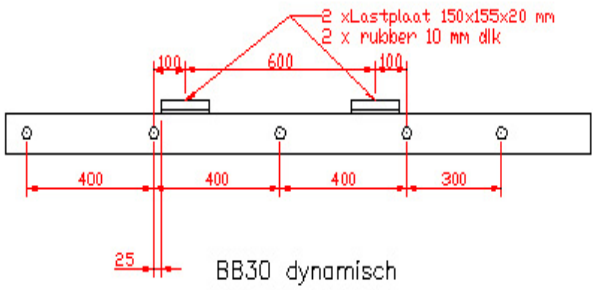

Figure 3-21 – Loading scheme of fatigue test no. 4

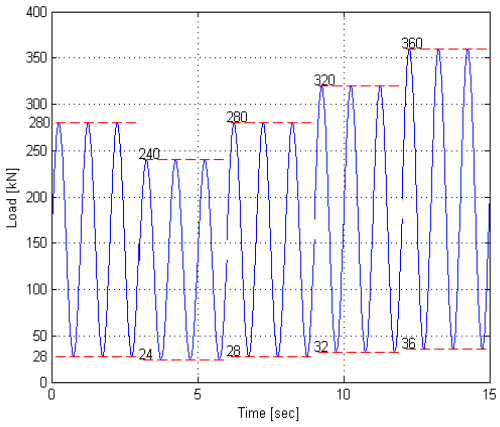

Figure 3-22 – Loading sequence for fatigue test no. 4 [15]

Figure 3-23 – Failure pattern of fatigue test no. 4 [15]

The last fatigue test was located again between two prestressing bars and had a large steel plate of 200 x 200 mm^2 for transferring the load. The main difference from the other tests performed previously is that for the present one the cycles that had a higher maximum value of the load were applied before the ones with a lower load. In the first part of the test, a 240 kN maximum load was applied, with a corresponding min. load of 24 kN. After 100000 cycles the load was decreased to 200 kN since the crack width had a large value (0.7 mm). With the smaller maximum load, failure occurred at approx. 283000 cycles. Following the test, it seems that by applying the loads in this order (max. to min.) the fatigue life of the specimen is considerably reduced [15].

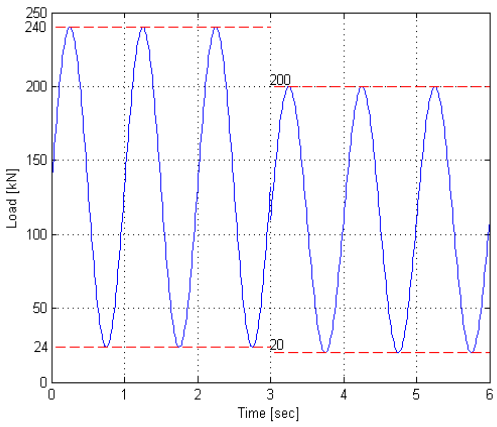

Figure 3-24 - Loading sequence for fatigue test no. 5 [15]

Figure 3-25 - Failure pattern of fatigue test no. 5 [15]

3.2.4 Results

The structural system on which all the test were conducted tried to replicate as close as possible a real life bridge, at a 1:2 scale. In order to predict the failure load at a certain number of cycles, namely the upper limit for the second fatigue test performed during the initial set of experiments, a whole range of results were considered, including the ones from four static tests

previously performed, the ones resulting from the acoustic emissions tests and the ones from the first fatigue test carried out [15].

For the static tests, the average value of the failure load was determined and this was the one used for predicting the failure load after a certain number of cycles. The mean value was 333.5 kN. In case of the acoustic emissions tests, the load was applied in steps that were each repeated 3 times and had the targeted load value being maintained for 10 minutes. For these tests failure came after 5 and 8 hours and had a mean value of the load of 283 kN, corresponding to almost 15 cycles. From the result of the first fatigue test (approx. 21000 cycles at a max. load of 200 kN), an extrapolation was made for 1 million cycles. The result obtained for the maximum value of the load (150 kN) is subsequently used for the second fatigue test. When performing the test, no failure occurred after 1.5 million cycles, therefore the slab was subjected to static loading, with failure occurring at 330 kN. This meant that the fatigue loading had no effect on the final bearing capacity as the slab failed at a value almost identical to the one from the static tests. Furthermore, the failure pattern was similar to the one from the static tests [15].

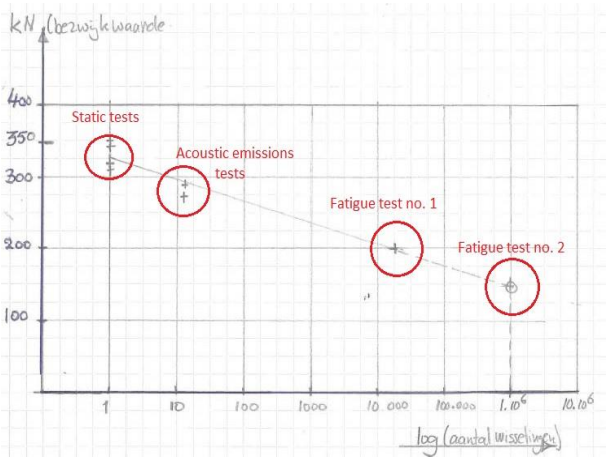

Figure 3-26 – Failure load as a function of the no. of cycles [15]

In the real bridge, the distance between the casing tubes that hold the prestressing bars is up to 800 mm. Based on this value, the 400 mm distance was chosen for the scaled model used for the experimental program. Due to the strange failure pattern along the casing tubes, it is not certain if during a fatigue test, by choosing the maximum distance between the prestressing bars, this results in the lower limit for the element's resistance [15].

The diameter of the tubes was also changed from 40 mm to 30 mm and the distance between them was reduced to 300 mm. These modifications in the structural system seemed to have no impact on the failure load but it must be taken into account that the dimensions of the steel plate was also changed for the second part of the research study on fatigue [15].

Following a conservative approach in analyzing the results of the research, a formula that considers the ratio between the fatigue load and the static load is presented for the second series of tests: $F_{fat}/F_{stat} = 1 - 0{,}0737 \log N$ [15].

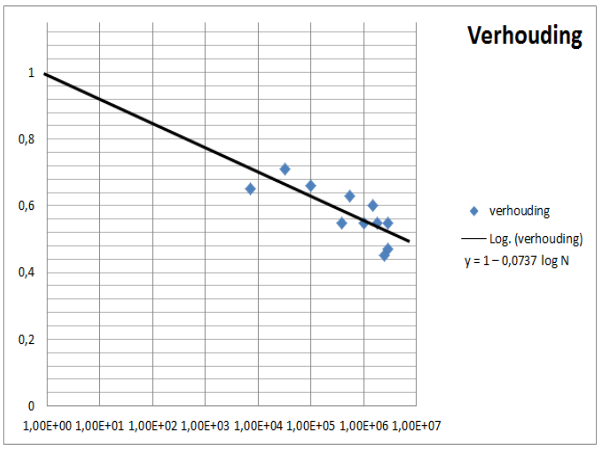

Figure 3-27 - Relative load value F_{fat}/F_{sta} as a function of the no. of loading cycles for the 2nd series of tests [15]

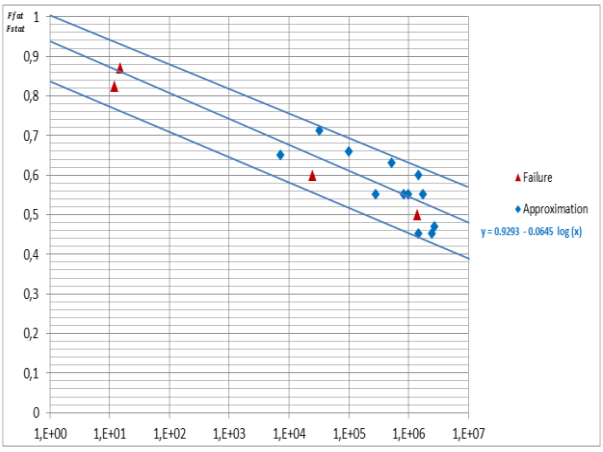

Figure 3-28 - Relative load value F_{fat}/F_{sta} as a function of the no. of loading cycles for all the tests [15]

The previous formula does not take into account the results from the original structural system and the ones from the acoustic emissions tests. When these are also taken into account, the formula becomes: $F_{fat}/F_{stat} = 0.93 – 0.065 \log N$ [15].

The expression given by the previous formula is presented in the upper graph on the right (Figure 3-28) together with the 95% confidence value. It is approximated an average relative fatigue value of 0.54 and 0.41 at 1 and 100 million cycles. At 1 million cycles it can be seen that for the fatigue load a value of 54% of the static load is given. This is a conservative assumption following from a limited number of observations [15].

An important observation regards the outcome from reversing the order of the magnitude of the load during the loading cycles. If initially a higher maximum load is considered for the first loading cycles, followed by loading cycles at a lower maximum load, then the fatigue life seems to be reduced quite considerably [15].

3.2.5 Conclusions

For a single point (wheel) load, a relationship was found between the relative value of the fatigue load and the logarithm of the number of cycles to failure. The relative fatigue load value is given as a ratio between the fatigue load and the static load. The values at 1 million and 100 million cycles are approximated to 0.54 and 0.41. In case of a double wheel load, the same results apply for fatigue loading. In order to obtain the static failure value of the load in this case (double point load), it is sufficient to multiply the static failure value of one single point load by 1.4 [15].

There seems to be no influence due to the different diameter of the casing tube (30 and 40 mm), nor due to the center to center distance between these tubes (300 and 400 mm). In both cases a similar failure load is obtained. This outcome might be the result of using different steel loading plates, smaller in size [15].

3.3 Studies outside the Netherlands

3.3.1 Introduction

In this section, a number of experimental programs from all around the world that dealt with the fatigue of concrete deck slabs will be presented. Already, in the literature survey part of the Master's Thesis, certain scientific articles were detailed and an overview of those studies was performed. Nevertheless, the main ideas that are needed for a comparison with the TU Delft research program will be addressed here again, thus having a more condensed data compendium, with this assuring a cursive flow for the said comparison. In general, for all the studies presented in this chapter, it will be shown the way those studies were conducted, characteristics of the structural systems or elements, the approach towards the testing of the elements, procedures and results. All this will be accounted for in the following.

3.3.2 Research programs and characteristics

In reference no. 12, the study performed by Graddy et al. on the punching shear behavior of bridge decks under fatigue loading was presented. The tested specimens were meant to simulate a real bridge deck at the point of application of the wheel point load, being both precast and prestressed (with a cast in-situ topping) or cast in-situ only [12].

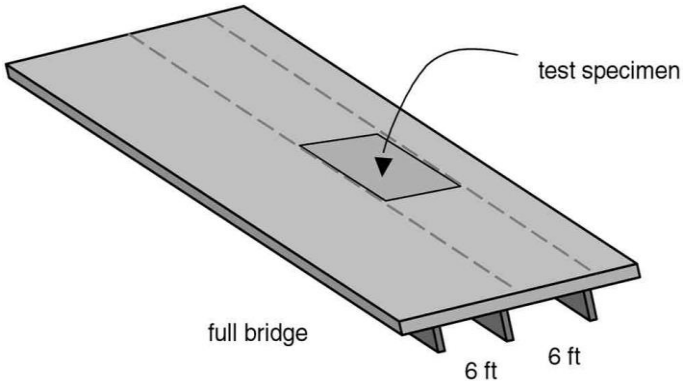

Figure 3-29 – Tested specimens as component of a bridge [12]

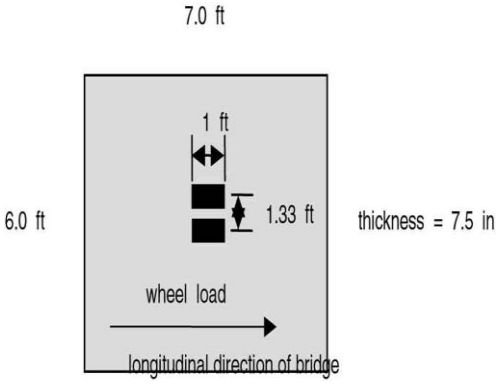

Figure 3-30 – Loading of specimen for analytical studies [12]

For the analytical evaluation of the proposed specimens, the applied load was idealized as a double point load, each footprint having an in-plane dimension of 0.30 (1 ft.) x 0.20 (8 in.) m^2 and a center to center distance of 0,405 m (1,33 ft.). The dimensions of the specimens were ≈1.80 m (6 ft.) x ≈2.10 m (7 ft.). Finite element and analytical models were used for the development and verification of the capacities of the specimens. The calculation, using the analytical model, of the transverse membrane forces of the full bridge and the transverse membrane forces of the proposed test specimen proved to have very similar results, validating the suitability of the proposed specimens for testing. The punching shear capacities were determined from AASHTO and ACI codes, following a similar procedure and also from the general punching shear model (Tsui, Burns, Klingner) [12].

The testing of the specimens was performed using a steel frame, ensuring that the bearing of the slabs on the frame was uniform. For the cyclic tests, a sinusoidal load was applied whose minimum value was approximately 10% of the maximum one with a frequency between 1 and 4.5 Hz. The cast in-situ specimens were 1.83 m (6 ft.) by 2.13 (7 ft.) with a thickness of 191 mm and had a high amount of flexural reinforcement in order to prevent bending failure. The precast and prestressed specimens were composed out of a precast prestressed panel and a cast in-situ topping that had regular reinforcement. The dimensions of these specimens were 2.44 m (8 ft.) by 2.13 (7 ft.) with a thickness of approx. 185 mm [12].

Figure 3-31 – Test setup [12]

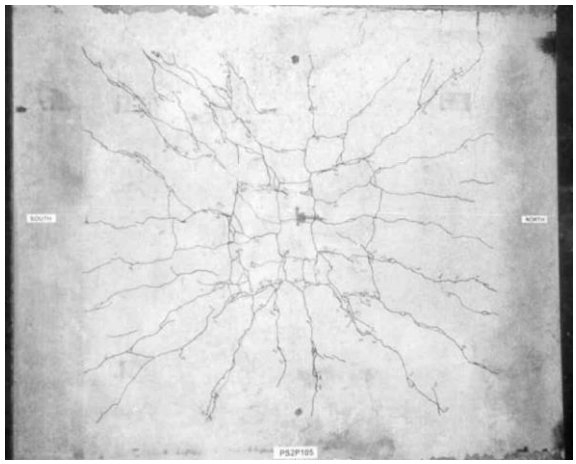

Figure 3-32 – Crack pattern at failure for precast specimens [12]

The loading of the specimens was performed using a hydraulic ram. In case of the static and cyclic tests for the cast in-situ specimens, each footprint from the pair of loading plates had an area of 356 x 610 mm^2. For the precast specimens this area was reduced to 445 x 254 mm^2 in order to increase the punching shear stresses. During the fatigue tests, strains, loads and deflections were recorded after the first cycle and, subsequently, after a predefined number of cycles until failure occurred [12].

Two static tests were performed for the cast in-situ specimens, both ending in punching shear failure. Bending cracks started forming at low values of the force and propagated in both directions. During the pulsating fatigue tests, the majority of flexural cracks formed during the first loading cycle, propagating into the specimen and towards the supports. Fatigue deterioration was observed with the increase in the number of cycles, presenting wide cracks and considerable loss of material after more than 500000 cycles. Two static tests were also performed on the precast specimens, in both cases failure occurring due to punching shear, with the failure load being smaller than the one for the cast in-situ specimens. The number of fatigue tests was also two, with many flexural cracks forming during the first loading cycle [12].

The specimens that were subjected to static loading failed in punching shear whilst the ones that were subjected to cyclic loading failed by delamination of the neutral axis. For the precast specimens, the failure load was smaller than the one predicted, most likely due to a combined failure mode. The support conditions used to increase the bending capacity had a contribution to the mode of failure. The predicted punching shear capacities were modified to take into account the failures of the precast specimens by including only the areas for which it

was certain that punching failure occurred. The nominal punching shear stresses at failure were normalized and plotted against the no. of cycles to failure. The arching action appeared to only slightly increase the capacity of simply supported slabs [12].

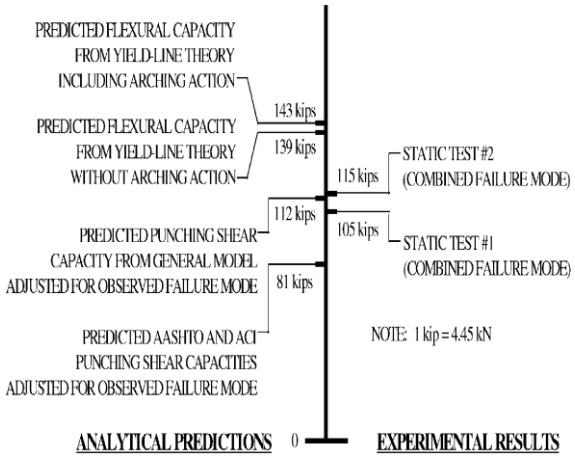

Figure 3-33 – Predicted and observed results for precast specimens [12]

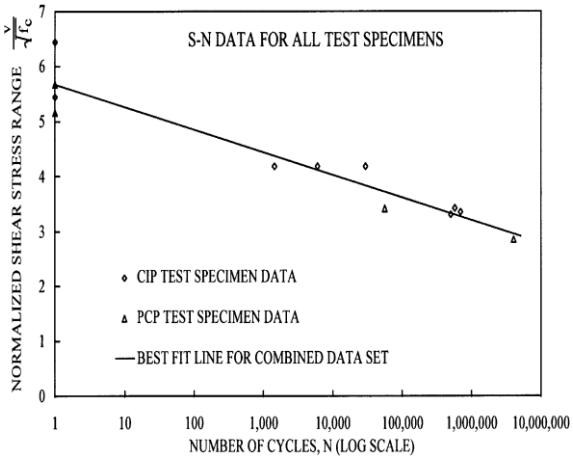

Figure 3-34 – S-N diagram for all specimens [12]

Reference number 5 detailed a research program that involved the fatigue behavior of bridge deck slabs reinforced with GFRP bars. For the experimental part, the tested specimens simulated an actual bridge deck slab, having real scale dimensions: 5000 x 2480 x 200 mm^3. The adopted wheel load had a 50% increase compared to the maximum one from the codes, having a value of 140 kN, with the contact area of the wheel being reduced to 200 x 300 mm^2. These values were adopted in order to reduce the number of cycles to failure [5].

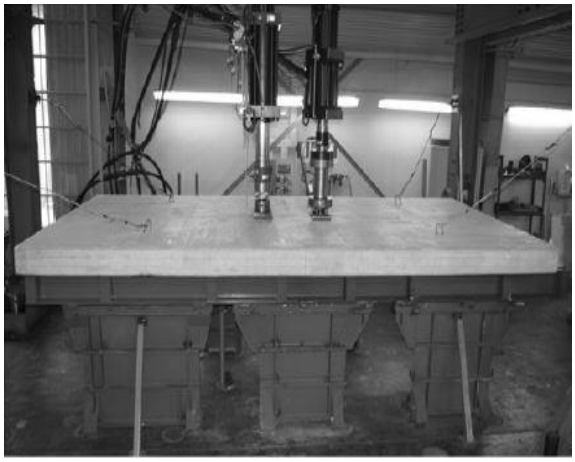

Figure 3-35 - Experimental setup [5]

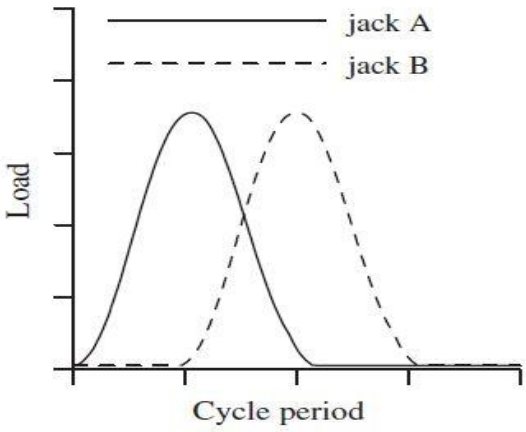

Figure 3-36 - Shape of load variation [5]

The concrete under cyclic compressive loading must have its strength verified by means of the Palmgren-Miner rule, according to the European codes. Also the punching shear strength is determined following the codes. For the experimental part, the slabs were considered simply supported in the attempt to recreate as accurately as possible the real structural system. For this purpose, the slabs were restrained on two sides by beams. Hydraulic jacks were used to apply the load, with its frequency varying between 0.2 and 1.25 Hz. The loading was applied in such a way that it mimicked the real wheel load, always having one jack delivering the maximum

load, whilst the other one was at its minimum. Two of the slabs were subjected to cyclic and static loading, one slab only to cyclic loading and the last one only to static loading [5].

The slabs that underwent cyclic loading but did not fail (S1 and S2) were subsequently statically loaded with a single concentrated load, up to failure. Slab S1, which had a maximum load value of 140 kN, did not fail after 1.5 million cycles and had a mid-span displacement of 1,8 mm in the beginning of the test and 2,5 mm after the cyclic test. The second slab, S2, was subjected to a maximum load of 290 kN and did not fail after 140000 cycles but the tests was stopped due to the large displacement at the mid-span (≈12 mm). The last slab that was subjected to a fatigue type of loading (S3) had a maximum value of the load of 440 kN and failed after approx. 400 cycles. Slab S4 underwent only static loading and failed at a value of 592 kN. When compared to this value, the reduction of the maximum static load for slabs S1 and S2 was extremely small, being less than 3,5% [5].

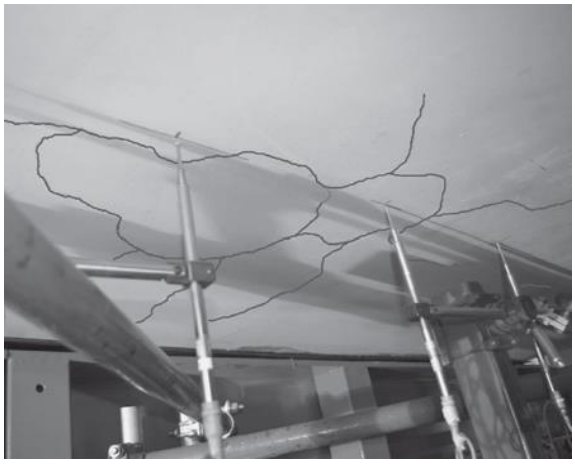

Figure 3-38 – Cracks in slab S1 after the cyclic test [5]

Figure 3-37 – Slab S1 at failure after static loading [5]

Slabs S1 and S2 behaved much better than predicted, since, according to the codes, they should have failed. The displacement of these slabs increased during the first period of cycle loading, matching the predictions from literature, namely, that the strain in the concrete increases until the stability curve is reached. The failure mechanism of the slabs was punching shear [5].

The study performed by Hwang et al. which was denoted as reference 7, researched the punching and fatigue behavior of long-span prestressed concrete deck slabs. Tests of both nature, static and cyclic, were carried out on scaled models of an actual bridge deck in order to come up with reliable formulas that would be used for assessing these two phenomena in such a structural system. For having a wider range in assessing the punching shear and fatigue performances, a number of current formulas were used, 4 for punching shear and one for fatigue [7].

Within the experimental program, 10 one-way (for reducing the weight) slab specimens were produced and tested. These models were scaled 1:3 out of a real bridge, having identical sectional details. They had 5 different levels of prestressing, from fully prestressed to none. The other variable was the concrete class. In terms of dimensions, the slabs had a total length of 4.3

m, with a span length of 2.7 m and two cantilevers of 0.8 m. The other in-plane dimension was 5 m, with the specimens being 115 mm thick. The slabs were connected to the supporting girders by shear connectors [7].

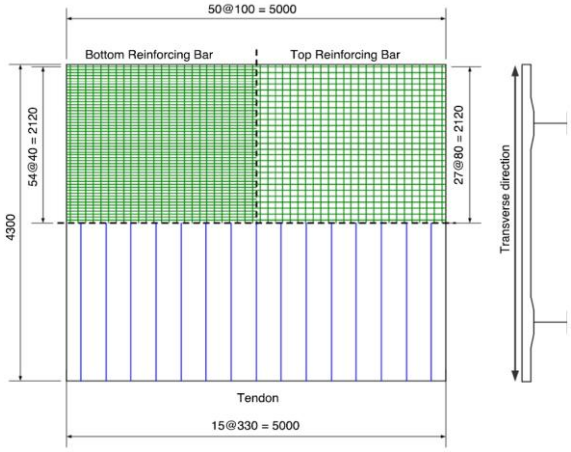

Figure 3-39 – Geometry and reinforcement layout of the specimens [7]

Figure 3-40 – Tests setup for (moving wheel) fatigue test [7]

Static load tests were performed in order to determine the static strength that served as a comparative value in estimating the cumulative damage that followed from the cyclic loading, where the strength of the specimen decreases with the increase in the number of cycles. An equipment that had loading capacities of 500 kN (for fatigue, simulating the passing of a wheel) and 1000 kN (for static) was used for the tests. The steel loading blocks were 192 x 77 mm^2 in dimension and were used as a runway during the fatigue tests. Due to their setup, the specimens were considered to have fixed and fully supported boundary conditions. During the tests, the strains and the deflections were measured [7].

Following the static tests, it was noted that the specimens subjected to punching exhibited different behaviour depending on the concrete strength and the level of prestressing. Their ultimate failure load ranged between 216 and 325 kN, with the mode of failure being punching shear or a combination of this and flexure. Prestressing increases the arching action, therefore influences the mode of failure. The deflection at failure appears to be inversely proportional to the level of prestressing. In the case of the specimen without prestressing, longitudinal cracks started at the bottom of the slab during the early stages of the loading, propagating towards the edges of the specimens and having a diagonal orientation as the load increased, this cracking pattern being associated with flexure. In the end, this slab had a combined failure mode. For the specimens that were prestressed, the cracks had a radial pattern. Failure occurred before yielding of the tendon and reinforcing bars in the longitudinal direction, though the reinforcement in the transverse direction did yield. All the prediction formulas used for the ultimate strength gave a lower value than the one obtained from the tests, with an accuracy between 60 and 85%. The formula from the Eurocode is considered to be reasonable for the estimation of punching strength since it is easy to use and has a good accuracy, although the one developed by Graddy et al. gives the best prediction. The punching strength appears to be proportional with the level of prestressing [7].

Even though the cyclic wheel loading produces more conservative results compared to a fixed point loading, still it was decided to perform the fatigue tests in this manner in order to shorten the testing period by applying high loads and load increments. By making use of Miner's rule and the determined static strength, an estimation of the punching strength of the fatigue specimens is performed [7].

For the first two specimens tested, the applied load was kept constant until failure. A value of 168 kN of the load led to failure after 35000 cycles, whilst a value of 141 kN led to failure after ≈32000 cycles. The values for de loads were chosen to represent a certain percentage of the static strength. For the last two fatigue tests, the load was applied in steps. For specimen no. 3, a first loading step of 29 kN resulted in 500000 cycles without failure, followed by an increase of the load to 141 kN and failure after ≈22000 cycles. For the last specimen, the first step had a 78 kN load which resulted in 800000 cycles without failure. Subsequently the load was increased to 141 kN and failure occurred after 1000 cycles. Specimens failed by sudden subsidence at the centre of the slab. At the bottom of the slabs, the transverse cracks progressed to form a grid shape, with a distribution similar to that of the punching cone from the static tests [7].

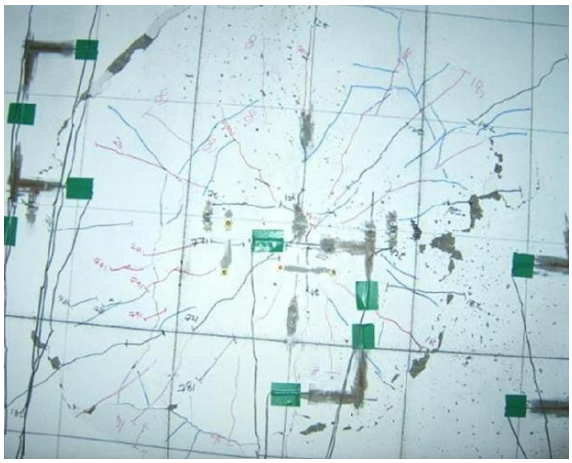

Figure 3-41 – Failure of specimen after static tests [7]

Figure 3-42 – Failure of specimen after fatigue test [7]

Without having clear guidelines for the evaluation of fatigue, it is generally accepted that minimum fatigue strength is thought of being achieved if after two million loading cycles there is no observable damage to the specimen. The predictions based on Miner's rule are considered to be too conservative, conclusion that is reached after comparing the results from the tests with the ones given by this method. The author derives a formula for predicting the fatigue life that is based on Miner's rule, but this also proves to be too conservative [7]

The study performed by El-Ragaby et al. (ref. 16) focused on the fatigue analysis of concrete bridge deck slabs reinforced with E-glass/vinyl ester FRP reinforcing bars. This type of reinforcement was chosen since it has a very good behaviour in corrosive environments. On the downside, the modulus of elasticity has a low value together with the transverse strength, resulting in elements with a lower shear capacity when compared to ones reinforced with steel. For the experimental program, a number of six bridge deck specimens were constructed (S0-steel, S1..5-GFRP), these having the dimensions 2500 x 3000 x 200 mm^3. Five of these slabs

were reinforced with GFRP bars having different reinforcement ratios and configurations, whilst the last slab was reinforced with steel. The concrete used had a targeted value for its compressive strength of 37 MPa at 28 days. After curing, the specimens were stored outdoors for more than a year in order to undergo environmental conditions similar to the ones from the service life of the structure. After this period, the properties of the concrete were concluded to have been stabilized at 42 MPa for the compressive strength and 34 GPa for the modulus of elasticity [16].

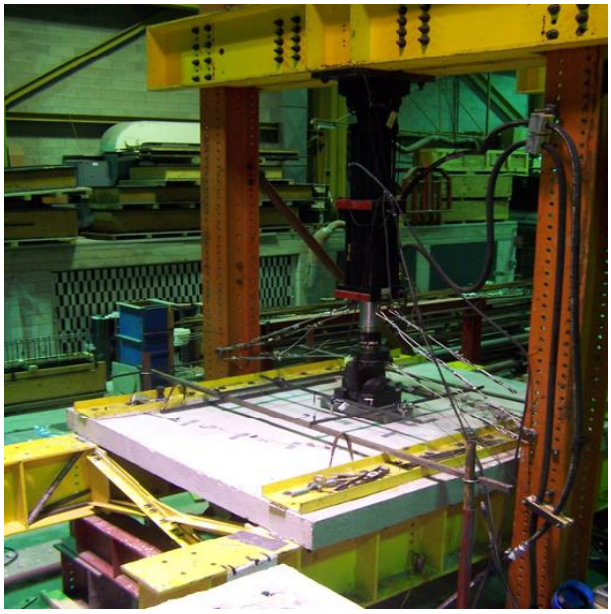

.

Figure 3-43 – Test setup [16]

The specimens were tested by applying a single point load at mid-span through a steel plate of 250 x 600 mm^2 in area and with a 75 mm thickness. Between the steel plate and the concrete it was positioned a 20 mm neoprene sheet used for avoiding stress concentrations. To ensure a partial end restraint for the slabs, these were connected to two supporting steel beams. For the fatigue loading, two different schemes were used: one with variable amplitude and one with constant amplitude. The variable amplitude fatigue loading consisted of a sinusoidal waveform of the applied load, between a minimum load level and a variable maximum level. The minimum load level was set to 15 kN, whilst the different maximum loads were selected based on the fatigue limit state given by the *Canadian Highway Bridge Design Code* [16].

Based on the regulations from CHBDC, the used maximum loads were 183.8, 245, 367.5, 450 and 490 kN. Each load step was applied for 10^5 cycles at a frequency of 2 Hz, the test continuing until failure if this would not occur during the specified number of cycles at the highest load. This loading scheme was applied to 4 slabs, namely S0, S1, S4 and S5. Slab S3 had a similar type of variable amplitude fatigue loading but with 3 additional load levels, all below the ones mentioned previously. The constant amplitude loading was applied to slab S2 for 4 million cycles at a peak load value of 122.5 kN, with a frequency of 4 Hz. The measurements performed on the specimens included strains of the reinforcing bars and concrete, deflections at the load area and the support, crack width [16].

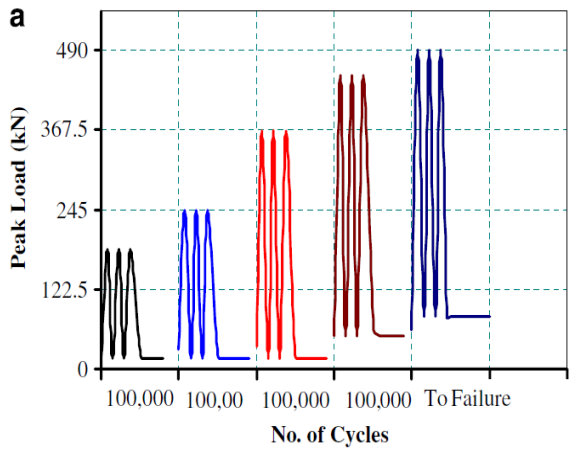

Figure 3-44 – Variable amplitude fatigue loading scheme [16]

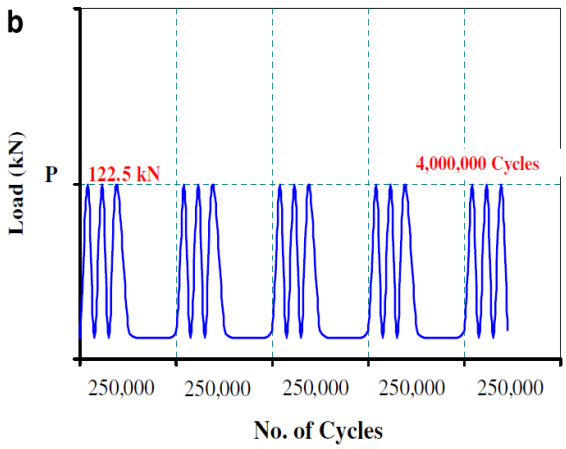

Figure 3-45 - Constant amplitude fatigue loading scheme [16]

For a better understanding of the loading effects that vehicles have on the deck slabs of bridges, the authors have performed a finite element analysis where the monotonic loading on such a system and its ultimate capacity were investigated. In order to do so, they had to choose a constitutive model for the concrete that would describe as accurately as possible its actual behaviour. This model was based on a smeared cracking methodology, took into account the non-linear properties of the material and the strain softening regime. The reinforcement is also taken into account in the model. The finite element model was validated based on results from previous experiments [16].

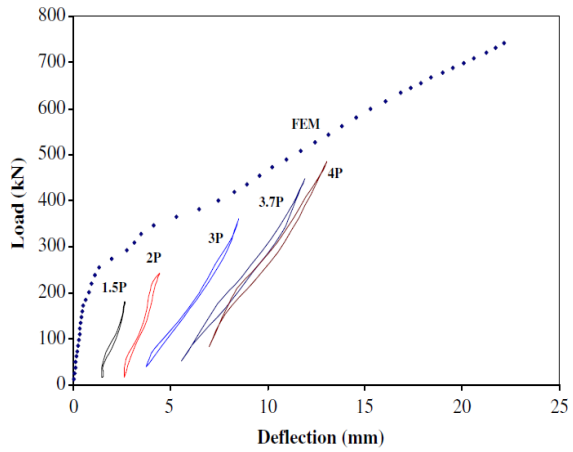

Figure 3-46 – Load-deflection behavior of slab S1 under static and cyclic loading [16]

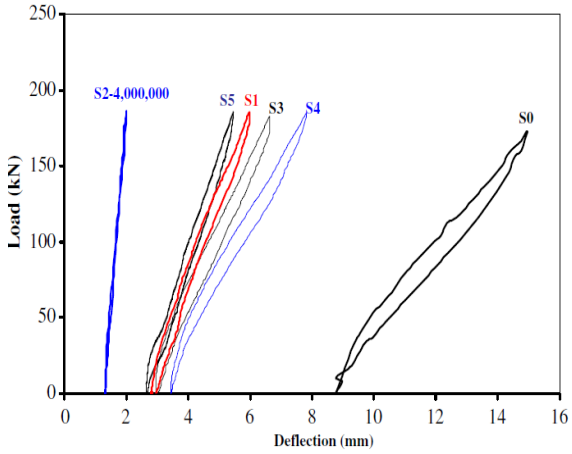

Figure 3-47 – Static response of the slabs after different fatigue loading steps (F_f=367 kN) [16]

In order to estimate the fatigue damage, the magnitude of the residual deflection was considered a proper measure for it. Following the finite element analysis that took into account only the static loading, it appears that the slabs have a very similar ultimate capacity (≈750 kN) despite the different top reinforcement ratios. The reduction in transverse reinforcement also seems to have no impact. From the analysis of the load-deflection behaviour of slab S1, it is shown that at the same load level, the deflection under cyclic loading is greater than the one under static loading. For slab S2, even after 4 million cycles, which is twice the expected lifetime of the structure, the deflection is below the allowable limit, this slab having the lowest residual deflection. For the slab reinforced with steel, S0, the damage was higher due to the

large difference between the elasticity moduli of steel and concrete and the mechanical bond [16].

The cracking pattern of the GFRP specimens was similar, with cracks being observed at the bottom of the slabs since the early stages. As the number of cycles and the load increased, the number of cracks became larger, with the cracks also getting wider. Excepting slab S2, which did not fail even after 4 million cycles, all the other slabs failed in punching shear [16].

Figure 3-48 – Crack pattern under fatigue loading [16]

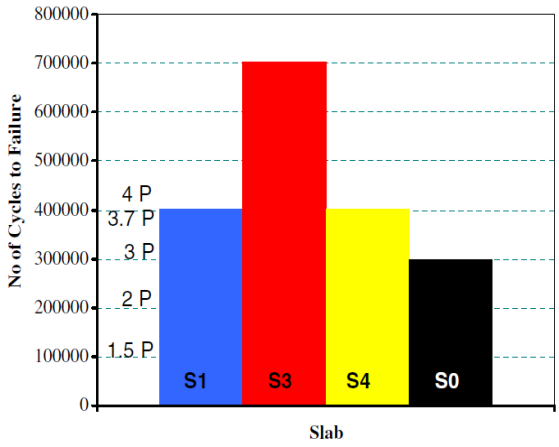

Figure 3-49 – Number of cycles to failure for each slab [16]

In other papers published recently and which have been examined (17, 18), the experimental programs and testing procedures follow a similar pattern to the studies that have been previously presented. Important aspects that must be mentioned are related to the testing frequency, which is mainly 1 Hz for the study performed by Natario et al. (17) and 1 or 2 Hz for the tests performed by Roesler & Barenberg (18). In both cases, the minimum load during the cycles was 10% of the maximum load.

3.4 Assessment of TU Delft testing program

3.4.1 General remarks

In this section, a general characterization of the testing procedures involving the concrete deck slabs under fatigue loading will be performed, with the framing of the study performed at TU Delft on this topic within the international research environment. The main aspects involved in such a study will be presented and comments will be made based on the previously presented papers.

The first main point of interest in such a study is represented by the specimens that need to be tested. These will try to replicate as accurately as possible the original structural system, often at a certain scale. If this is not entirely possible, then representative parts of that system, in terms of behaviour, will be manufactured. The complex structural system built by TU Delft for their research program was a 1:2 scale model of an actual bridge, being a mixture of pre-

cast and cast in-situ elements. It comprised precast prestressed longitudinal girders, post-tensioned transverse beams and a transversely prestressed deck. By building an actual structure, the researchers at TU Delft succeeded in creating a system that would behave almost identical to the full sized one, this being essential in order to obtain precise data that could be accurately extrapolated to real life situations.

For the other research programs that were studied, it must be noted that only scaled specimens were manufactured. From this point of view, the approach from TU Delft is considerably more beneficial. A certain degree of imperfection is another aspect that gives the specimen authenticity with respect to the behaviour of a real structure. This means, for instance, that the specimen can be subjected on purpose to an outdoor environment and its actions, like it was in the case of a previous study (16), or that it can suffer some structural flaws, like shrinkage cracks in the case of the TU Delft model. The scope in the end is to obtain a system that behaves as realistic as possible, scope that was achieved by the research program at TU Delft.

The testing setup, another point of interest, would usually involve a frame rigid enough to withstand the loading process of the specimens, this being performed by means of a hydraulic jack or an electro-hydraulic actuator. The applied load is normally a single point (wheel) load or a double point load that would simulate the loading from an actual wheel system. Such a frame was used for the loading process within the TU Delft research program. Depending on the type of research, the frame could be more complex and also be used for ensuring the support conditions of the specimens, providing the required degree of rigidity to its sides (12) and, for instance, being able to activate the compressive membrane action (CMA) of a slab. In the case of the TU Delft model, the structural system was conceived in such a way that it did not require additional restraints. Through the nature of the system itself and by making use of the transverse girders that would increase the rigidity, the arching action within the model was enabled.

Another aspect that is relevant for the test setup involves how the load is transferred to the specimen. This is done through the means of a steel plate that has realistic in-plane dimensions that are in accordance with the size of wheels given in the codes. If it is desired to decrease the number of cycles to failure without increasing the load, then the size of the steel plate can be reduced, resulting in a higher applied stress. In order to avoid or reduce as much as possible the risk of stress concentrations on the perimeter of the loaded area, usually a rubber sheet is applied between the steel plate and the concrete. This procedures were present in the studies that were described in the previous sections, with the program at TU Delft having a similar approach.

The instrumentation used for measuring the data within the tests is also part of the setup. A wide range of variables can be measured during testing, such as: applied load, deflections at the location of the load, deflections at the supports, strains of the reinforcing or prestressing steel, strains of the concrete, crack widths and patterns. It is of importance in the case of fatigue loading to assess what is happening to the specimen after one loading cycle, subsequently studying the outcome at a predefined number of cycles.

As mentioned earlier, the applied load would simulate the effect that an actual wheel from an automobile has on the bridge. Usually, the load would have a fixed point of application, resulting in a pulsating fatigue test, this being the case of the ones performed by TU Delft. In this situation, the load would have a sinusoidal waveform, with a minimum and a maximum value within each stress range, being applied for a certain number of cycles. Another type of loading system that might be used would be one that simulates the actual passing of a wheel over the specimen (7). Although it tries to be more realistic in terms of load application, it is considered that the results provided are too conservative. Pardikaris et al. (1988) came to the conclusion that one wheel load passage of such a system over the specimen is equivalent to 80-600 load cycles of a stationary pulsating load that has the same amplitude (16).

For the experimental program at TU Delft the applied stress was only of compressive nature, similar to the cases presented in Section 3, with the load consisting of a single or a double point load. The maximum value of the load within a stress range would represent a certain percentage out of the ultimate static strength, whilst the minimum value would represent 10% of the chosen maximum. This type of approach was adopted for the TU Delft tests but is also a common choice for other experimental programs (12, 17, 18). An interesting observation from the presented tests, including TU Delft, is that at a lower maximum value of the load, the fatigue loading does not seem to affect the ultimate static strength of the specimen. Another important aspect during fatigue loading is represented by the frequency of the load. The chosen value for this was 1 Hz, again a very common choice for this type of tests (12, 5, 17, 18). CEB's Bulletin no. 188 (3) and Mallett (2) state that, for plain concrete, higher frequencies, between 1 and 15 Hz, do not affect the fatigue strength if the maximum stress level is not higher than 75% of the static strength. A recent study performed by Medeiros et al. (19) confirms that fatigue life is reduced at lower frequencies for plain concrete. It can be concluded that the choice made by TU Delft with respect to the frequency is correct. In terms of load positioning, this would be applied at the position that is more susceptible to failure or where it would have an impact on the structural system (e.g. at the mid-span of the element).

Concerning the failure of the specimens, it is a general observation that for slabs where the compressive membrane action (CMA) is deployed, punching shear will be the failure mode. CMA increases the ultimate capacity of the slabs, with the flexural resistance becoming higher than the shear one, making the punching shear to be governing. This was also the failure mode for the tests performed by TU Delft and is in accordance with the other tests presented. In terms of cracking pattern, this was the well-known one for such a failure mode: cracks would form below the loading plate and would spread in a radial pattern, with their width being larger under the area where the force was applied, whilst outside that area they would have considerable smaller openings.

3.4.2 Comparison of experimental results

Following the experimental program performed by TU Delft and analysing the obtained results, a series of conclusion and observations were made, with the main ideas being presented

at the end of section 2 of this chapter. It was acknowledged that with the decrease of the fatigue load value, the fatigue life of the specimen was enhanced, namely the number of loading cycles to failure would increase. A descending trend is clearly visible in the graph that presents the relative load value (F_{fat}/F_{sta} - the ratio between the fatigue load and the static load) versus the number of cycles (Figure 3-50). Having a decrease in the fatigue life with the increase of the load is logical since, as deterioration begins, the element will undergo continuous damage at a certain rate, depending on the value of the cyclic load. Based on the formula that was derived by the researchers at TU Delft, it was approximated that the average value for the fatigue load at 1 million cycles is 54% of the static load, respectively 41% at 100 million cycles. These results will be compared in the following with results from other researches, with the purpose of assessing whether they fit within the general findings on this topic and additionally evaluating their degree of accuracy/reliability.

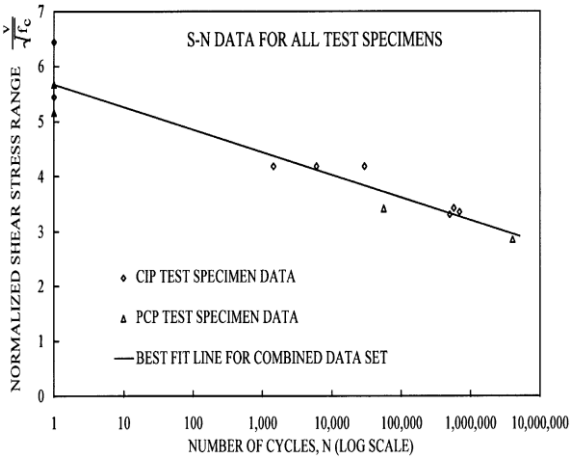

Figure 3-51 - S-N diagram for all specimens [12]

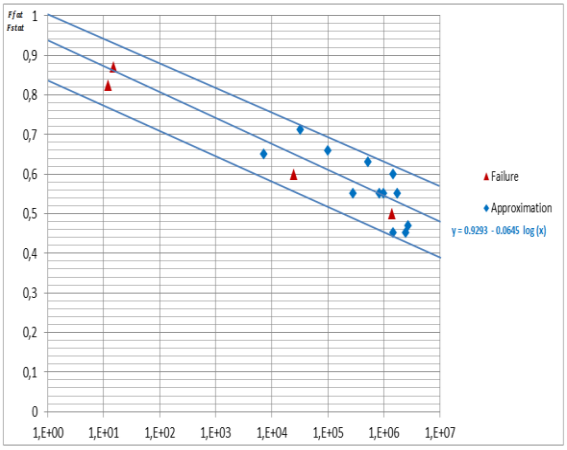

Figure 3-50 - Relative load value Ffat/Fsta as a function of the no. of loading cycles for all the tests [15]

The research presented as reference 12 focused on the fatigue testing of concrete deck slabs that tried to replicate as accurately as possible a part of a real bridge deck. These specimens were either cast in situ or a combination of prestressed and cast in situ concrete. With the obtained results following from the fatigue and static tests, the S-N diagram presented in Figure 3-51 was obtained. It can be observed immediately that also in this case the trend line is descending, meaning that with the increase in value of the applied stress, the number of cycles to failure is decreasing. This graph shows the normalized shear stress ratio plotted against the number of cycles to failure. This normalized stress was used in order to take into account the area of the specimen that failed in punching shear only.

Since this study (12) does not give a prediction formula nor an S-N graph that accounts for the ratio between the fatigue and static loads like it was in the case of the TU Delft research, an approximation was made in order to obtain an average value for the fatigue load at 1 million cycles. The procedure on how this value was obtained is described in *Annex 1* and is based on the data presented in the scientific paper (12). As a result of the calculations, it was estimated that at 1 million cycles the fatigue load would have a 51% value of the static load, result that is very similar to the one from the TU Delft research (54%).

In reference 7, a study investigating the punching and fatigue behaviour of long-span prestressed concrete deck slabs was presented. Following the testing program and the data processing, the authors derived a couple of prediction formulas for the fatigue load at a certain number of cycles. Being based on Miner's rule, they themselves acknowledge that the results provided by these formulas are conservative. In order to be able to compare their accuracy, they used an additional prediction formula derived by Higashiyama and Matsui (1998) which was recognized to provide more accurate results.

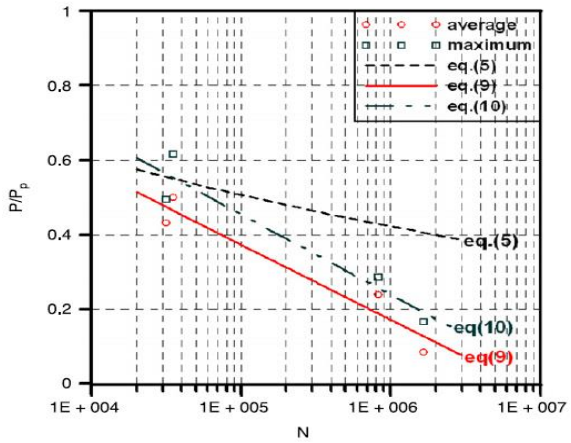

Figure 3-52 – S-N curve: tests and prediction from formulas [7]

Following their predictions, an S-N graph similar to the one from TU Delft was plotted (Figure 3-52), showing the ratio between the fatigue load and the static load versus the number of cycles to failure. A similar descending trend can be observed, with the increase in the number of cycles as the value of the load (ratio) is decreasing. On the graph, equations 9 and 10 denote the prediction formulas derived by the authors, whilst equation 5 denotes Higashiyama's and Matsui's formula. In case of the latter, it can visually be assessed that at 1 million cycles the fatigue load is around 42% of the static load. Although similar visual observations can be done with respect to the derived formulas, in their case the values are directly determined and can be verified in *Annex 1*. From the first formula (average wheel load considered) a fatigue load value of 17% of the static load is derived at 1 million cycles, whilst for the second formula (maximum wheel load considered) a value of 24% is obtained. These results are considerably smaller than the ones obtained within the TU Delft study. At 100 million cycles the formulas are not valid anymore since the results obtained have a negative value. As stated before, these formulas prove to be very conservative.

The study performed by Roesler and Barenberg that was presented in reference 18, researched the fatigue and static behaviour of concrete slabs. A series of tests were performed on fully supported slabs and simply supported beams and an S-N curved was derived based on the data from the tests. This curve is presented in Figure 3-53 and on the graph it can be observed its descending trend, with the increase in the number of cycles. The stress ratio that was plotted against the number of cycles to failure represented the ratio between the bending stress in the slab and the concrete modulus of rupture. Since not all the data required to perform an accurate calculation is presented in the paper and there is no prediction formula given, the value for this ratio at 1 million cycles is estimated visually from the graph. Subsequently, to

have a better estimation of the fatigue life, the modulus of rupture was replaced by the static strength. Therefore it can be assumed that the bending stress is directly linked to the fatigue load and therefore the ratio can be interpreted as being between a fatigue and a static load. At 1 million cycles this ratio is approximately 0.6, meaning that the fatigue load would have a value of around 60% of the static load, result that is close to the ones from the TU Delft research.

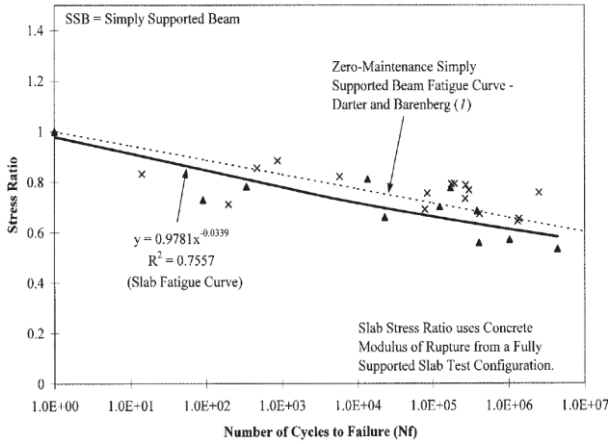

Figure 3-53 – S-N curve for fully supported slabs from Roesler and Barenberg study [18]

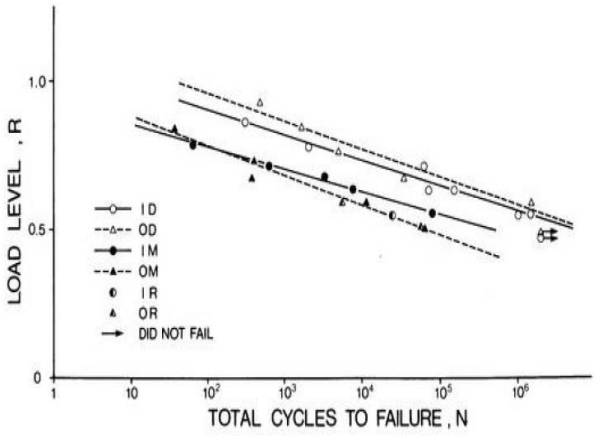

Figure 3-54 – S-N curve from the study performed by Sonoda and Horikawa [20]

Sonoda and Horikawa researched the fatigue strength of reinforced concrete bridge deck slabs under moving loads, this study being labelled as reference 20. For their experimental program they tested 20 slabs that were subjected to static loading, fixed point pulsating loading and moving loads. These slabs had either isotropic or orthotropic bottom reinforcement and were simply supported during the tests. Following the experimental program, prediction formulas and S-N curves were determined, this being presented in Figure 3-54. The load level "*R*" on the vertical axis represents the ratio between the applied (fatigue) load and the average static collapse load, this load level being plotted against the number of cycles. The same descending trend of the S-N curve can be observed. Of interest in this situation are the prediction formulas that relate to the fixed point pulsating tests since the same type of tests were performed during the research at TU Delft. Based on these prediction formulas, it is estimated that at 1 million cycles, for isotropic slabs, the fatigue load is 56% of the static load, whilst for orthotropic slabs the value is 58%. At 100 million cycles the values are 39% and 42%. These results are very similar to the ones from the study by TU Delft and they can be verified in *Annex 1*.

Another research performed by El-Ragaby et al. is presented in reference 21 and deals with the fatigue life of concrete bridge deck slabs reinforced with GFRP bars. A similar study performed by the same author was presented in reference 16 and these studies are most likely linked to one another. In the current paper, a series of deck slabs were tested under a fixed point pulsating load and subsequently the results were processed in order to obtain a fatigue life prediction formula based on which a S-N curve was plotted. Since the reinforcement consisted of GFRP bars, this had to be considered for the prediction, as the behaviour of such bars differs from the behaviour steel.

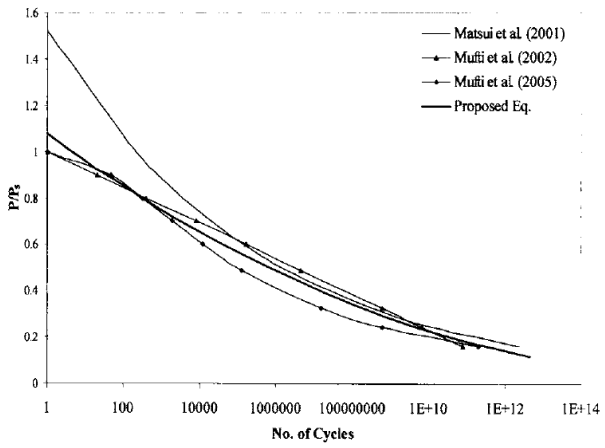

Figure 3-55 – S-N curves based on different prediction formulas [21]

Figure 3-55 presents the ratio between the fatigue and the static loads plotted against the number of cycles using several prediction formulas, including the one proposed for elements with GFRP bars. They all follow the same descending trend: as the ratio of the loads reduces, the number of cycles to failure increases. Based on the prediction formula by El-Ragaby, the fatigue load at 1 million cycles has a value of 48.5% of the static load. At 100 million cycles the prediction results in a value of 34%. In the same paper, a formula derived by Matsui et al. (2001) is also presented, this dealing with steel reinforcement. Following this formula, the prediction at 1 million cycles is 51.5%, whilst at 100 million cycles is 36%. These calculations can be verified in *Annex 1*. It can be stated that both the S-N curves and the results are similar to the ones from the TU Delft research.

It is a general observation that the lower the applied fatigue load is, the higher is the number of cycles required for failure of the specimen. Such descending trend was observed in each research that was presented and the study performed by TU Delft had the same outcome.

Overall, it can be concluded that the results from TU Delft's research are in good correlation with other researches performed worldwide, this giving them a high degree of reliability and credibility. Nevertheless, it must be kept in mind that fatigue testing is prone to a large scatter in the results due to the non-uniform properties of the material (concrete) and future usage of TU Delft's prediction formula should be accompanied by further testing in order to validate its accuracy.

3.4.3 Conclusions

The research program performed by TU Delft on the fatigue of concrete deck slabs was complex, from the point of view of the structural system and from the point of view of the variables within each test. A better understanding of the fatigue phenomenon was tried to be achieved and also a way of predicting the fatigue life of old and new structures.

As an overall review of the tests from the experimental program conducted by TU Delft, it can be acknowledged that these fit well within the general pattern of fatigue tests performed

on a global scale. The main points of interest for such tests align themselves to the international researches, as it was presented in the previous sections. There result also are in correlation with similar outcomes from studies performed across the globe. In The Netherlands there is no standardised procedure involving the fatigue testing of slabs, therefore an approach like the one used, more empirical, is legitimate. Outside The Netherlands, such standardized procedures can be found, like the one for "*Determining the fatigue failure of compacted asphalt concrete - ASTM D7460"*. Nevertheless, the way this research was conducted can be appreciated as being suitable for the topic and reliable.

A series of observations involving certain aspects of the testing procedure could be made. Related to the tests, since each one had its own characteristics, it would be of interest to confirm the result by performing a replication of this tests. This way any improbability or concern could be removed. Another aspect that might have had an influence on the results, although measures were taken in order to avoid a negative impact, was the fact that these test were performed at locations close to each other and the structural system could have given a slightly different response in case of test *n+1*, following test *n*. A final comment involves the order of the applied stress ranges. It was observed during the tests performed at TU Delft that an initial higher stress range might have a detrimental impact on the fatigue life, shortening it considerably. In the presented literature, such a case was not encountered so no other information can be given on this aspect. It is then one of the goals of this Master's Thesis to try and shed some light on this matter and see if there is indeed an impact caused by the loading sequence.

Chapter 4: Finite Element Analysis - Stage I

4.1 Introduction

The finite element analysis (FEA) is a powerful tool that can be used in order to evaluate in detail the behaviour of structures or elements within a structure, without having to perform costly and time consuming experiments. In order to benefit from the full usage of such a tool, it is required to understand how it works, how to operate it and how to interpret the results that follow from this type of analysis.

As the main goal of the Master's Thesis, it was set that a FEA model would be created in order to try to predict the fatigue damage of transversely prestressed thin bridge deck slabs. First, the model should be able to describe as accurate as possible the static capacity of the structural system from the previous experimental program (S. Amir's PhD Thesis, [14]). Subsequently, the model should be used for the fatigue prediction of the experiments described in TU Delft's report number 25.5-14-06 ([15]).

It was decided that the model would be a simple one, two-dimensional (2D), thus not having a high degree of complexity. By doing so, it must be understood that the model would have its drawbacks and limitations, since it won't be able to fully describe the real three-dimensional stress state. A complex 3D model was created by S. Amir for her PhD thesis and experimental program ([14]) and it is presented in Figure 4-1.

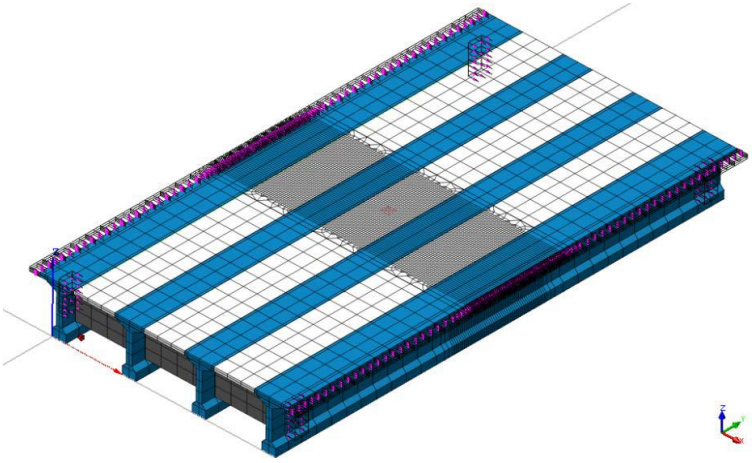

Figure 4-1 – 3D solid finite element bridge model, S. Amir [14]

As part of the numerical analysis section of the Master's Thesis, this first stage of FEA presents the development of the model, with all the necessary steps required to reach a suitable result, including its calibration.

The software used for this section was DIANA FEA (version 10.0). This is a multi-purpose software package that is widely used in different branches of the civil engineering field and it was developed in The Netherlands by DIANA FEA BV, company that has its origins at the Computational Mechanics department of TNO Building and Construction Research Institute in Delft.

4.2 Development of the FEA model

4.2.1 Plane Stress model

When analysing what type of simplified model to be used in order to describe as accurate as possible the stress state, it was clear from the beginning that a one dimensional (1D) model was not an option, this not being capable of presenting a desirable state of the stresses. For instance, such a model would not be able to develop the compressive membrane action (CMA) that is characteristic to the bridge deck slabs. Therefore it became clear that a 2D model should be created and the choice between a plane stress and a plane strain approach had to be made.

Considering the real life structure, a long motorway bridge, more often the choice would be for a plane strain method. In this case however, the plane stress was thought to be suitable for performing the intended analyses, as the concrete is assumed to no longer have any effect or contribution in the direction of the width of the element, once cracking occurs. This was one of the first assumptions that were made during the development stages of the FEA model.

The plane stress state implies that there are no stresses in the direction of the width: the normal stress $\sigma_z = 0$ and the shear stresses $\tau_{xz} = 0$, $\tau_{yz} = 0$. Only in-plane stresses are allowed (here, it was considered that the X and Y axes define our plane and the Z axis is out of plane) and these are assumed to be constant over the width of the model.

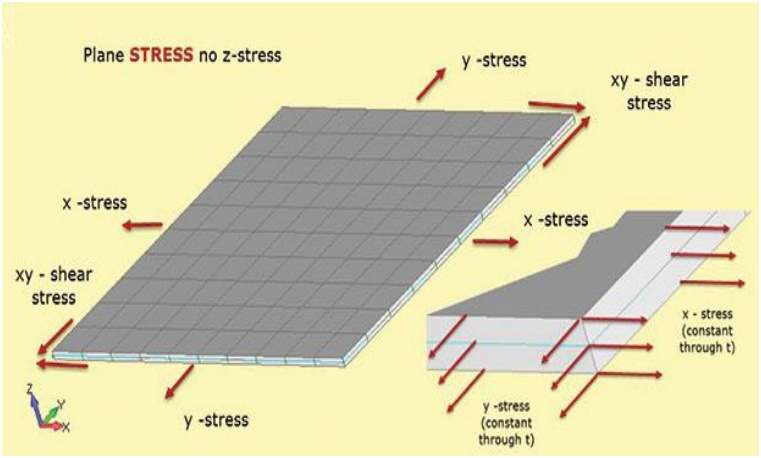

Figure 4-2 – Plane stress state [24]

4.2.2 Geometry and support conditions of the model

The structural system that underwent testing was a 1:2 scale model of a real bridge, therefore its dimensions were quite large (Figure 3-2), having a total area of the deck of approximately 77 m^2. It was composed of four long precast longitudinal girders, two cast in-situ end beams and a cast in-situ deck, having three spans.

For reasons of simplification, only the deck was modelled (in the transverse direction), considering the top midpoints of the precast longitudinal girders as the locations of the supports. Since it had 3 spans, the first set of analyses tried to replicate only the middle span, this being the one that was loaded by a point load. This was done in order to assess how the model behaves and reacts having different support conditions: simply supported and one time statically indeterminate. The anticipated increase of the initial stiffness and capacity and decrease of the vertical deflection at the mid-span of the model were observable and can be seen in Graph 4-1 below. For reasons of comparison, the outcome of considering the full transverse cross section is also presented, this being closer to a clamped situation.

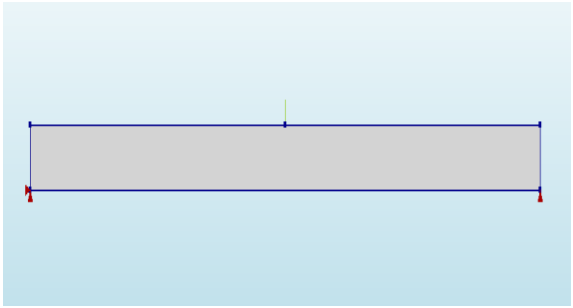

Figure 4-3 – First FEA model, simply supported

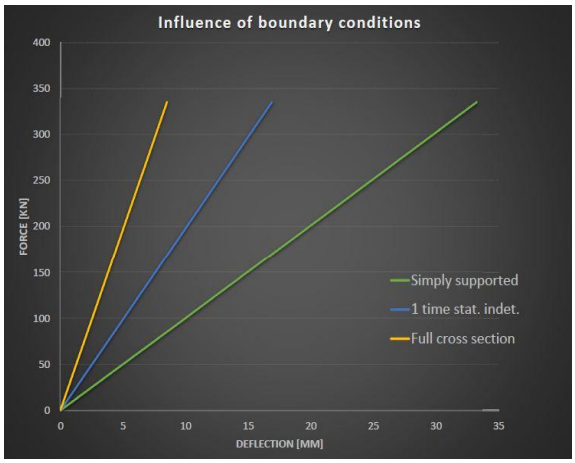

Graph 4-1 - Influence of boundary conditions (following from the linear analyses)

After the first series of analyses, it was understood that by modelling only the loaded span of the actual bridge, the capacity of the model was extremely low. For the simply supported conditions it had a value between 12 and 15 kN (following from the nonlinear analyses), a very low value compared to the mean static capacity of the structural system (considered to be 335 kN, according to [15]). Therefore it was decided to define as geometry of the FEA model the full transverse section of the bridge deck as a continuous element, assuming that the precast girders and the cast in-situ deck had the same material properties.

Since the full transverse section was modelled, this was considered as a beam on multiple supports, with the supports being positioned at the location of the longitudinal girders in the real structure. A main reason for choosing this type of schematization was that, by doing so, the ultimate capacity would increase substantially and the compressive membrane action was able to develop and be assessed in the model. Its in-plane dimensions were 6.40 meters by 0.10 meters. Regarding the supports, all of them ended up having fixed translations on both X and Y axes, but in-plane rotation was allowed.

At the supports and at the location of the applied force, steel plates were added to the model in order to avoid stress concentrations, a phenomenon that occurred during the first analyses performed. Similar plates were added to the sides of the model for the same reason, since the prestressing load was applied as an external lateral load. All the steel plates were 200 mm in length, 20 mm in height and 200 mm in the out-of-plane direction. Between the steel

plates and the concrete section, an interface was defined for the same purpose of avoiding the stress concentrations.

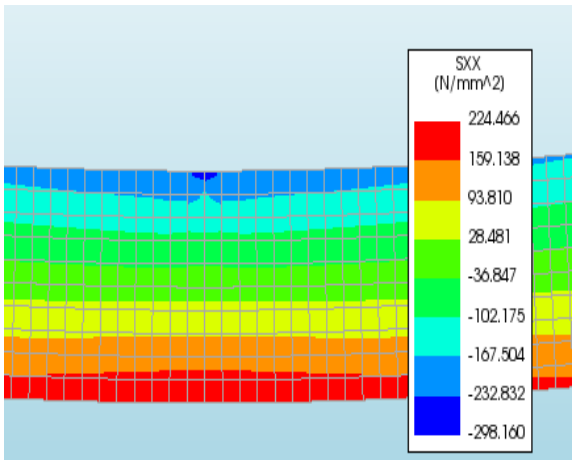

Figure 4-4 - Lack of plate in the model (linear analysis)

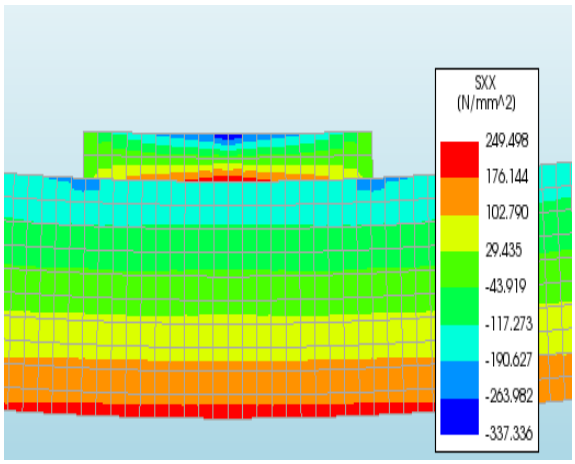

Figure 4-5 – Effect of the loading plate on the stress distribution (linear analysis)

Although the conducted analyses were of a 2D plane stress type, also a dimension for the out-of-plane direction had to be considered – an effective width. The final model had a width 1.95 meters and in the section of this chapter regarding the calibration, it will be presented how this value was reached.

4.2.3 Reinforcing and prestressing steel

Following the design of the real structure presented in S. Amir's thesis ([15]), reinforcement was also added to the model. Having assumed a certain effective width (1.95 meters) which would theoretically be influenced by the load, the real area of reinforcement distributed over that width was assigned to the model. The reinforcement was schematized as horizontal embedded bars at the top and bottom of the FEA model, running across the full transverse section. This was done although in the real structural system the bars which are of interest were distributed in those parts of the deck that were cast in-situ. But because the precast girders contained enough reinforcement in the top flange, the assumption of continuous reinforcement in the model was made. The concrete cover was considered to be 10 mm. The amount of reinforcement that was assigned at either sides of the model was 311 mm^2, since the reinforcement was Φ6/200: there were considered 11 bars for the effective width of 1.95 meters, the first one being laid down at "0" meters. Shear reinforcement was not provided for the actual deck therefore such a type of reinforcement was of no interest.

Although the prestressing force was applied as an external load, the number of prestressing bars that had been spread over the assumed effective width were schematized in the model as a bar placed at the centre of the section, having an equivalent area to that of the actual bars. This was done in order to represent as accurate as possible the real life situation. The area considered for the prestressing steel was 883 mm^2: 5 bars of Φ15/400. In the section

that deals with the calibration of the model it will be discussed about the impact of this bar, taking into account whether it was bonded or not.

The following figure presents the final model used, having the previously specified geometry (with the steel plates included), support conditions and steel (reinforcing or prestressing):

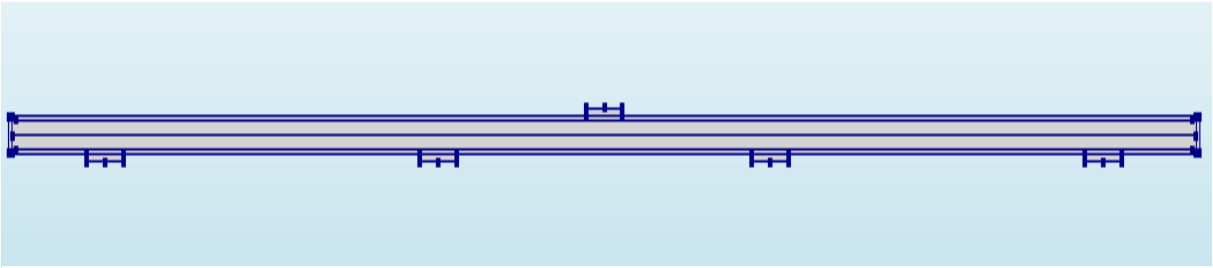

Figure 4-6 – FEA model displaying the geometry and the reinforcing/prestressing bars

4.2.4 Element types of the model

4.2.4.1 Plane stress elements

The main element of the constructed FEA model, used for both deck and plates, is defined in DIANA with the indicative CQ16M. According to the software's manual, reference [25], this is an eight-node quadrilateral isoparametric plane stress element, which is based on quadratic interpolation and Gauss integration. By default, DIANA applies 2 x 2 integration points (deemed as optimal), but it can also use a 3 x 3 integration scheme.

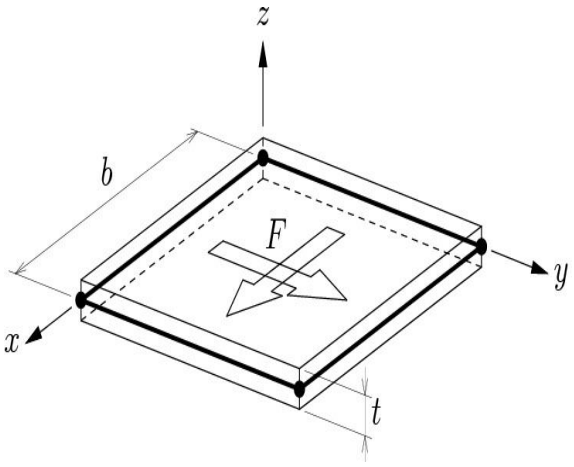

Figure 4-7 – Plane stress element as defined by DIANA [25]

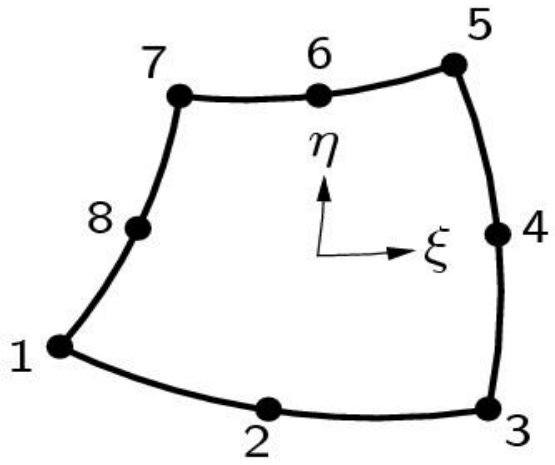

Figure 4-8 – CQ16M element of DIANA [25]

As characteristics for a plane stress element it is stated that its nodes must be in a flat plane, that its width must be smaller than the in-plane dimension(s) or that the loading must be in the plane of the element. It was already mentioned that the stresses in the direction of the

width are assumed to be 0 ($\sigma_z = 0$). The element cannot be used in the case of out-of-plane bending [25].

For CQ16M, the determination of the displacement in both directions, u_i (i = x, y), makes use of following quadratic polynomial expression:

$$u_i(\xi,\eta) = a_0 + a_1\xi + a_2\eta + a_3\xi\eta + a_4\xi^2 + a_5\eta^2 + a_6\xi^2\eta + a_7\xi\eta^2 \quad [25]$$

By using the above relationship, the strains can be determined. ε_{xx} varies linearly on X and quadratically on Y, ε_{yy} varies linearly on Y and quadratically on X, whilst the shear strain varies quadratically in both directions [25].

4.2.4.2 Interface elements

Generally, such interface elements describe the behaviour with respect to normal and shear tractions and normal and shear displacements across the interface. The elements used in the FEA model were of type CL12I as defined by DIANA and are used as interfaces between two lines of adjacent elements in a 2D state, being based on quadratic interpolation and, by default, a 3 point integration scheme [25].

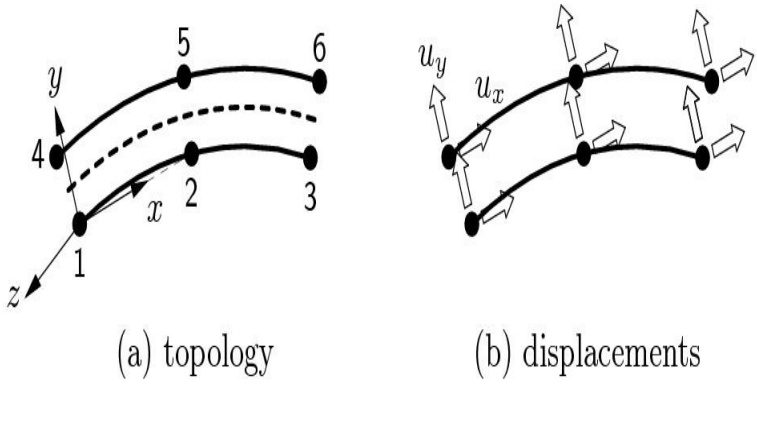

Figure 4-9 – CL12I interface element [25]

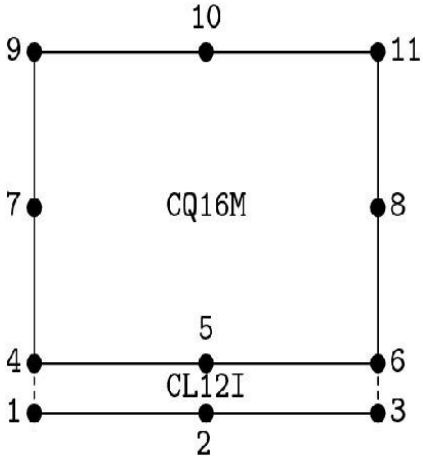

Figure 4-10 – Connection of CL12I to another element [25]

4.2.4.3 Reinforcement elements

The reinforcement bars were considered as being embedded into the mother element, therefore not allowing any slip (perfect bond) and adding stiffness to the FEA model. DIANA treats them as bars and assesses these elements as having the shape of a line, dividing them into so called particles, performing for each particle a separate numerical integration. The output is composed of stresses and strains which are oriented along the axis of the element. In order to have a bar embedded in a plane stress element, DIANA requires for each plane stress element the location points of each particle of the bar embedded into that element [25].

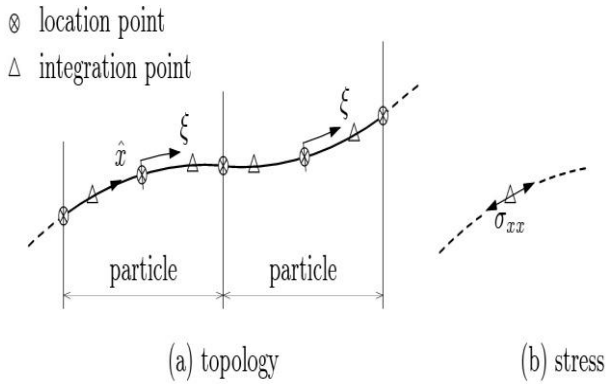

Figure 4-11 – Reinforcement bar as considered by DIANA [25]

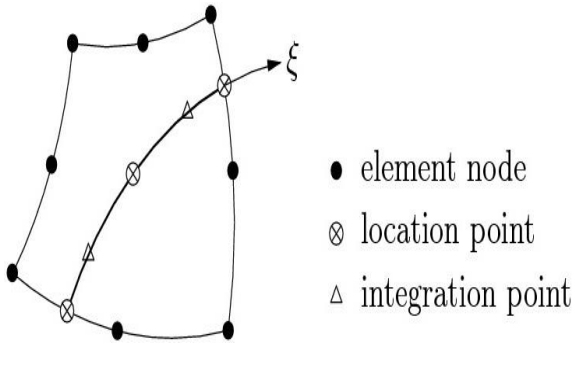

Figure 4-12 - Bar particle in a plane stress element [25]

4.2.5 Constitutive (material) models

In order to analyse a structure, one major part of this process is represented by how the physical behaviour of the materials used in the said structure are modelled for the finite element analysis, behaviour that is based on the knowledge about what kind of failure mechanisms can occur in the material. DIANA offers an extensive library of material models that can be used in order to describe as realistic as possible the way a certain material behaves, considering different loading hypotheses and types of structures.

To be sure that a right constitutive model is used for the FEA, the Guidelines for Nonlinear Finite Element Analysis of Concrete Structures released by Rijkswaterstaat [26], the DIANA manual [25] and S. Amir PhD thesis [14] were examined.

4.2.5.1 Concrete

Being the main material used for the structure tested during the experimental programs related to static [14] and fatigue [15] loading, concrete is known for having a very complex behaviour, being influenced by the stresses that it must bear and by the fact that it is not a homogeneous material. Concrete can be labelled as a composite material, made up of different components, each with specific properties that influence in the end the characteristics of the final product. The structures that are constructed out of reinforced concrete have their behaviour influenced by that of the main constitutive materials: concrete, with its proneness to cracking (tensile behaviour) or crushing (compressive behaviour) and steel, with its proneness to yielding.

In order to obtain results that were in accordance with the previously performed experimental programs and FEA analyses, certain material properties were borrowed from S. Amir's PhD thesis [14]. Among these properties, for concrete it is mentioned the mean compressive strength, the mean tensile strength, the modulus of elasticity and the tensile fracture energy, all of these being based on results from tests. The coefficient of lateral

contraction (Poisson's coefficient) was taken from the guidelines for nonlinear analysis of Rijkswaterstaat [26], although analyses performed with both values showed no difference in behaviour. For the determination of the tensile fracture energy, according to [14], a mean value was considered, between the results provided by Model Code 90 and Model Code 2010. The guidelines for Rijkswaterstaat [26] use only the approach from MC2010:

$$G_F = 73 * f_{cm}^{0.18}$$

All the considered properties for concrete will be presented in a table at the end of this subsection.

Material	Component	f_{cm} [MPa]	f_{ctm} [MPa]	f_{sy} [MPa]	E [MPa]	ν	G_f [N/mm]
Concrete	Girders	75	6.31	-	41000	0.2	-
	Slab	65	5.41	-	39000	0.2	0.15
	Transverse beams	65	5.41	-	39000	0.2	-
Steel	Slab	-	-	525	200000	0.3	

Figure 4-13 – Material properties of concrete and steel from S. Amir's PhD thesis [14]

For the cracking behaviour of concrete, a smeared cracking approach was adopted. Such a concept allows for cracking to develop in the element once the cracking initiation conditions are met, with the cracks being allowed to form freely in the model, anywhere and in any direction. This is opposite to a discrete cracking procedure, where the location of a crack is more or less imposed or known. Rots in his article [27] describes these two approaches and presents the characteristic features of each.

When the principal tensile stresses exceed the tensile strength of the concrete, a crack is initiated, with its direction being perpendicular to that of the principal tensile stresses [28]. For the smeared cracking procedure, the opening of the crack is smeared all across the considered element, being represented by the strains of the crack. These strains are dependent on the displacement of the crack surface and the band width of the crack (length over which the displacement is distributed) [14]. Another important parameter that influences the smeared crack propagation is the fracture energy, which is in close correlation with the tension softening stress-strain diagram [28].

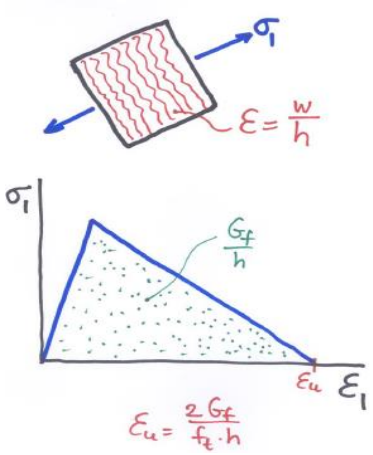

Figure 4-14 – Smeared cracking approach [28]

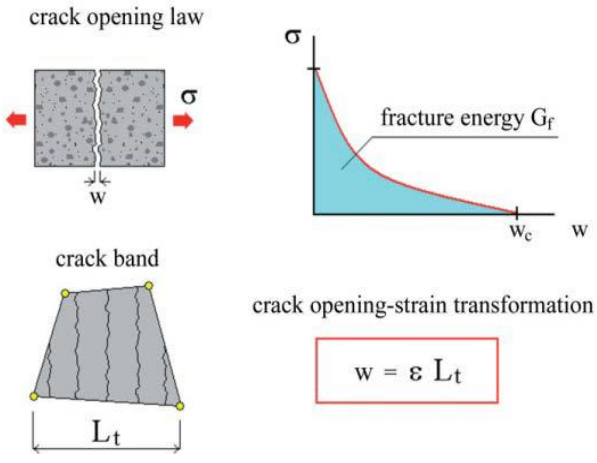

Figure 4-15 – Smeared crack model, tensile behaviour [14]

Within the smeared cracking concept, a total strain based crack model with rotating cracks was adopted (cracks rotate with the axes of the principal strain), as recommended by the guidelines from Rijkswaterstaat [26] and similar to S. Amir's finite element analyses [14]. The benefit of using such a model is represented by the avoidance of stress locking. The value for the crack bandwidth was equal to the dimension of the discretized element, 10 mm.

For the tensile behaviour of the concrete (cracking), DIANA offers a wide range of predefined tension softening functions. Rijkswaterstaat [26] recommends the use of an exponential function since it will result in more localized cracks, avoiding scattered cracking. In order to see how the FEA model behaves, analyses were conducted with a Hordijk, an exponential and a linear type of softening. The behaviour turned out to be significantly influenced by the choice of the softening function, the linear type of softening giving the best results. This will be presented in the section that deals with the calibration of the model.

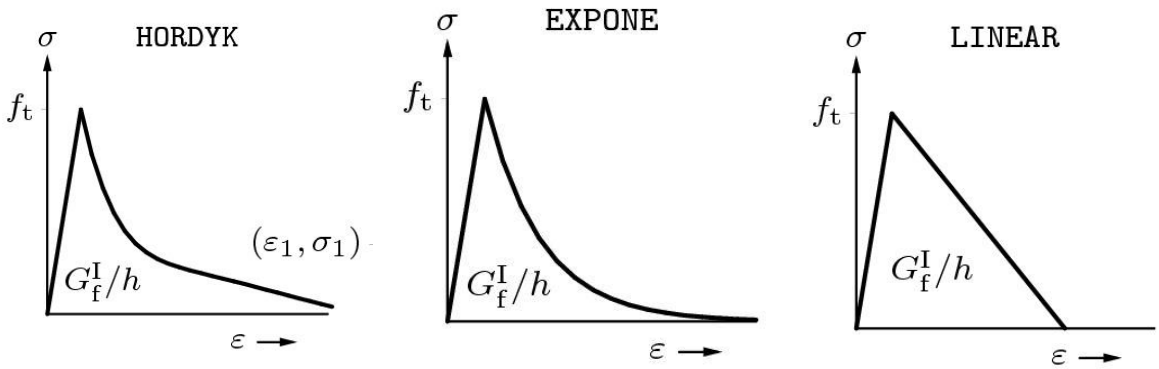

Figure 4-16 – Tension softening functions: Hordijk (left), Exponential (centre) and Linear (right) [25]

The tension-compression interaction, namely the reduction of the compressive strength due to lateral cracking, is taken into account, as the guidelines [26] suggest, by using the reduction model of Vecchio and Collins from 1993, with a value of 0.4 as the lower bound of the reduction curve. For the Poisson's ratio reduction due to cracking, a damaged based reduction model was chosen, meaning a decrease of the ratio with increasing damage due to cracking.

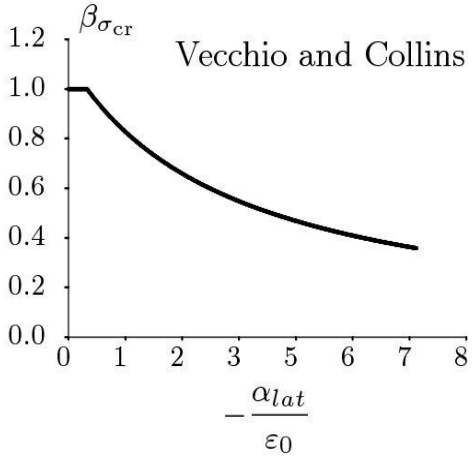

Figure 4-17 – Vecchio and Collins reduction factor due to lateral cracking [25]

The compressive behaviour of concrete (crushing) can also be modelled in a high variety of ways, as DIANA offers again a wide range of predefined functions to account for this type of material behaviour. According to Rijkswaterstaat's guidelines [26], a parabolic stress-strain diagram with a softening branch should be used in order to limit the maximum compressive stress. In order to assess their impact, both a parabolic and an ideal (constant) curve were used, the outcome showing a considerably better behaviour in case of the parabolic function. This will be presented in the subsection regarding the calibration of the model. The increase in compressive strength due to the lateral confinement is taken into account by using the model proposed by Selby and Vecchio. For the parabolic curve it was necessary to determine the compressive fracture energy which was done by consulting the guidelines [26]:

$$G_C = 250 * G_F \quad [26]$$

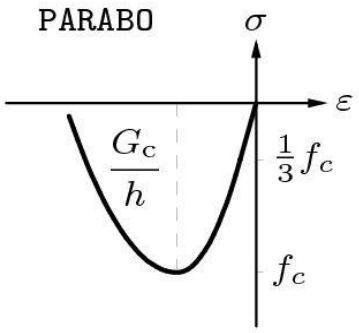

Figure 4-18 – Parabolic compression curve [25]

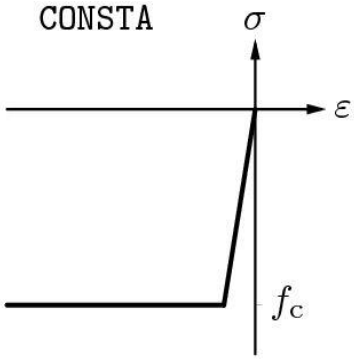

Figure 4-19 – Ideal (constant) compression curve [25]

The characteristics of the constitutive model for concrete are summed up in Table 4-1:

Table 4-1 – Properties of the constitutive model for concrete

Element class	Regular plane stress
Material class	Concrete and Masonry
Model for concrete	Total strain based crack model with rotating cracks
Elasticity modulus	39 GPa
Poisson's ratio	0.15 or 0.20
Mass density	2500 kg/m^3
Tensile curve	Hordijk, Exponential or Linear - crack energy
Tensile strength	5.41 MPa
Tensile fracture energy (G_F)	0.15 N/mm
Reduction due to lateral	Vecchio & Collins '93 model; lower bound factor: 0.4
Poisson's ratio reduction	Damage based reduction model
Compression curve	Parabolic or Ideal (Constant)
Compressive strength	65 MPa
Compressive fracture energy	37.5 N/mm (250 x G_F)
Stress confinement	Selby & Vecchio model

4.2.5.2 Reinforcing steel

For the reinforcing steel, the recommendation from Rijkswaterstaat [26] states that an elasto-plastic material with hardening should be used, where the elastic limit is represented by the steel's yield strength.

In S. Amir's thesis, tests were conducted in order to determine the properties of the reinforcing steel, properties such as the mean yield and ultimate tensile strengths and the modulus of elasticity. Although no hardening was considered for the FEA model from the PhD thesis [14], based on the determined properties, a hardening branch was considered for the material model of this thesis. As it was done for concrete, also in the case of the steel the same material properties would be used in order to obtain results close to the experimental ones and to the ones from the PhD's FEA.

Component	Property	Value	Units
Deck slab and transverse beams	Mean yield strength, f_{sy}	525	MPa
	Mean ultimate tensile strength, f_{su}	580	MPa
	Modulus of elasticity, E_s	200000	MPa

Figure 4-20 – Reinforcing steel properties from S. Amir's PhD thesis [14]

The plastic behaviour of the reinforcing steel, which in DIANA was modelled as an embedded bar, was defined using the Von Mises plasticity model for the yielding of the reinforcement, having a total strain - yield stress criterion. Within the model, the hardening branch was specified based on the previously determined material properties. In the analyses, two values for the ultimate strain were considered, 5.5% (minimum value from the tests) and 7% (considered average value of the tests) but no influence was observed on the behaviour of the model. In order to be sure that there will be no problems related to the iterative process during the finite element analysis, an abrupt descending branch was provided to the stress-strain diagram of the steel.

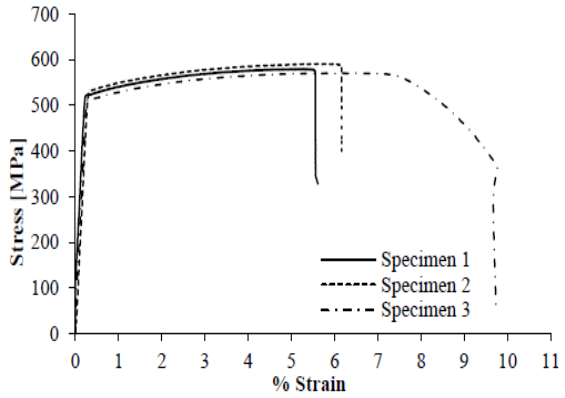

Figure 4-21 – Strain curves of steel from the experimental program [14]

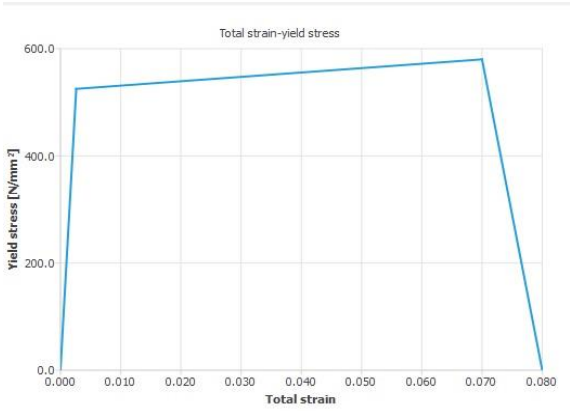

Figure 4-22 – Stress-strain diagram used for the FEA model of the Master's Thesis

In DIANA also a hypothesis for hardening must be considered, therefore a strain hardening hypothesis was chosen. For the hardening type an isotropic hardening was considered.

The properties of the reinforcing steel used for the FEA model are summed up in the following table:

Table 4-2 – Properties of the constitutive model for reinforcing steel

Class	Reinforcement and pile foundation
Material model	Von Mises plasticity
Elasticity modulus	200 GPa
Plastic hardening	Total strain – Yield stress
Yield stress	525 MPa
Ultimate stress	580 MPa
Strain at yield stress	2.625×10^{-3}
Strain at ultimate stress	7% (0.07) or 5.5% (0.055)
Hardening hypothesis	Strain hardening
Hardening type	Isotropic hardening

4.2.5.3 Prestressing steel

Since the prestressing load was applied on the FEA model as an external lateral load, the modelling of the prestressing bar was done just to be in accordance with the real structure. As a consequence, the bar was modelled as a reinforcing bar, having however different properties than the reinforcing steel. For this bar, a higher yield strength (equal to the 0.1% proof stress for Y1100H type of steel used in the structure) and a higher modulus of elasticity were considered. Although the Von Mises plasticity was taken into account, no hardening was considered.

The properties of the "prestressing" steel used for the FEA model are presented in the following table:

Table 4-3 – Properties of the constitutive model for prestressing steel

Class	Reinforcement and pile foundation
Material model	Von Mises plasticity
Elasticity modulus	205 GPa
Plastic hardening	Total strain – Yield stress
Yield stress	900 MPa

In the real structure the prestressing bars were not bonded to the concrete since they had a plastic tube through which they passed, with the tube remaining not grouted after the bars were installed and subsequently tensioned. Nevertheless, analyses were performed considering this bar both bonded and not bonded and the results will be presented and discussed in the section that deals with the calibration of the FEA model.

4.2.5.4 Steel for plates

Like it was previously mentioned, the steel plates used at the loading positions and at the supports were added to the model in order to avoid stress concentrations and a premature failure, assuring a proper force transfer to the concrete element. The behaviour of these plates was not a part of the object of the study, consequently the material for them was considered to have only a linear elastic behaviour.

The properties of the steel plate material are presented below:

Table 4-4 – Properties of the constitutive model for the steel plates

Element class	Regular plane stress
Material class	Steel
Material model	Linear elastic isotropic
Elasticity modulus	200 GPa
Poisson's ratio	0.3
Mass density	7850 kg/m^3

4.2.5.5 Interface

The interface was used between the steel plates and the concrete element for the same reason of ensuring that there will be no stress concentrations at the points where the loads were applied. For the interface material to be able to do this, a very high stiffness modulus in the normal direction was assumed, combined with a very low shear stiffness modulus. The width of the interface (on Z direction) was assumed to be equal to the one of the steel plates (200 mm). For the determination of the two stiffness's the following formulas were used:

$$K_n = \frac{E_s}{h} * 1000 \quad \text{– Normal stiffness modulus}$$

$$K_s = \frac{E_s}{h*1000} \quad \text{– Shear stiffness modulus}$$

E_s is the modulus of elasticity of steel and h is the dimension of the discretized element.

The properties of the interface material are presented in the following table:

Interface type	Connected
Element class	Structural interfaces
Material class	Interface elements
Material model	Linear elasticity
Type	2D line interface
Normal stiffness modulus	2E07 N/mm^3
Shear stiffness modulus	20 N/mm^3

4.2.6 Loads acting on the model

The applied loads that act on the model are described in this section.

- Self-weight of the concrete (γ_c = 25 kN/m^3)

- Prestressing load: the requirement during the experimental programs [14] and [15] was that a constant compressive stress of 2.5 MPa (maximum level of transverse prestressing considered) should be in the deck, thus implying that a force of 100 kN would be applied in each prestressing bar, since the bars were positioned at a distance of 400 mm from each other and the deck was 100 mm in height. In the case of the FEA model from this thesis, the applied lateral load was dependent on the assumed effective width of the model and the prestressing bars that were distributed over that width. As a consequence of this, the value of the applied lateral load varied with the value of the considered effective width. For a width of 1.95 meters, a lateral load of 487.5 kN was applied (on both sides of the model).

- Point or distributed load / Imposed displacement: The applied point load (or distributed load if it was applied over the whole length of the loading plate) had a value of 335 kN since this was the mean force at which the deck failed during the static tests (according to research on fatigue [15]). For the imposed displacement analyses, a vertical displacement of 5 mm was considered to be sufficient, this value being in accordance with the results from the PhD thesis of S. Amir [14].

4.2.7 Mesh properties

The size of the used mesh was in accordance with the guidelines on nonlinear analysis from Rijkswaterstaat [26]. In order to have a smooth stress field, a minimum of 6 elements over the height should be used. In the case of the FEA model, a number of 10 elements over the height were used. Each meshing element had an in-plane dimension of 10 x 10 mm^2, with the same mesh size being used for all the components of the model. The use of a slightly coarser mesh that would still comply with the guidelines was tried, but the outcome showed no difference.

According to the guidelines, the maximum element size can be determined as follows:

$$\text{Maximum element size} = \min\left(\frac{l}{50}, \frac{h}{6}\right) = \min\left(\frac{1800}{50}, \frac{100}{6}\right) = \min(36, 16.7) = 16.7mm$$

l = 1800 mm (span of model), h = 100 mm (height of model)

Since the maximum allowed size of the element was 16.7 mm and requiring at least 6 element over the height, the choice of having 10 element of 10 mm over the height of the FEA model complies with the requirements. There is no requirement for a minimum size of the element.

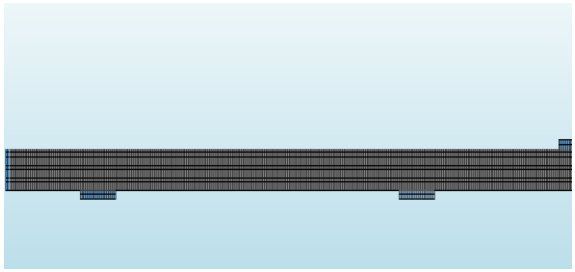

Figure 4-23 – Meshed FEA model, presented half due to symmetry

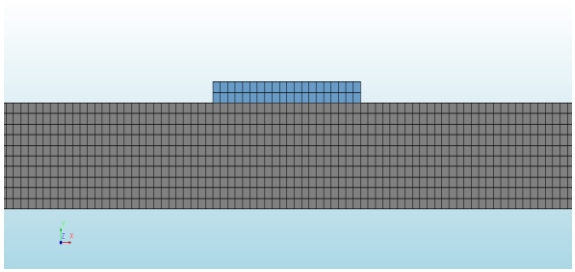

Figure 4-24 – Close-up of the mesh for assessing the discretization elements

4.2.8 Features of the performed analyses

In order to assess the behaviour of the finite element model under the loads described in subsection 4.2.6, three types of analyses were performed: linear, nonlinear and phased, with the mention that the latter comprised a series of nonlinear analyses carried out in succession.

- The linear static analysis was mainly performed in order to see whether the model would give reliable results that could be hand checked, thus being able to assess if the model was behaving in a correct manner. In *Annex 2* such hand calculations will be presented alongside the values obtained following the linear analysis from DIANA and a comparison between them will be made.

- In case of the nonlinear analysis, this represents the main point of interest for the FEA since, based on it, the fatigue behavior of the structure will be subsequently evaluated. By using such an analysis, the properties of the material can be altered in a way that a fatigue type of loading can be simulated and the impact on the structure can be assessed. The main characteristics of the performed nonlinear analyses are presented and discussed in the following part of this section, with them complying with the guidelines of Rijkswaterstaat [26] and being in accordance with the numerical analysis part of the previous research program [14].

  For the FEA model, a physical type of nonlinearity was considered, this referring to how the material behaves. Effects such as plasticity, creep or cracking were taken into account by DIANA.

  Within the analysis, the self-weight and the prestressing load were applied in this order in one loading step each, before the external load was applied. The external load, whether it was a point load, a distributed load or an imposed displacement, had a number of 100 loading steps which were equal in size. This number was chosen in order not to have a too high increase in the force that could lead to an early failure of the FE model.

  It was determined that the model subjected to a point or distributed load having the arc-length control as an incremental procedure gave the best results in terms of the model's

capacity. This aspect will be emphasized more in the calibration related section of this chapter.

The arc-length method, that can adapt its step size depending on the results in the current step, is used to overcome too large displacement predictions that emerge when a load increment is prescribed. By using this method, behaviours such as snap-through and snap-back, that otherwise would lead to divergence, can be analysed. The size of the increment is adapted automatically within the iteration process and no longer depends on the one imposed at the beginning of the increment [25].

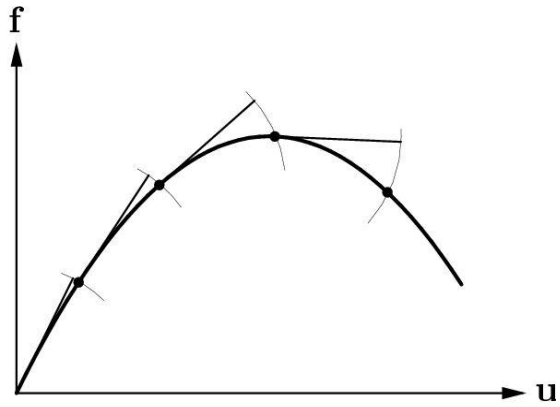

Figure 4-25 – Snap-through [25]

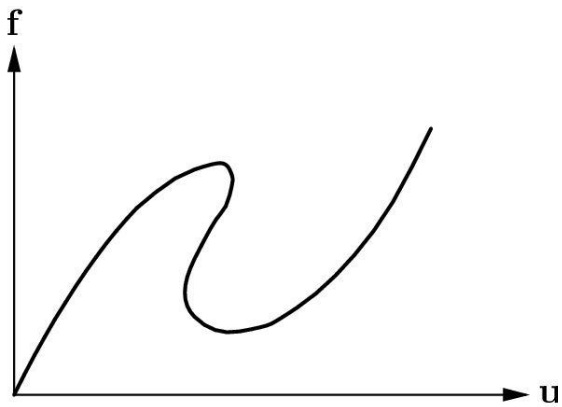

Figure 4-26 – Snap-back [25]

For the iterative method, the modified Newton-Raphson was used, considering a maximum of 50 iterations per loading step. This method, although it may require a higher number of iterations, is faster than the regular Newton-Raphson and can converge in situations where the latter is not able to do that, evaluating the stiffness at the start of the increment and not for every iteration [25].

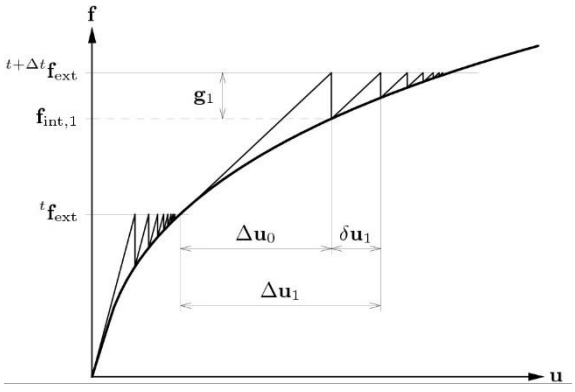

Figure 4-27 – Modified Newton-Raphson method [25]

The convergence norms for an applied load were displacement and energy based, whilst for an imposed displacement they were force and energy based. With respect to the tolerances, their values were taken from the guidelines [26]: 0.001 for an energy norm and 0.01 for an unbalanced force.

- The phased analysis was used in two situation. First, when an imposed displacement was acting on the model and there was a need for adding an extra support at the location of the displacement in order to apply this deformation. Second, when a series of nonlinear analyses had to be performed successively, with the materials (concrete) within the model having their properties changed. This was done in order to simulate the effect of fatigue. Basically, a phased analysis was used when either geometrical or material changes had to be done to the model within the same extended analysis, with the results from the previous phases being used as initial values for the next phase.

4.3 Calibration of the FEA model

In order to calibrate the FEA model as accurate as possible, the results from the previous experimental programs, [14] and [15], were needed for comparison. To achieve this, the first step was to obtain from the PhD thesis of S. Amir [14] the data required to plot the force – deflection behaviour of the structural system during the experiments and from the FEA analysis. Since this data was not directly available, use was made of one of the graphs (from an image) from the thesis, this containing the previously mentioned information that was of interest. A software named ENGAUGE DIGITIZER was used to recover the data points from the said graph that was in the image file. Based on those points, a new graph was created and the plotted curves (reference) served as the basis for comparing the results obtained from the FEA model. The graph taken from the PhD thesis [14] was created for a transverse prestressing level (TPL) of 2.5 MPa and an applied single point load at the mid-span of the deck slab, the same characteristics being valid for the FEA model of this thesis.

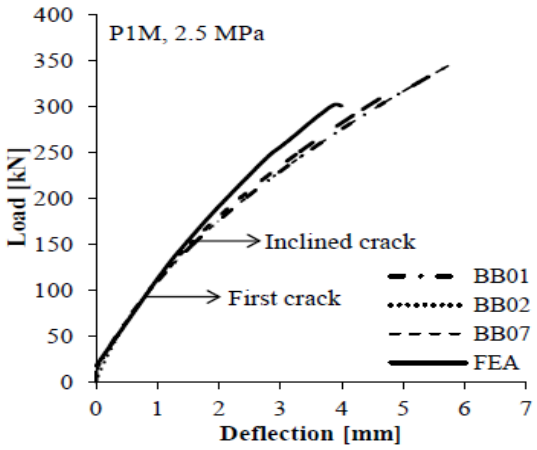

Figure 4-28 – Load-deflection behaviour for a single point load at mid-span and a TPL of 2.5 MPa [14] (image used to obtain Graph 4-2)

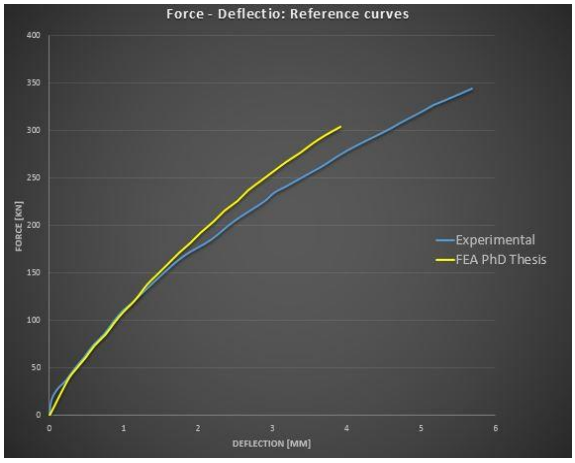

Graph 4-2 – Load-deflection behaviour following from the experimental program and the FEA of S. Amir

Having managed to obtain the behaviour of the structure during both the experiment and FEA 3D model (the reference curves), the following step was to perform a static calibration of this thesis's FEA model, before moving to the assessment and prediction of the fatigue damage. The goal was to create a model that would behave similar to the cases already

mentioned and depicted in Graph 4-2. During this process, it was noticed that a number of parameters had an impact on the model's behaviour and they will be individually discussed in the following. It must be noted that the influence of some of these parameters was assessed before reaching the model that was considered to have the best behaviour, therefore the variables within these transition models might have had different values than the final ones, but is important to understand that here the sensitivity of the model was assessed with respect to these parameters.

It must be mentioned that for all the graphs that will be presented in this Master's Thesis and are related to the force-deflection behaviour of the model, only the external applied force was considered for this plots. The contribution to this behaviour of the self-weight or prestressing load was disregarded, due to its small impact and because it would have had the same effect on a model with the same width but a variation in other parameters.

4.3.1 Initial model based on the width from the experimental programs

This subsection presents the model that ensued by following the results and the data from both experimental programs, [14] and [15]. Although it was labelled as the *initial model*, this was because it was the first complex model that included all the parameters from the research, the previous models being very simplistic when related to this aspect.

Having established how the in-plane geometry of the FEA model would be defined - its shape, steel plates and position of bars - a realistic value for the considered effective width was necessary for the plane stress model. After studying S. Amir's thesis [14] and the report on the fatigue tests [15], a width (in Z direction) of 1.40 meters was considered to be in good correlation with the real experiments. This choice was based on assessing the observed cracking pattern and punching cone in the previously mentioned sources, but it must be noted that those were real life experiments having a three dimensional stress state.

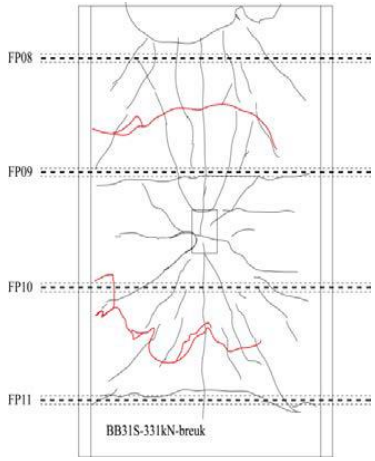

Figure 4-29 – Cracking pattern due to static loading [15]

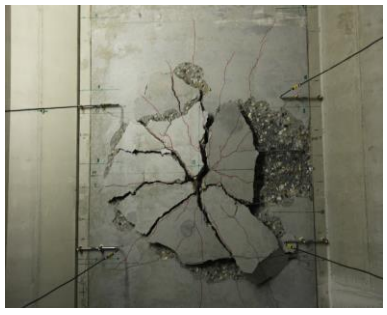

Figure 4-30 – Failure due to fatigue loading [15]

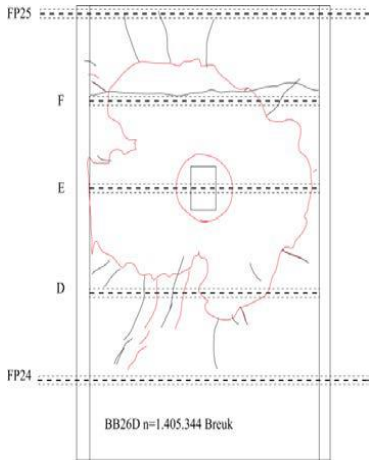

Figure 4-31 – Punching cone contour and crack pattern due to fatigue loading [15]

As a consequence of the chosen effective width, other parameters such as the area of reinforcement or the lateral prestressing load had to be adjusted accordingly. For instance, in order to have a 2.5 MPa stress level in the concrete, the lateral load had to be increased to 350 kN. As reinforcement, 8Φ6 bars were considered at each side (top and bottom) and 4Φ15 for the area of prestressing steel. Regarding the supports, the left one had fixed translations on both X and Y axes, whilst the other supports had a fixed translation only on the Y axis, trying to replicate the conditions from S. Amir's thesis [14]. It must be mentioned that whilst in the case of S. Amir's research the supports were considered at the bottom side of the longitudinal girders ends, in the FEA model of this thesis they are considered at the level of the deck since only this element was modeled. The external force had a value of 335 kN as it was described in section 4.2.6. If this was distributed over the length of the plate, its value would be 1675 N/mm.

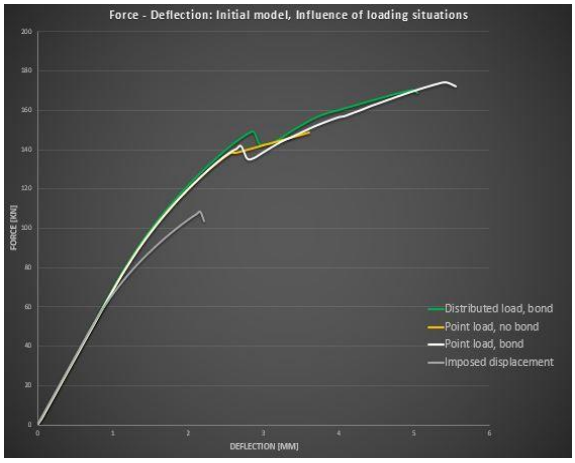

Graph 4-3 – Force-deflection behaviour of the initial model for different loading situations

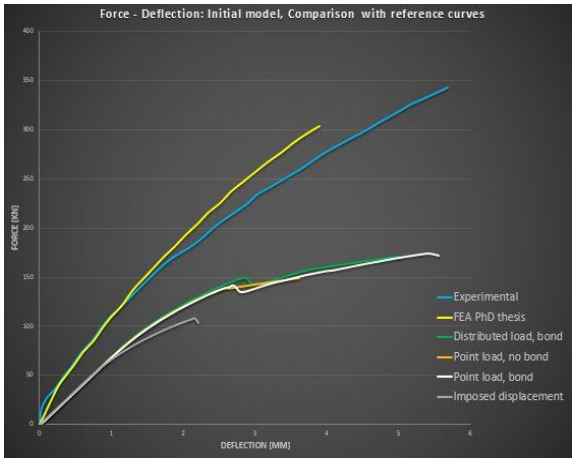

Graph 4-4 – Different force-deflection behaviours of the initial model compared to the reference curves

In the above graphs, the force-deflection behaviour of the initial model is presented. A series of analyses were conducted within which the external load was applied in different manners: as a point load acting on the loading plate in the middle of the span, as a uniformly distributed load acting over the length of the steel plate or as an imposed displacement. Another important parameter studied was the bond of the prestressing steel and its impact.

4.3.1.1 Behaviour of the initial model

Following the analyses, it was very clear that the behaviour of the initial model was far from the experimental and the 3D FEA results, especially in terms of initial stiffness and capacity. However, a series of observations were made which allowed for the continuous development of the model.

It was observed that an applied point load, in an analysis with arc-length control, gives better results in terms of capacity than an applied uniformly distributed load (UDL). At the opposite end, an imposed displacement gives by far the lowest estimation of the model's capacity.

Although when a UDL is applied and the first part of the force-deflection curve before the drop is higher, in the end the capacity of the model that has an applied point load surpasses the UDL one. The reason for the drop in the curve is that, due to a substantial increase in the crack width, the steel consequently reaches and exceeds the yielding value of the stress at that particular load step (value of the force). The stress in the concrete increases too, but not significantly. The model fails and the analysis stops when the strain of the steel exceeds its ultimate limit of 7% and the equivalent ultimate stress, with the failure mode being of flexural nature.

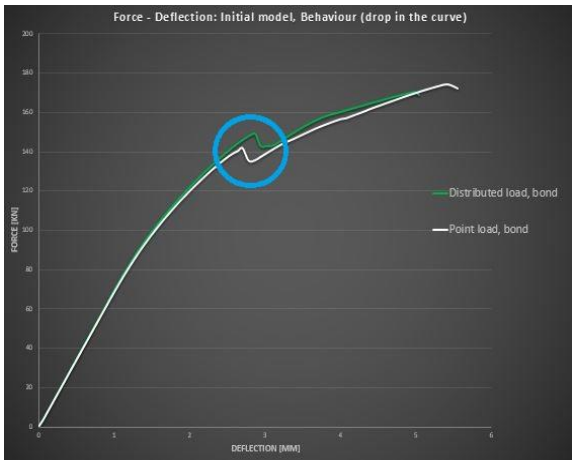

Graph 4-5 – Behaviour of the initial model due to the exceeding of the yield stress of steel

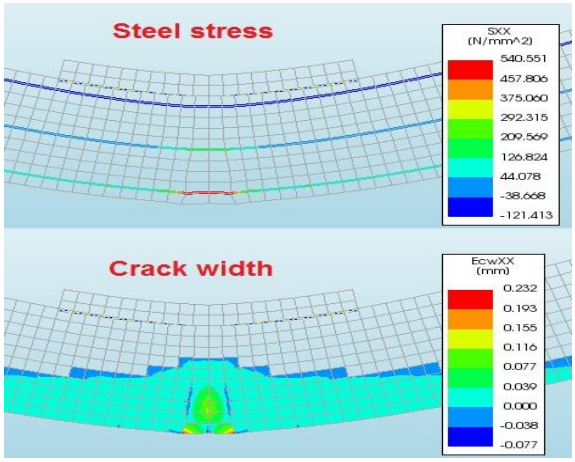

Figure 4-32 – Increase in the steel stress over the yield value as a consequence of the increase in crack width

An explanation for the higher value of the force before the drop in case of the uniformly distributed load might be that, since the load is applied on the whole plate and not concentrated in one single point, it will take an additional increase of the force in order to make the steel yield at two locations instead of one (the plate's extremities).

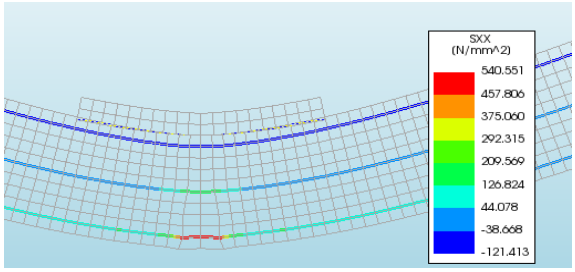

Figure 4-33 – Yielding of steel at one location in the initial model loaded by a point load

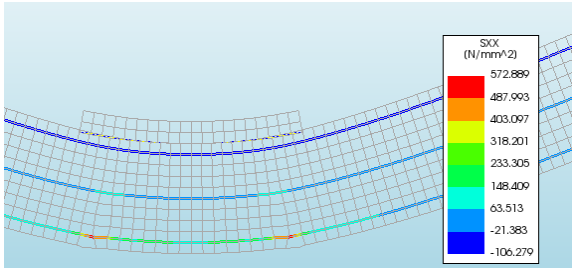

Figure 4-34 – Yielding of steel at two locations in the initial model loaded by a distributed load

Another observation that was made involved the influence of the prestressing bar. If this was considered as being bonded, which was not the case in the experiments, a significant increase in the capacity and the ductility of the model would occur. Based on this observation, it was decided to further study this behaviour and see whether or not, by making such an assumption, the behaviour of one of the models would come close to the actual behaviour described in references [14] and [15]. The influence of the bond can be assessed in Graph 4-6.

Another parameter that was varied was the ultimate strain of the reinforcing steel. Its increase from a value of 5.5% to a value of 7% had as effect an extremely small increase in the ductility of the model. Overall it can be concluded that the variation of the ultimate steel strain has no major impact on the behaviour of the model. This can also be seen in Graph 4-7, with both of the curves overlapping each other.

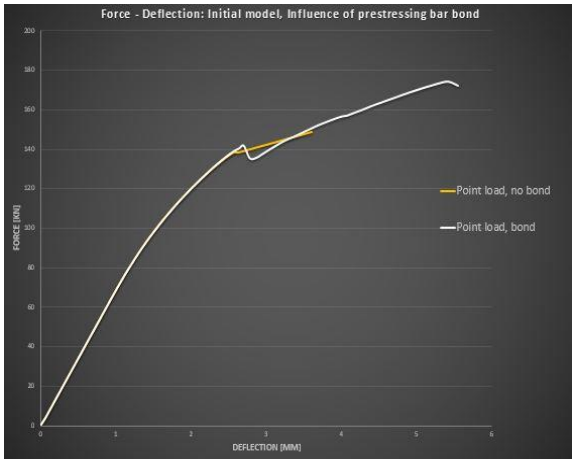

Graph 4-6 - Influence of the prestressing bar's bond on the behaviour of the initial model

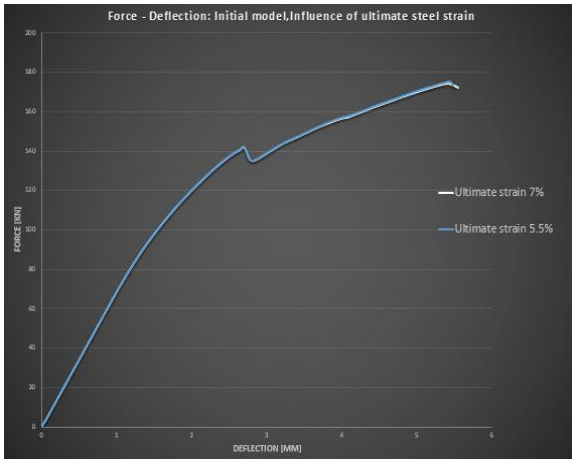

Graph 4-7 – Influence of the ultimate steel strain on the behaviour of the initial model

One important observation concerns the sensitivity of the model to the value of the applied force and number of loading steps, seeming that these influence substantially the force-deflection behaviour. Although a high number of equal loading steps (100) was considered especially to avoid higher load increments that could lead to early failure, it appears that for the parameter combination within the model, there is a range of applied force values for which this early failure manifests itself. This can be assessed in Graph 4-8.

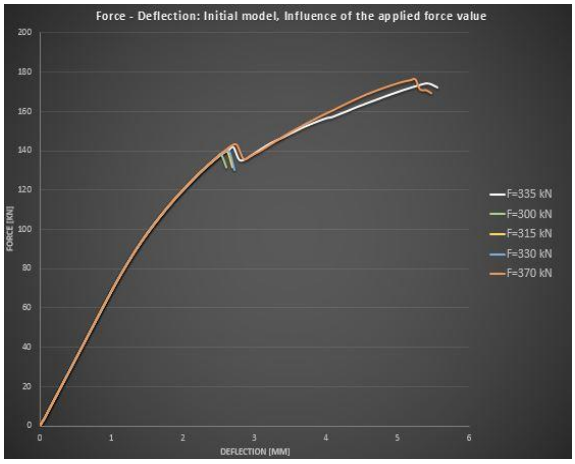

Graph 4-8 – Influence of the value of the applied force

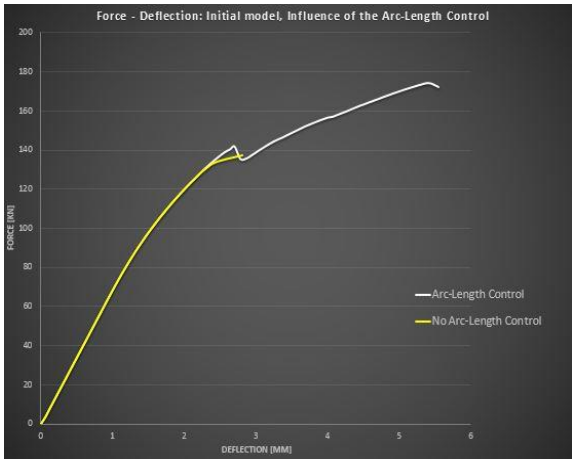

Graph 4-9 – Influence of the arc-length control method

Having an applied external force, it was necessary to use the arc-length method for the nonlinear finite element analysis in order to have convergence for as many load increments as

possible and avoid or delay the occurrence of divergence. The lack of the arc-length method from the analysis setup will lead to early failure. Its influence is presented in Graph 4-9.

Another important remark refers to the development of the compressive membrane action within the model. As it was thought, this phenomenon occurs in the deck slab and is a result of slab's supporting conditions and restraints. The CMA can be observed in the figure below:

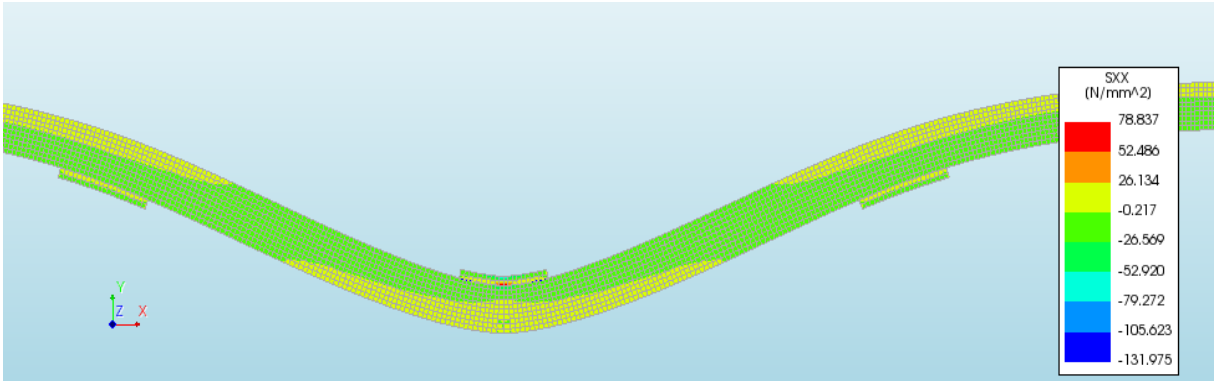

Figure 4-35 – Development of the compressive membrane action (CMA) within the initial FEA model

4.3.1.2 Conclusions regarding the initial model

This subsection presents briefly the main conclusions that followed from the series of analyses performed on the initial complex model, all of these representing the main basis for improvement and further development of the FEA model, with the goal of creating one that depicts a behaviour similar to the reference curves.

- The failure of the model is of flexural nature
- The phenomenon of compressive membrane action develops within the FEA model
- The initial stiffness and overall capacity of the model must be considerably improved in order to obtain a behaviour similar to the reference curves
- Applying a point load (concentrated force) gives the best results in terms of capacity and ductility
- The use of the arc-length method is mandatory to avoid premature failure when a point load is applied to the model
- Considering the prestressing bar as being bonded, assumption that does not reflect the situation within the real structure, increases substantially the behaviour of the model

Most of the parameters assessed in subsection 4.3.1 will also be analysed with respect to the final FEA models and it will be shown that they influence the model's behaviour a manner similar to what was described previously.

4.3.2 Impact of the considered effective width

Following the analyses performed on the initial complex model, it was concluded that a substantial increase in the model's initial stiffness is required. To achieve this, the effective width of the FEA model, which emerged as a fundamental parameter, was increased step-wise, assessing its impact for each individual value. Together with the increase of the width, also an increase in the areas of reinforcing and prestressing steel and the prestressing load was performed, since they were tightly correlated to each another. The areas of steel because of the number of bars distributed over the considered width and the prestressing load due to the fact that a uniform compressive stress of 2.5 MPa had to be achieved in the deck slab.

Such a realistic value, in terms of its magnitude, for the effective width was considered in order to have a behaviour for the FEA model that would be as close as possible to the ones determined in the previous research [14]. Taking into account that the used model already had a series of major assumptions that influenced its behaviour, it was though that a simplification in terms of width size (effective width) would lead to certain drawbacks. The FEA model tried to replicate on a 1:1 scale the real structural system so that a similar behaviour would be obtained. Using a two-dimensional model to reproduce a three-dimensional stress state proved already its limitations, therefore it was tried to avoid the potential disadvantages and insufficiencies that might have occurred by using a scaled down value for the width. In essence, it was thought that by reproducing the life-sized structure, the stress state and the behaviour would be more accurate.

By successively varying the value of the width it was determined that the plane stress model in DIANA has a size limitation of 2 meters with respect to this. According to the manual, the plane stress model is dependent on the geometry, not allowing the width to be too large compared to the in-plane dimensions, as stated in subsection 4.2.4.1. In the end, the final width of the FEA model, as previously mentioned in subsection 4.2.2, had a value of 1.95 meters, this giving the best behaviour with respect to the reference curves. The equivalent steel areas are the ones presented in subsection 4.2.3 and the prestressing load in subsection 4.2.6.

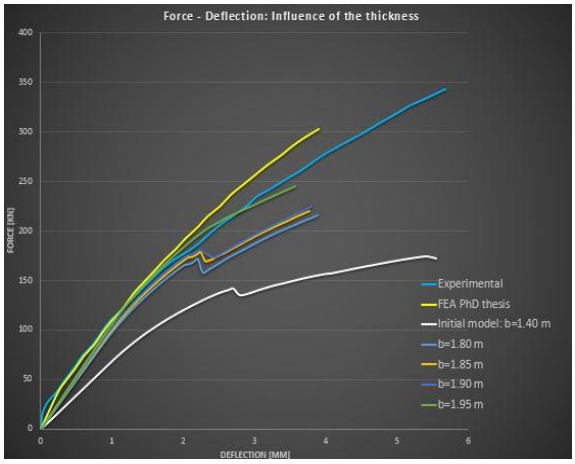

Graph 4-10 – Impact of the effective width on the FEA model's behaviour

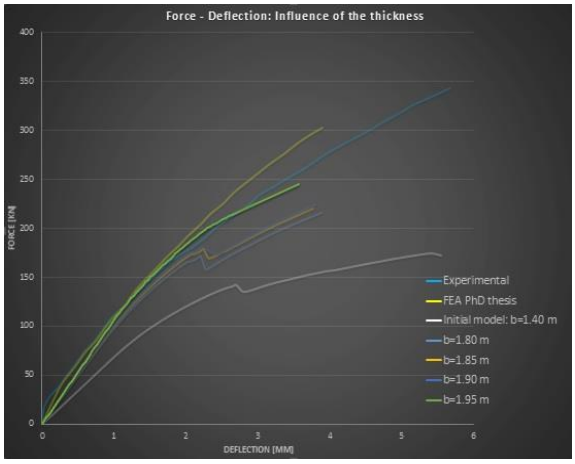

Graph 4-11 – Best behaviour obtained for a width of 1.95 meters

The previous graphs present the impact of the considered width on the behaviour of the FEA model, with the substantial increase of the initial stiffness being extremely clear.

4.3.3 Impact of the degrees of freedom at the supports

After studying the behaviour of the initial model, modifications to the supports were performed since it was obvious that the results were very far from those obtained by S. Amir [14]. It must be mentioned that in the actual experiment (S. Amir), as part of the structural system, two end cross-beams were present at each end of the concrete deck, these completely restraining its horizontal movement. As a consequence, the translations on both directions (X and Y) for all supports were blocked, this action resulting in a substantial increase in the initial stiffness of the FEA model and a more realistic behaviour that was similar to the actual structure. As it was outlined in subsection 4.3.1, in the real structure the supports were considered at the bottom side of the longitudinal girder's ends, whilst the deck was overall monolithically connected (the flanges of these girders with the concrete cast in-situ between them). This gave a higher degree of restraint to the deck, considering that only rotations were allowed at the location of the girders. Since in the FEA model the supports were part of the deck, the assumption of translations blocked on both directions seems sound, allowing only rotations. The influence on the model of the previously mentioned rotations will also be analysed later in this section.

The downside of fixing both translations meant that the required compressive stress of 2.5 MPa within the concrete slab was no longer achievable since the supports restricted the transfer of the prestressing load across the slab. Nevertheless, a compressive stress of 1.7 MPa on average was obtained due to the bending moment resulted at the supports from the action of the laterally applied prestressing load. The small loss in the compressive stress was deemed to be acceptable, considering the substantially improved behaviour of the FEA model.

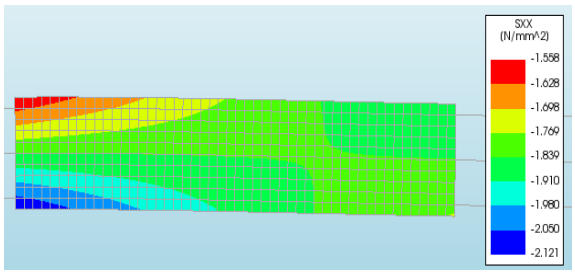

Figure 4-36 - Compressive stress in the deck slab after blocking both translations at the supports

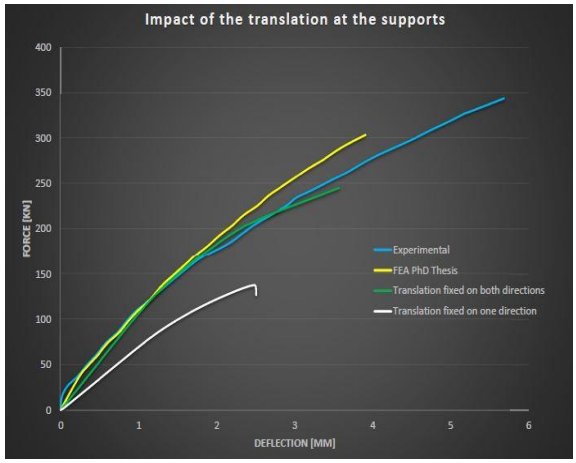

Graph 4-12 – Impact of the translation restraint at the supports

4.3.4 Impact of the prestressing bar's bond

As it was observed for the initial model, whether the prestressing bar is considered bonded or not has a large influence on the model's behaviour. In reality the bar was not bonded, as it was described in subsection 4.2.5.3, but seeing that it can increase the model's capacity

quite substantially and give a behaviour that is similar to the reference curves, it was decided to create also a model where the prestressing bar is bonded. The outcome was in accordance to what was previously mentioned, obtaining results that were closer to the experimental capacities of the structural system. This is presented below:

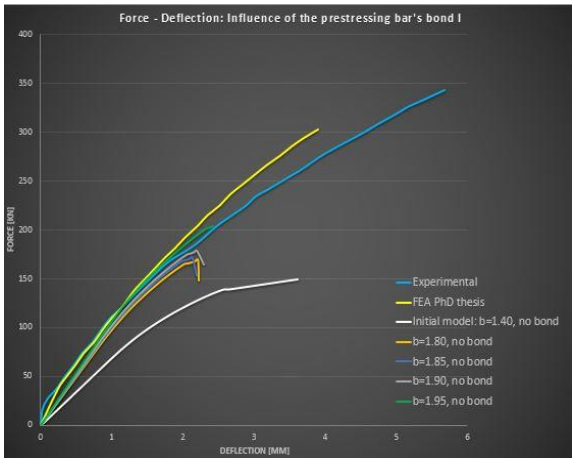

Graph 4-13 – Influence of the prestressing bar's bond on the capacity of the model: no bond considered

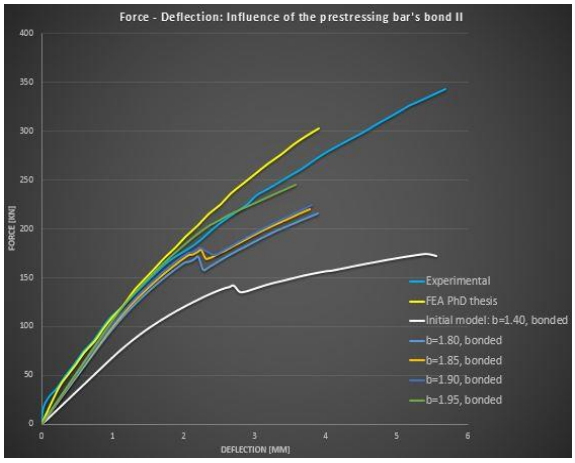

Graph 4-14 - Influence of the prestressing bar's bond on the capacity of the model: bond considered

Another aspect that was also studied was the relevance of modelling the prestressing bar in the situation that this was not bonded to the mother element. Since the prestressing load was applied to the model as an external lateral load and also because there would be no contribution in terms of stiffness or capacity when the bar would be modelled without bond, it seemed that the absence of the prestressing bar element from the FEA model would be justified. The performed analyses showed indeed that the behaviour of a model that does not contain the prestressing bar is similar to that of a model that contains the bar, but this is not bonded.

In the following graph, the behaviour of the FEA model with different widths and having the prestressing bar modelled with no bond or not modelled at all, can be observed. It is clear that for the same width, the force-deflection curves are identical and overlap each other for both previously mentioned situations.

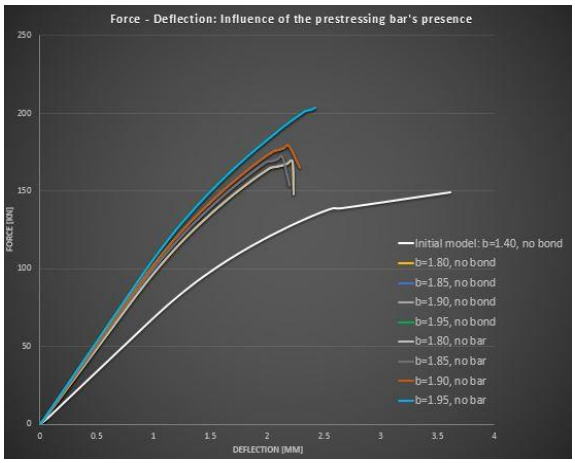

Graph 4-15 – Behaviour of the FEA model without the prestressing bar and with the bar not being bonded

4.3.5 Impact of the Arc-Length Control (ALC) method

The arc-length control method, assessed also for the initial model in subsection 4.3.1.1, was used within the nonlinear FEA in order to avoid early divergence during the iterative process. Its impact was clear following the analyses, this method assuring the convergence of a higher number of incremental steps. As a direct outcome from the usage of ALC it can be mentioned the higher capacity of the FEA model that resulted from the analyses. For the final width of 1.95 meters such a study was performed and the result is presented in Graph 4-16.

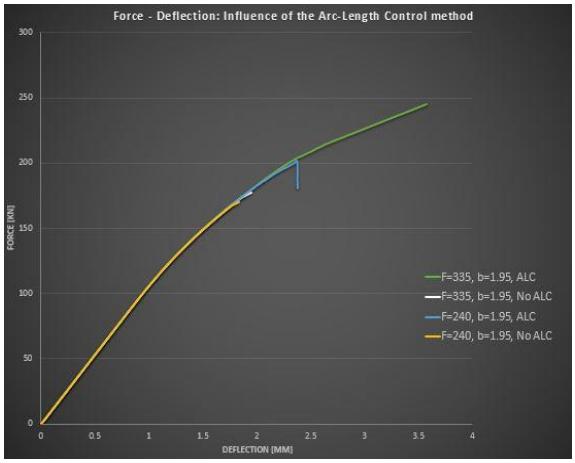

Graph 4-16 - Influence of the Arc-Length Control method; final effective width (1.95 m) considered

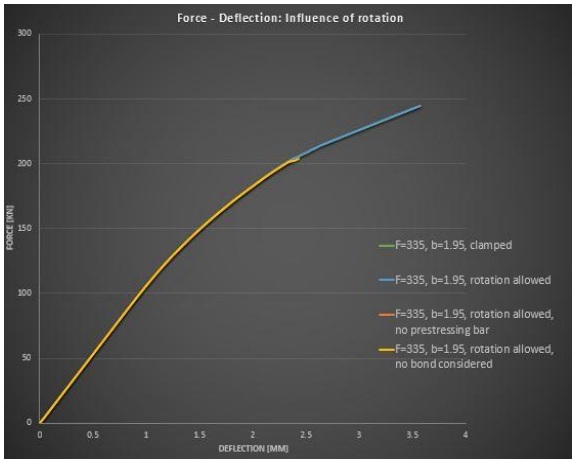

Graph 4-17 - Influence of the rotation at the supports on the behaviour of the FEA model

4.3.6 Impact of the rotation at the supports

Due to the simplifications, in terms of modelling of the structure, that were already mentioned in this section, at the location of the supports in the FEA model the translations were blocked on both directions, whilst the rotations were permitted. This was done in order to replicate more accurately the real life situation.

Because an increase in capacity and stiffness were the goals throughout the calibration stage of the FEA model, a number of analyses were also performed by assuming that the model is fully clamped: all translations and rotations were blocked. However, the outcome was identical to the situation where rotations were permitted, not existing any difference in the behaviour of the model. In Graph 4-17 the impact of the rotation can be assessed for an applied force of 335 kN (mean static strength from the experiments) and different configurations of the model, with the graphs overlapping each other (2 pairs).

4.3.7 Impact of the compressive behaviour of concrete

In order to assess the compressive behaviour of concrete, two models were tested, as it was mentioned in subsection 4.2.5.1. The guidelines from Rijkswaterstaat [26] recommend that a parabolic function with a softening branch should be used. Apart from this model, a constant

one (ideal: elastic-perfectly plastic) with no softening branch was also tested since such a function was used by S. Amir in her thesis [14]. Following the performed analyses it was concluded that a parabolic model would give a better behaviour for this FEA model. This is presented in Graph 4-18.

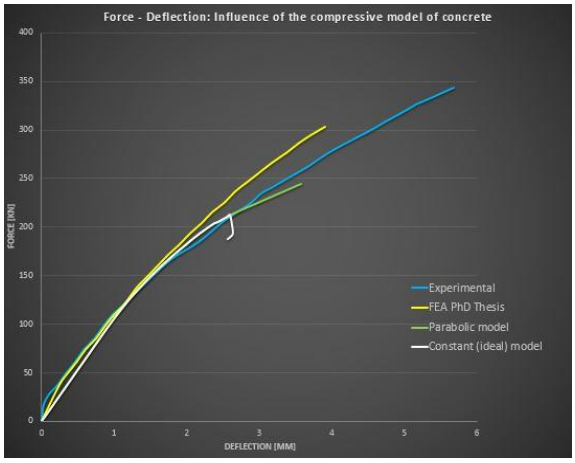

Graph 4-18 - Influence of the compressive model of the concrete on the FEA model's behaviour

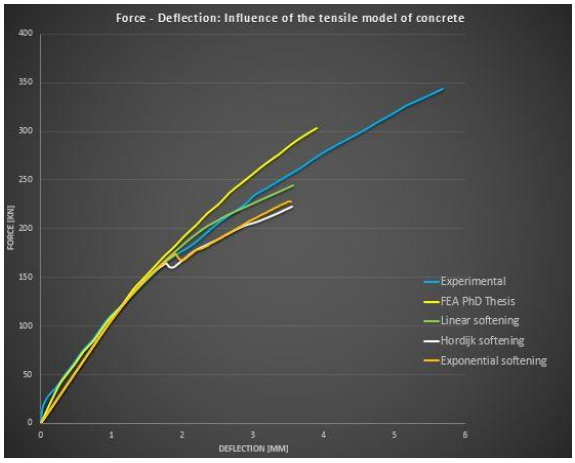

Graph 4-19 - Influence of the tensile model of concrete on the FEA model's behaviour

4.3.8 Impact of the tensile behaviour of concrete

For the tensile behaviour of concrete a series of tension softening functions were considered, as described in subsection 4.2.5.1: exponential softening - which is recommended by Rijkswaterstaat [26], Hordijk softening – used by S. Amir [14] and linear softening. Following a series of analyses performed using each of these functions, the results showed that a linear softening model gives a better behaviour. This can be assessed in Graph 4-19.

4.3.9 Chosen FEA models

After performing an extensive number of analyses and studying the impact of a series of parameters that influenced the behaviour of the FEA model, two final variations of this model were chosen for the fatigue prediction analyses.

The first of these models gave the best behaviour when compared to the reference curves, but, in its case, the assumption of having the prestressing bar bonded to the mother element was made in order to increase the capacity. It was discussed previously that this was not the case with the real structure, but for the purpose of calibrating the model as accurately as possible this assumption was adopted. All the other parameters were in accordance with the real structure. This was deemed as the "best behaviour model" (BBM). The second FEA model used was very similar to the first one, the only exception being that the prestressing bar was not bonded. Since in this case all the parameters, including areas of steel and prestressing load, were in line with the tested structure, this was deemed as the "realistic model" (RM).

The majority of the properties or parameters of these models were presented in section 4.2. Following the calibration process, the other important parameters were obtained and are described in the current section, 4.3. One major parameter that must be mentioned due to its contribution to the stiffness of the model and its overall behaviour is the considered effective width, this having a value of 1.95 meters. The two final models, based on this width, are presented in the graph below:

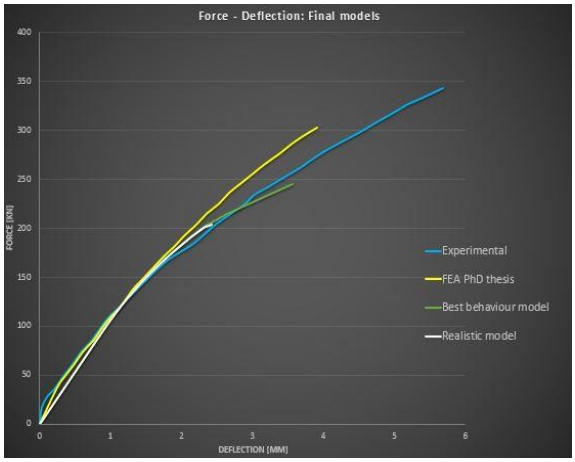

Graph 4-20 - Final FEA models

4.4 Final models and their behaviour

4.4.1 Linear analysis checks

In order to be sure that the general FEA model behaves as intended and it is reliable, a series of hand calculations were performed and their results were compared with the outcomes from the linear analysis performed on the model. For assessing the linear behaviour, the following were checked: vertical deflection, stresses at top and bottom side of the section and the moment of cracking. The results showed a good correlation between the hand-checked calculations and the data obtained from DIANA, this being presented in *Annex 2*.

4.4.2 Capacity of the models

Following the performed nonlinear analyses for the calibration process, it was concluded that the two FEA models selected for the fatigue prediction stage proved to have a lower overall capacity than the reference curves based on the experimental programs [14] and [15]. This was to be expected since the plane stress model refers to a bi-dimensional (2D) stress state, whilst in the real life structure a three-dimensional stress state defines the behaviour. As a consequence, there are limitations to the 2D FEA model and a completely accurate description of the real behaviour is hard to achieve.

Although the externally applied point load had a value of 335 kN, as it was described in subsection 4.2.6, none of the two models was able to reach it. The one that exhibited the best behaviour (BBM) had a final static capacity of approximately 245 kN, this representing 73% of the value from the tests. The second model (RM), having the prestressing bar not bonded, had its capacity equal to approximately 203 kN, meaning 60% of the mean static capacity from the tests [15].

In case of the first model (BBM), divergence occurred during the nonlinear analysis and the iterative process together with the analysis was halted. For the second model, all the load increments converged, but after reaching a peak value, the force started a continuous decrease. This was the moment when the steel exceeded its ultimate stress value, but with the strain remaining below the ultimate limit according to DIANA. This will be presented in the subsection related to the realistic model (RM). For defining this model's behaviour, only the first part of the curve was considered, the second branch being truncated. This is presented in the graph below. The failure modes of both models are assessed in the next subsection.

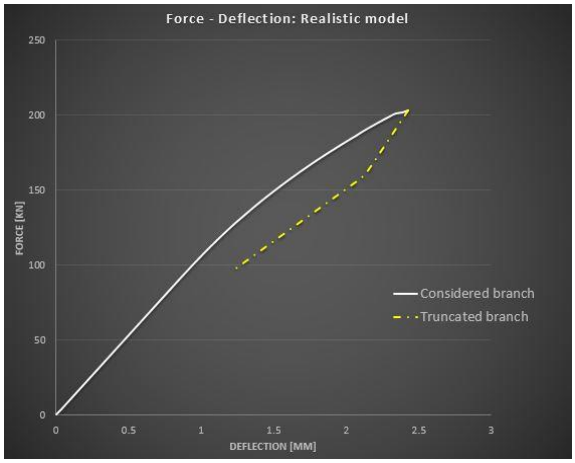

Graph 4-21 – Behaviour of the "realistic model' (RM)

4.4.3 Failure modes

The real structural system, from [14] and [15], failed exclusively through punching shear during all the tests that were performed on it, this being a three-dimensional mode of failure. In case of the FEA model, since this was of a two-dimensional plane stress type, for all the analyses performed, the failure mode was of flexural nature. In the following, the behaviour of both chosen models (BBM and RM) will be presented.

4.4.3.1 Best behaviour model (BBM)

The FEA model that presented the best behaviour (BBM) failed as the stress in the reinforcing steel exceeded the yield limit and almost reached the ultimate value of 580 MPa,

this happening at an applied force of ≈245 kN. The value of the strain increased substantially at failure, to 1.3%, but was still well below the ultimate value of 7%. This large difference might be due to how DIANA considers the strains, calculating an average over the length of one discretized element, with the outcome being a smaller value.

The concrete compressive stress was smaller than its compressive strength, whilst the tensile stress was higher than the tensile strength, with cracking occurring in the initial loading stages at ≈90 kN of the applied force (or 27%). It can be stated that once the concrete has cracked, the steel starts to take over most of the load, with a redistribution of stresses also taking place.

In the case of this FEA model, it was also studied what impact would the choice of presenting the results in the nodes of the plane stress elements or in the integration points have. It was observed that the results that are given in nodes are higher than the ones from the integrations points. This occurs due to the extrapolation that is performed from the integration points to the nodes. When the results are determined in the integration points, DIANA still presents them as being in the nodes. What happens here is that the software takes the results from the integration points and attributes them to the nodes without any extrapolation, therefore having lower values.

The following subsections present the results from the analysis, showing the stresses and strains of steel and concrete, crack widths, deflections, occurrence of CMA.

4.4.3.1.1 Stresses and strains in the reinforcing steel

The following figures present the stress in the steel at the moment of failure, with the values exceeding the yield stress. The difference between the results in the nodes (left figure) and the ones in the integration points (right figure) is clearly visible, having higher values in the nodes of the plane stress element. The reason behind this matter was explained in the previous paragraph.

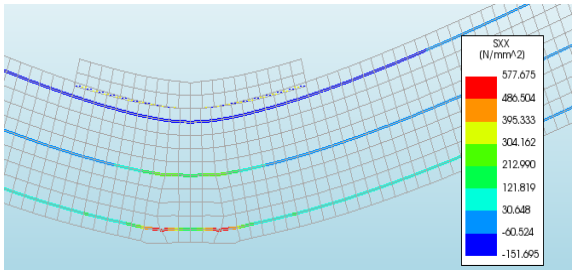

Figure 4-37 – Stresses in the steel at failure (presented in the nodes)

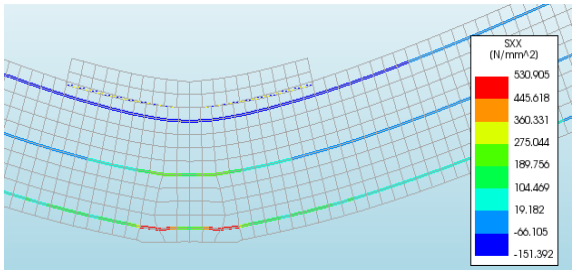

Figure 4-38 - Stresses in the steel at failure (presented in the integration points)

The values of the strains are presented below, in the nodes and in the integration points, with the observations made earlier being valid also in this case. A possible explanation for the low value of the strain at such a high stress was given at the beginning of subsection 4.4.3.1.

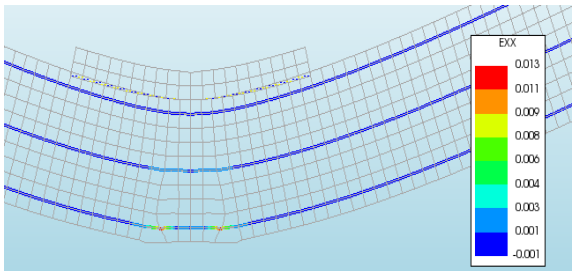

Figure 4-39 – Strains in the steel at failure (presented in the nodes)

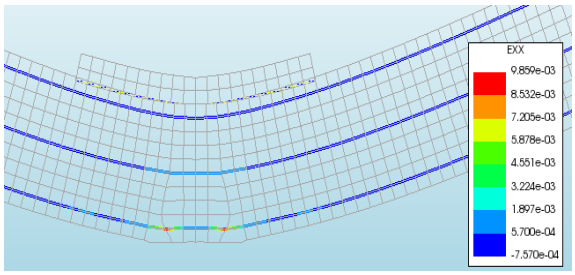

Figure 4-40 - Strains in the steel at failure (presented in the integration points)

The variation of the stress in the steel with the increase in the force was also studied and is presented in the following graph. It can be observed that after a long period of slow and gradual increase, there is an abrupt rise in the value of the stress, up to failure.

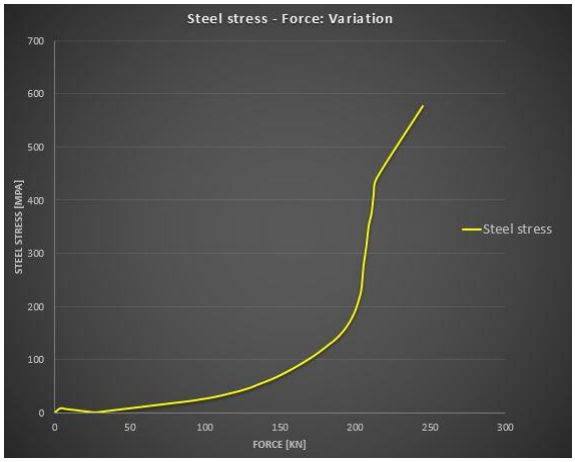

Graph 4-22 – Steel stress variation in the best behaviour model

4.4.3.1.2 Stresses and strains in the concrete

The stresses in the concrete clearly show that high values were reached at the moment of failure, with the increase in the compressive stress being higher than the increase of the tensile one, when compared to the second to last loading step. The compressive strength of the concrete (65 MPa) is not reached but the tensile strength (5.41 MPa) is exceeded by 40% at the moment of failure, with cracking occurring in the early loading stages at an applied load of ≈90 kN. It must be mentioned that in the case of the results given in the integration points, once the concrete cracks, the value of the tensile stress does not change, only the height of the tensile zone. In the following figures only the most relevant part of the deck is presented, which is at the location of the applied load. The loading plate is not included in the plots.

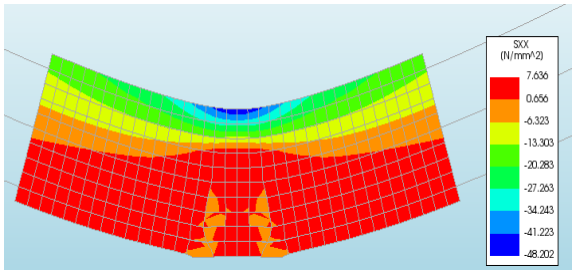

Figure 4-41 – Stress in the concrete at failure (presented in the nodes)

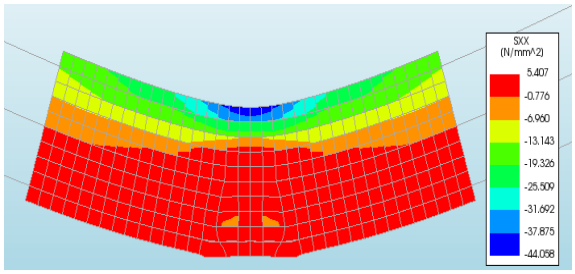

Figure 4-42 - Stress in the concrete at failure (presented in the integration points)

The strains of the concrete are presented below and they clearly show the locations where the cracks were formed. Again, the values presented in the nodes are higher that the results obtained in the integration points. An observation can be made regarding the values in the nodes. Since these are determined via extrapolation, the unrealistic situation when to the strains in a crack a negative value is attributed, can occur. Here the loading plate is included in the plot since in this case it does not have an impact on the results.

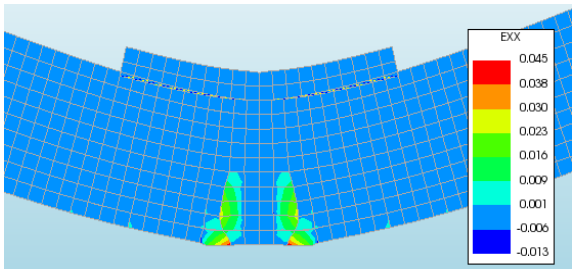

Figure 4-43 - Strain of the concrete at failure (presented in the nodes)

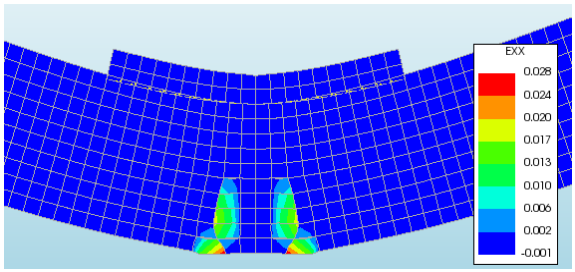

Figure 4-44 - Strain of the concrete at failure (presented in the integration points)

4.4.3.1.3 Crack width

The location of the cracks is in correlation with the strains showed earlier, as anticipated. The way DIANA determines the crack widths is by multiplying the strains with the crack bandwidth (h_{cr}). For a two-dimensional element, the crack bandwidth is equal to the square root of the element's area. Since in this case the element was defined as having a 10 x 10 mm^2 area (subsection 4.2.7), the value for h_{cr} was 10 mm. The resulting crack width can be easily checked by multiplying the values of the strains with 10.

In order to check whether the obtained results have a realistic fundament, reference is made to the tests performed within the research [15]. According to the obtained results in test number BB25, at a loading between 200 and 250, the crack width ranged between 0.35 and 0.5 mm. Subsequently the specimen failed at 330 kN and a crack width of 0.9 mm. For test BB31 similar values are obtained, having a crack width of 0.5 mm at a load that varied between 200 and 250. However, test BB27 displayed much lower crack widths, between 0.05 and 0.15 mm for the same loading range.

For the BBM, it was observed that at the moment of failure there was a substantial increase in the crack width. The crack widths are presented in the figures below and it can be observed that they have the same order of magnitude with the previous presented results.

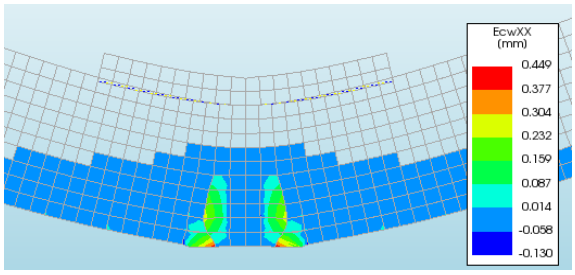

Figure 4-45 – Crack width at failure (presented in the nodes)

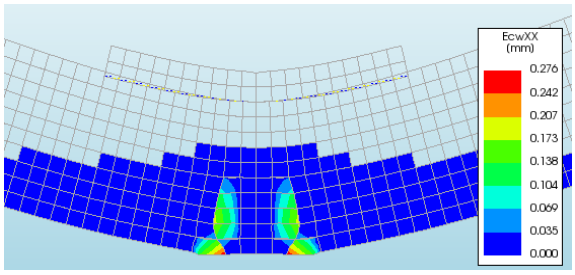

Figure 4-46 - Crack width at failure (presented in the integration points)

4.4.3.1.4 Deflection at mid-span

In order to verify if the value for the obtained deflection at mid-span was realistic, a comparison was made with the deflections obtained in S. Amir's thesis [14], both experimental and FEA. It must be kept in mind that the values from the experimental tests are the outcome of an average applied force of 335 kN and the value from the FEA is obtained under a load of ≈300 kN. Since the static capacity of the BBM is ≈245 kN, the obtained lower value for the deflection is thought to be justified and to have the same order of magnitude.

#	Test	Designation	TPL	$P_{CRi,T}$	$P_{CR0.1,T}$ (0.1 mm)	S_T	P_T	FMODE
			[MPa]	[kN]	[kN]	[mm]	[kN]	
1.	BB1	C-P1M-ST	2.5	75	150	5.8	348.7	BP
2.	BB2	A-P1M-SK	2.5	75	150	4.92	321.4	BP
3.	BB7	C-P1M-ST	2.5	75	125	5.77	345.9	BP
4.	BB19	B-P1M-SK	2.5	75	125	4.15	317.8	BP

Figure 4-47 – Deflection values from the experimental tests [14]

No.	TPL	Designation	P_{FEA}	S_{FEA}	$P_{CR,FEA}$
5.	2.5	A/C-P1M	302.3	3.9	93.2
6.	2.5	A/C-P1J	429.9	5.05	107.1
7.	2.5	A/C-P2M	529.9	7.4	151.8
8.	2.5	A/C-P2J	537.1	5.2	165.2

Figure 4-48 - Deflection values from the FEA [14]

It was observed that the deflection was identical for both types of outputs, in the nodes or in the integration points. As a consequence only one plot will be presented.

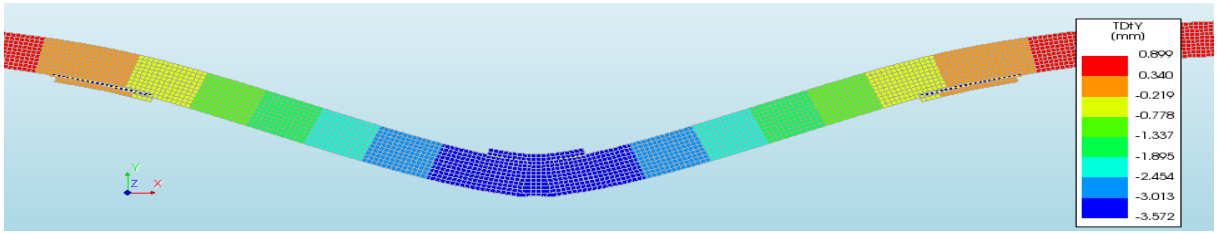

Figure 4-49 – Deflection of the best behaviour FEA model

4.4.3.1.5 Compressive membrane action (CMA)

As expected, the FEA model was able to develop the compressive membrane action, by doing so the moment of failure being delayed. This can be assessed in the following figure. In

order for it to be more clearly visible, the value of the maximum and minimum stresses were chosen accordingly.

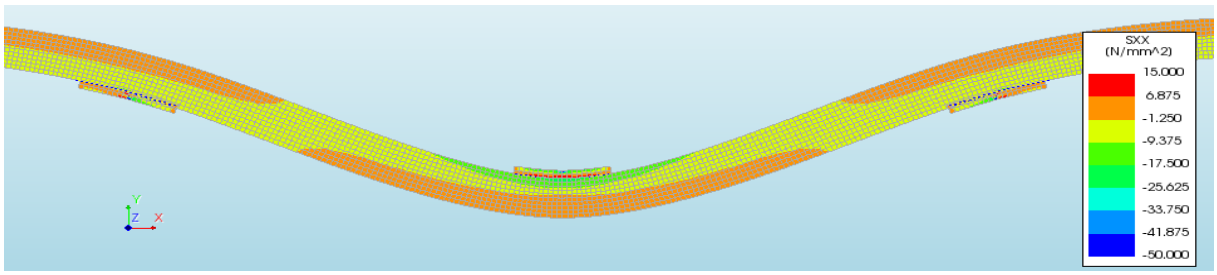

Figure 4-50 – Development of the Compressive Membrane Action in the BBM FEA model

4.4.3.2 Realistic model (RM)

The FEA model that was deemed as the realistic model (RM) due to the fact that its parameters were in accordance with the real structural system, failed as the stress in the reinforcing steel exceeded the ultimate limit of 580 MPa, this happening after a force of ≈203 kN was applied. Nevertheless, the value of the strain remained extremely low, occurrence which is thought that it should not have happened. This aspect is presented in the following subsection.

It was already mentioned and presented in subsection 4.4.2 that after reaching the peak value, the force started a continuous decrease and the analysis did not stop. It is thought that this happened due to the inaccurate value of the strain computed by DIANA. Nevertheless, this part of the curve was not considered for the model's behaviour, as it can be seen in Graph 4-21.

The compressive stress in the concrete was well below the compressive strength, whilst the tensile stress was higher than the concrete's tensile strength. Cracking started at a value of the force of ≈90 kN. At the moment when the stress in the steel exceeded its ultimate limit, considered to be the failure moment of the model, the compressive stress had a small increase of ≈1.5 MPa, whilst the tensile stress had a very small decrease of ≈0.3 MPa. At this stage the crack widths grew substantially.

Like in the case of the BBM, also for the realistic model the following subsections present the results from the analysis, showing the stresses and strains of steel and concrete, crack widths, deflections, occurrence of CMA.

4.4.3.2.1 Stresses and strains in the reinforcing steel

As it was mentioned earlier, after the applied load of 203 kN, the stresses in the steel exceeded the ultimate value. As a consequence, the strain should have had also a value

associated with the stress, above its ultimate one. However, this did not happen, with DIANA calculating much lower values for the strain. This phenomenon is presented in the following figures.

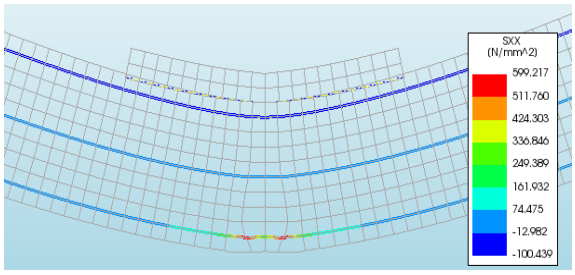

Figure 4-51 – Steel stress at the assumed failure

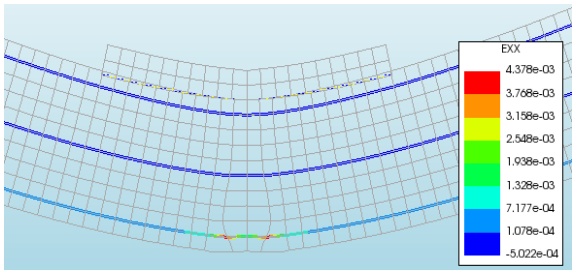

Figure 4-52 – Value of the strain at the assumed failure

4.4.3.2.2 Stresses and strains in the concrete

Regarding the compressive stresses, it can be seen from the bottom figure that their values was half the value of the compressive strength and considerably lower than the ones from the best behaviour model. The tensile stresses were higher than the tensile strength with about 25%, with cracking starting in the early stages of loading, as previously mentioned. The strains in the concrete presented the location where cracks were formed in the model.

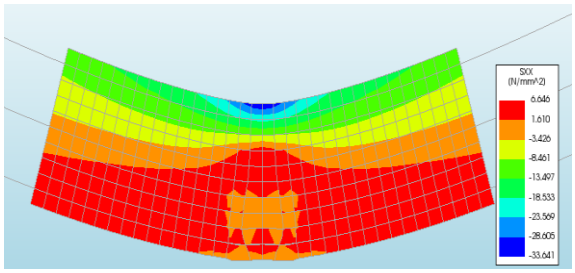

Figure 4-53 – Concrete stresses at the assumed failure

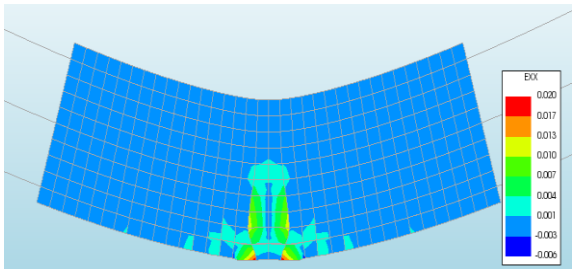

Figure 4-54 – Concrete strains at the assumed failure

4.4.3.2.3 Crack width

The cracks were formed at the locations previously observed in the plot referring to the strains. In section 4.4.3.1.3 it was described how DIANA calculates their values.

Similar to the BBM case, also for this FEA model the result can be compared to the previous ones described in reference [15], in order to have an idea about the validity of the outcome and an order of magnitude as reference. From the report on fatigue tests [15], under a force of around 200 kN, the values from the tests present crack widths of 0.35-0.4 mm (tests BB25), 0.05-0.01 mm (tests BB27) and 0.35 (tests BB31). Comparing the obtained result with these values shows a similar range for the crack width, slightly lower in case of this FEA model. The crack widths were lower also than the ones from the best behaviour model, probably because of the reduced value of the acting load. Such differences however are to be expected

considering the two-dimensional nature of this plane stress model and the real three-dimensional state.

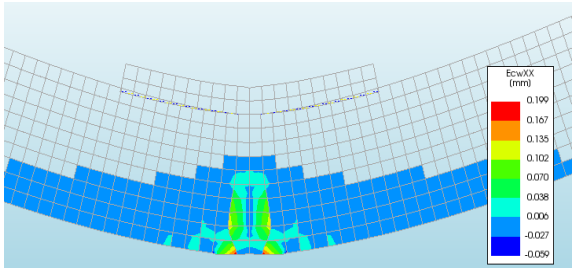

Figure 4-55 – Crack widths at the assumed failure

4.4.3.2.4 Deflection at mid-span

The obtained deflection of this model can also be compared with the results from the previous experimental tests and FEA described in subsection 4.4.3.1.4. Since this model had an overall reduced capacity, it was to be expected that also the deflection would have a lower value, smaller than the one from the best behaviour model and previous tests.

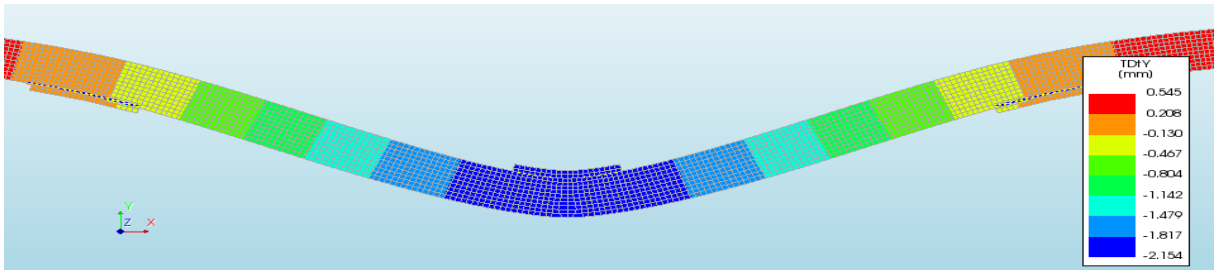

Figure 4-56 – Deflection of the realistic FEA model

4.4.3.2.5 Compressive membrane action (CMA)

The compressive membrane action also developed in this FEA model, as anticipated. Like in the case of the BBM, for the CMA to be more clearly visible, the value of the maximum and minimum stresses were chosen accordingly.

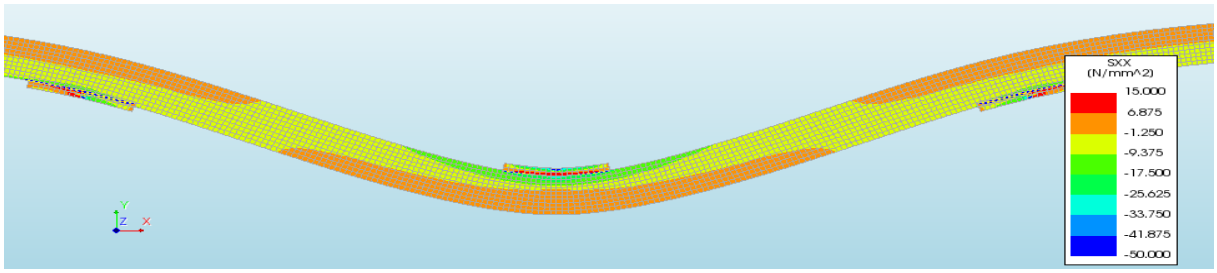

Figure 4-57 – Development of the Compressive Membrane Action in the RM FEA model

4.5 Conclusions of FEA – Stage I

For the first stage of the finite element analysis, the construction of a model that would replicate as accurately as possible the results obtained by TU Delft's experimental programs [14] and [15] was performed. The behaviour of a transversely prestressed concrete deck slab had to be modelled using the software package DIANA FEA and calibrated accordingly.

The departure point for this phase was the choice of using a two-dimensional model in order to describe and assess the behaviour of the real structure, this being a three-dimensional situation. The simplified approach involving a 2D plane stress model was chosen, acknowledging the limitations that would come with the use of such a model. Although simplistic from a geometrical point of view, the FEA model had a high number of parameters that influenced its behaviour during the analyses and the obtained results. Among these parameters, the ones that had a large impact on the outcome were the support conditions, the material properties, the considered effective width of the model, the bond of the prestressing bar, the incremental method, the way the external force was applied and the accuracy in reproducing the real structure that was tested. Nonlinear analyses were performed in order to reflect more realistically the behaviour and also for the ability to subsequently modify the properties of the materials for the second stage of the FE analysis, the one related to fatigue.

The material models had a decisive role in describing as realistic as possible the behaviour of the FEA model. For this, different functions were considered for simulating the compressive and tensile behaviour of the concrete, choosing in the end the ones that gave the best results. Another parameter that proved to be decisive was the considered width of the plane stress model. Its value was essential for obtaining an initial stiffness similar to the ones from the experimental program. The degrees of freedom of the supports also had a significant impact. Whether the prestressing bar was considered bonded or not had a large influence on the capacity of the model.

Overall, the influence of many parameters was studied and in the end the choice was made to use two models for the second FEA stage. One of these models presented the best behaviour (BBM) when compared to the results of previous experiments [14] and [15]. Nevertheless, in order to achieve such results the assumption of a bonded prestressing bar was made, this being contrary to the real structure. The other model was in accordance with the parameters from the structure and therefore was deemed as the realistic model (RM), its behaviour however not being as good as for the other model.

The capacity of both FEA models was found to be lower than the previous experimental and FEA results, but this was to be expected considering that a plane stress model was used. The failure modes were analysed, studying the steel and concrete stresses and strains, the crack widths, deflections and the development of the compressive membrane action, which occurred as expected. Whilst in reality the structure experienced a punching shear type of failure given the three-dimensional stress state, in the case of the FEA plane stress model the failure was of flexural nature.

Chapter 5: Finite Element Analysis - Stage II

5.1 Introduction

The stated main goal of this Master's Thesis was to create a FEA model that could predict the fatigue behaviour of transversely prestressed concrete deck slabs. During the first stage of the finite element analysis, two very similar models were created in order to replicate this behaviour, both being calibrated according to the previous researches performed at TU Delft, [14] and [15]. One of these experimental programs [15] studied the effect of fatigue on such a structural system described earlier and represents the benchmark of this chapter.

This chapter describes how the created FEA models tried to replicate the previously obtained test results and also assesses the accuracy of their prediction of the fatigue behaviour, when this is compared with the outcome of the prediction formula derived at TU Delft for the experiments described in reference [15]. Changes in material properties, namely concrete, were performed in order to simulate the damage due to fatigue. The changes were directly linked to the number of loading cycles and the loading range that acted on the structure.

The tests performed during the experimental program [15] were of compressive nature only and had either one or multiple loading ranges. Apart from assessing the behaviour of the structure under a single range, it was also of importance to analyse whether the loading sequence in case of more than one range had any impact. For this however, only a single test was performed, therefore there is no much data on such a behaviour. The effect of the loading sequence is the object of the next research on fatigue at TU Delft, the experimental program starting in the near future. This will be presented in the next chapter of the thesis.

Since an actual fatigue analysis cannot be performed in DIANA, the ones performed for this chapter were still static analyses, where the reduction of material properties was taken into account in the FEA models to simulate the fatigue behaviour. For all the analyses performed for this part of the thesis, the value of the load that was applied to the FEA models was represented by the static capacity of each model, since the loading range from the tests was taken into account within the modified material parameters.

5.2 Changes in material properties

As concrete is subjected to cyclic loading, micro cracks and, subsequently, cracks start to develop slowly in the concrete. By doing so, the material's properties are getting altered continuously, with the initial characteristics being reduced over time.

In the case of the deck slabs, with the load acting repeatedly on the structure, the reduction of material properties starts with the assumption that the concrete's compressive strength is the main parameter that influences the behaviour. In the following it will be presented to what extent the main properties of concrete influence the assumed fatigue behaviour and it will be shown how these are correlated with each other.

5.2.1 Compressive strength and compressive fracture energy of concrete

As a direct consequence of the repeated loading, the cracked concrete reduces its bearing capacity, with the compressive strength being directly influenced by this phenomenon. The reduction in the compressive stress that the structure can withstand is dependent on the number of loading cycles and the loading range. A simplified approach used in order to determine the maximum compressive stress in a structure after the action of a cyclic type of loading is given by the formula:

Equation 5-1 – Determination of the maximum compressive stress

$$\frac{\sigma_{c.max}}{f_c} = 1 - \beta * (1 - R) * logN$$ [29], where

- β is a coefficient: $0.064 < \beta < 0.080$, here it was considered that $\beta = \frac{1}{14}$
- $R = \frac{\sigma_{min}}{\sigma_{max}}$ is the ratio between the minimum and maximum stresses (loads) in the cycle
- *N* represents the number of cycles within a loading range
- f_c is the compressive strength of the concrete (assumed to be the mean one for the analyses)

During the performed tests, it was decided that for all of them the minimum load value within a loading range would be 10% of the maximum one. As a consequence, in the above formula, the ratio "*R"* between the minimum and maximum stresses (or loads) always had a value of 0.1. Inserting into the formula the number of cycles along with the ratio of the stresses (or loads) and the value for the initial compressive strength of the concrete, the result would give a reduced compressive stress that, in theory, would be the maximum value that the concrete could bear after the fatigue loading cycles.

This obtained value was used in the FEA model as the new and modified compressive strength, representing the main parameter for assessing the fatigue behaviour. When considering the crushing behaviour of concrete, apart from its strength, also the compressive fracture energy plays a role and this was one of the parameters that served as an input for the FEA model. Since these two are linked to each other, it was assumed that the same reduction that was obtained for the compressive strength was also valid for the fracture energy.

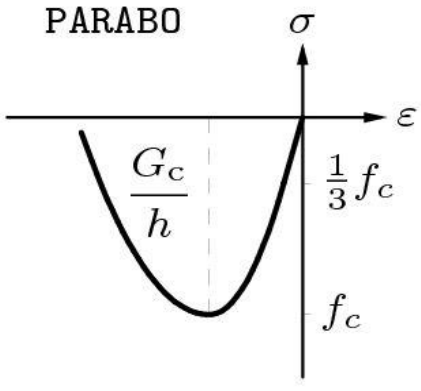

Figure 5-1 – Compressive fracture energy dependence on the compressive strength [25]

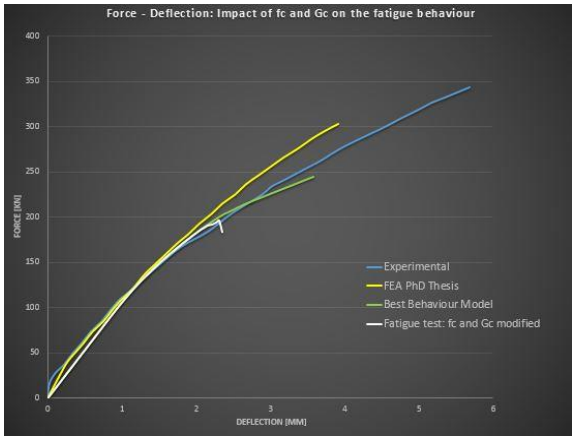

Graph 5-1 – Impact of the modified compressive strength and fracture energy on the FEA model

In Figure 5-1 the influence of the compressive strength on the compressive fracture energy is presented for the parabolic function used in order to describe the compressive behaviour of the concrete within the FEA model.

Following a series of analyses, it was observed that by modifying only the compressive strength and the compressive fracture energy, the FEA model would not behave realistically. This modifications led only to a decrease in the final capacity of the model, with no deterioration of the stiffness, as it can be seen in Graph 5-1. A decrease in the stiffness should have occurred since the concrete starts developing more and more cracks.

As the outcome from changing only the before mentioned parameters was considered not to be satisfactory from a realistic point of view, the change of other parameters within the FEA model was subsequently considered and performed.

5.2.2 Modulus of elasticity of concrete

As a consequence of the repeated loading, the concrete will crack and its stiffness will be reduced. However, it was observed that during the initial finite element analyses related to fatigue, the stiffness suffered no modifications after the parameters described in subsection 5.2.1 were altered. Therefore it was thought to study the impact of a modified modulus of elasticity, this having a direct impact on the stiffness. The amount of reduction was thought to have the same percentage as for the previous parameters. The outcome of modifying also the value for the modulus of elasticity within in the FEA model can be observed in the following graph.

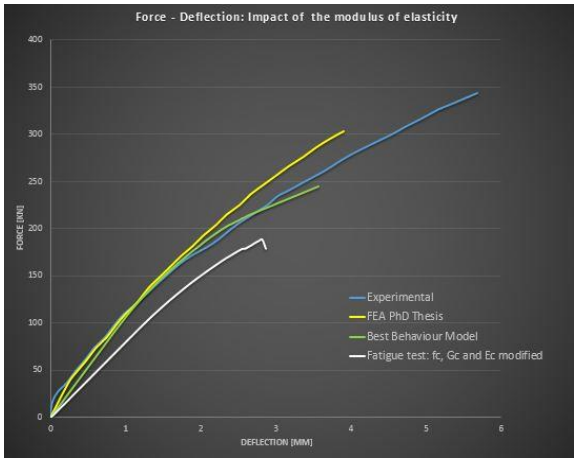

Graph 5-2 – Impact of the elasticity modulus on the fatigue behaviour

Again, after a series of analyses that had the same outcome outlined by Graph 5-2, it was clear that also by modifying the elasticity modulus of concrete, the end result would not properly describe the real situation. In this case, the stiffness is completely different than the ones obtained during the previous research programs right from the beginning of the analysis. Since this is far from a real description of the behaviour, other parameters were modified.

5.2.3 Tensile strength and tensile fracture energy of concrete

With the previous modified material parameters not being able to describe a behaviour that could have been considered realistic when related to the fatigue loading, thought was given in altering also the tensile strength and the tensile fracture energy of the concrete, with the latter being dependent on the former.

In order to come up with the best possible result, a series of combinations in terms of considered parameters were taken into account and also several approaches in determining the degree of reduction for the tensile strength and fracture energy.

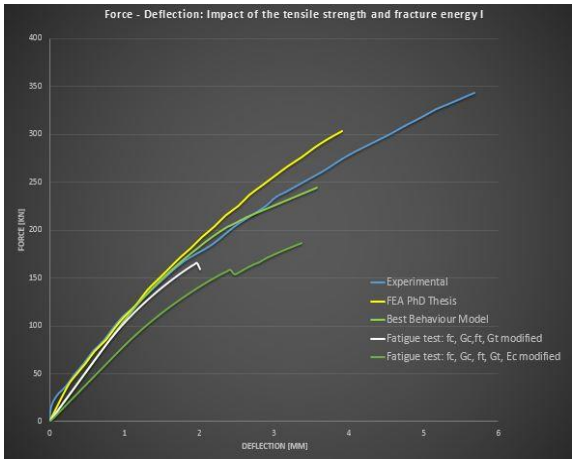

Graph 5-3 – Behaviour of FEA model depending on the parameters considered for modification

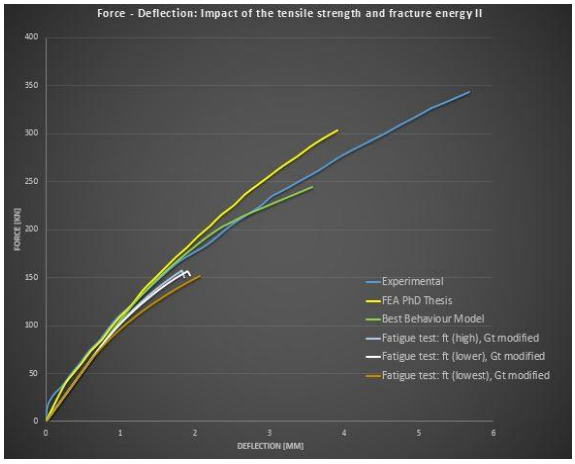

Graph 5-4 – Impact of different approaches in determining the tensile strength and fracture energy

In Graph 5-3 the combination that would lead to a more realistic behaviour of the FEA model can be observed, with the parameters that were taken into account being both strengths of the concrete and their associate fracture energies. The modulus of elasticity was assumed not to have its value modified, with the tensile strength determining the loss in stiffness once the concrete starts to crack.

Graph 5-4 presents the outcome of different approaches that involved the way the reduction of the tensile strength and fracture energy were considered. These two parameters are also linked to the compressive strength, therefore were highly influenced by it. These approaches were thought of in this form so that a behaviour closer to a real situation would be simulated.

Table 5-1 – Approaches for determining the reduced tensile strength and tensile fracture energy

Outcome	Parameters				
High tensile strength	$f_{ck}^{fatigue} = \sigma_{c.max}$			$f_{ctm}^{fatigue} = 0.3 f_{ck}^{fatigue\frac{2}{3}}$	$G_f^t = \frac{G_f^c}{250}$
Lower tensile strength	$f_{cm}^{fatigue} = \sigma_{c.max}$		$f_{ck}^{fatigue} = f_{cm}^{fatigue} - 8MPa$	$f_{ctm}^{fatigue} = 0.3 f_{ck}^{fatigue\frac{2}{3}}$	$G_f^t = \frac{G_f^c}{250}$
Lowest tensile strength	$f_{cm}^{fatigue} = \sigma_{c.max}$	$f_{ck}^{fatigue} = f_{cm}^{fatigue} - 8MPa$	$f_{ctm}^{fatigue} = 0.3 f_{ck}^{fatigue\frac{2}{3}}$	$f_{ctk.min}^{fatigue} = 0.7 f_{ctm}^{fatigue}$	$G_f^t = 73 f_{ctm}^{fatigue^{0.18}}$

For the formulas in Table 5-1, the guidelines from Rijkswaterstaat [26 - table on page 11] were used, but not necessarily in the order presented there. The calculation process was started by knowing the amount of reduction for the compressive stress and compressive fracture energy. As a result, the tensile compressive energy was determined based on the compressive tensile energy (for the first two methods) and not on the tensile strength, as would have been done in [26]. By following the above mentioned approaches, it was observed that a too high tensile strength might not lead to a failure associated with fatigue, the model behaving similar to the static tests. On the other hand, a too low tensile strength could make the model fail sooner than desired. It was also observed that the value of the tensile strength affects the ductility of the model and not its capacity. As a consequence of all these observation, the second approach was chosen in the end, this being the one that would result in a lower tensile strength (second line of the table), between the two extremes.

Having determined what parameters influence the behaviour of the FEA model related to the fatigue prediction analyses, the next step consisted of replicating the results from the research on fatigue [15] and also determining the degree of accuracy of the FEA model with respect to the prediction formula derived from the experimental tests described in reference [15]. All of these are presented in the next subsections of the thesis.

5.3 Single cyclic loading range analyses

Within the experimental program related to fatigue [15], a series of single point load tests were conducted by applying only a single load range on the structure. Like mentioned previously, all the tests were of compressive nature, with the minimum load value being 10% of the maximum one, the latter having always smaller value than the static strength of the structure. Based on the results from these tests, but also from the ones with multiple stress ranges, double point load or acoustic emissions, all described in reference [15], a prediction formula was derived by the researchers from TU Delft, formula with which the theoretical maximum force that could act on a structure after a certain number of cycles would be determined.

Equation 5-2 – Force prediction formula

$$\frac{F_{fat}}{F_{sta}} = 0.93 - 0.065 * logN \qquad \text{[15], where}$$

- F_{fat} is the force predicted after N loading cycles to be resisted by the element/structure
- F_{sta} is the static capacity of the element/structure
- N represents the number of loading cycles

Based on this formula, a value for the force after a certain number of cycles is obtained, this being subsequently compared with the one resulting from the fatigue analysis performed in DIANA, analysis that implies the modification of material properties. Furthermore, the results from the FEA will be plotted against the ones from the tests and their accuracy will be assessed.

5.3.1 Test BB23_200

Being the first fatigue test with a single load range and applied point load, this had a maximum force value of 200 kN and a minimum one of 20 kN, as presented in Figure 5-2. The number of cycles to failure was 24800. The prediction according to the previous formula was done based on the static capacity of the two FEA models: the one with the best behaviour (BBM) and the realistic one (RM). For both models a nonlinear analysis was performed using DIANA.

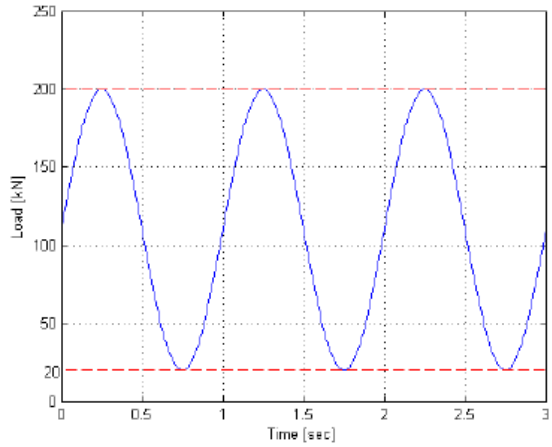

Figure 5-2 - Cyclic loading range for test BB23_200 [15]

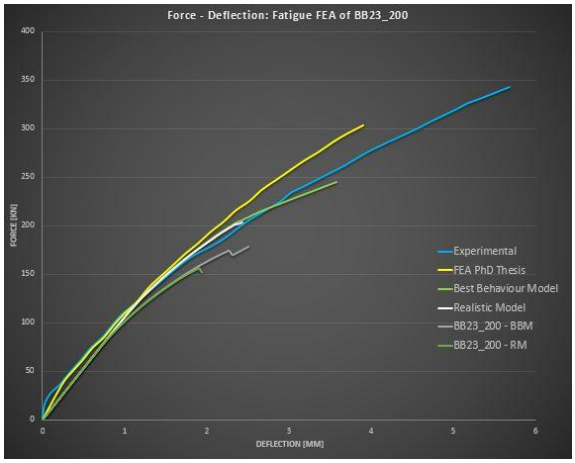

Graph 5-5 – Fatigue FEA of test BB23_200

It can be observed from Graph 5-5 that the capacity and ductility of the models are considerably reduced following the fatigue FE analyses. Nevertheless, the resulting forces are higher than the ones predicted by Equation 5-2 and can be assessed in the following table:

Table 5-2 – Test BB23_200 FEA results and prediction

FEA model	Static capacity (F_{sta}) [kN]	Predicted force (F_{fat}) [kN]	FEA result [kN]
BBM	244.86	157.78	178.25
RM	203.38	131.05	156.31

In case of the BBM all loading steps converged (applied 73% of load), with the steel stress being just slightly below the yield limit and the steel strain having a very small value at the end of the analysis. The compressive stress in the concrete was considerably low compared to the compressive strength, whilst the tensile stress was larger than the tensile strength as cracking occurred in the early loading stages. The strain in the tensioned zone had a large value.

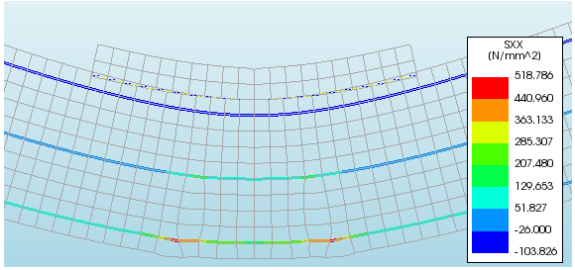

Figure 5-3 – Steel stress at the end of the analysis, BB23_200 - BBM

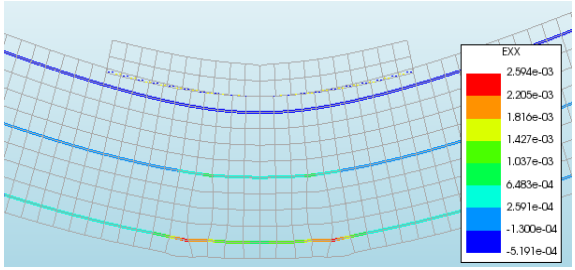

Figure 5-4 – Steel strain at the end of the analysis, BB23_200 - BBM

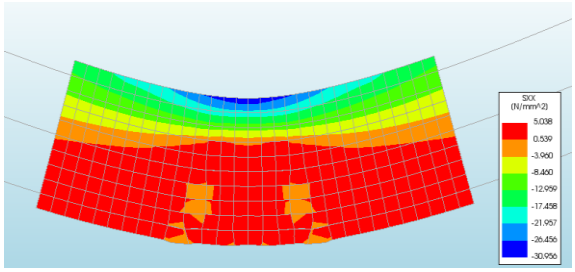

Figure 5-5 – Concrete stresses at the end of the analysis, BB23_200 - BBM

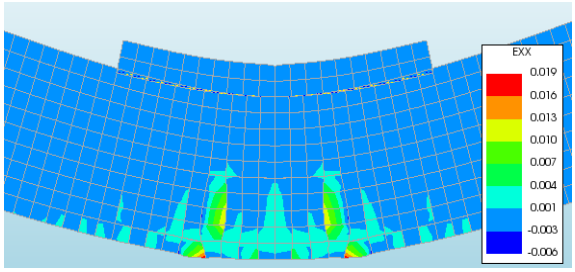

Figure 5-6 –Concrete strains at the end of the analysis, BB23_200 - BBM

The drop in the force - deflection curve, followed by a rise, is the result of a very large and instant increase in the steel stress (by more than 50%), caused by an increase of the crack width. It was observed that once the curve in the graph starts to rise again, the stress in the concrete varies only to a small extent, whilst the stress in the steel continues to constantly increase its value until the end of the analysis. The output in terms of crack width from DIANA (≈0.2 mm), seen in Figure 5-7, showed a similar magnitude to the crack width measured in the test (0.4 mm). It was also clear that the CMA had developed within the model as presented in Figure 5-8.

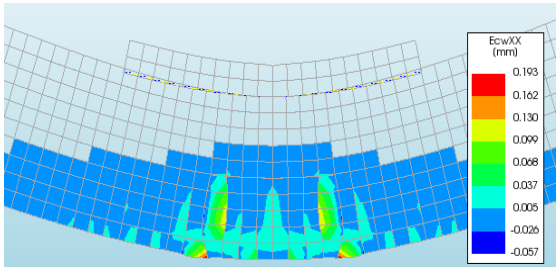

Figure 5-7 – Crack width, BB23_200 - BBM

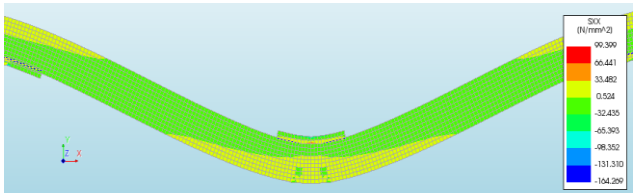

Figure 5-8 – Development of CMA, BB23_200 - BBM

In case of the realistic model (RM) the analysis diverged towards the end. The failure was of flexural nature, most likely due to the concrete failing in tension, this being combined with the effect of the steel stresses, although the latter did not exceed its yield values. The steel stress had a value far from the yielding one, but at failure the stress increased by more than 40%. Nevertheless, the steel strain remained at a low value.

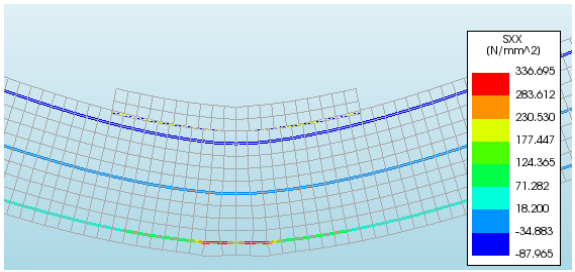

Figure 5-9 – Steel stress at failure, BB23_200 - RM

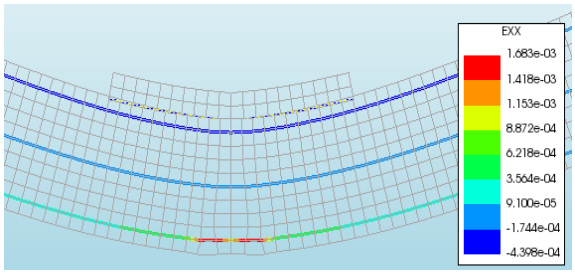

Figure 5-10 – Steel strain at failure, BB23_200 - RM

Like for the BBM, the compressive stress in the concrete was considerably lower than the compressive strength, with the tensile stresses being larger than the tensile strength. At failure, the increase in their value was extremely small but the crack width increased

significantly, almost doubling its value. The strain had a high value in the tensioned zone. The compressive membrane action had developed within the model also during this analysis.

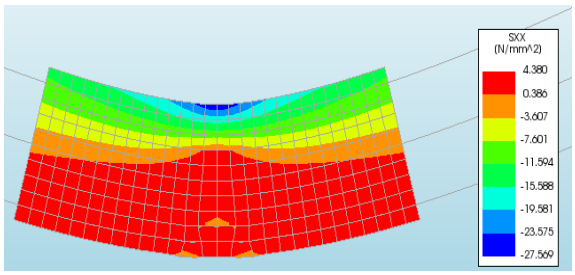

Figure 5-11 – Concrete stress at failure, BB23_200 - RM

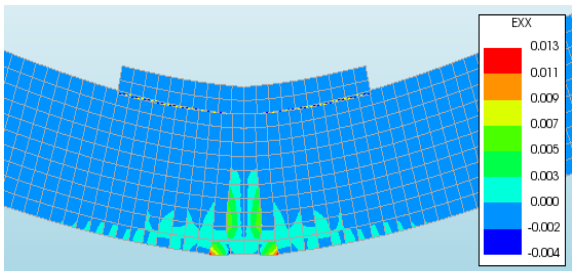

Figure 5-12 – Concrete strain at failure, BB23_200 -RM

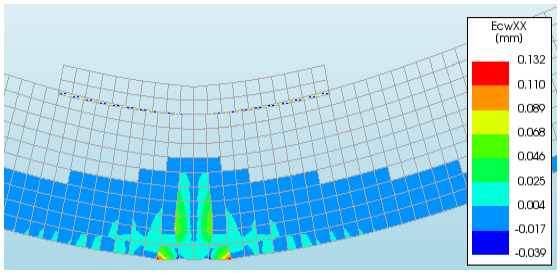

Figure 5-13 – Crack width, BB23_200 - RM

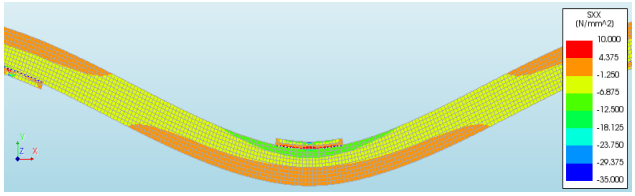

Figure 5-14 – Development of CMA, BB23_200 - RM

5.3.2 Test BB24_150

This was the second test that had a single load range, with the loading being applied at one location. The maximum value of the load was 150 kN and the minimum one was 15 kN. After 1.5 million cycles the concrete deck slab still did not fail and subsequently was statically loaded to failure, this occurring at 330 kN. Only the fatigue loading was analysed in DIANA.

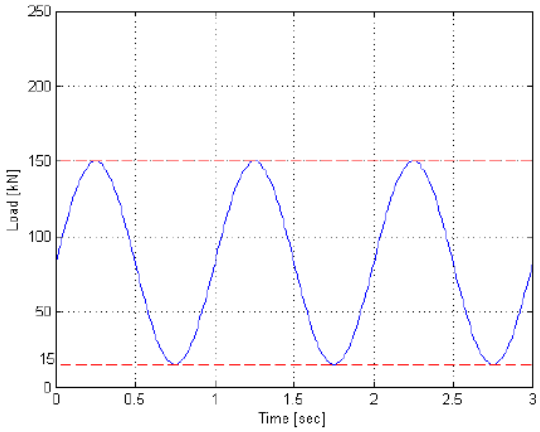

Figure 5-15 - Cyclic load range for test BB24_150 [15]

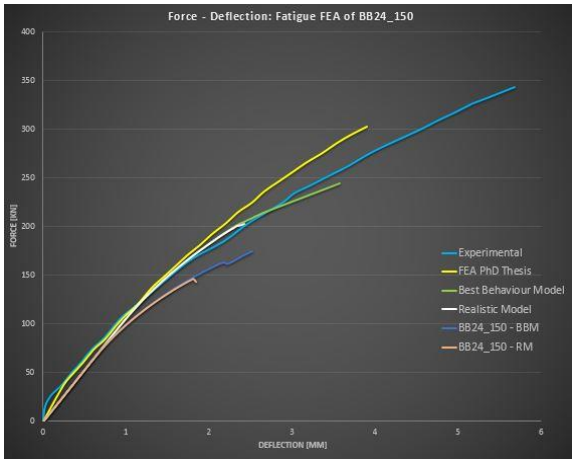

Graph 5-6 - Fatigue FEA of test BB24_150

The outcome of the analyses for both FEA models was similar to the first test. It can be observed that the capacity and the ductility are reduced when compared with the ones from the static loading. Another similarity was that the resulting forces from the FE analyses had larger values than the ones predicted by Equation 5-2, this being presented in Table 5-3.

Table 5-3 - Test BB24_150 FEA results and prediction

FEA model	Static capacity (F_{sta}) [kN]	Predicted force (F_{fat}) [kN]	FEA result [kN]
BBM	244.86	129.42	174.89
RM	203.38	107.50	146.49

In the case of the BBM all the loading steps converged, with the analysis ending at about 71% of the applied load. At the end of the analysis the stress in the steel had a value close to the yield one, with the strain being relatively low.

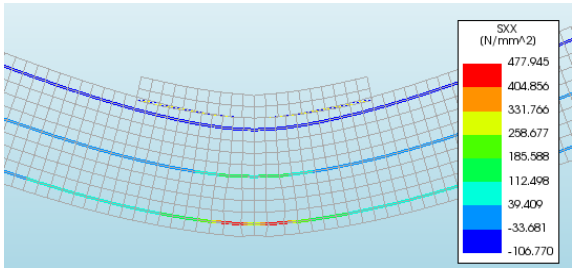

Figure 5-16 - Steel stress at the end of the analysis, BB24_150 - BBM

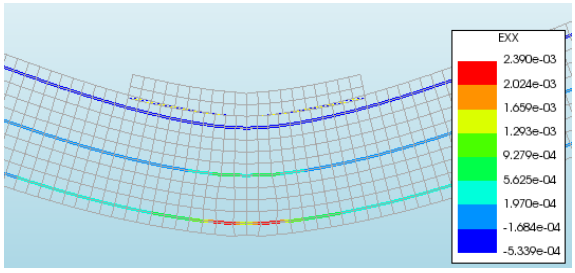

Figure 5-17 - Steel strain at the end of the analysis, BB24_150 - BBM

The concrete tensile stress exceeded the tensile strength, with the height of the tensile zone being more than 70% of the section's height. The compressive stress was lower than the strength. The strain of the concrete had quite a large value in the tension zone. Since the model did not fail by the end of the analysis, the cracks continued to grow. The development of the compressive membrane action was clearly visible in the model. Like in the case of the first test, the decrease and subsequent rise in the force - deflection curve is due to a sudden opening of the cracks and increase in the steel stress, increase that was not as high as the one from BB23_200. At the same time a small decrease in the tensile stress of the concrete is noticeable.

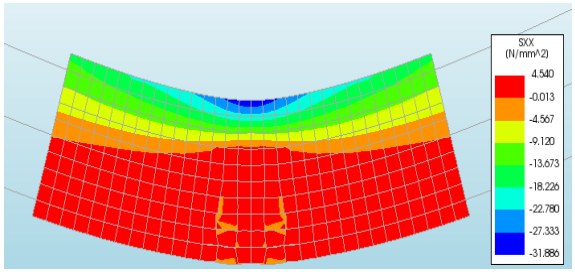

Figure 5-18 - Concrete stresses at the end of the analysis, BB24_150 - BBM

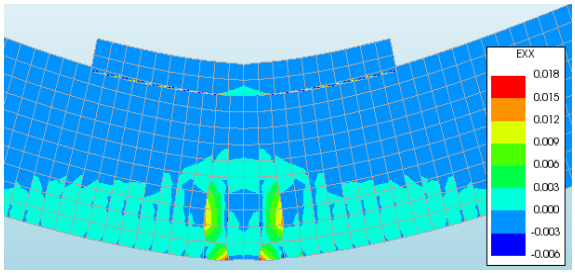

Figure 5-19 - Concrete strains at the end of the analysis, BB24_150 - BBM

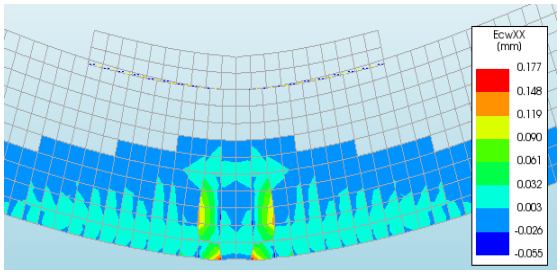

Figure 5-20 - Crack width, BB24_150 - BBM

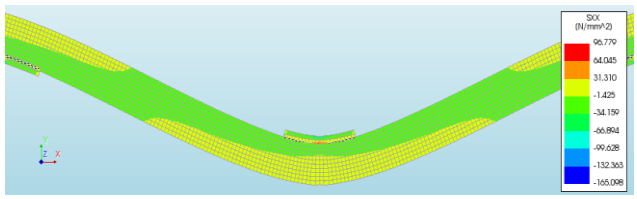

Figure 5-21 – Development of CMA, BB24_150 - BBM

For the realistic model (RM), the behaviour was almost identical to its equivalent from test BB23_200. The analysis stopped before finishing all load increments, with the model experiencing flexural failure. The steel stress increased by more than 35% when the model failed, but still it had a low value, around half of its yield one. A high growth in the crack opening is believed to be the cause of the behaviour of the steel. The steel strain had a low value.

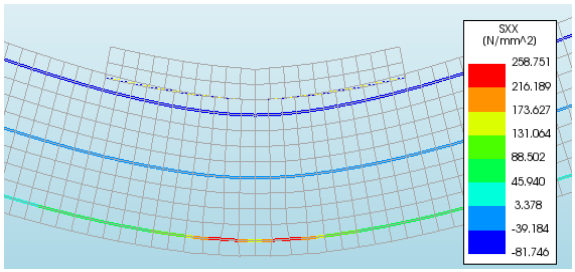

Figure 5-22 - Steel stress at failure, BB24_150 - RM

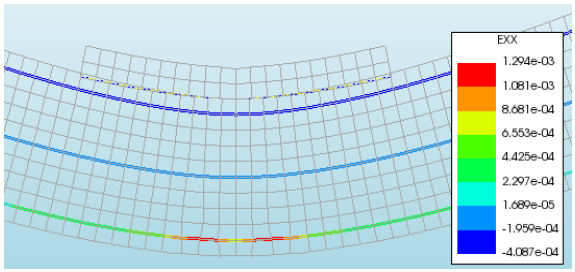

Figure 5-23 - Steel strain at failure, BB24_150 - RM

The compressive stress in the concrete did not exceed the compressive strength but the tensile one did. At failure, the tensile stress increased by more than 25% but the concrete was already cracked since the early loading stages.

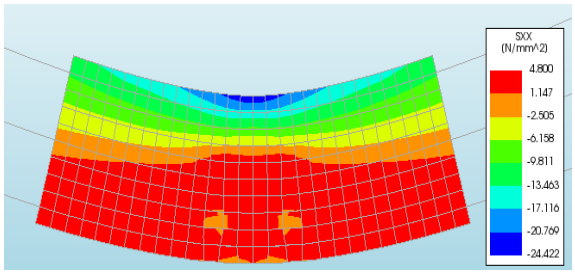

Figure 5-24 - Concrete stress at failure, BB24_150 - RM

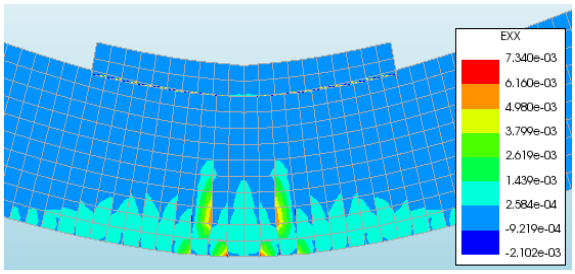

Figure 5-25 - Concrete strain at failure, BB24_150 - RM

The crack width that resulted from the analysis had a noticeably smaller value (0.07 mm) compared to the one that was measured in the test (0.6 mm). The strain in the area under tension was higher than 0.7%. Regarding the compressive membrane action, once again this was observed to develop in the FEA model.

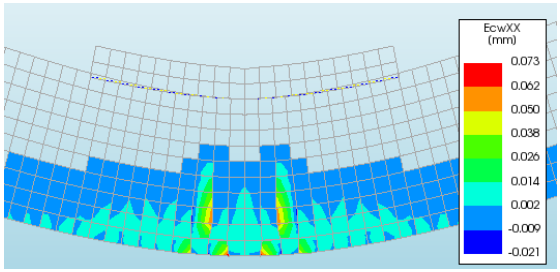

Figure 5-26 – Crack width, BB24_150 - RM

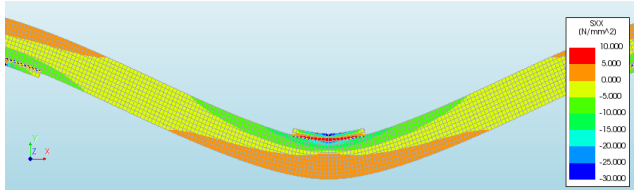

Figure 5-27 – Development of CMA, BB24_150 - RM

5.3.3 Test BB26_165

Being the last of the tests involving a single load range, this had a maximum load value of 165 kN and a minimum of 16.5 kN, with failure occurring after a little over 1.4 million cycles.

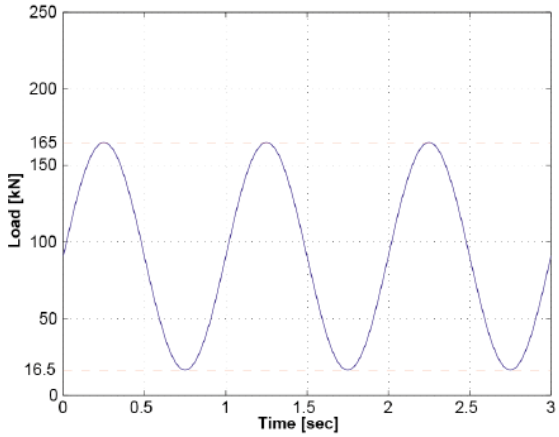

Figure 5-28 – Cyclic load range for test BB26_165

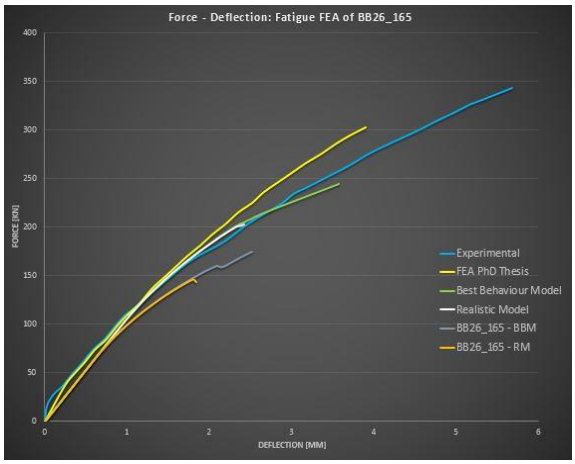

Graph 5-7 - Fatigue FEA of test BB26_165

The overall behaviour of this test was also very similar to the previous two tests. The same decrease in capacity and ductility of the models can be seen. Regarding the prediction of the force after the number of loading cycles (using Equation 5-2), again the value resulted from the FE analyses proved to be higher. It must be mentioned that the values obtained from the FEA were almost identical to the ones from tests BB24_150, although the material parameters were modified in accordance with the procedure described in subsection 5.2.

Table 5-4 - Test BB26_165 FEA results and prediction

FEA model	Static capacity (F_{sta}) [kN]	Predicted force (F_{fat}) [kN]	FEA result [kN]
BBM	244.86	129.87	174.94
RM	203.38	107.87	146.44

For the best behaviour model all the loading steps converged and the analysis ended at around 71% of the applied load. Again, the steel stress proved to be very high but still it did not reach the yielding value. Its strain was also below the yield value.

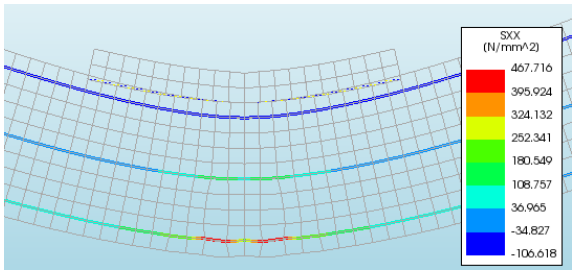

Figure 5-29 - Steel stress at the end of the analysis, BB26_165 - BBM

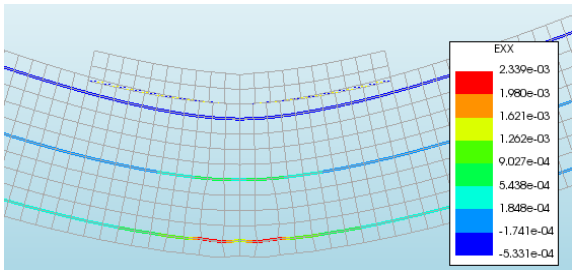

Figure 5-30 - Steel strain at the end of the analysis, BB26_165 - BBM

As in the previous tests, the compressive stress in the concrete was below the compressive strength and the tensile one was above the tensile strength, with the tensile zone

spreading over more than 70% of the section's height. The strain had a large value in the tensile area. Like before, the decrease and subsequent rise in the force - deflection curve is due to a sudden opening of the cracks and increase in the steel stress. After the curve started to go up again, the stresses in the concrete had a very small variation. The cracks continued to grow until the analysis was finished. The compressive membrane action was again present in the model.

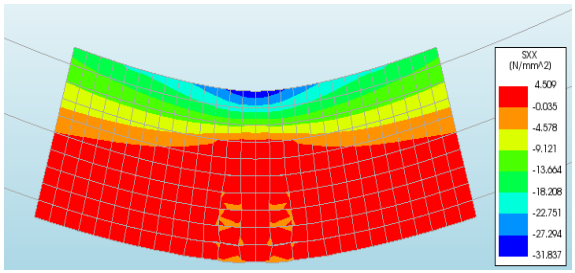

Figure 5-31 - Concrete stresses at the end of the analysis, BB26_165 - BBM

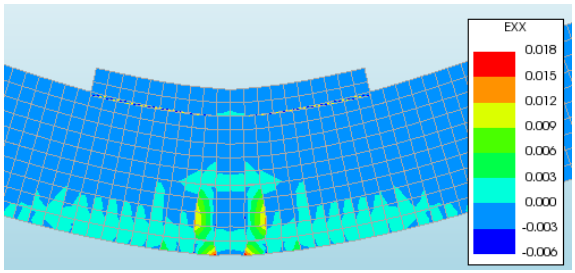

Figure 5-32 - Concrete strains at the end of the analysis, BB26_165 - BBM

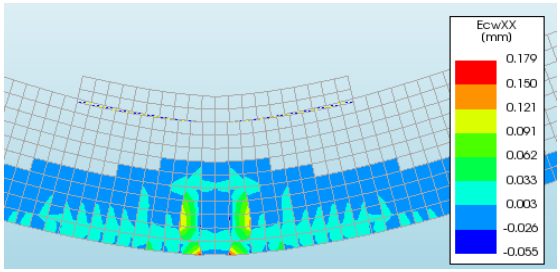

Figure 5-33 Crack width, BB26_165 - BBM

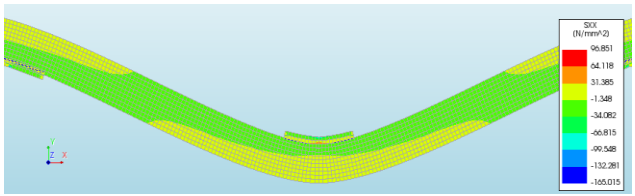

Figure 5-34 – Development of CMA, BB26_165 - BBM

The realistic model had a behaviour that was similar to the ones from the previous tests. It failed before all the loading steps were applied, with the type of failure being flexural. At failure, the stress in the steel increased by almost 55%, but still had a lower value compared to the yield stress. This behaviour is thought to have happened due to large increase in the crack width, which got enlarged by more than 50%. The value of the strain was quite low, obviously not reaching the yield limit.

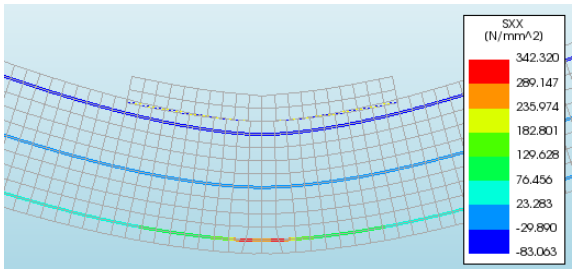

Figure 5-35 - Steel stress at failure, BB26_165 - RM

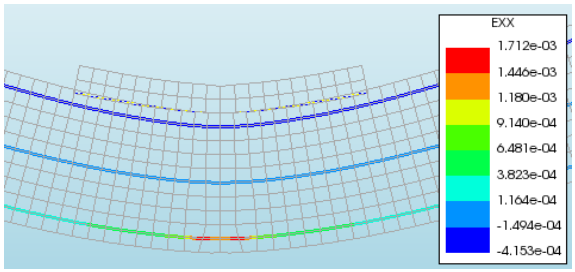

Figure 5-36 - Steel strain at failure, BB26_165 - RM

The tensile stress of the concrete exceeded the tensile strength, but this happened in the early stages of loading when cracking occurred. At failure only a small increase was observed. The compressive stress was lower than the equivalent strength. The strain of the concrete had a value of ≈1% in the area under tension. The cracked width increase substantially at failure, more than doubling its value. The compressive membrane action was observed also for this FEA model.

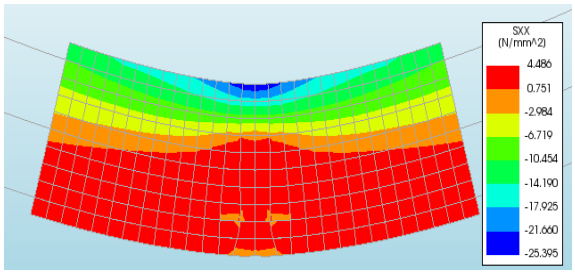

Figure 5-37 - Concrete stress at failure, BB26_165 - RM

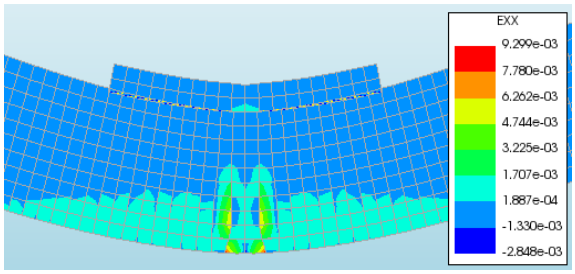

Figure 5-38 - Concrete strain at failure, BB26_165 - RM

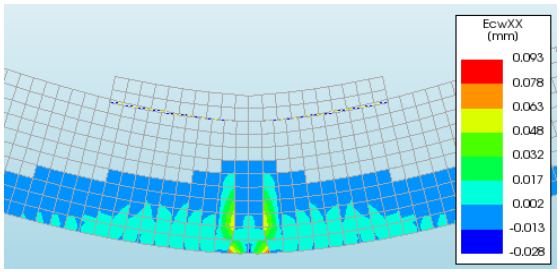

Figure 5-39 – Crack width, BB26_165 - RM

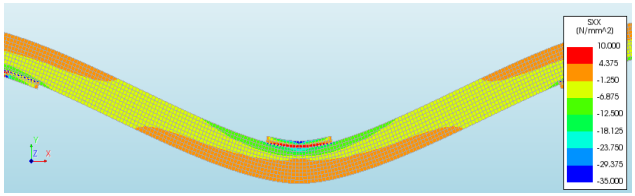

Figure 5-40 – Development of CMA, BB26_165 - RM

5.3.4 Accuracy of the results

Having performed the analyses that involved the single load range fatigue tests, it was of interest to see where they fit compared with the previous results and how accurate can the FEA models be considered. In order to do this, use was made of Figure 3-28, originating from the report on the fatigue tests [15]. This contained all the previous results, the prediction given by Equation 5-2 and the 95% confidence interval. The data points from the image were retrieved by using again the software ENGAUGE DIGITIZER. These were plotted together with the results from the FEA tests for both models and their theoretical predictions. Of interest for the plot was the ratio between the fatigue force from the FEA tests or the one predicted and the static capacity of the models, together with the number of cycles for each loading range.

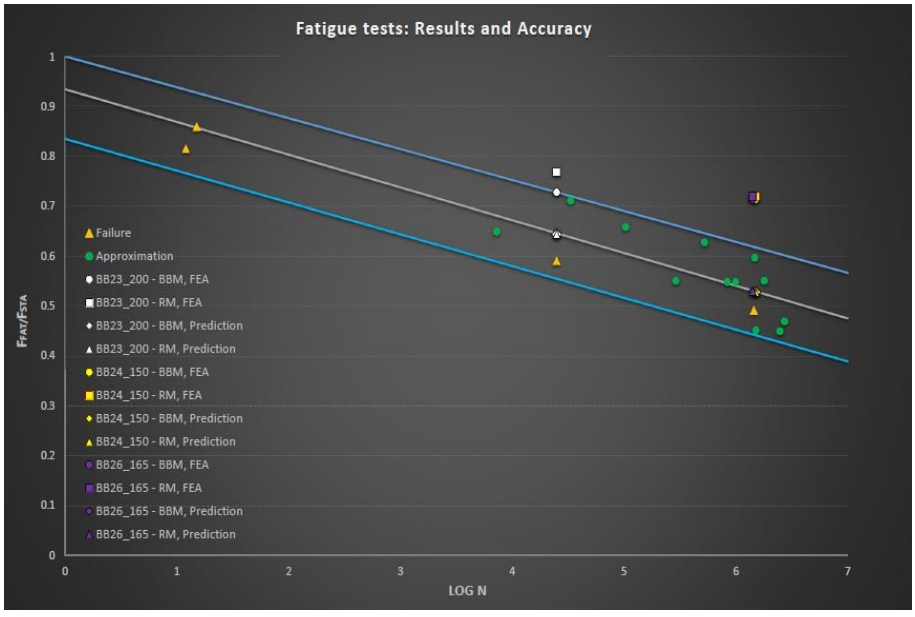

Graph 5-8 – Fatigue tests: Results and accuracy; F_{fat}/F_{sta} vs. logN

It can be observed in the graph that the results from the FE analyses are at some distance from the confidence interval, with only one test, BB23_200 – BBM, being exactly on the upper boundary of the interval. Two of the tests, BB24_150 and BB26_165 had almost an identical outcome, mostly due to a very close number of loading cycles. The predictions for the tests that follow from the formula derived at TU Delft, Equation 5-2, are located as expected on or near the prediction trend line.

Based on the plotted results, it appears that the model is not yet accurate enough to predict in a satisfactorily manner the fatigue damage suffered by a concrete deck slab, with a number of reasons being considered to influence this outcome. This will be discussed in subsection 5.5, where the conclusion of the second stage of the FEA are presented.

5.4 Multiple cyclic loading ranges analyses

Apart from the single load range tests that were performed during the research on fatigue [15], also tests that included multiple load ranges were conducted. In order to try and simulate these tests using the finite element method, a phased analyses was considered as a primary option. Such an analysis is meant to execute all the loading ranges one after the other, with the influence of the previous phase being taken into account in the next one. Since in subsection 5.3 it was observed that the realistic model (RM) always failed for an applied single loading range, for this subsection only the best behaviour model (BBM) will be considered for the FEA analyses. For each phase of an analysis, a progressive reduction of the material properties was considered, the reduction being performed as it was described in subsection 5.2.

Besides the phased analysis, another approach was tried in order to see how the outcome would differ and what additional observations could be made. This approach implied running each loading range within a test as a separate analysis, but having the material properties modified for each subsequent load range. Like stated before, a progressive reduction was thought to be more accurate. For the sake of comparison between the approaches, the BBM was also used for this one.

Apart from the performed FE analyses regarding multiple loading ranges, the question related to the impact of the sequencing effect still remained. In order to try and see whether some clarifications could be obtained related to this topic, a series of analyses were performed especially for this. The outcome will also be presented in the following.

5.4.1 Performed tests

For assessing the behaviour of the models under multiple loading ranges, two experimental tests from the fatigue research [15] were considered: BB28 and BB29.

5.4.1.1 Phased analysis approach

Test BB28 was composed of three different loading ranges. The maximum values in each range were 165, 200 and 240 kN, in this order, with the minimum values being 10% of the maximum ones, similar to the single load range tests. The first cyclic range did not fail after 1.5 million cycles, with the second one not failing also after 1 million cycles. Eventually the specimen failed after 7144 cycles during the last loading range.

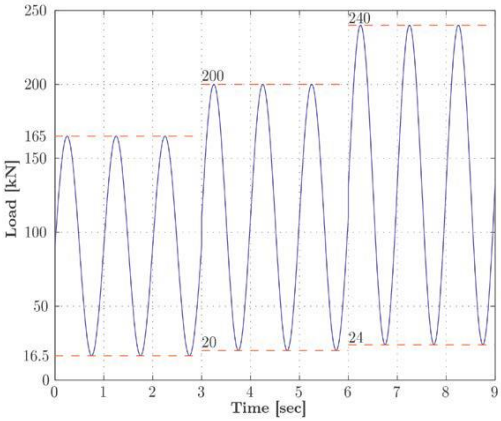

Figure 5-41- Loading ranges for test BB28 [15]

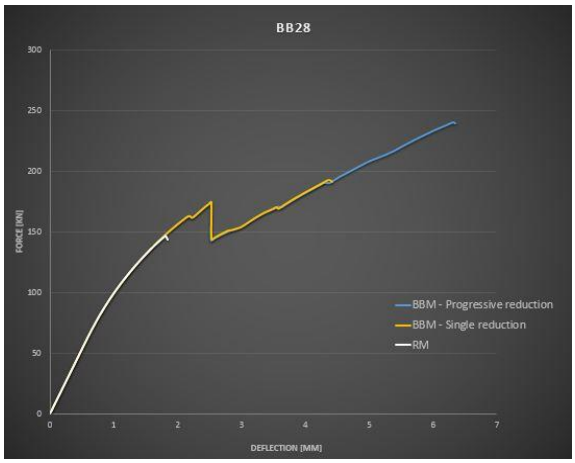

Graph 5-9 - FE analyses of test BB28

For each phase of the analysis, the material parameters were changed in order to reflect the theoretical damage caused by the cyclic loading. For the second phase the reduction was based on the values of the compressive strength and fracture energy from the first phase, whilst for the third one the reduction was based on the values of the same parameters of the second phase. The other modified parameters were the tensile strength and the tensile fracture energy.

Graph 5-9 presents the outcome of a series of analyses, including one on the RM model. This was performed just to confirm that for this FEA model, failure occurs during the first phase. The other two curves are the result of two analyses performed on the BBM, both failing during the second phase. The difference in behaviour was given by the assumed reduction in the material. A progressive reduction, as it was described in the previous paragraph, resulted in a better behaviour (blue curve). The earlier failure in the second stage (orange curve) was caused by assuming the same compressive strength for the reduction of each phase. For the BBM it is clear that the analysis was terminated due to divergence before starting its third phase.

The small decrease and subsequent increase of the curve in the first phase of the analysis was caused by a widening of the cracks and subsequent increase in the steel stress, behaviour similar to the single loading range models. The big drop in the curve marks the transition between the first and second phases of the analysis. It is thought that this behaviour might be caused by the decrease in the properties of the FEA model as a consequence of the assumed fatigue damage. It is essential to mention that as soon as the second phase started, the steel stress had exceeded the yield value and the concrete stress had exceeded the compressive strength, but did not exceed its ultimate strain. This was eventually exceeded, strangely, quite some load steps before failure. Until the analysis stopped, the stresses continued to grow, but

the steel stress did not reach its ultimate value. It is not understood why, based on the values from the second phase, the analysis did not stop much earlier, even at the beginning of this phase. It can be concluded that the FEA model presented a strange behaviour that can be deemed as unreliable and unrealistic.

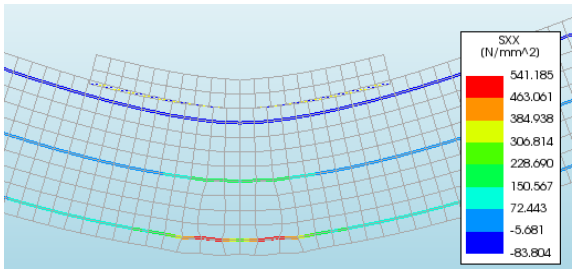

Figure 5-42 – Steel stress at the beginning of the second phase, BB28

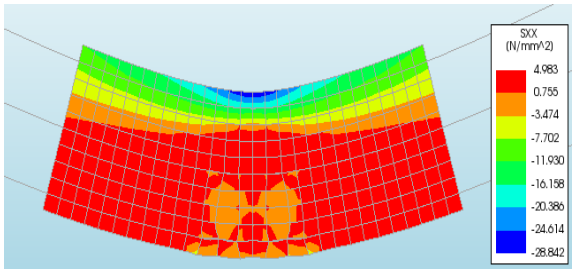

Figure 5-43 - Concrete stress at the beginning of the second phase, BB28

Test BB29 was composed of two load ranges, having maximum values of 200 and 220 kN. For the first range a number of 1.5 million cycles were performed whilst for the second, just under 265 thousands.

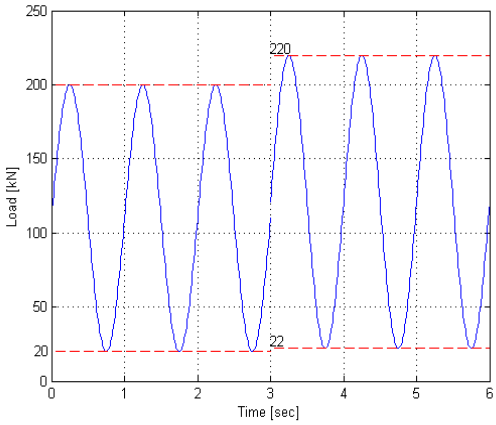

Figure 5-44 – Loading ranges for BB29 [15]

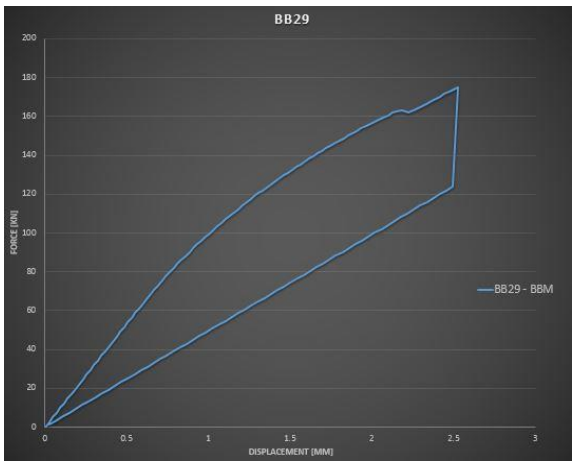

Graph 5-10 - FE analysis of test BB29

As it can be seen from Graph 5-10, the result of the FE analysis does not describe correctly the behaviour of the test BB29. The first phase of the analysis and the transition between phases followed the same trend as the one described by test BB28. When it came to the second phase however, the FEA model presented a decrease in both force and deflection. Such an occurrence cannot happen and it is unclear why the model behaved in such a manner. All the steps performed for the previous analyses regarding tests BB28 were followed also for this test, however the behaviour was very different. This might be due to the sensitivity of the model to certain parameters. Multiple analyses were performed in order to find what might be causing this behaviour but the same outcome was obtained every time.

5.4.1.2 Separate analyses approach

For this approach, all the loading ranges were analysed individually and subsequently plotted in order to assess the behaviour of the model, namely, its deterioration caused by each

loading range. The downside of this approach was that every analysis started with the same initial stiffness, the original one, whilst in the actual tests the stiffness had decreased constantly with the increase in the number of loading cycles and modification of the range. Such a change in stiffness was not performed for the second or third load ranges since it was not known how this would have been affected by the loading. The modification in the stiffness throughout the analysis was accounted for only by the tensile properties of the concrete. Nevertheless, the results can give an idea about how the fatigue damage, which was reproduced through the properties of the material, affected the capacity and the ductility of the structure.

For tests BB28 and BB29, three, respectively two separate analyses were performed accounting for the different cyclic ranges within each test. The outcome can be observed in the following graphs:

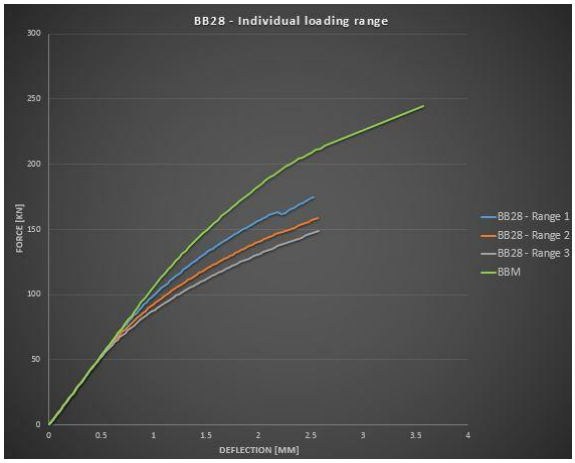

Graph 5-11 - Individual FEA for each loading range of test BB28

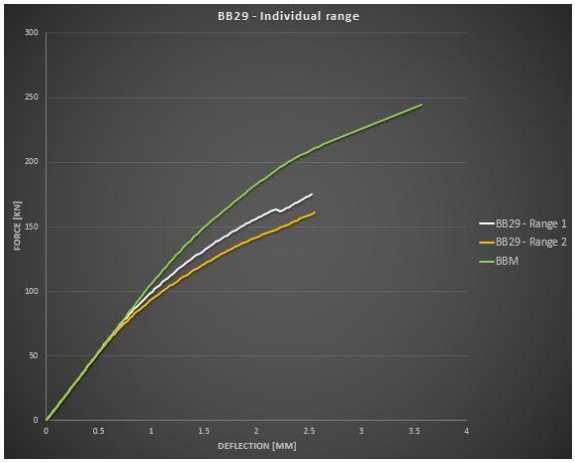

Graph 5-12 - Individual FEA for each loading range of test BB29

It can immediately be seen that there is a reduction in capacity with the increase in the loading range. This outcome is deemed as correct, since it was expected that, with the increase in the loading range, the model would not be able to bear higher loads due to the changes in the material's properties that accounted for the actual fatigue loading.

The curve for the first range had a small drop and rise due to the growth of crack widths and, simultaneously, increase in the steel stress. Such a behaviour was assessed previously in subsection 5.3. The curves for the other ranges were smoother, with the concrete and steel stresses having lower values than for the first range. Taken individually, the force resulted from the analysis of each range was higher than the predicted force given by Equation 5-2. This was also mentioned in subsection 5.3.

The first method tried to present the combined effect of the loading ranges by attempting to reach the static capacity of the model, this being considered as failure for the FE analysis. In case of the separate range approach, this tried to show the impact of the cyclic ranges on the model, presenting the progressive deterioration of the FEA model.

Since the best behaviour model was used (BBM) as it was mentioned earlier, all the loading steps converged, meaning that the model did not technically fail. Nevertheless, its

behaviour suggests that a flexural type of failure would eventually occur, similar to the case of the realistic model (RM).

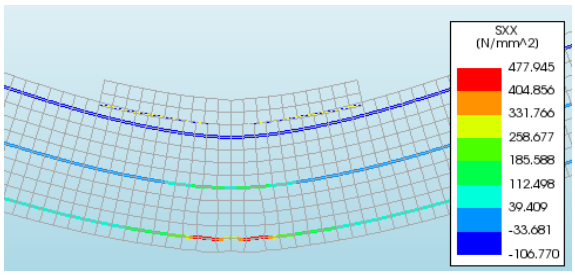

Figure 5-45 – Steel stress at the end of FEA for loading range 1 of test BB28

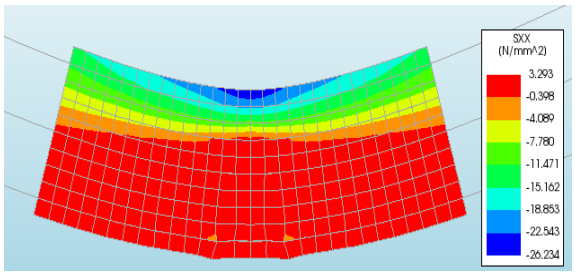

Figure 5-46 - Concrete stress at the end of FEA for loading range 2 of test BB29

5.4.2 Sequence effect

Within the fatigue tests that were performed and had multiple loading ranges, there was a test that had first a higher loading range, followed by a lower one. This led to an earlier failure of the specimen and the question whether such an outcome is just a random occurrence or an earlier failure can be caused by applying the cyclic load in such a manner.

The next research on fatigue that will be performed by TU Delft and will start in the near future, will specifically study this sequence effect with the hope of finding a conclusive answer. In this subsection of the thesis, it will also be tried, using finite element analyses, to study whether this effect can be replicated and, if so, assess its impact.

5.4.2.1 Palmgren-Miner rule

For an easy, fast and acceptable assessment of the fatigue damage, the Miner's rule can be applied. This describes a linear cumulative damage that is used to estimate the impact of cyclic loading. Miner's rule can be schematized as follows:

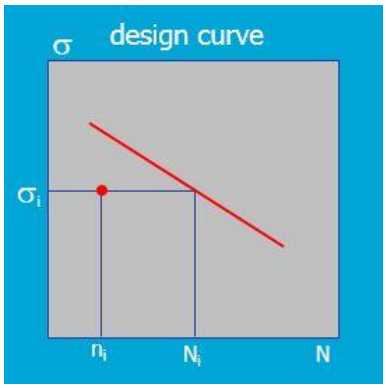

Figure 5-47 – Schematization of Miner's rule, design curve [29]

The general formulation for Miner's rule is given as:

Equation 5-3 – Formulation for Miner's rule

$$\sum_{i=1}^{k} \frac{n_i}{N_i} = 1 \quad [29] \text{ , where:}$$

- n_i represents the number of applied cycles within a certain stress/load range

-N_i represents the number of cycles to failure for a certain stress/load range

One major limitation of this method is that it does not take into account the sequence effect, more specifically, the order of loading is of no importance. This does not correspond with results from tests, where an impact of the sequence was observed. Another limitation of Miner's rule refers to the accumulation of damage, which is considered to be independent of the stress level. Again, this is a too simplistic assumption. [29]

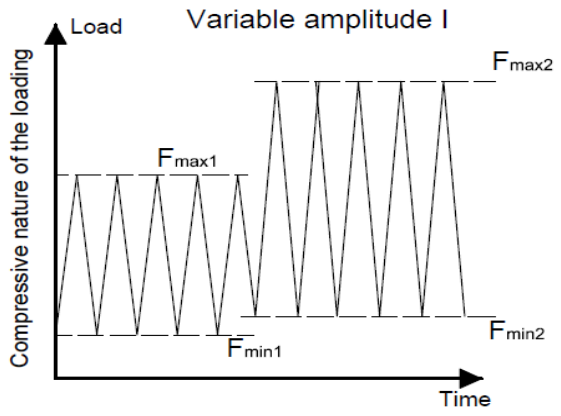

Figure 5-48 – Loading sequence, type I

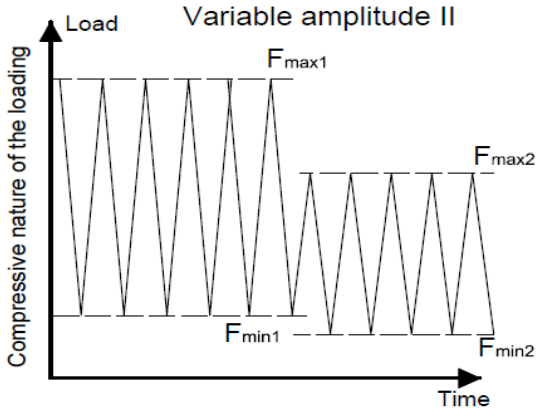

Figure 5-49 – Loading sequence, type II

Since the Miner's rule cannot provide a proper assessment of the sequence effect, in the following a numerical approach will be used for this purpose.

5.4.2.2 Phased analysis approach

For this approach, two loading ranges were assumed, one with a maximum value of 150 kN and 1.5 million cycles and a second range with a maximum value of 200 kN and 1 million cycles. Such a high number of cycles was chosen since it was observed that a proper reduction in the material's parameters occurred only at high values. The minimum load value within each range was 10% of its maximum, as before. The reduction in material properties was done for each loading range as it was described in subsection 5.4.1.1.

Two analyses were performed on the best behaviour model (BBM), one where the first loading range had a smaller maximum value than the second range (low to high) and a second analysis that had first a higher range, followed by a smaller one (high to low).

Following the analyses, a similar behaviour to the one described in subsection 5.4.1.1 was observed, with the outcome being almost identical for both of the FEA models. Based on this observation, it seemed that there was no impact of the load sequence, at least not for this model. Graph 5-13 presents the results of the phased analyses.

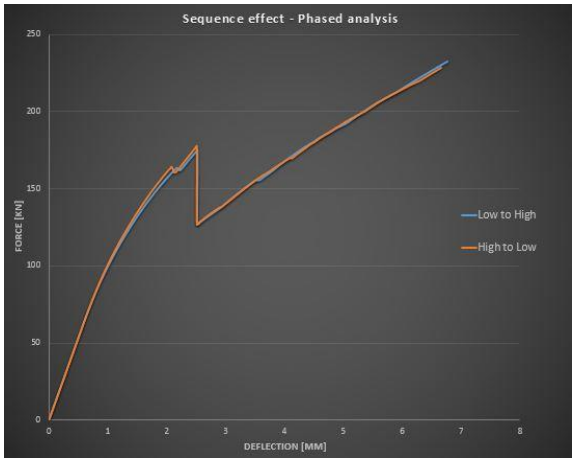

Graph 5-13 – Sequence effect, phased analysis

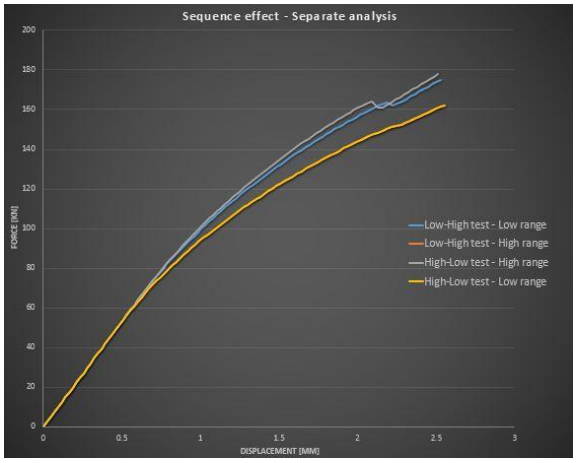

Graph 5-14 – Sequence effect, separate analysis

5.4.2.3 Separate analysis approach

For the separate approach the same stress ranges as for the phased analysis were considered. In this case, two sets of analyses were performed, one for each type of sequence, low to high and high to low. Within each set, individual analyses were performed for each loading range using the best behaviour model. The stiffness was considered to be the original one in all the analyses, as it was explained in subsection 5.4.1.2.

As it can be seen in Graph 5-14, also for this approach the FEA model does not seem to be sensitive to the loading sequence. The resulting curves describe almost the same behaviour, with two of them, the ones at the bottom, overlapping each other. The curves at the top represent the outcome of the first loading range within each set of analyses, whilst the curves at the bottom are the result of the second loading ranges.

5.5 Conclusions of the FEA – Stage II

Having created and calibrated the FEA model in Chapter 4, the first part of this chapter tried to replicate the single load range fatigue tests that were described in reference [15]. In order to do that, changes in the material's parameters of the FEA model had to be made for simulating its deterioration as a consequence of the cyclic loading. The effect of fatigue meant a decrease in the capacity and ductility of the model.

The main point of departure for this stage was the consideration of a uniform reduction in the material properties with an impact at the structural level. It was assumed that the

compressive strength of the concrete was the main material parameter and the rest were dependent on its variation. The decrease in this strength, which was based on Equation 5-1, led to an overall diminishment in the behaviour of the FEA models. Directly affected were the tensile strength and both fracture energies. For the tensile strength, different approaches were considered for its reduction, choosing the one that seemed more fitting. This had no influence on capacity of the model, only on its ductility.

In the case of the BBM, this had that extra capacity and increase in the curve probably due to the bond of the prestressing bar, with the CMA being also more easily noticeable. The RM had a not so common mode of failure, with the stresses still being well below their ultimate value, except the tensile one in the concrete. It is thought that the strain capacity of the concrete was exceeded due to a sudden increase of the crack width, in combination with a similar increase in the steel stress, this being the main reason for failure.

Following the FE analyses, all the tests presented a significant reduction in terms of capacity and ductility of the model when compared to the static tests, reduction that was expected to occur with the simulation of the fatigue loading. Nevertheless, when the results were plotted against the ones from the experimental tests, the outcome presented quite a discrepancy from what was presumed to be obtained. These were out of the confidence interval, with a single exception, and also the reduction in material properties seemed insufficient. By assessing Graph 5-8, it could be estimated that the model would present a higher accuracy for lower numbers of loading cycles. As a general remark, both FEA models present a higher value for the fatigue force than the one given by the prediction formula (Equation 5-2).

A major reason for this behaviour is thought to be the reduction in the compressive strength of the concrete. According to Equation 5-1, this reduction depends on the number of cycles, on the ratio of the minimum and maximum values of the applied stress (force) and on the compressive strength of the concrete. Whilst the former and latter have values that, righteously, can be considered as constants (fixed values) for a single analysis, assuming that the influence of the loading range can be expressed only through its force ratio seems not realistic in terms of the actual impact of the loading on the structural system. Based on the ratio, no matter how high or low the applied maximum force within a stress range is, it will lead to the same impact. Maybe it is assumed that the applied value of the load can be reflected in the number of cycles to failure (the higher the value, the lower the number of cycles), but this would also be a partially wrong assumption, since it is known about the large scatter in the results of fatigue tests.

An eloquent example can be seen in Graph 5-8 for the tests BB24_150 and BB26_165, which displayed an almost identical behaviour. This happened although there was a difference in the number of cycles of ≈100000, but also a difference in the value of the load.

Coming back to the formula for determining the maximum compressive stress (Equation 5-1), this might be deemed as being not accurate enough for properly describing the reduction of the compressive strength due to a cyclic loading. The value of the load should have a higher impact on the reduction by taking into account the stress range in a more realistic

manner. If such a correlation would be possible, then a more accurate reduction in the material's parameters would lead to a highly realistic scenario of assessing fatigue, this being of utmost importance.

The prediction formula for the fatigue force, Equation 5-2, might also have an impact on the range of the results. This takes into account only the number of cycles and based on this it predicts the ratio between the fatigue and static forces. Not taking into account at all the loading range might seem too simplistic and not sufficiently accurate. It might be that an altered formula that takes into account the values of the load would give results closer to the FEA analysis.

The second part of this chapter dealt with tests that had multiple loading ranges and also with the impact of the load sequence on the behaviour of the model. In order to simulate a test with multiple ranges, two different approaches were used: one dealt with phased analyses whilst the other used separate analyses for each range. A phased analysis meant that the loading ranges were analysed one after the other, having a continuity of the stress state.

For replicating the behaviour of the structural system as close as possible to the one damaged by fatigue, each loading range from an analysis had its material properties modified. Both strengths, together with the fracture energies, ended up being altered, with the compressive strength being considered the main parameter in simulating the damage due to the cyclic loading. It was observed that a high number of cycles was required in order to witness a proper reduction.

Following the multiple range analyses, it was observed that both of the approaches used, phased and separate, had difficulties in describing accurately the behaviour from the experimental tests. The outcome presented strange results that could be attributed to the FEA model itself, but also to the user of DIANA, due to a lack of experience and expertise with this type of analyses. Like stated previously, the phased analysis tried to present the combined effect of the loading ranges. This was done by attempting to reach the static capacity of the FEA model, since this was considered to be the failure criterion of the FE analysis. As for the separate range approach, this analyses tried to show the impact of the cyclic ranges on the model, presenting its progressive deterioration, with this type of behaviour being observed following the analyses.

In order to assess the impact of the loading sequence, use was made again of the previously mentioned approaches. Following the obtained results, it might seem that the sequence of loading does not have any impact on the behaviour of the model. Nevertheless, a conclusive answer cannot be given, since the behaviour of the model is influenced by a high range of parameters, with the model also presenting a series of limitations, as it was stated from the beginning. The reduction in the properties of the material plays also a significant role, together with the number of assumed cycles to failure. Also the user component has to be taken into account, as it was stated before.

Chapter 6: Future research program

In this chapter, the preparations for the future research program on fatigue that will be performed at TU Delft in the near future will be described. This program is a follow-up to the one that was done in the past [15] and focuses on the impact of the loading sequence. In the initial research there was only one test during which a higher loading range preceded a lower one, usually being vice versa. The result showed a detrimental effect on the structural system of such a type of sequencing. This contradicted Miner's rule for cumulative damage, according to which the sequencing should have no impact on the final outcome. This rule, which is known for its limitations towards sequencing, was presented in subsection 5.4.2.1. It is the purpose of this future study to shed light on the matter of loading sequence and its impact, hoping to reach a series of generally valid conclusions.

During the summer of 2016, starting with the end of June and until the end of August, work was done in order to finalize the structural system that will undergo testing. Like in the previous research, the system was a scaled model (1:2) of a concrete bridge, being made up out of three precast prestressed longitudinal girders, two cast in-situ end beams that were subsequently prestressed and a cast in-situ deck slab which was transversely prestressed also.

Between the previously tested and the current structure, there are a few major differences that are mentioned in the following:

- number of longitudinal girders: 4 in the case of the previous research, 3 for the current study

Figure 6-1 – Number of longitudinal girders for the previous structural system [14]

Figure 6-2 – Number of longitudinal girders for the current structural system

- cross section of the longitudinal girders: for the initial research, the girders had both a top and bottom flange, having also larger dimensions than the ones used for the current system, with the latter also lacking the top flange

- concrete deck slab: the first structural system had the deck slab composed out of the flanges of the longitudinal girders and cast in-situ concrete strips, these being casted between the flanges; for the current system, the deck slab has been monolithically cast in-situ over its whole area

- thickness of the deck slab: the first system had a 100 mm thick cast in-situ part of the deck, adjacent to the flanges; for the current one, the deck slab has also 100 mm in the

central area between the girders, where the tests will be performed; at the extremities of the girders however, in order to account for the top flange, the thickness of the slab is more than twice the previously mentioned one

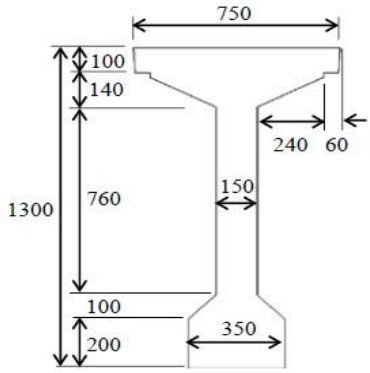

Figure 6-3 - Cross section of longitudinal girders from previous study [14]

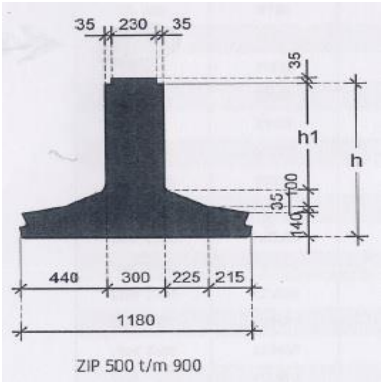

Figure 6-4 - Cross section of longitudinal girders from current study

The precast longitudinal girders were manufactured by Spanbeton and delivered to TU Delft's Stevin II laboratory where they were placed on their final position (Figure 6-2), taking into account the geometry of the structural system.

The next stage after positioning the longitudinal girders was the construction of the formwork for the transverse end beams, placement of their reinforcement and PVC tubes for the prestressing bars, followed by the casting operation. Each end beam was composed of two different but symmetric segments, positioned between the girders. It must be mentioned that all the required reinforcement for the structure was delivered to TU Delft already assembled.

Figure 6-5 – Formwork and reinforcement for end beams

Figure 6-6 – Transverse end beams after casting

Following the casting of the end beams, the challenging task of building the formwork for the deck slab ensued. The difficulty of this assignment was represented by the need to have a 100 mm thick deck, with a margin of error of 2 mm, all while the precast prestressed beams had a pre camber in their middle zone. This task was additionally made more difficult by the material that was used and the size of its boards, as the formwork had to have a slightly concave shape. Also a high number of wooden frames were required for the stability of the formwork.

Figure 6-7 – Wooden frames for supporting the formwork

Figure 6-8 – Completed formwork for the deck slab

After finishing with the erection of the formwork, the next stage in the construction of the structural system was represented by the placement of the reinforcement inside the formwork. The bars had already been assembled and delivered in a cage type of format. With the aid of a moving crane, all the parts were placed at their required positions. Following the placement of the reinforcement, the PVC tubes for the prestressing bars within the deck were mounted.

Figure 6-9 – Structure after positioning of the reinforcement ant PVC tubes

Figure 6-10 – Close-up with the reinforcement and the plastic tubes

Once the structural system had the reinforcement and the plastic tubes for the prestressing bars installed at the required locations, the casting of the concrete followed. This was a continuous operation that was performed in one go, starting with the casting at one side of the deck slab and finishing at the other end. Used was made again of the moving crane, this moving the concrete bucket from which the concrete was poured inside the formwork. Throughout the casting procedure, the concrete was vibrated in order to obtain a better compaction and remove the air pockets.

After the casting was finalized, the surface of the concrete was smoothened using a long aluminium beam and subsequently it was covered with a plastic foil in order to prevent the water from evaporating, therefore assuring a proper hydration process.

Figure 6-11 – Casting and smoothing the surface of the concrete

Figure 6-12 – Concrete covered with a plastic foil to prevent water evaporation

A week after the casting, the transverse prestressing bars were installed at their position and at the beginning of October, after it was considered that the concrete had developed the required strength, they were also tensioned. After tensioning the bars, the preparation for the testing setup began. A large metal frame was moved in position and a loading device was eventually attached to it. The full setup consists of a high number of sensors and measuring devices for forces and deflections, all connected to a system for data acquisition.

In the following months, both static and fatigue tests will be performed on the structural system, with the stated goal of clarifying whether there is an effect of the loading sequence within the fatigue tests.

Figure 6-13 – Tensioning of the prestressing bars

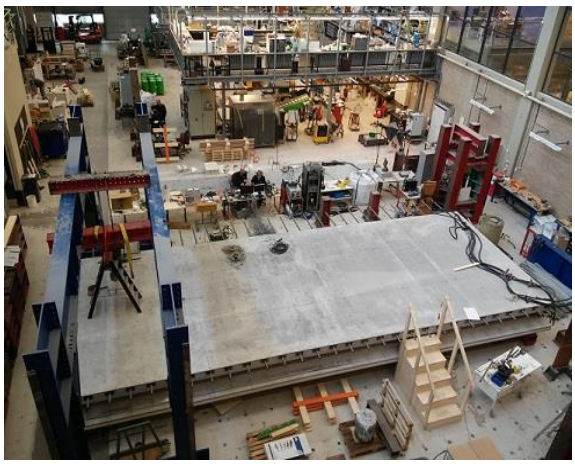

Figure 6-14 – Structural system prepared for tests

Chapter 7: General conclusions

This chapter will present in a more fluid and concise manner the conclusions that accompanied the previously discussed segments of this Master's Thesis. Each previous chapter introduced a specific part that was required to properly describe the theme that was addressed in this thesis. In the following, the essential ideas, observations, viewpoints and conclusions will be outlined so that a full image of the accomplished work will be portrayed.

The thesis started with the idea of creating a simplified FEA model that would describe the effect of fatigue on a structure, more specifically on a concrete bridge deck slab that was transversely prestressed. Before tackling this numerical approach, insight into the topics of fatigue and compressive membrane action (CMA) had to be gained. These are two phenomena that affect the service life of a bridge, fatigue in a negative manner, whilst the CMA has a positive effect.

As the main topic around which this thesis was constructed, fatigue was described as a complex phenomenon, being presented how it affects and damages the individual materials, concrete and steel, but also the reinforced concrete structures. In case of the materials, the emphasis was put on the behaviour of concrete under different stress situations such as compression, tension and alternating stresses, presenting the material's response under the cyclic loading. In terms of structures, the impact of fatigue on concrete deck slabs was mainly discussed. As a general conclusion related to the impact of fatigue, it is stated that, although it did not cause a direct failure of a structure, its contribution cannot be ignored during the service life of structures that are prone to this phenomenon. For the other approached topic, CMA, it is found that this forms in concrete slabs and increases the capacity of the structure, being dependent on the degree of restraint.

The previous research program on fatigue of concrete deck slabs performed at TU Delft was assessed from the point of view of the results, the structural system and the variables within each test and was considered to fit well with the other studies performed on this topic on a worldwide scale. The obtained results are in correlation with similar outcomes from studies performed across the globe, this giving a high degree of trust to the research. This study represented one of the primary sources for the development of the FEA model, with the other major source being the research on CMA of prestressed concrete deck slabs performed around the same time also at TU Delft.

The method used for the development of the FEA model comprised a series of steps and suppositions that were followed in order to obtain an outcome that was as accurate as possible. During this process, a couple of fundamental points of departure had to be considered. The first one implied the use of a two-dimensional model for describing the stress state, whilst the other made use of the assumption of a uniform reduction in the material properties on a structural level. Both of these had a decisive contribution to the behaviour of the model and the results.

The scope of the FEA model, developed using DIANA FEA, was to replicate as accurately as possible the results from the previously mentioned experimental programs. For its development, a two-dimensional plane stress model was chosen, acknowledging the limitations of such a model when describing a three-dimensional stress state. In terms of

geometry, it was decided to define the whole cross section of the structure since it was observed that, by doing so, the behaviour was more realistic. For the supports, the fixed translation on both directions combined with an allowed rotation presented the best outcome by having a substantial contribution to the increase in the initial stiffness of the model. The chosen effective width of the model proved to be essential in obtaining an initial stiffness that was similar to the one from the previous studies. Based on this width, the directly proportional quantity of reinforcement was assigned to the model and also the equivalent prestressing load. These last two parameters had a vital contribution to the capacity of the model. A high contribution to the overall behaviour was also obtained by considering that the prestressing bar was bonded.

The chosen material models were in accordance with the guidelines from Rijkswaterstaat and proved to have a considerable impact on the model's behaviour as well. For the concrete, a total strain based crack model with rotating cracks and smeared cracking was used. Its compressive behaviour was defined using a parabolic model, whilst for the tensile behaviour a linear softening model was used, this giving a better behaviour than the exponential one recommended by the guidelines. For the reinforcing steel, a model based on Von Mises plasticity was used, with a user defined stress-strain diagram that included a hardening branch and a downward branch considered for the iterative process.

Applying the external force as a point load was found to give better results than a distributed load or a prescribed displacement. In order to avoid early divergence of the iterative procedure, the arc-length control method was used. Linear analyses were performed only to check the reliability of the model. Nonlinear analyses were performed in order to reflect more realistically the behaviour of the model and also for the possibility to subsequently modify the parameters of the materials for the second stage of the FE analysis, the one related to fatigue. The mesh size used was in accordance with the guidelines also.

After considering and assessing the influence of a wide range of parameters, it was decided to use two models for the fatigue related stage of the FE analysis. The first model gave the closest results to the ones from the previous studies and it was named the "best behaviour model" (BBM). In its case it was used the assumption that the prestressing bar is bonded. The second model did not consider the bond of the prestressing bar, being in accordance with the real structure. This was named the "realistic model" (RM) and had a lower capacity than the previous one. Overall, the capacity of both FEA models was found to be lower than the capacities obtained in the previous studies, but this was expected considering that the FEA model was built using a simplified approach. It was observed that within the models, the CMA had developed. The failure mode was of flexural nature, this being the result of the two-dimensional plane stress model used.

For simulating the deterioration of the structure due to fatigue, modifications of the material parameters of concrete in the FEA model were performed, with the effect of fatigue being a reduction in capacity and ductility. This reduction was considered to be uniform and at a structural level. The main material parameter that was modified was the compressive strength of the concrete and, based on it, the tensile strength and the fracture energies were modified also. For the determination of the maximum compressive stress allowed after the cyclic loading,

a reduction formula was used, this being dependent on the number of cycles and the ratio between the minimum and maximum values of the stresses/loads within a loading range.

Following the FE analyses, the expected reduction in capacity and ductility was witnessed, with the BBM having a better behaviour than the RM. When the results were plotted against the previous ones from the experiments, it was observed that they had an offset from the confidence interval given by a prediction formula developed at TU Delft, with one single exception. As a general observation, both FEA models present a higher value for the fatigue force than the one given by the prediction formula, with the RM giving the highest ratios between the fatigue force and the static force. It was observed that in order to obtain a proper reduction in the material properties a high number of cycles was required.

A main cause for this behaviour, apart from the limitations of the FEA model itself, is thought to be an insufficient reduction in the previously mentioned material properties, the main considered parameter being the compressive strength. Its reduction, which is based on the number of cycles and the ratio of the stresses/loads, seems to be too simplistic, with the actual impact of the loading being disregarded. By considering only the ratio, no matter how high or low the applied maximum force within a stress range is, it will lead to the same effect. If it is assumed that the magnitude of the applied load is reflected in the number of cycles, this would also be a partially wrong assumption, since it is known about the large scatter in the results of fatigue tests. The opinion is that the reduction formula for the compressive stress is not accurate enough and does not describe properly the full effect of the fatigue loading. On a similar note, the prediction formula for the fatigue force might also be too simplistic since it disregards the loading effect altogether and considers only the influence of the number of cycles and the static strength.

For the tests involving multiple loading ranges two different approaches for the analyses were used, phased and separate. The phased analysis tried to present the combined effect of the loading ranges, whilst the separate analysis tried to show the impact of the cyclic ranges on the model, presenting its progressive deterioration. Like in the case of single loading ranges, also here a reduction in the material parameters was performed for each individual range, the same properties as the ones mentioned before being modified. Having performed the analyses, it was acknowledged that both of the approaches used had difficulties in describing accurately the behaviour from the experimental tests. It is thought that the results could be attributed to the FEA model itself, but also to the DIANA user, due to a lack of experience and expertise with this type of analyses.

The last attended matter was represented by the impact of the loading sequence. The same two approaches, phased and separate, were used in order to describe the behaviour of low-to-high or high-to-low loading cycles. Based on the results it seems that the sequence has no impact on the behaviour of the model, but it is thought that a conclusive answer cannot be given. This is due to the limitations of the model and the assumptions taken for its development, the high number of parameters that interact with each other and influence its behaviour. The way the reduction in the properties of the material is performed or the user component must also be considered.

The FEA model that was developed to serve as topic for this Master's Thesis proved its limitations when compared to the results obtained from the previous research programs. This was not something unexpected, considering that a simplified approach was taken for its development. It was shown that its behaviour is influenced by a high number of parameters, being sensitive to their variation, but also proved to be flexible in response.

Chapter 8: Recommendations

The 8th and final chapter of this Master's Thesis presents a series of recommendations that aim at improving the approach towards the studied topic and its desired outcome. The improvements can be done on different levels as it will be outlined below.

For the actual FEA model, considering other material models for the behaviour of concrete under compression and tension might lead to a change in the results and possibly a better outcome. For this thesis, a number of such constitutive models were considered, taking also into account the guidelines on nonlinear analysis of concrete structures from Rijkswaterstaat, but DIANA offers a higher number of predefined material functions. It might be that by using other material models the behaviour of the FEA model will be noticeably improved.

If a two-dimensional model would still be desirable, then a plane strain one could be used. The choice of the plane stress model for this thesis was deemed to be accurate enough and its choice was explained. Nevertheless, a plane strain model might present an improvement of the stress state and of the general behaviour, being closer to the real structure.

For a complex and realistic assessment of the structure, a three-dimensional model could be created. This would present as close as possible the actual behaviour of the structural system, being defined by a high complexity and the lack of simplifications or assumptions required for a two-dimensional model. However, the high fidelity of its behaviour has a series of downsides, such as the time required to actually develop the model, the duration of the performed analyses, this increasing exponentially compared to the simple 2D model, or the amount of computational power required to perform such complex analyses.

Upgrades to the formula that determines the maximum compressive stress bearable by the structure after cyclic loading should be performed. It was discussed that it appears to be too simplistic to consider only the ratio of the stresses/loads within a range, this leading to an effect of the fatigue that is thought not to be correctly described. As a consequence, a higher contribution of the loading range must be considered.

Modifications could be done also to the prediction formula for the fatigue force so that this would take into account the force values of a loading range, not only the number of cycles and the static capacity of the structure. It is believed that, by doing so, a more accurate force prediction will be obtained.

Further fatigue tests should also be performed in order to gain additional knowledge related to this phenomenon and assess better the impact of the loading sequence and its minimum and maximum values.

Annex 1

Estimation of the fatigue load value

1) Reference no. 12 - study by Graddy et al.

In the article, besides the S-N line, the essential data used to obtain the graph is presented for each specimen (Table 4). In order to estimate a value at 1 million cycles, a series of assumptions are made, these being presented in the following.

For the prediction, a number of 3 tests is considered since they were identical and the scatter in the results, in terms of numbers of cycles to failure, is small compared to other tests, having the same range for the magnitude. The codes of the specimens were S1P110, S2P110 and S3P110.

The tests taken into account had only cast in situ specimens but the estimation for the fatigue load will also be extrapolated to the prestressed + cast in situ specimens since the S-N graph takes them into account also.

From the graph, it is approximated that the value for the normalized stress range at 1 million cycles is 3.25.

The value for the static load will be the average of the ones obtained following the static tests.

The value for the concrete compressive strength will be the average value of the strengths of the specimens.

The Imperial unit system will be used, as it is used throughout in the scientific paper.

The formulas used for the nominal punching shear and for the normalized stress are the ones presented and used in the article.

$\upsilon := \frac{P}{b_0 \cdot d_{eff}}$ - Nominal punching shear stress

$\frac{\upsilon}{\sqrt{f_c}}$ - normalized stress

$f_{c.average} := \frac{5490psi + 5710psi + 5870psi}{3} = 5.69 \times 10^3 \cdot psi$ - Average value for the concrete compressive strength

$b_0 \cdot d_{eff} := 395in^2$ - Effective area $A_{eff} := 395in^2$

$\frac{\nu_{assumption}}{\sqrt{f_{c.average}}} := 3.25$ - approximated normalized stress at 1 million cycles

$\upsilon_{assumption} := 3.25\sqrt{psi} \cdot \sqrt{f_{c.average}} = 245.154 \cdot psi$

$P_{fatigue} := A_{eff} \cdot \upsilon_{assumption} = 9.684 \times 10^4 \cdot lbf$ - Estimated value of the fatigue load at 1 million cycles

$P_{static} := \frac{173kip + 205kip}{2} = 1.89 \times 10^5 \cdot lbf$

$\frac{P_{fatigue}}{P_{static}} = 51.236 \cdot \%$ - The ratio between the estimated fatigue load at 1 million cycles and the static load

2) Reference no. 7 - study by Hwang et al.

Prediction from formula no. 1, based on the average wheel load:

$$\frac{P}{P_p} := -0.2019 \cdot \log(N_c) + 1.384$$

$N_{c1} := 10^6$ $\frac{P}{P_p} := -0.2019 \cdot \log(10^6) + 1.384 = 0.173$ - Prediction for 1 million cycles

P is the fatigue load and P_p is the static load.

Prediction from formula no. 2, based on the maximum wheel load:

$$\frac{P}{P_p} := -0.2157 \cdot \log(N_c) + 1.535$$

$N_{c2} := 10^6$ $\frac{P}{P_p} := -0.2157 \cdot \log(10^6) + 1.535 = 0.241$ - Prediction for 1 million cycles

At 100 million cycles the result is negative, the formulas not being able to predict the fatigue load:

$\frac{P}{P_p} := -0.2019 \cdot \log(10^8) + 1.384 = -0.231$ - First formula

$\frac{P}{P_p} := -0.2157 \cdot \log(10^8) + 1.535 = -0.191$ - Second formula

3) Reference no. 20 - study by Sonoda and Horikawa

Prediction formula for isotropic slabs under fixed point pulsating load:

$$\frac{F_{fatigue}}{F_{static}} := 1.08 - 0.086 \cdot \log\left(N_{cycles}\right)$$

The 1.08 and 1.14 values are not found in reality as a load higher than the static one (presumed to be 1) cannot be considered.

Estimation at 1 million cycles: $\frac{F_{fatigue}}{F_{static}} := 1.08 - 0.086 \cdot \log\left(10^6\right) = 56.4 \cdot \%$

Estimation at 100 million cycles: $\frac{F_{fatigue}}{F_{static}} := 1.08 - 0.086 \cdot \log\left(10^8\right) = 39.2 \cdot \%$

Prediction formula for orthotropic slabs under fixed point pulsating load:

$$\frac{F_{fatigue}}{F_{static}} := 1.14 - 0.093 \cdot \log\left(N_{cycles}\right)$$

Estimation at 1 million cycles: $\frac{F_{fatigue}}{F_{static}} := 1.14 - 0.093 \cdot \log\left(10^6\right) = 58.2 \cdot \%$

Estimation at 100 million cycles: $\frac{F_{fatigue}}{F_{static}} := 1.14 - 0.090 \cdot \log\left(10^8\right) = 42 \cdot \%$

4) Reference no. 21 - study by El-Ragaby et al.

Prediction formula resulted from this study:

$$\frac{P}{P_s} := 0.0034 \cdot \left(\log\left(N_{cycles}\right)\right)^2 - 0.11873 \cdot \log\left(N_{cycles}\right) + 1.0752$$

Estimation at 1 million cycles:

$$\frac{P}{P_s} := 0.0034 \cdot \left(\log\left(10^6\right)\right)^2 - 0.11873 \cdot \log\left(10^6\right) + 1.0752 = 48.522 \cdot \%$$

Estimation at 100 million cycles:

$$\frac{P}{P_s} := 0.0034\cdot\left(\log\left(10^8\right)\right)^2 - 0.11873\cdot\log\left(10^8\right) + 1.0752 = 34.296\cdot\%$$

The prediction formula derived by Matsui et al. (2001) that deals with reinforcing steel:

$$\log\left(\frac{P}{P_s}\right) := -0.07835\cdot\log\left(N_{cycles}\right) + \log(1.52)$$

Estimation at 1 million cycles: $\frac{P}{P_s} := 10^{\left(-0.07835\cdot\log\left(10^6\right)+\log(1.52)\right)} = 51.492\cdot\%$

Estimation at 100 million cycles: $\frac{P}{P_s} := 10^{\left(-0.07835\cdot\log\left(10^8\right)+\log(1.52)\right)} = 35.896\cdot\%$

Annex 2

Linear and nonlinear analysis checks

For these checks, the steel plates were not considered in the hand calculations or the FEA analysis since their behaviour could influence the results.

1) Deflection at mid-span due to self-weight (linear):

The part of the deck is schematized as a beam clamped at both ends.

$l_{span} := 1.80m$ - length of the span

$h := 0.10m$ - height of the deck

$b := 1.95m$ - considered thickness of the model

$\gamma_c := 25\frac{kN}{m^3}$ - specific weight of concrete

The load per linear meter is equal to: $q := \gamma_c \cdot h \cdot b = 4.875 \cdot \frac{kN}{m}$

$E_c := 39000MPa$ - modulus of elasticity of concrete

$I := \frac{b \cdot h^3}{12} = 1.625 \times 10^{-4} m^4$ - moment of inertia of the deck

The deflection at mid-span due to the self-weight is equal to: $\delta_G := \frac{q \cdot l_{span}^4}{384 \cdot E_c \cdot I} = 0.021 \cdot mm$

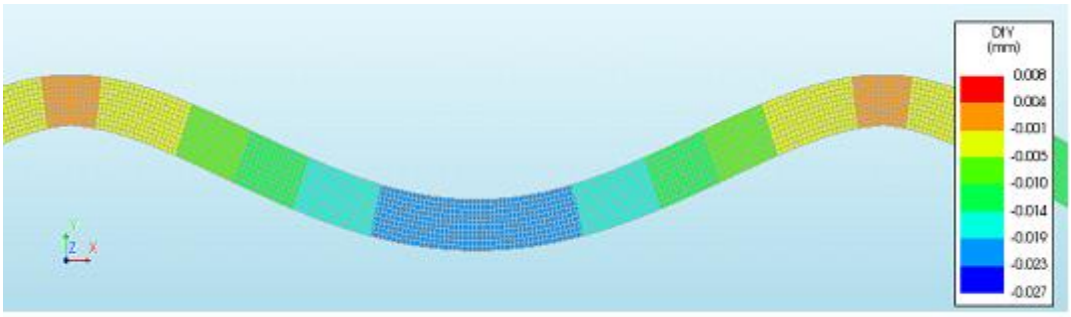

Figure 1 - Deflection of the FEA model due to self-weight

It can be seen that the calculated value of the displacement is similar to the value determined by DIANA following the linear analysis.

2) Stresses at the outer fibers due to self-weight (linear):

$M_G := \frac{q \cdot l_{span}^2}{24} = 6.581 \times 10^5 \cdot N \cdot mm$ - moment due to self-weight

$W_{section} := \frac{b \cdot h^2}{6} = 3.25 \times 10^6 \cdot mm^3$ - section modulus

The stress at the outer fibres due to self-weight is: $\sigma_G := \frac{M_G}{W_{section}} = 0.203 \cdot MPa$

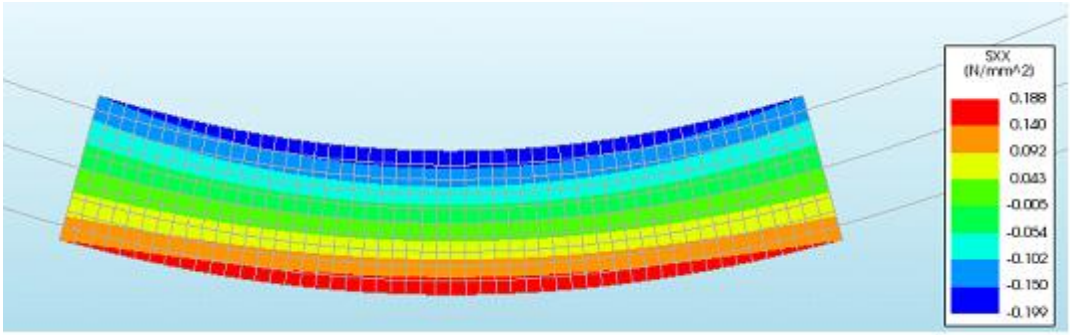

Figure 2 - Stresses at the outer fibers due to self-weight in the FEA model

It can be seen that the calculated value of the stresses at the outer fibres is similar to the values determined by DIANA following the linear analysis.

3) Force at cracking (nonlinear):

$f_{ct} := 5.41MPa$ - tensile strength of the concrete

$M_{cr} := \left(f_{ct} + 2.5MPa\right) \cdot W_{section} = 25.708 \cdot kN \cdot m$ - cracking moment of the section considering also the effect of the prestressing

General formulation for the cracking moment: $M_{cr} = \frac{q \cdot l_{span}^2}{24} + \frac{F_{cr} \cdot l_{span}}{8}$

$F_{cr} := \frac{8 \cdot M_{cr} - \frac{q \cdot l_{span}^2}{3}}{l_{span}} = 111.331 \cdot kN$ - cracking force determined analytically

In the FEA model the cracking occurs at a value of approximately 90 kN, a lower value than the one calculated previously. This difference is thought to be the result of how DIANA uses, within the nonlinear analysis, the material models considered for the concrete in combination with a smeared cracking approach.

4) Deflection due to the point load (linear):

$F_{pl} := 335kN$ - external point load applied to the deck

The deflection at mid-span due to the point load is equal to: $\delta_F := \frac{F_{pl} \cdot l_{span}^3}{192 \cdot E_c \cdot I} = 1.606 \cdot mm$

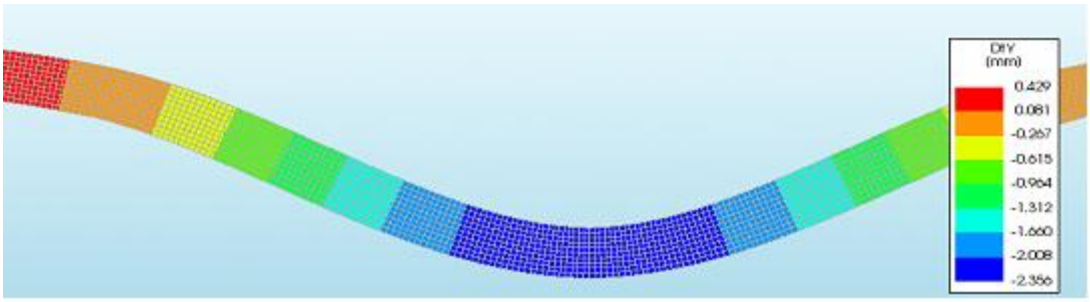

Figure 3 - Deflection due to the external force of the FEA model

In case of the deflection due to the external force, the value resulted from the FEA linear analysis is slightly larger than the computed one.

5) Stresses at the outer fibers due to the point load (linear):

$M_F := \frac{F_{pl} \cdot l_{span}}{8} = 75.375 \cdot kN \cdot m$ - moment due to the point load

$\sigma_F := \frac{M_F}{W_{section}} = 23.192 \cdot MPa$ - stress in the outer fibres

The stresses obtained from the FEA are very close to tha calculated value. In the plot below, the stress at the top should have a similar value with the one at the bottom, but this differs since the point load is applied in this case directly on the concrete element, therefore having a stress concentration in that area.

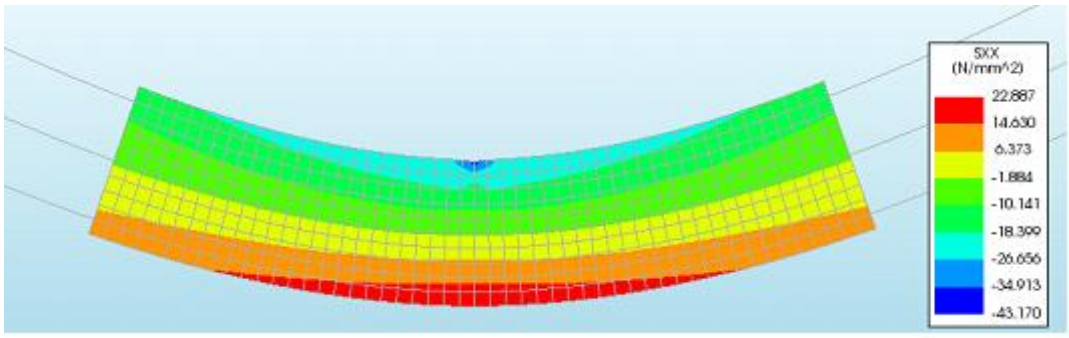

Figure 4 - Stresses at the outer fiber due to the point load in the FEA model

List of Figures

Figure 1-1 – Dutch road network: e.g. The Ridderkerk interchange (source: Wikipedia) 19
Figure 1-2 - Constant amplitude fatigue loading..... 20
Figure 1-3 - Variable amplitude fatigue loading (I)..... 20
Figure 1-4 - Variable amplitude fatigue loading (II)..... 20
Figure 1-5 – Structural behaviour 22
Figure 1-6 – Behaviour due to cyclic loading in compression [29] 22
Figure 2-1 - Development of fatigue damage [2, 3]..... 27
Figure 2-2 - Example of a Wohler diagram (S-N curves) [2, 3] 27
Figure 2-3 - Example of a Goodman diagram [3]..... 27
Figure 2-4 - Development of cyclic strain [2, 3]..... 28
Figure 2-5 - Cyclic stress-strain curve for concrete in compression [2, 3] 28
Figure 2-6 – Cyclic stress-strain curve for concrete in tension [3] 29
Figure 2-7 – Development of the tensile strain components [3] 29
Figure 2-8 - Cyclic stress-strain for reversals 29
Figure 2-9 – Detrimental effect of stress reversals [2, 3]..... 29
Figure 2-10 - S-N diagrams for wet (left) and dry (right) concrete [2, 3]..... 30
Figure 2-11 - Stress-strain relation with post-peak cycles for concrete in compression [3].... 31
Figure 2-12 - Stress-strain relation with post-peak cycles for concrete in tension [3] (from Reinhardt, Cornelissesn and Hordijk, 1986) 31
Figure 2-13 - Linear softening relations and an experimentally determined relation [13] 31
Figure 2-14 - σ-w relations, and data points [13]..... 31
Figure 2-15 - Size effect on bars [2]..... 32
Figure 2-16 - S-N curves for wires and bars [2, 3] 33
Figure 2-17 - Influence of frequency [2, 3]..... 34
Figure 2-18 – Fretting at different frequencies [2, 3]..... 34
Figure 2-19 - Failure modes for beams without stirrups (left) and with stirrups (right) [2, 3] 36
Figure 2-20 - Specimen dimension, reinforcement and loading setup [5] 37
Figure 2-21 - Experimental setup [5] 38
Figure 2-22 - Shape of load variation [5]..... 38
Figure 2-23 - Influence line for a moving load – stress reversal occurrence [6] 40
Figure 2-24 – Static test [7]..... 41
Figure 2-25 – Wheel load fatigue test [7] 41
Figure 2-26 - Failure shape of fatigue test specimen, top [7]..... 42
Figure 2-27 - Failure shape of fatigue test specimen, bottom [7] 42
Figure 2-28 - Arching in concrete element [1]..... 43
Figure 2-29 - Compressive membrane action in bridge deck [1]..... 44
Figure 2-30 - Components of load deflection curve for a partially restrained slab [8]..... 45
Figure 2-31 - Punching failure model, boundary forces [8]..... 45
Figure 2-32 - Punching failure model, forces on sector element [8]..... 45
Figure 2-33 - Variation of punching load with boundary forces [8] 46
Figure 2-34 - Idealized mode of arching action [1] 47
Figure 2-35 - Arching moment of resistance [1]..... 47
Figure 2-36 - Test slab and lateral restraint configuration [10] 48
Figure 2-37 - Test setup, laboratory [11] 49
Figure 2-38 - Test setup, scheme [11]..... 49
Figure 2-39 - Punching failure load predictions: EC2, ACI [11]..... 50

Figure 2-40 - Punching failure load calculated from UK BD81/02 with CMA [11] 50
Figure 2-41 - Scheme of reduced effectiveness of arching action due to multiple close loads [12] 51
Figure 2-42 - Pattern of cracking on bottom surface of cast-in-place specimens after punching shear fatigue failure [12] 52
Figure 2-43 - Load-deflection behavior of cast-in-place specimens under fatigue [12] 52
Figure 2-44 - Schematic plan view of combined failure mode for precast specimens [12] 52
Figure 2-45 - Schematic section view of combined failure mode for precast specimens [12] 52
Figure 3-1 – T girders before casting of the deck and the cross-beams [14] 55
Figure 3-2 – Structural system after casting of the deck and the cross-beams [14] 55
Figure 3-3 – Loading setup scheme: single load and double load [14] 55
Figure 3-4 – Loading scheme for static (blue line) and alternating loading [15] 56
Figure 3-5 – Position of the fatigue tests [15] 57
Figure 3-6 – Position of the applied load [15] 57
Figure 3-7 – Loading during the first fatigue test [15] 57
Figure 3-8 – Failure of specimen during the first fatigue test [15] 57
Figure 3-9 – Crack pattern at failure, fatigue test no. 2 [15] 58
Figure 3-10 – Crack pattern at 330 kN [15] 58
Figure 3-11 - New deck slab before casting [15] 58
Figure 3-12 – Position of static and dynamic tests [15] 58
Figure 3-13 - Crack pattern at failure, static test no. 1 [15] 59
Figure 3-14 - Crack pattern at failure, static test no. 2 [15] 59
Figure 3-15 – Load values for fatigue test no. 1 [15] 60
Figure 3-16 – Failure pattern for fatigue test no. 1 [15] 60
Figure 3-17 – Loading sequence for fatigue test no. 2 [15] 60
Figure 3-18 – Failure pattern of fatigue test no. 2 [15] 60
Figure 3-19 - – Loading sequence for fatigue test no. 3 [15] 61
Figure 3-20 – Crack pattern at failure, fatigue test no. 3 [15] 61
Figure 3-21 – Loading scheme of fatigue test no. 4 61
Figure 3-22 – Loading sequence for fatigue test no. 4 [15] 62
Figure 3-23 – Failure pattern of fatigue test no. 4 [15] 62
Figure 3-24 - Loading sequence for fatigue test no. 5 [15] 62
Figure 3-25 - Failure pattern of fatigue test no. 5 [15] 62
Figure 3-26 – Failure load as a function of the no. of cycles [15] 63
Figure 3-27 - Relative load value F_{fat}/F_{sta} as a function of the no. of loading cycles for the 2nd series of tests [15] 64
Figure 3-28 - Relative load value F_{fat}/F_{sta} as a function of the no. of loading cycles for all the tests [15] 64
Figure 3-29 – Tested specimens as component of a bridge [12] 65
Figure 3-30 – Loading of specimen for analytical studies [12] 65
Figure 3-31 – Test setup [12] 66
Figure 3-32 – Crack pattern at failure for precast specimens [12] 66
Figure 3-33 – Predicted and observed results for precast specimens [12] 67
Figure 3-34 – S-N diagram for all specimens [12] 67
Figure 3-35 - Experimental setup [5] 67
Figure 3-36 - Shape of load variation [5] 67
Figure 3-37 – Slab S1 at failure after static loading [5] 68
Figure 3-38 – Cracks in slab S1 after the cyclic test [5] 68
Figure 3-39 – Geometry and reinforcement layout of the specimens [7] 69
Figure 3-40 – Tests setup for (moving wheel) fatigue test [7] 69

Figure 3-41 – Failure of specimen after static tests [7] 70
Figure 3-42 – Failure of specimen after fatigue test [7] 70
Figure 3-43 – Test setup [16] 71
Figure 3-44 – Variable amplitude fatigue loading scheme [16] 72
Figure 3-45 - Constant amplitude fatigue loading scheme [16] 72
Figure 3-46 – Load-deflection behavior of slab S1 under static and cyclic loading [16] 72
Figure 3-47 – Static response of the slabs after different fatigue loading steps (F_f=367 kN) [16] 72
Figure 3-48 – Crack pattern under fatigue loading [16] 73
Figure 3-49 – Number of cycles to failure for each slab [16] 73
Figure 3-50 - Relative load value Ffat/Fsta as a function of the no. of loading cycles for all the tests [15] 76
Figure 3-51 - S-N diagram for all specimens [12] 76
Figure 3-52 – S-N curve: tests and prediction from formulas [7] 77
Figure 3-53 – S-N curve for fully supported slabs from Roesler and Barenberg study [18] 78
Figure 3-54 – S-N curve from the study performed by Sonoda and Horikawa [20] 78
Figure 3-55 – S-N curves based on different prediction formulas [21] 79
Figure 4-1 – 3D solid finite element bridge model, S. Amir [14] 82
Figure 4-2 – Plane stress state [24] 83
Figure 4-3 – First FEA model, simply supported 84
Figure 4-4 - Lack of plate in the model (linear analysis) 85
Figure 4-5 – Effect of the loading plate on the stress distribution (linear analysis) 85
Figure 4-6 – FEA model displaying the geometry and the reinforcing/prestressing bars 86
Figure 4-7 – Plane stress element as defined by DIANA [25] 86
Figure 4-8 – CQ16M element of DIANA [25] 86
Figure 4-9 – CL12I interface element [25] 87
Figure 4-10 – Connection of CL12I to another element [25] 87
Figure 4-11 – Reinforcement bar as considered by DIANA [25] 88
Figure 4-12 - Bar particle in a plane stress element [25] 88
Figure 4-13 – Material properties of concrete and steel from S. Amir's PhD thesis [14] 89
Figure 4-14 – Smeared cracking approach [28] 89
Figure 4-15 – Smeared crack model, tensile behaviour [14] 89
Figure 4-16 – Tension softening functions: Hordijk (left), Exponential (centre) and Linear (right) [25] 90
Figure 4-17 – Vecchio and Collins reduction factor due to lateral cracking [25] 90
Figure 4-18 – Parabolic compression curve [25] 91
Figure 4-19 – Ideal (constant) compression curve [25] 91
Figure 4-20 – Reinforcing steel properties from S. Amir's PhD thesis [14] 92
Figure 4-21 – Strain curves of steel from the experimental program [14] 92
Figure 4-22 – Stress-strain diagram used for the FEA model of the Master's Thesis 92
Figure 4-23 – Meshed FEA model, presented half due to symmetry 96
Figure 4-24 – Close-up of the mesh for assessing the discretization elements 96
Figure 4-25 – Snap-through [25] 97
Figure 4-26 – Snap-back [25] 97
Figure 4-27 – Modified Newton-Raphson method [25] 97
Figure 4-28 – Load-deflection behaviour for a single point load at mid-span and a TPL of 2.5 MPa [14] (image used to obtain Graph 4-2) 98
Figure 4-29 – Cracking pattern due to static loading [15] 99
Figure 4-30 – Failure due to fatigue loading [15] 99
Figure 4-31 – Punching cone contour and crack pattern due to fatigue loading [15] 99

Figure 4-32 – Increase in the steel stress over the yield value as a consequence of the increase in crack width 101
Figure 4-33 – Yielding of steel at one location in the initial model loaded by a point load .. 101
Figure 4-34 – Yielding of steel at two locations in the initial model loaded by a distributed load 101
Figure 4-35 – Development of the compressive membrane action (CMA) within the initial FEA model 103
Figure 4-36 - Compressive stress in the deck slab after blocking both translations at the supports 105
Figure 4-37 – Stresses in the steel at failure (presented in the nodes) 111
Figure 4-38 - Stresses in the steel at failure (presented in the integration points) 111
Figure 4-39 – Strains in the steel at failure (presented in the nodes) 112
Figure 4-40 - Strains in the steel at failure (presented in the integration points) 112
Figure 4-41 – Stress in the concrete at failure (presented in the nodes) 113
Figure 4-42 - Stress in the concrete at failure (presented in the integration points) 113
Figure 4-43 - Strain of the concrete at failure (presented in the nodes) 113
Figure 4-44 - Strain of the concrete at failure (presented in the integration points) 113
Figure 4-45 – Crack width at failure (presented in the nodes) 114
Figure 4-46 - Crack width at failure (presented in the integration points) 114
Figure 4-47 – Deflection values from the experimental tests [14] 114
Figure 4-48 - Deflection values from the FEA [14] 114
Figure 4-49 – Deflection of the best behaviour FEA model 114
Figure 4-50 – Development of the Compressive Membrane Action in the BBM FEA model 115
Figure 4-51 – Steel stress at the assumed failure 116
Figure 4-52 – Value of the strain at the assumed failure 116
Figure 4-53 – Concrete stresses at the assumed failure 116
Figure 4-54 – Concrete strains at the assumed failure 116
Figure 4-55 – Crack widths at the assumed failure 117
Figure 4-56 – Deflection of the realistic FEA model 117
Figure 4-57 – Development of the Compressive Membrane Action in the RM FEA model 117
Figure 5-1 – Compressive fracture energy dependence on the compressive strength [25] 121
Figure 5-2 - Cyclic loading range for test BB23_200 [15] 125
Figure 5-3 – Steel stress at the end of the analysis, BB23_200 - BBM 125
Figure 5-4 – Steel strain at the end of the analysis, BB23_200 - BBM 125
Figure 5-5 – Concrete stresses at the end of the analysis, BB23_200 - BBM 126
Figure 5-6 –Concrete strains at the end of the analysis, BB23_200 - BBM 126
Figure 5-7 – Crack width, BB23_200 - BBM 126
Figure 5-8 – Development of CMA, BB23_200 - BBM 126
Figure 5-9 – Steel stress at failure, BB23_200 - RM 126
Figure 5-10 – Steel strain at failure, BB23_200 - RM 126
Figure 5-11 – Concrete stress at failure, BB23_200 - RM 127
Figure 5-12 – Concrete strain at failure, BB23_200 -RM 127
Figure 5-13 – Crack width, BB23_200 - RM 127
Figure 5-14 – Development of CMA, BB23_200 - RM 127
Figure 5-15 - Cyclic load range for test BB24_150 [15] 127
Figure 5-16 - Steel stress at the end of the analysis, BB24_150 - BBM 128
Figure 5-17 - Steel strain at the end of the analysis, BB24_150 - BBM 128
Figure 5-18 - Concrete stresses at the end of the analysis, BB24_150 - BBM 128
Figure 5-19 - Concrete strains at the end of the analysis, BB24_150 - BBM 128

Figure 5-20 - Crack width, BB24_150 - BBM 128
Figure 5-21 – Development of CMA, BB24_150 - BBM 128
Figure 5-22 - Steel stress at failure, BB24_150 - RM 129
Figure 5-23 - Steel strain at failure, BB24_150 - RM 129
Figure 5-24 - Concrete stress at failure, BB24_150 - RM 129
Figure 5-25 - Concrete strain at failure, BB24_150 - RM 129
Figure 5-26 – Crack width, BB24_150 - RM 129
Figure 5-27 – Development of CMA, BB24_150 - RM 129
Figure 5-28 – Cyclic load range for test BB26_165 130
Figure 5-29 - Steel stress at the end of the analysis, BB26_165 - BBM 130
Figure 5-30 - Steel strain at the end of the analysis, BB26_165 - BBM 130
Figure 5-31 - Concrete stresses at the end of the analysis, BB26_165 - BBM 131
Figure 5-32 - Concrete strains at the end of the analysis, BB26_165 - BBM 131
Figure 5-33 Crack width, BB26_165 - BBM 131
Figure 5-34 – Development of CMA, BB26_165 - BBM 131
Figure 5-35 - Steel stress at failure, BB26_165 - RM 131
Figure 5-36 - Steel strain at failure, BB26_165 - RM 131
Figure 5-37 - Concrete stress at failure, BB26_165 - RM 132
Figure 5-38 - Concrete strain at failure, BB26_165 - RM 132
Figure 5-39 – Crack width, BB26_165 - RM 132
Figure 5-40 – Development of CMA, BB26_165 - RM 132
Figure 5-41- Loading ranges for test BB28 [15] 134
Figure 5-42 – Steel stress at the beginning of the second phase, BB28 135
Figure 5-43 - Concrete stress at the beginning of the second phase, BB28 135
Figure 5-44 – Loading ranges for BB29 [15] 135
Figure 5-45 – Steel stress at the end of FEA for loading range 1 of test BB28 137
Figure 5-46 - Concrete stress at the end of FEA for loading range 2 of test BB29 137
Figure 5-47 – Schematization of Miner's rule, design curve [29] 137
Figure 5-48 – Loading sequence, type I 138
Figure 5-49 – Loading sequence, type II 138
Figure 6-1 – Number of longitudinal girders for the previous structural system [14] 143
Figure 6-2 – Number of longitudinal girders for the current structural system 143
Figure 6-3 - Cross section of longitudinal girders from previous study [14] 144
Figure 6-4 - Cross section of longitudinal girders from current study 144
Figure 6-5 – Formwork and reinforcement for end beams 144
Figure 6-6 – Transverse end beams after casting 144
Figure 6-7 – Wooden frames for supporting the formwork 145
Figure 6-8 – Completed formwork for the deck slab 145
Figure 6-9 – Structure after positioning of the reinforcement ant PVC tubes 145
Figure 6-10 – Close-up with the reinforcement and the plastic tubes 145
Figure 6-11 – Casting and smoothing the surface of the concrete 146
Figure 6-12 – Concrete covered with a plastic foil to prevent water evaporation 146
Figure 6-13 – Tensioning of the prestressing bars 146
Figure 6-14 – Structural system prepared for tests 146

List of Graphs

Graph 4-1 - Influence of boundary conditions (following from the linear analyses) 84
Graph 4-2 – Load-deflection behaviour following from the experimental program and the FEA of S. Amir 98
Graph 4-3 – Force-deflection behaviour of the initial model for different loading situations 100
Graph 4-4 – Different force-deflection behaviours of the initial model compared to the reference curves 100
Graph 4-5 – Behaviour of the initial model due to the exceeding of the yield stress of steel 101
Graph 4-6 - Influence of the prestressing bar's bond on the behaviour of the initial model . 102
Graph 4-7 – Influence of the ultimate steel strain on the behaviour of the initial model..... 102
Graph 4-8 – Influence of the value of the applied force 102
Graph 4-9 – Influence of the arc-length control method 102
Graph 4-10 – Impact of the effective width on the FEA model's behaviour 104
Graph 4-11 – Best behaviour obtained for a width of 1.95 meters 104
Graph 4-12 – Impact of the translation restraint at the supports 105
Graph 4-13 – Influence of the prestressing bar's bond on the capacity of the model: no bond considered 106
Graph 4-14 - Influence of the prestressing bar's bond on the capacity of the model: bond considered 106
Graph 4-15 – Behaviour of the FEA model without the prestressing bar and with the bar not being bonded 106
Graph 4-16 - Influence of the Arc-Length Control method; final effective width (1.95 m) considered 107
Graph 4-17 - Influence of the rotation at the supports on the behaviour of the FEA model.. 107
Graph 4-18 - Influence of the compressive model of the concrete on the FEA model's behaviour 108
Graph 4-19 - Influence of the tensile model of concrete on the FEA model's behaviour 108
Graph 4-20 - Final FEA models 109
Graph 4-21 – Behaviour of the "realistic model' (RM) 110
Graph 4-22 – Steel stress variation in the best behaviour model 112
Graph 5-1 – Impact of the modified compressive strength and fracture energy on the FEA model 121
Graph 5-2 – Impact of the elasticity modulus on the fatigue behaviour 122
Graph 5-3 – Behaviour of FEA model depending on the parameters considered for modification 123
Graph 5-4 – Impact of different approaches in determining the tensile strength and fracture energy 123
Graph 5-5 – Fatigue FEA of test BB23_200 125
Graph 5-6 - Fatigue FEA of test BB24_150 127
Graph 5-7 - Fatigue FEA of test BB26_165 130
Graph 5-8 – Fatigue tests: Results and accuracy; F_{fat}/F_{sta} vs. logN 132
Graph 5-9 - FE analyses of test BB28 134
Graph 5-10 - FE analysis of test BB29 135
Graph 5-11 - Individual FEA for each loading range of test BB28 136
Graph 5-12 - Individual FEA for each loading range of test BB29 136
Graph 5-13 – Sequence effect, phased analysis 139
Graph 5-14 – Sequence effect, separate analysis 139

List of Tables

Table 4-1 – Properties of the constitutive model for concrete 91
Table 4-2 – Properties of the constitutive model for reinforcing steel 93
Table 4-3 – Properties of the constitutive model for prestressing steel 93
Table 4-4 – Properties of the constitutive model for the steel plates 94
Table 5-1 – Approaches for determining the reduced tensile strength and tensile fracture energy 123
Table 5-2 – Test BB23_200 FEA results and prediction 125
Table 5-3 - Test BB24_150 FEA results and prediction 128
Table 5-4 - Test BB26_165 FEA results and prediction 130

List of Equations

Equation 5-1 – Determination of the maximum compressive stress 121
Equation 5-2 – Force prediction formula 124
Equation 5-3 – Formulation for Miner's rule 138

References

[1] ICE Manual for bridge engineering, Institution of Civil Engineers, 2008

[2] G. P. Mallett, Fatigue of reinforced concrete, HMSO, Transport and road research laboratory, 1991

[3] Comité européen du beton, Bulletin No. 188, 1988

[4] Ahsan R., Fatigue in concrete structures, BSRM Seminar on fatigue properties of construction steel

[5] V. Carvelli, M. A. Pisani, C. Poggi, Fatigue behaviour of concrete bridge deck slabs reinforced with GFRP bars, Composites: Part B Engineering 41(7):560-567 · October 2010

[6] M. Schlafli, E. Bruhwiler, Fatigue of existing reinforced concrete bridge deck slabs, Engineering Structures, Vol. 20, No. 11, pp. 991–998, 1998

[7] H. Hwang, H. Yoon, C. Joh, B-S. Kim, Punching and fatigue behavior of long-span prestressed concrete deck slabs, Engineering Structures 32 (2010) 2861-2872

[8] B. deV. Batchelor, Membrane Enhancement in Top Slabs of Concrete, Concrete Bridge Engineering: Performance and advances, CRC Press 1987

[9] The Highways Agency, Use of compressive membrane action in bridge decks - Summary of correction – BD 81/02 Volume 3, Section 4, Part 20, Design manual for roads and bridges, 2007

[10] Y. Zheng, C.H. Li, J.B. Yang, C. Sun, Influence of arching action on shear behaviour of laterally restrained concrete slabs reinforced with GFRP bars, Composite Structures 132 (2015) 20–34

[11] S. Amir, C. van der Veen, J.C. Walraven, A. de Boer, Bearing capacity of prestressed concrete decks slabs. In CR Alimchandani (Ed.), Proceedings of the 4th international FIB congress (pp. 1-10). Himayatnagar: Universities Press. (TUD), 2014

[12] J. C. Graddy, J. Kim, J. H. Whitt, N. H. Burns, R. E. Klingner, Punching-Shear Behavior of Bridge Decks under Fatigue Loading, ACI Structural Journal 99(3):257-266, Title no. 99-S27 · May 2002

[13] D. A. Hordijk, Local approach to fatigue of concrete, Technische Universiteit Delft, 1991

[14] S. Amir, Compressive Membrane Action in Prestressed Concrete Deck Slabs, PhD thesis, TU Delft, 2014 – from TU Delft repository

[15] C. van der Veen, A. Bosman, Vermoeiingssterkte voorgespannen tussenstort" - report number 25.5-14-06, TU Delft, December 2014

[16] A. El-Ragaby, E. El-Salakawy, B. Benmokrane, Fatigue analysis of concrete bridge deck slabs reinforced with E-glass/vinyl ester FRP reinforcing bars, Composites Part B: Engineering, 38 (2007) 703–711

[17] F. Natário, M. F. Ruiz, A. Muttoni, Experimental investigation on fatigue of concrete cantilever bridge deck slabs subjected to concentrated loads, Engineering Structures 89 (2015) 191–203, 2015

[18] J. R. Roesler, E. J. Barenberg, Fatigue and Static Testing of Concrete Slabs, Transportation Research Record, No. 1684, Pag. 71-80, Nov. 1999

[19] A. Medeiros, X. Zhang, G. Ruiz, R. C. Yu, M. de Souza Lima Velasco, Effect of the loading frequency on the compressive fatigue behaviour of plain and fiber reinforced concrete, International Journal of Fatigue 70 (2015) 342–350, 2015

[20] K. Sonoda, T. Horikawa, Fatigue strength of reinforced concrete slabs under moving loads, IABSE reports, 37 (1982)

[21] A. El-Ragaby, E. El-Salakawy, B. Benmokrane, Fatigue Life Evaluation of Concrete Bridge Deck Slabs Reinforced with Glass FRP Composite Bars, Journal of Composites for Construction © ASCE / May/June 2007, J. Compos. Constr., 2007, 11(3): 258-268

[22] E. Lantsoght, C. van der Veen, A. de Boer, J. Walraven, Recommendations for the Shear Assessment of Reinforced Concrete Solid Slab Bridges, PowerPoint presentation at IABMAS 2014, 7th International Conference on Bridge Maintenance, Safety and Management, 7th-11th of July, Shanghai, China

[23] S. Amir, Compressive Membrane Action in Concrete Decks, Proc. of the 9th fib International PhD Symposium in Civil Engineering July 22 to 25, 2012, Karlsruhe Institute of Technology (KIT), Germany – from TU Delft repository

[24] Digital Engineering, Online engineering platform and magazine
http://www.digitaleng.news/de/simplifying-fea-models-plane-stress-and-plane-strain/

[25] DIANA 10.0 Manual, Website of DIANA FEA,
http://dianafea.com/manuals/d100/Diana.html

[26] Guidelines for Nonlinear Finite Element Analysis of Concrete Structures, Rijkswaterstaat Technical Document (RTD), Doc. nr. : RTD 1016-1:2016, Version: 2.0, Status: Final, Date: 24 June 2016

[27] J. G. Rots, J. Blaauwendraad, Crack models for concrete: Discrete or Smeared? Fixed, multi-directional or rotating? , Heron, Vol. 34, 1989, No. 1

[28] Computational Modelling of Structures Course (CIE5148), Faculty of Civil Engineering and Geosciences, Technical University of Delft, 2015/2016

[29] Fatigue Course (CIE5126), Faculty of Civil Engineering and Geosciences, Technical University of Delft, 2015/2016